

# The Science of Nuclear Energy: Fission and Fusion

Robert J. Goldston



Dedicated to my wife Ruth, my sons Josh and Jake,  
my daughter-in-law Katie, and especially to my grandsons, Max and Ezra,  
who will have to live with all the decisions we make and do not make.

## Preface



Lise Meitner, circa 1930

At this point we both sat down on a tree trunk, and started to calculate on scraps of paper. ... When the two drops separated they would be driven apart by their mutual electric repulsion and would acquire a very large energy, about 200 MeV in all; where would that come from? Fortunately Lise Meitner remembered how to compute the masses of nuclei from the so-called packing fraction formula, and in that way she worked out that the two nuclei formed by the division of a uranium nucleus would be lighter than the original uranium nucleus by about one-fifth the mass of a proton. Now whenever mass disappears energy is created, according to Einstein's formula  $E = mc^2$ , and one-fifth of a proton mass was just equivalent to 200 MeV. So here was the source for that energy; it all fitted!

---

Otto Frisch

The science of nuclear energy can be viewed from two different perspectives, and we will explore both of them: the beauty and simplicity of the underlying science, and the scientific underpinnings of the implications for

society of the resulting technology. This dual perspective is unusual for a textbook like this.

First, the underlying science is indeed beautiful. We will sit on the tree trunk with refugee Lise Meitner and her nephew Otto Frisch in the snowy woods in Sweden in December 1938. We will share their “Aha!” experience as we understand when they find – and then explain to the world – that nuclear fission has been observed for the first time. The measurements had been taken on Meitner’s insistence in the laboratory in Germany she had been forced to abandon in July, and she was the first to interpret them. We will also follow Enrico Fermi in discovering the subtle – but ultimately simple and beautiful – physics of neutron thermalization and diffusion, required to design a self-sustaining chain reaction. Amazingly, he achieved this goal only four years later, in December 1942.

We will also study the new science of plasma physics, the physics of ionized gases, developed in large part to make fusion energy possible. We will have eyewitness access to the development of the experimental and theoretical understanding of the macroscopic stability limits of fusion plasmas, of the micro-scale turbulent processes that govern how heat is transported across magnetic fields, and the physics that determines the narrow layer through which heat escapes from a plasma.

Throughout this book you will be sharpening, deepening, and extending your understanding of concepts that are useful in many areas of the physical sciences and technology. Some of the exercises include fun options to develop simple but powerful Monte Carlo computational simulation tools to test some of the analytic theories we will develop. These can be extended into midterm projects that examine more subtle issues.

Looked at from the second perspective, societal implications, nuclear energy is a low-carbon source of electrical energy and process heat, and so can contribute to the advancement of global development without adding to climate change. However it also brings with it risks associated with safety, waste and nuclear proliferation. We will stand next to the operators of the Fukushima Daiichi nuclear power station and understand their actions as they carefully switch on and off the emergency core cooling system to control the cool-down of Unit 1 – until the tsunami hits and they lose control. We will also probe the aftermath, and the root causes of the accident. We will see why it is so hard to open a geological repository for civilian nuclear waste. We will also sit with U.S. Secretary of Energy Ernie Moniz and understand as he negotiates the scientific aspects of the recent Joint Comprehensive Plan of Action with his counterpart, Iran’s Ali Ahkbar Salehi. Finally, we will peek under the hood of future technologies for nuclear fission.

We will learn about the great successes and tough challenges facing the development of practical fusion energy. We will talk about the scientific progress and prospects for the massive international fusion energy experiment in France, ITER, which involves China, the European Union, India, Japan, Russia, South Korea, and the U.S. We will also look at the scientific issues that remain before fusion can be commercialized.

With the understanding we will develop, you will be in a position to form your own considered opinions about the important policy issues surrounding nuclear energy. Society grants scientists the privilege and the great pleasure of studying and learning; it is reasonable that we should give back to society our best, honest understanding of the societal issues on which we are best informed.

What background do you need to benefit from this book? The science and mathematics we use should be familiar to third-year university students in the physical sciences and engineering. However very well prepared first-year students and interested fourth-year students, also graduate students, have benefited from this course. We use vector calculus extensively, for example Gauss's and Stokes's theorems, and we will get to know the partial differential diffusion equation, in some depth. We will use elementary thermodynamics and quantum mechanics. We will present the nuclear physics we will need in the context of the basic elements of non-relativistic quantum mechanics.

Scientists and engineers from other fields of research who want to understand the ideas behind nuclear energy may find that this book gives them a useful perspective. It should be particularly helpful to those interested in arms control and nuclear non-proliferation, which we cover in some depth. Policymakers, even those with a technical bent, may not want to follow all of the derivations (nor do all of the exercises!), but they may be able to glean enough useful technical perspective on key issues to orient themselves, and to ask the right questions of experts.

You can use this book as an introduction to the science of nuclear fission by reading Chapter 1 and all of part I. Section 1.2 will give you a helpful self-contained perspective on fusion energy. If instead you are looking for an introduction to nuclear fusion science, you can read all of Chapter 1, getting a quick perspective on fission, sections 2.1 - 2.3 to understand reaction rates, 4.1 - 4.5 to understand the diffusion equation, and all of part II.

At Princeton we have 12-week semesters, and I have taught the course associated with this book in two 80 minute sessions per week, plus one evening precept for Q&A. Chapter 1 is longer than most; I don't cover section 1.2.3 in class, since these topics are covered more deeply later. It is

included here to provide an overview of fusion for those primarily interested in fission. Chapters 3, 4, 5, 6 and 10 have about twice the content of the others. These longer chapters each form a logical unit, and are each covered in two lectures. I have used the last lecture period for student presentations.

A comment about the questions that appear in the text: I find that it is a good idea to break up lectures every so often with simple, enlightening questions. The questions every few pages in the text are an attempt at reproducing the spirit of this in book form.

All units are SI, unless otherwise specified with a subscript. We frequently use a unit of energy that is common in both fission and fusion research, the “electron Volt,” or eV. 1 eV equals the energy that an electron gains when it is accelerated across a potential difference of 1 V in free space,  $e$  Joules, where  $e$  is the magnitude of the elementary charge in Coulombs,  $1.60 \cdot 10^{-19}$  C. Thus energy expressed in eV,  $E_{eV}$ , and energy expressed in the SI energy unit, Joules,  $E$ , are related by  $E = eE_{eV} = 1.60 \cdot 10^{-19} E_{eV}$ . The units of  $E_{eV}$ , like those of the electrostatic potential,  $\Phi$ , are Volts, since  $eE_{eV}$ , like  $e\Phi$ , gives an energy in Joules.

I would like to thank all of the clever and energetic students who have taken this course over the last eight years, asked great questions that helped deepen my understanding and clarify my explanations, completed innumerable exercises, some of which really needed the clarification that is included here, and wrote overwhelmingly thoughtful essays. I would also like to thank my dedicated Assistants in Instruction, Tyler Abrams, Abraham Fetterman, Laura Berzak Hopkins, Sébastien Philippe, Jacob Schwartz and David Turnbull, who helped with the teaching, with the precepts, and with developing and grading the exercises.

I would particularly like to thank Prof. Alex Glaser, with whom I shared this course for the first three years, and from whom I have learned a great deal about nuclear fission energy and nuclear proliferation.

Rob Goldston  
February 7, 2018

# Contents

<b>Preface</b>	<i>page</i> iii
<b>1 Fission and Fusion</b>	1
1.1 Fission	3
1.1.1 Self-sustaining fission reactions	3
1.1.2 Safety, waste, nuclear proliferation	10
1.1.3 Past may be prologue, but what is it telling us?	17
1.1.4 Prospects	21
1.2 Fusion	21
1.2.1 Self-sustaining fusion reactions	21
1.2.2 Why fusion?	29
1.2.3 Scientific progress	32
1.2.4 Prospects	48
Resources	49
Exercises	50
 <b>PART ONE FISSION</b>	53
<b>2 Neutron Interactions with Matter</b>	55
2.1 Cross sections	56
2.2 Beam attenuation and mean free path	57
2.3 Reaction rates	58
2.4 Elements of non-relativistic quantum mechanics	59
2.5 Elements of nuclear physics	62
2.6 Fission	70
2.7 Radiative Absorption	76
2.8 Elastic and Inelastic Scattering	78
2.9 Try This at Home	80
Resources	81
Exercises	82
<b>3 Neutron Energy Distribution</b>	86
3.1 Energy change in elastic scattering	87
3.2 Logarithmic energy decrement	92
3.3 Slowing Down Time	95
3.4 Neutron flux vs. energy, $\phi(E)$ , and vs. lethargy, $\phi(u)$	96
3.5 Fast energy region $\phi_F(E)$	98
3.6 Intermediate energy region $\phi_I(E)$	106
3.7 Thermal energy region $\phi_T(E)$	114

	<i>Contents</i>	ix
3.8	Visualizing the four-factor formula	120
3.9	Neutron flux spectrum in the example Light Water Reactor	121
3.10	Fast reactors	125
3.11	Neutron flux spectrum in the example Fast Reactor Review	131
	Resources	133
	Exercises	133
<b>4</b>	<b>Neutron Spatial Distribution</b>	<b>135</b>
4.1	Neutrons as a one-speed gas	136
4.2	The one-speed neutron diffusion equation	140
4.3	1-D $\delta$ -function initial condition without boundaries	144
4.4	Statistical interpretation of the neutron diffusion equation	145
4.5	1-D $\delta$ -function steady source without boundaries	147
4.6	Boundary conditions	151
4.7	Bounded Systems	153
4.8	Non-leakage probability	163
4.9	Spatial diffusion in thermal reactors	164
4.10	Spatial diffusion in fast reactors	168
4.11	Integrated numerical modeling	169
	Review	169
	Resources	169
	Exercises	169
<b>5</b>	<b>Safety</b>	<b>172</b>
5.1	The neutron “kinetic” equation	172
5.2	Including delayed neutrons	172
5.3	Consequences for reactor stability	172
5.4	Behavior over longer time scales	172
5.5	Chernobyl	172
5.6	Fukushima	172
5.7	Regulatory response	172
5.8	Effects of radiation on human health	172
5.9	Impacts of Chernobyl and Fukushima	172
	Review	172
	Resources	172
	Exercises	172
<b>6</b>	<b>The Nuclear Fuel Cycle</b>	<b>173</b>
6.1	Mining	173
6.2	Enrichment	173

6.3	Burnup	173
6.4	Interim storage	173
6.5	Geological repository	173
6.6	Reprocessing for thermal reactors	173
6.7	Fast reactors and reprocessing	173
	Review	173
	Resources	173
	Exercises	173
<b>7</b>	<b>Nuclear Weapons and Nuclear Proliferation</b>	174
7.1	How nuclear weapons work	175
7.2	History of nuclear proliferation	175
7.3	Proliferation risks going forward	175
7.4	Means to manage risks	175
	Review	175
	Resources	175
	Exercises	175
<b>8</b>	<b>Advanced Reactors</b>	176
8.1	Generation III and III+ reactors	176
8.2	Generation IV reactors	176
8.3	Thorium cycle	176
8.4	Breed and burn in place	176
	Review	176
	Resources	176
	Exercises	176
	<b>PART TWO FUSION</b>	177
<b>9</b>	<b>Power and Particle Balance</b>	179
9.1	Fusion reactions	179
9.2	Plasma heating	179
9.3	Heat loss	179
9.4	Energy gain!	179
9.5	Particle balance	179
	Review	179
	Resources	179
	Exercises	179
<b>10</b>	<b>Particle Motion</b>	180
10.1	Uniform electric and magnetic fields	180
10.2	Curved magnetic field	180

	<i>Contents</i>	xi
10.3	Perpendicular gradient in magnetic field strength	180
10.4	Parallel gradient in magnetic field strength	180
10.5	Drifts in toroidal magnetic field	180
10.6	Passing particle orbits	180
10.7	Trapped particle orbits	180
10.8	Bootstrap current	180
	Review	180
	Resources	180
	Exercises	180
<b>11</b>	<b>Plasmas as Fluids</b>	181
11.1	Plasmas as fluids?	181
11.2	Equilibrium in a cylinder	181
11.3	Plasma control	181
11.4	Stellarators	181
11.5	2-fluid model and parallel force balance	181
	Review	181
	Resources	181
	Exercises	181
<b>12</b>	<b>Macroscopic Stability</b>	182
12.1	Ideal MHD stability	182
12.2	Interchange and ballooning modes	182
12.3	Kink modes	182
12.4	Plasma shaping	182
12.5	Stellarators	182
	Review	182
	Resources	182
	Exercises	182
<b>13</b>	<b>Collisions and their Effects</b>	183
13.1	Coulomb collisions	183
13.2	Debye shielding	183
13.3	Small-angle scattering	183
13.4	Collisional cross-field transport	183
13.5	Other collisional effects	183
	Review	183
	Resources	183
	Exercises	183
<b>14</b>	<b>Turbulent Transport</b>	184
14.1	Bohm and GyroBohm	184
14.2	Turbulence and flows – simulation	184

14.3	Turbulence and flows – measurement	184
14.4	Transport barriers	184
14.5	Global scaling	184
	Review	184
	Resources	184
	Exercises	184
<b>15</b>	<b>Divertors, Scrape-off layers, and Plasma-Facing Components</b>	
15.1	Divertors	185
15.2	Scrape-off layers	185
15.3	Transient events	185
15.4	Plasma-facing components	185
	Review	185
	Resources	185
	Exercises	185
<b>16</b>	<b>Neutron Interactive Materials, Blankets; Safety, Waste and Proliferation</b>	
16.1	Neutron interactive materials	186
16.2	Blanket designs	186
16.3	Safety	186
16.4	Waste	186
16.5	Nuclear proliferation	186
	Review	186
	Resources	186
	Exercises	186
<b>17</b>	<b>Inertial Fusion Energy</b>	
17.1	Vision and status	187
17.2	Batch burn vs. hot-spot ignition	187
17.3	Drivers	187
17.4	Targets and chambers	187
	Review	187
	Resources	187
	Exercises	187
<b>18</b>	<b>Power Plant Concepts, Development Path and Deployment</b>	
18.1	Power plant concepts	188
18.2	Development path	188
18.3	Deployment	188
	Review	188

<i>Contents</i>	xiii
Resources	188
Exercises	188



# Chapter 1

## Fission and Fusion



what's past is prologue; what to come,  
In yours and my discharge

---

The Tempest, William Shakespeare

In this opening chapter we will explore some of the general features of fission and fusion. We will first address the basic physical requirements for sustainment of both kinds of reactions. Then we will take a look at the societal implications of the underlying technologies of fission and fusion, and finally we will review progress and prospects for each. All of this, of course, will be covered more thoroughly in the chapters that follow, but here we will get an overview, and develop a sense of what is to come.

As shown in figure 1.1, the mass-energy of most nuclei is  $8 \pm 1$  MeV/nucleon below the mass-energy of the free nucleons, protons and neutrons that form them. This nuclear potential energy is the negative of the conventional “Curve of Binding Energy,” or “packing fraction” curve. It better expresses the analogy of the lower gravitational potential energy of a ball at the bottom of a well as compared with at the top. The nucleons have, in effect, “fallen” together, because the strong short-range nuclear force of attraction has overcome the average long-range mutual electrostatic repulsion, and created a deep potential well that contains the nucleons. The potential energy per nucleon is evidently lower near the bottom of the curve and if a group of nucleons move from either end towards the lowest point, their nuclear potential energy drops. This reduction in potential energy makes

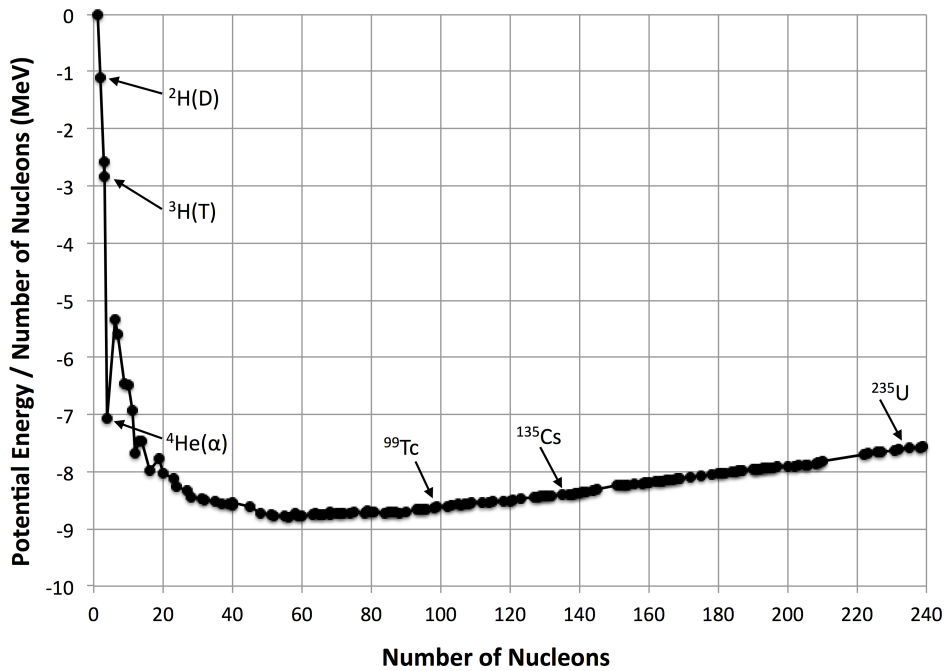


Figure 1.1 Curve of the potential energy per nucleon (protons + neutrons) in nuclei, over a wide range in mass. This is the average mass-energy ( $mc^2$ ) per nucleon less the average mass-energy per nucleon of the free protons and neutrons (938 and 940 MeV respectively) from which they are formed. Negative potential energy, in the form of reduced rest mass compared with free particles, binds the nuclei together. Some nuclei are tagged that participate in fusion (to the left) or fission (to the right) as reactants or products.

energy available to take other forms, in particular the kinetic energy of the reaction products.

**Warm-up Question:** Why is the  $^1\text{H}$  nucleus at zero potential energy?

Figure 1.1 shows that if a heavy nucleus, such as uranium, fissions into two nuclei averaging about half its weight, a bit less than 1 MeV per nucleon is freed up for a total of  $\sim 200$  MeV. On the other hand, if we can arrange for two light nuclei to fuse together to form a heavier nucleus (helium looks like a particularly promising candidate for the heavier nucleus) then a total of  $\sim 18$  MeV is released, or about 3.6 MeV per nucleon. This is far and away more energy per unit mass than is available from chemical reactions, of order a few eV per molecule, and molecules can contain many nucleons.

## 1.1 Fission

### 1.1.1 Self-sustaining fission reactions

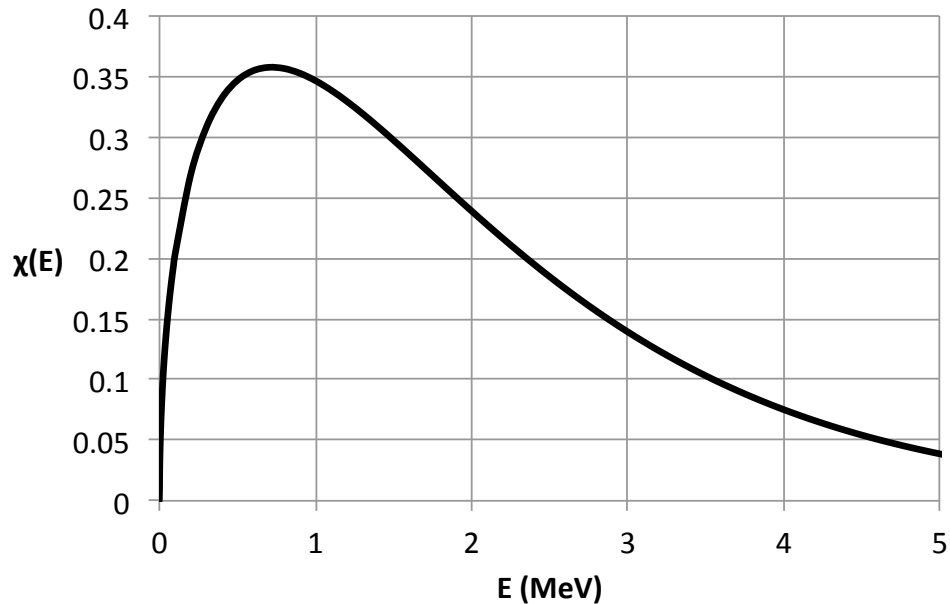


Figure 1.2 Probability distribution of neutrons produced by fission

Figure 1.2 shows the probability distribution of neutrons that emerge from fission of  $^{235}\text{U}$ . Evidently neutrons boil out of the fission process with energies in the general range of the potential energy release per nucleon, but also below and significantly above. Note that the spectrum has been normalized such that  $\int_0^\infty \chi(E)dE_{\text{MeV}} = 1$ , where the subscript “MeV” indicates that  $E$  is measured in MeV. This means, for example, that about 1/3 of the neutrons are emitted with energies in the 1 MeV wide range from 0.5 MeV to 1.5 MeV, and about 1/2 of the neutrons are emitted in the 2 MeV wide range from 1 MeV to 3 MeV.

The speed of a non-relativistic neutron is  $1.38 \cdot 10^7 \sqrt{E_{\text{MeV}}} \text{ m/s}$ . We will be studying neutrons up to at most 14.1 MeV, and since relativistic effects scale as  $(v/c)^2$ , where  $c = 3.00 \cdot 10^8 \text{ m/s}$ , there should be only weak relativistic effects. Another way to see this is to note that the rest mass of the neutron is about 940 MeV, so we are making errors in the range of  $10^{-3} - 10^{-2}$  by ignoring relativistic effects. The other simplifying approximations we will use produce greater inaccuracies. We acknowledge this fact, in a limited way, by only evaluating numerical results to three significant figures.

While the neutrons from various fusion reactions are born at energies of up to 14.1 MeV, and fission neutrons are born generally in the low MeV range, we will also be interested in the behavior of neutrons as they lose energy and ultimately thermalize with their near room-temperature surroundings. In addition we will be interested in hot fusion fuel in the ionized state, with electrons stripped from nuclei, called “plasma.” This also tends to have a thermal, or Maxwellian, distribution of velocities – just with a very high temperature. Thus we are interested in thermal distributions of particles.

You should be familiar with the fact that the average kinetic energy of a molecule in a gas of temperature,  $T_K$  (temperature expressed in Kelvins), is given by

$$\langle E \rangle = (3/2) kT_K = (3/2) \cdot 1.38 \cdot 10^{-23} T_K \quad (1.1)$$

This is  $(1/2)kT_K$  for each of the three degrees of freedom of motion, where  $k$  is Boltzmann’s constant.  $kT_K$ , as an energy, is thus  $2/3$  of the average particle energy in the distribution. In fusion plasma physics, we tend to subsume Boltzmann’s constant into the definition of temperature, expressing temperature,  $T$ , directly in SI energy units, Joules, in our equations. On the other hand, we tend to *talk* about temperature in units of eVs,  $T_{eV}$  (temperature expressed in electron Volts).  $T_{eV}$  is the electrical potential,  $\Phi$ , measured in Volts, that is required to accelerate an elementary charge,  $e$ , to the energy  $kT_k$ , or  $2/3$  of the average particle energy. Now we can derive the relationship between  $T_{eV}$  and  $T_K$ :

$$kT_K = eT_{eV} \quad (1.2)$$

$$\frac{T_K}{T_{eV}} = \frac{e}{k} = \frac{1.60 \cdot 10^{-19}}{1.38 \cdot 10^{-23}} = 11,600 \quad (1.3)$$

It is instructive to survey some energies and temperatures, and associated speeds, we will be studying.

- Birth energy of neutrons from the  ${}^2\text{H} + {}^3\text{H}$  (deuterium + tritium) reaction: 14.1 MeV,  $v_n = 5.19 \cdot 10^7$  m/s.
- Average birth energy of neutrons from thermal fission of  ${}^{238}\text{U}$ : 2 MeV,  $v_n = 1.96 \cdot 10^7$  m/s.
- Typical temperature of a fusion plasma:  $T_{eV} = 10$  keV,  $T_K = 116\text{M}^\circ$  K. Deuteron, triton, and electron speeds:  $v_d = 9.78 \cdot 10^5$  m/s,  $v_t = 7.98 \cdot 10^5$  m/s,  $v_e = 5.85 \cdot 10^7$  at  $E = 10$  keV.
- Room temperature:  $T_K = 293^\circ$  K,  $T_{eV} = 0.0253$  eV.  $v_n = 2200$  m/s at  $E_n = 0.0253$  eV.

Now we are prepared to consider how to sustain a fission reaction in uranium. First let us note that the number of protons in a nucleus is its atomic number, denoted by “ $Z$ .” This defines its electronic configuration, and so its chemistry. Thus  $Z$  indicates the chemical element under discussion. The total number of nucleons in a given nucleus is its atomic mass, denoted “ $A$ , and for our purposes we take it to have integer value. Two nuclei with the same  $Z$ , but different  $A$ , are called isotopes of one another. These can have very different nuclear properties, such as radioactivity or ability to undergo fission.

By definition a uranium nucleus contains 92 protons. The two predominant isotopes found in nature are  $^{238}\text{U}$  and  $^{235}\text{U}$ , which have atomic abundances of 99.27% and 0.710% respectively. (There is also a tiny fraction of  $^{234}\text{U}$ .) A nucleus of  $^{238}\text{U}$  contains 146 neutrons, while a nucleus of  $^{235}\text{U}$  contains, evidently, 143. As we will see in Chapter 2,  $^{235}\text{U}$  fissions when struck by neutrons of any energy, but with especially high probability when struck by thermal or near-thermal neutrons.  $^{238}\text{U}$ , on the other hand, only fissions with significant probability when struck by neutrons above about 1 MeV, and then the reaction probability is at most only about 40% of that of  $^{235}\text{U}$ . The good news is that when either of them fissions, while they consume a neutron, they produce, on average, 2 – 3 neutrons.

This could also be considered the bad news. When neutron emission during fission was discovered in 1939, soon after fission itself was discovered, many physicists deduced immediately that an explosive chain reaction, on an energy scale  $\sim 10^6$  times greater than that of chemical explosions, might be possible. Nuclear fission research results were no longer published in physics journals, but not before the critical measurement of neutron production was public.

**Question:** What effects, both positive and negative, could this silence have had on the Axis powers’ motivation and ability to develop a nuclear weapon? On balance, was it a good idea?

To get a first look at how much the neutron population in a fission reactor changes from one generation of neutrons to the next, consider neutron balance in a highly simplified situation. Imagine that there are neutrons present at only one specified energy in a large mass of pure uranium, containing a specified percentage of  $^{235}\text{U}$ . In this situation the fraction of this first generation of neutrons that drive fission, rather than become absorbed without fission, is determined by the underlying nuclear physics. A fission event driven by a room-temperature (“thermalized”) neutron in uranium provides a gain of 2.44:1, on average 2.44 neutrons out from a fission event

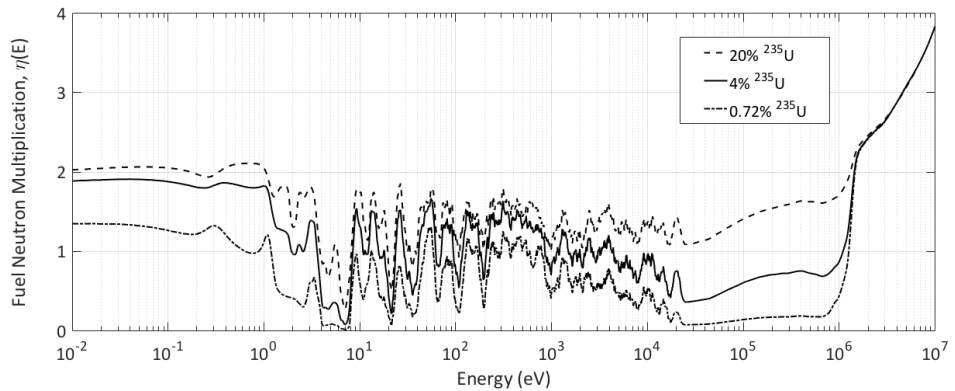


Figure 1.3 Fuel gain in number of neutrons from one generation to the next, at fixed neutron energy. Smoothed to average over resonances in mid-energy range.

per neutron in, to drive that event. (In general a little higher for energetic neutrons than for thermal ones, and a somewhat higher for plutonium than for uranium. See table 2.2.) If the fraction of fission events divided by all absorption events, fission plus absorption without fission, is greater than  $\sim 40\%$ , then the neutron gain at the specified energy,  $\eta(E)$ , is greater than unity, and sustained fission may be possible. Not surprisingly, the neutron gain will always be higher with uranium more enriched in  $^{235}\text{U}$ , as can be seen in figure 1.3.

To put this figure into perspective, we need to recognize that in the real world you cannot pin neutrons at a given energy as suggested by plotting  $\eta(E)$ . Furthermore, there will always be other losses from the neutron population than fission-less absorption by uranium nuclei. The coolant that is needed in a real power plant absorbs neutrons, as does the fuel cladding and structure. We will discuss these in Chapters 2 and 3. Furthermore, some neutrons escape from the reactor, as we will discuss in Chapter 4, so  $\eta(E) > 1$  represents a *bare minimum* requirement.

In general it is key, in both thermal and fast reactors, that the number of fissions stay very precisely constant from one generation to the next. This is a topic of much of the discussion in Chapters 3, 4 and 5.

**Question:** If each succeeding generation makes 1% more neutrons than the one before it, how many generations does it take to double the power being produced? And if 2% more are produced? 7%? In finance, this pattern is called the rule of 70. See exercise 1.4 to explore it some more.

Self-sustainment in the range of 100 keV requires fuel enriched to about

20%. This is the energy range of “fast reactors”, FRs, so named because they utilize energetic and therefore fast neutrons. These reactors need coolant that neither absorbs fast neutrons significantly nor slows them down too quickly into the range where gain is too low. In this intermediate energy region, neutrons are eaten up by absorbing resonances of  $^{238}\text{U}$ , a process we will study in chapters 2 and 3. Liquid sodium is used in the world’s two operational commercial-scale fast reactors, in Russia, but other coolants such as lead, lead-bismuth and helium gas, which is basically transparent to neutrons, are being considered, as discussed in Chapter 8. One potential advantage of fast reactors, discussed in Chapter 6, is that they can in principle produce more fission fuel than they consume, because most of the absorption of neutrons can be by  $^{238}\text{U}$ . In so-called “breeder” reactors as much as  $\sim 50\%$  more  $^{238}\text{U}$  can be converted to Pu than  $^{235}\text{U} + \text{Pu}$  is burned. By reprocessing the fuel and extracting the fissile material as well as the unburned  $^{238}\text{U}$ , most of the natural uranium dug from the earth can in principle be burned, stretching by a factor  $\sim 90$  the amount of energy that can be extracted from a given amount of natural uranium. The reprocessing step, however, is expensive and messy, and presents a serious nuclear proliferation risk, as described in Chapter 7.

The other energy range that is practicable is the thermal range. In this case while neutrons are born in the MeV range, they are very rapidly slowed down past the resonances to 5 eV and below, in order to minimize the chance of being absorbed in the resonance region. Ultimately they drive fission in the thermal energy region, where  $^{235}\text{U}$  is very reactive. Figure 1.4 illustrates a chain reaction in a thermal reactor. As with fast reactors (FRs) Pu is produced even in thermal reactors, but considerably less than in breeders. In all cases the number of neutrons in each generation must precisely equal the number in the preceding generation.

As discussed in Chapter 3, the best materials for causing rapid slowing-down, or “moderation,” of neutrons, with very little absorption of the slowed-down neutrons, are pure graphite and heavy water,  $\text{D}_2\text{O}$ . ( $\text{D}$  represents deuterium,  $^2\text{H}$ , the isotope of hydrogen with one proton and one neutron.) In fact graphite and heavy-water systems are so efficient in their neutron economy that reactors that use them can be fueled with natural uranium. They can also be prodigious producers of weapon-grade plutonium as we will discuss in Chapter 7. The great majority of the world’s fission reactors are “light-water reactors,” LWRs. In this case regular water,  $\text{H}_2\text{O}$ , is used both to moderate the neutrons and to carry away the nuclear heat, a great simplification. LWRs, however, do require uranium to be enriched, because while the protons in  $\text{H}_2\text{O}$  are excellent at slowing down neutrons, even better than

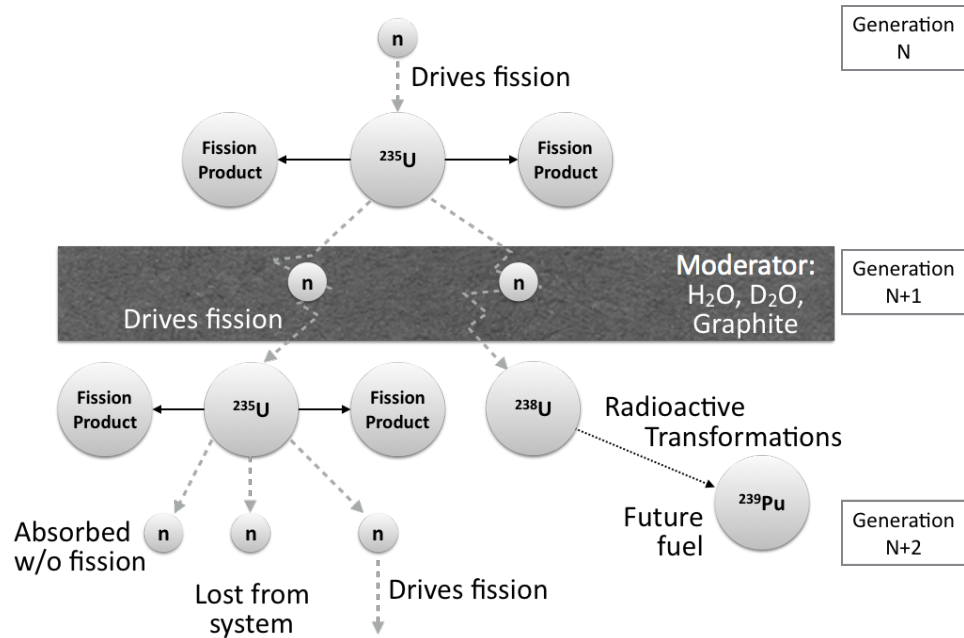


Figure 1.4 Fission, moderation and Pu production in a thermal reactor. Generations of neutrons are indicated.

the deuterons in  $\text{D}_2\text{O}$  and C in graphite, they compete with the uranium fuel in absorbing thermalized neutrons. Because of this absorption, there is less production of Pu in LWRs, but it is still significant. Over time as it builds up and fissions it adds to the total energy that is extracted from the fuel. In fact, by the time fuel is unloaded from an LWR, about as much Pu has burned as  $^{235}\text{U}$  is left unburned,  $\sim 1\%$  out of  $\sim 4\% \text{ }^{235}\text{U}$ .

There are two kinds of LWRs, pressurized water reactors, PWRs, shown in figure 1.5, and boiling water reactors, BWRs. The majority of operating fission reactors, and most new designs, are PWRs (see table 1.1), in which the cooling water that passes through the reactor core is highly pressurized, and so does not boil. A secondary cooling loop, in which the water is allowed to boil and form steam, provides extra isolation from the reactor, but adds complexity and requires a larger containment vessel. In a boiling-water reactor the water boils in the reactor core itself, and the resulting steam is transported directly to the turbines that generate electricity. Both of these reactor designs deliver net electrical efficiency in the range of 33%, so about 3000 MW of thermal power, denoted 3000 MW(th), is required to generate 1000 MW of electricity, denoted 1000 MW(e) = 1 GW(e). Generally 5 – 10% of the gross electricity generated is required to power the reactor systems

themselves, including the massive water pumps. Unless otherwise noted, net electricity generation is usually reported.

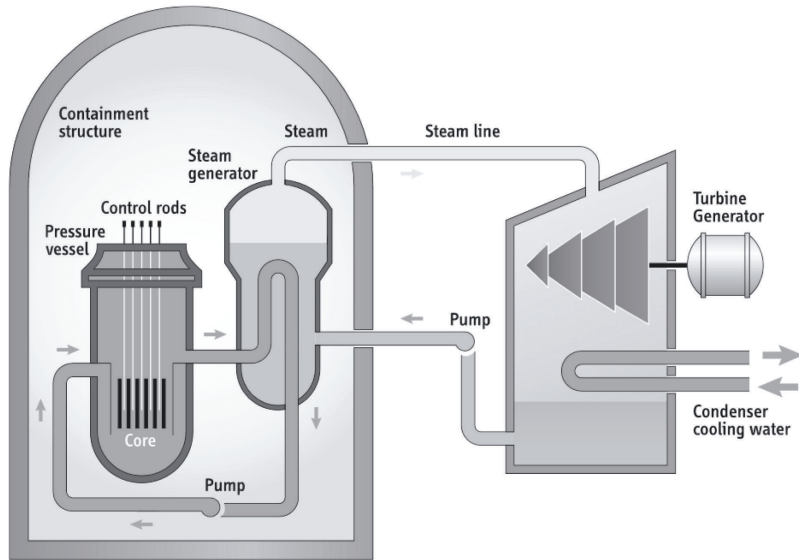


Figure 1.5 Diagram of a pressurized water reactor, PWR.

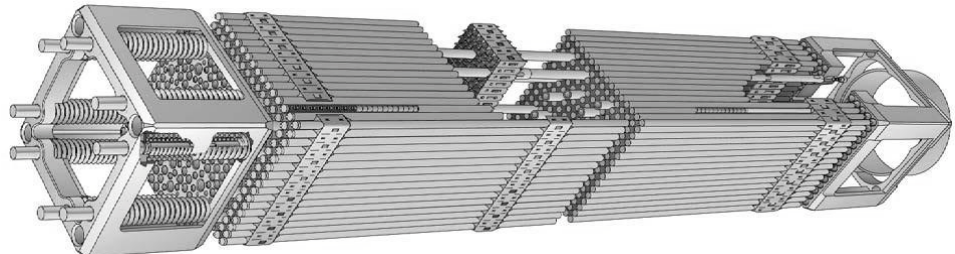


Figure 1.6 PWR fuel assembly (set sideways).

The neutron-absorbing control rods that are used to regulate the fission reaction are inserted from the top in PWRs (and from the bottom in BWRs). These rods, which can be of various shapes, penetrate into the core region occupied by the reacting fuel, as shown in figure 1.5. Figure 1.6 shows a PWR fuel assembly. Thin fuel pins, or rods,  $\sim 1$  cm in diameter and  $\sim 4$  m in length, hold ceramic pellets of  $\text{UO}_2$  within zirconium-alloy cladding that absorbs very few neutrons. The fuel pins are bound together into fuel

Table 1.1 *Distribution of reactor types.*  
*Source: IAEA Technology Review, 2015*

%		Type of Reactor
63.2	PWR	Pressurized (Light) Water Reactor
16.3	BWR	Boiling (Light) Water Reactor
11.2	PHWR	Pressurized Heavy Water Reactor
11.2	LWGR	Light Water (Cooled) Graphite (Moderated) Reactor
3.4	GCR	Gas Cooled (Graphite Moderated) Reactor
0.5	FR	(Liquid Metal) Fast Reactor

assemblies of perhaps 250 pins. Water flows freely between the individual fuel pins and fuel assemblies, both moderating (rapidly slowing down) the MeV neutrons that easily escape from the thin fuel pins and also carrying off the heat emanating from the fuel.

The distribution nuclear power reactors types as of 2014 is shown in table 1.1.

**Question:** What are some reasons why water is such a commonly used coolant in different technologies, from the little heat pipes in your laptop, to automobiles, to coal-fired power plants?

### *1.1.2 Safety, waste, nuclear proliferation*

There are three technical issues that have dogged nuclear fission power throughout its development. The first is safety, discussed in Chapter 5, which is headlined by the major accidents at Chernobyl in 1986 and at Fukushima in 2011. These were both “Level 7” accidents, the highest level on the International Nuclear and Radiological Event Scale. Each of these resulted in the dispersal of large amounts of radioactivity and the long-term evacuation of large areas of land. The second is waste, discussed in Chapter 6, which is headlined in the U.S. by the failure to open a geological repository for long-lived civilian nuclear waste despite 60 years of effort. The third is the link between the technologies of peaceful nuclear energy and nuclear weapons, discussed in Chapter 7, which has been headlined recently by the difficult agreement reached between China, France, Germany, Great Britain, Russia, the U.S. and Iran to verifiably limit Iran’s nuclear program to energy appli-

cations, as well as by the international failure to prevent North Korea from developing thermonuclear weapons of comparable yield to those in the U.S. stockpile.

### *Safety*

The proximate cause of the Chernobyl accident was “prompt criticality.” Each thermal nuclear fission reaction, as we discussed, emits about 2.44 neutrons. It is crucial to the controllability of the fission chain reaction that a small fraction,  $\beta \sim 0.65\%$  for uranium, of these neutrons are emitted with an average delay of 12.9 seconds, again for uranium. The delayed neutrons are emitted in the decay chains of the fission products, which naturally begin rich in neutrons. In Chapter 5 we will see that a nuclear reactor is controllable only for very small values of positive reactivity  $\rho \equiv (k - 1)/k$ , where  $k$  is the gain from generation to generation of the neutron population. The ratio  $\rho/\beta$  is so important to nuclear engineers that it is measured in dollars (\$), as shown in figure 1.7. If  $\rho/\beta > \$1.00$  a reactor has gone into “prompt criticality,” meaning that its power production can take off without waiting for any delayed neutrons, running away on the “prompt” neutrons alone, and so extremely rapidly. The reactor time,  $T$ , represents the characteristic time over which the power changes. In the course of disassembling itself, Chernobyl reactor #4 reached at least 10x its normal operating power. We will discuss the root causes that allowed this Level 7 “criticality accident” to occur, but most analysts believe that prompt criticality can be reliably avoided in light water reactors. Water-cooled graphite-moderated reactors like Chernobyl, and fast reactors, however, may be more susceptible to this mode of failure.

A failure mode that light water reactors still face, however, is associated with the decay heat from fission. About 94% of the power from uranium fission is emitted promptly; radioactive decay of the fission products emits the remaining 6%. As shown in figure 1.8, the power released by decay heat drops to about 2% by 15 minutes after all fission reactions have stopped, but falls quite slowly thereafter. Nothing can prevent this heat from being emitted. If it is not removed, in about five hours all of the water in the reactor vessel will have boiled away, and the overheated fuel assemblies that make up the core of the reactor will begin to melt and slump down in the reactor vessel. This happened in 1979 at the Three Mile Island Unit #2 accident in the U.S., and in the three reactors at the Fukushima Daichi plant in Japan that lost core cooling in 2011, leading to breaches of the reactor containment structures and widespread contamination. There was also a concern that the fuel cooling pool located high up in Unit #4 was losing water. If it had

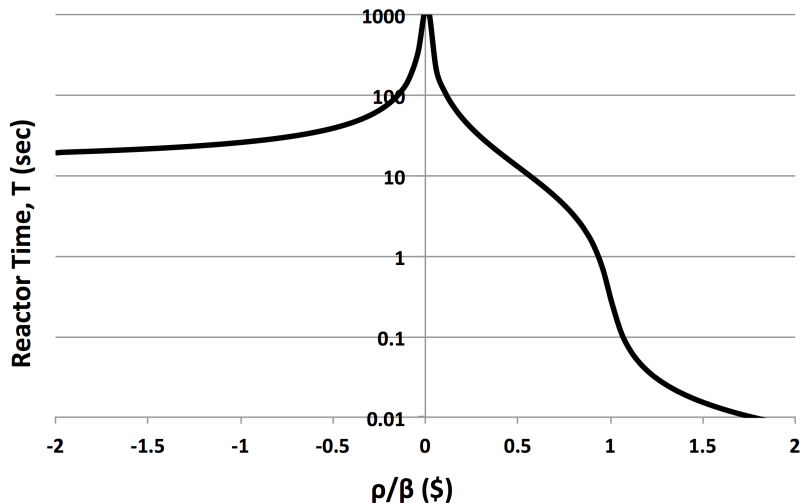


Figure 1.7 Characteristic reactor response time vs. reactivity divided by delayed neutron fraction.

drained and overheated, it could have caught fire and caused much greater radioactive contamination. Again we will discuss the root causes that allowed the accident to occur. We will also look at actions taken since the Fukushima accident to reduce risks. Minimizing the possibility of a core meltdown due to decay heat, and minimizing the consequences, are a major focus of new PWR fission reactor designs. In general fast reactors are believed to be more difficult to protect against core meltdown and its consequences.

**Questions:** What was your response to the Fukushima accident? What did you expect to be the near-term consequences for nuclear power? What is your impression of what actually happened?

Before we leave the topic of safety, we should consider the possibility of terrorist attacks, by insiders, by armed outsiders, or by commercial aircraft as in the 2001 attacks in the U.S. Each of these is a concern. In 2014 an insider sabotaged a turbine for generating electricity at the Doel-4 nuclear reactor in Belgium, by draining its oil and causing it to overheat. The reactor shut down without incident, but the cost of repair was over 100 M€. Damage to other targets might have been significantly more consequential. A sufficient force of armed outsiders could, in principle, use a missile or explosive charge to drain the water from a fuel cooling pool. This could lead to a fuel fire and major wide-area contamination. Studies of the effects of commercial airliner impacts on nuclear reactors and fuel cooling pools are

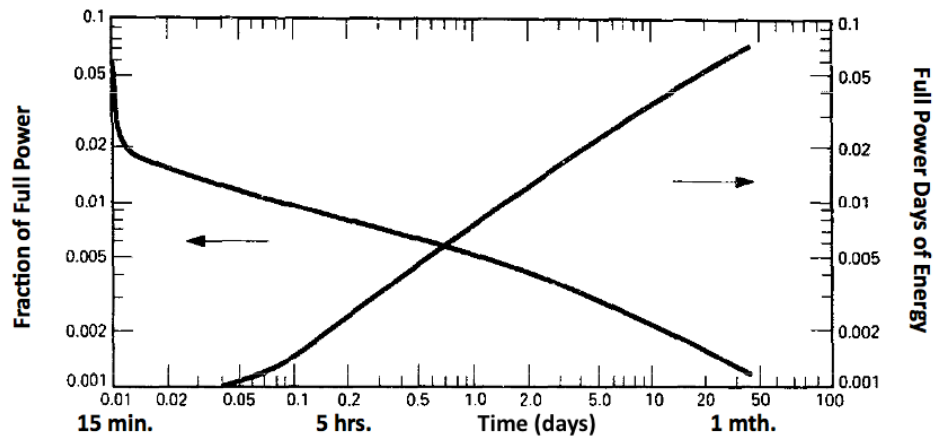


Figure 1.8 Decay power, as fraction of pre-shut-down total thermal power, on left axis. Decay energy (time-integral of decay power after shut-down) on right axis vs. time in days.

classified. Remarkably, one of the tapes recovered in Kandahar, Afghanistan after the 2001 attacks showed Osama Bin Laden explaining that Al Qaeda decided not to attack nuclear reactors with commercial aircraft, because it “could get out of hand.”

### *Waste*

The second tough problem faced by nuclear fission is the disposal of long-lived, high-level nuclear waste, which requires geological storage. The mass and volume of high-level nuclear waste is small compared with those of waste from, for example, coal-fired power plants, but it is lethally radioactive for a very long period of time. Human society has never had to deal with a problem of this nature, and we have not developed a consensus on how to balance risks to our current citizens vs. risks to those living 10,000 or even 100,000 years from now. On the one hand, we are unable to justify burdening many future generations with the risks associated with waste created during the next few generations. On the other hand, at the rate of scientific progress we see today, it seems likely that we will have a cure for radiation-induced cancers and/or much more sophisticated ways of dealing with environmental contaminants 10,000 years from now. Another societally difficult balancing act, and in practice the most *politically* difficult one, is tied to the question, “Why should the citizens of one region be required to live in the vicinity of the nuclear waste produced by a whole nation?” As we will discuss in Chapter 6, there is some progress being made, particularly in

Finland and Sweden, by making the site selection process more transparent, and by providing rewards to communities offering to host waste facilities.



Figure 1.9 Dry cask storage facility near a nuclear power plant.

Currently, spent fuel is first stored in cooling pools, for a period of at least five years. As more waste is produced these pools are being modified to accommodate more spent fuel assemblies, and as we noted these pools may be vulnerable to attack. Eventually the spent fuel is transferred to dry storage casks (figure 1.9). Each cask can handle about 10 t of spent fuel, which comes to about two casks per reactor-year. These are now building up at reactor sites, as there is no agreement on what to do with them. They are stable, resistant to forceful attack, and believed to be safe from theft – in part because if they are opened the radiation levels would be very high. They are generally licensed for 50 years. However no long-term geological storage facility has been licensed anywhere in the world to isolate commercial nuclear waste from the environment, so the ultimate fate of this waste is uncertain.

In principle fast reactors, FRs, can reduce the burden of nuclear wastes. Most, but not all, of the longest-lived waste products are actually not the products of fission, but rather nuclei that have absorbed neutrons and transmuted to plutonium ( $Z = 94$ ) and other members of the actinide family, neptunium ( $Z = 93$ ), americium ( $Z = 95$ ) and curium ( $Z = 96$ ). In principle

these can be fissioned in a fast reactor. If fuel is removed from a thermal or fast reactor, it can be reprocessed to extract the actinides, including  $^{238}\text{U}$ , for later burning in an FR. This can increase the utilization of the nuclear energy in the original uranium, which is normally less than 1%, since it is most of the  $^{235}\text{U}$  and some of the small fraction of  $^{238}\text{U}$  transmuted to Pu that is fissioned in a thermal reactor. The increased utilization can, in principle, be a factor  $\sim 90$ . (Actually reprocessed Pu can be fissioned for one cycle even in a thermal reactor, but this only increases the energy utilization by  $\sim 1/6$ .) FR's have proven difficult to build, reprocessing has proven to be very expensive, and it is not clear that the advantages of removing actinides from the waste stream are as high as originally expected. Furthermore, the price of uranium has remained low, so there is little economic incentive now to extract energy from it more efficiently. A central problem with reprocessing is that the Pu in the fuel that is produced is easily chemically separated, and is usable, if not ideal, for nuclear weapons.

**Questions:** Why is element 94 called plutonium? (Hints: It is not named for the Roman god of the underworld. What is element 93 called?)

#### *Nuclear proliferation*

A final, but very important, problem that needs to be considered is nuclear proliferation. Nuclear fission was discovered in 1938, and its first application was in the form of nuclear weapons in 1945. Nuclear weapons run on fast, prompt neutrons, and at very high fractions of  $^{235}\text{U}$  and/or  $^{239}\text{Pu}$ , in order to maximize the increase of the fission rate from generation to generation, resulting in a powerful explosion. Processes for the enrichment of uranium in  $^{235}\text{U}$  and the production of nearly pure  $^{239}\text{Pu}$  in nuclear reactors were developed to provide the immensely powerful explosive materials for nuclear weapons. Unfortunately, much of the technology that is used for nuclear energy production is “dual-use,” applicable both for civilian and military purposes. Most troubling, the scale of facilities for uranium enrichment or extraction of plutonium from spent fuel needed for energy production is much greater than that needed to produce nuclear weapons. For example we will see in Chapter 7 that a commercial enrichment plant sized to provide the fuel needs for ten LWRs, if redirected to making weapons material, can produce enough highly enriched uranium for 70 weapons per month. The trick for doing this so quickly is to start from reactor fuel. We will show, surprisingly, that 4% enriched uranium is  $2/3$  of the way to 90%, in terms of the required enrichment work.

This scale difference introduces three problems. First, as just mentioned, a



Figure 1.10 Centrifuge hall in commercial-scale enrichment plant. Source: URENCO

large enrichment or reprocessing facility, even if declared and safeguarded by the IAEA, can be rapidly redirected to military application. This is called “breakout.” Second, a clandestine facility that produces enough material for a few weapons per year can be much smaller than a commercial facility, and can be difficult to detect. A hall containing centrifuges for uranium enrichment only 1600 m<sup>2</sup> in area, and consuming only 300 kW of power, can be disguised as a commercial facility while producing enough highly-enriched uranium for one weapon per year. This option of clandestine nuclear materials production has recently been dubbed, “sneakout.” Finally, in a “diversion” scenario, a small fraction of the production of a declared and safeguarded facility is covertly diverted, providing material for bomb production. In all of these cases, breakout, sneakout, and diversion, the actions can be taken by a nation-state, and in the latter two cases one has to consider non-state actors, perhaps working in collusion with insiders.

If some of the safeguards innovations in the recent Iran Agreement (the Joint Comprehensive Plan of Action, JCPOA) can be applied more broadly, it will help with the problem of nuclear proliferation based on uranium enrichment. However the agreement itself, the IAEA Board of Governors, and UN Security Council Resolution 2231 all take pains to point out that the JCPOA does not set any precedents. Nonetheless, new unattended real-

time monitoring tools currently under development should provide assurance against misuse of declared facilities, and increased use of IAEA inspection authorities can help against “sneakout.” A complementary approach is to encourage multi-national enrichment facilities, where the multiple parties will provide brakes on each other. On the other hand it is not clear what technical or organizational mechanism can be used to assure that owners of reactors that burn Pu in their fuel do not use this Pu for weapons, so non-proliferation concerns weigh heavily against reprocessing.

It will remain a major challenge to avoid the proliferation of nuclear weapons capability to many more countries if nuclear energy spreads and grows significantly. Countries actively engaged with the International Atomic Energy Association (IAEA) in 2017 in planning for new nuclear power programs include Bangladesh, Belarus, Egypt, United Arab Emirates, and Viet Nam. The IAEA also reported that Argentina, Azerbaijan, Belarus, Belgium, Bolivia, Brazil, Ethiopia, France, Ghana, India, Kenya, Kuwait, Lebanon, Malaysia, Mongolia, Myanmar, Netherlands, Nigeria, Philippines, Russia, Senegal, South Africa, South Korea, Saudi Arabia, Sudan, Tajikstan, Thailand, Tanzania, Thailand, Tunisia, United States, and Viet Nam are building or considering building new research reactors. A research reactor was commissioned in Jordan in 2017.

### ***1.1.3 Past may be prologue, but what is it telling us?***

The history of nuclear fission power is unusual. Figure 1.11 shows that electricity production rose very rapidly from 1971 to 1990, increasing from 2% to 16% of world electrical power production. After 1990, however, growth slowed, and its fraction peaked at 18% of world production in 1996. Some of the slowing may have been driven by the Chernobyl accident in 1986, but a larger factor was likely rising costs and longer construction times. Since 1990 a large part of the growth in nuclear electrical energy production has come from better operation of the existing power plants. For example, in the U.S. the nuclear power plant capacity factor (yearly average power production divided by name-plate rating) has risen from 65% to 90% since 1990. After the accident at Fukushima in 2011, absolute world nuclear energy production fell and it now constitutes only 11% of world electricity production. On the other hand, as shown in tables 1.2 and 1.3 some 58 new nuclear power reactors are currently under construction, as compared with the ~408 currently operating. Because older plants will be coming off line, the IAEA projects nuclear electric capacity in 2030 to be between the current level

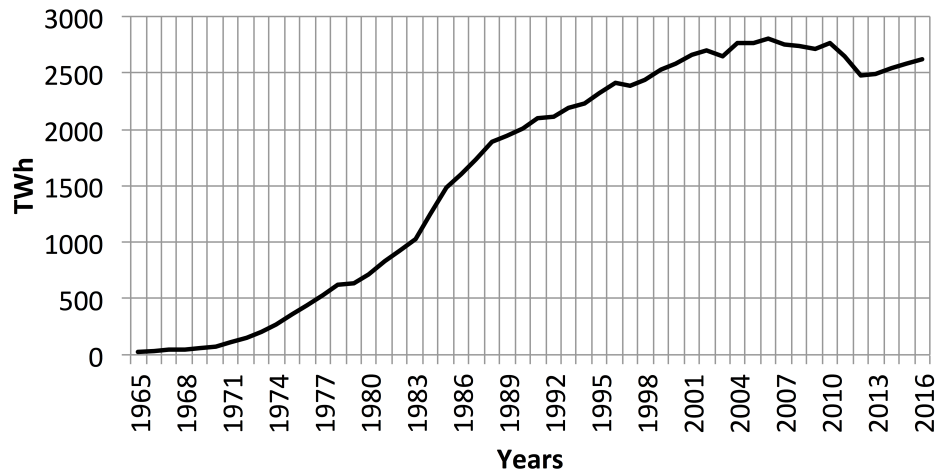


Figure 1.11 Terawatt-hours of nuclear electricity produced per year. 1 GW-yr = 8.77 TWh. Data Source: BP Tools

and 1.5x higher. It projects nuclear electric capacity in 2050 to be between the current level and 2.3x higher.

The factors that drive a nation to construct nuclear power plants are complex. In the U.S. natural gas is so inexpensive that nuclear power cannot compete in unregulated electricity markets, and even some older operating nuclear power plants that are completely paid for are slated to be shut down. In many countries, however, fossil fuels, especially natural gas, are much more expensive than in the U.S., while the labor required to construct nuclear plants is less expensive. Furthermore, in most countries the electric power industry is less strongly driven by market forces, and more by government policies and direct or indirect government investment. In this case society-wide issues like national energy security, including diversity and security of fuel supply, and/or limitation on CO<sub>2</sub> emission, play a stronger role. These factors have driven a significant increase in reactor construction over the last decade, particularly in the Far East, and especially in China, as shown in table 1.2. On the other hand the number of reactors under construction has tapered off recently, as shown in table 1.3.

The United Arab Emirates has contracted with South Korea to build four new LWRs. It has committed not to enrich uranium, nor to reprocess fuel, thereby providing favorable assurances to the international community against nuclear proliferation risks. This is sometimes called the “gold standard.” Another recent innovation is that Russia is offering to Build, Own

Table 1.2 *Reactors under construction as of January 1, 2018.*  
*Source: World Nuclear Association*

Country	Units	Gross MWe
Argentina	1	27
Bangladesh	1	1200
Belarus	2	2388
Brazil	1	1405
China	20	21,546
Finland	1	1720
France	1	1750
India	6	4350
Japan	2	2756
S. Korea	4	5600
Pakistan	2	2322
Russia	7	5904
Slovakia	2	942
United Arab Emirates	4	5600
United States	2	2500
Totals	58	62,710

Table 1.3 *Reactors under construction, by year.*  
*Source: IAEA Technology Review, 2017*

Year	2004	2005	2006	2007	2008	2009	2010
Units	27	26	28	35	45	57	68

Year	2011	2012	2013	2014	2015	2016	2017
Units	65	66	72	70	68	61	58

and Operate new reactors, as well as to provide fresh fuel and take back spent fuel – also mitigating proliferation risks – in exchange for a guaranteed price for electricity generated. This “BOO” model may be an effective

commercial approach in the future, since the capital cost of fission reactors is a major barrier to entry for many nations.

**Question:** What are the advantages and disadvantages, including risks, for the buyer and the seller in a “BOO” deal?

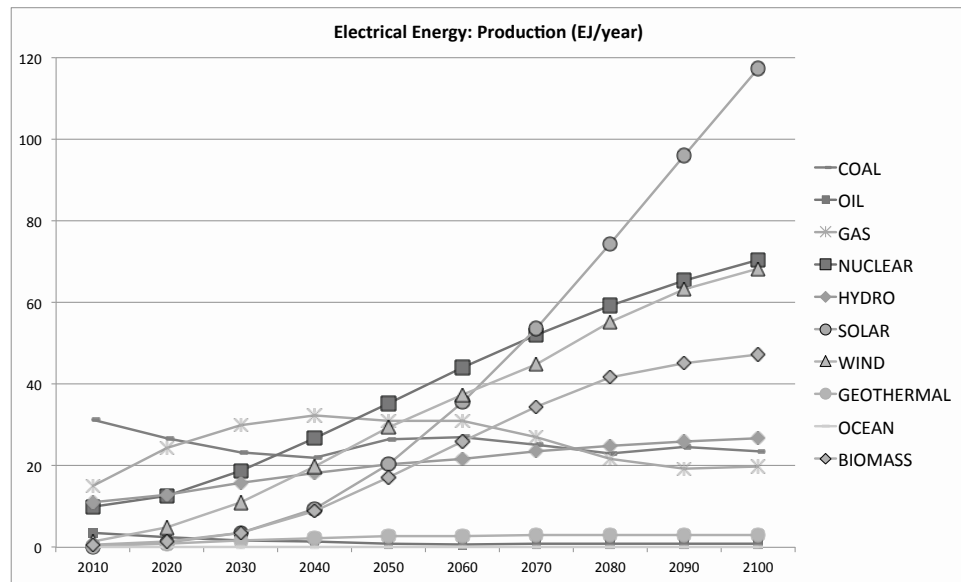


Figure 1.12 Mean electrical power production by technology, Energy Modeling Forum 27 model runs that limit global warming to 2° C in 2100. 1 EJ = 31.7 GWe-yr.

Nuclear power may have an important role in mitigating climate change. The Intergovernmental Panel on Climate Change (IPCC) worked with energy/environment modeling groups to project the pathway to a world where global warming is constrained to no more than 2° C above pre-industrial in the year 2100. Figure 1.12 shows the mean of the results from a set of models, EMF-27, that succeed in constraining global warming to the IPCC target value. Nuclear power is one of the major technologies these models rely upon, and nuclear’s market share increases moderately as its total yearly production rises a factor of seven by 2100. The values projected for 2030 and 2050 are above the high end of those projected by the IAEA, indicating that the models call for a strong enhancement of nuclear power.

The IAEA, in collaboration with the OECD-NEA, publishes estimates of world-wide uranium resources. These estimates have limitations, and certainly more uranium will be available at higher prices than considered in these reports, as discussed in Chapter 6. On the other hand, by 2055 the

nuclear energy scenario in figure 1.12 burns and commits to burn 100% of reported world-wide known and projected uranium resources, based on the sum of the IAEA/OECD-NEA categories of “Reasonably Assured,” “Inferred,” “Prognosticated,” and “Speculative” resources. Since uranium reserves are very unevenly distributed relative to human populations (for example there is a much greater uranium resource in Australia than in all of China), some nations will have more reason to be concerned about domestic reserves than others. These include China, India, Japan, South Korea, and countries in the Middle East. Concerns about national energy security may lead to the adoption of fast reactors later in the century, allowing more efficient use of uranium resources and some mitigation of the problems of waste storage, but introducing new safety risks and a substantially increased risk of nuclear proliferation.

#### 1.1.4 Prospects

The future of nuclear fission energy is uncertain. After the Fukushima accident Germany decided to phase out nuclear power, and only four of Japan’s 48 in-principle operable reactors are now in operation. On the other hand, after some review, China is continuing to build 20 new reactors and there appears to be growing interest in nuclear power in many areas of the world, as a form of secure domestic energy with low carbon emissions. In the U.S. and Europe the cost of nuclear power is a deterrent to its application. Progress is needed on safety, waste disposal, and the limitation of nuclear proliferation to reduce the risks associated with nuclear fission. In Chapter 8 we will examine designs of fission reactors that attempt to make progress against some or all of these goals, particularly “passively” safe LWRs, molten-salt-cooled reactors that use thorium to breed  $^{233}\text{U}$  for fuel, and fast reactors that maximize the efficiency of breeding Pu without employing reprocessing.

**Question:** What do you now think is the future of fission power, considering both the pro and con arguments? Leave mental room for your opinion to change as you learn more.

## 1.2 Fusion

### 1.2.1 Self-sustaining fusion reactions

For fusion, energy is extracted from the fusion of two light nuclei to form a heavier one. At distances large compared with a nuclear radius, even low-Z nuclei are kept apart by their electrostatic repulsion. If they approach closely

enough, however, then the strong – but short-range – nuclear force dominates and the nuclei can be attracted together and fuse. There are multiple possible fusion reactions, but the easiest to access for energy applications is



Here D represents deuterium, the isotope of hydrogen containing one proton and one neutron,  $^2\text{H}$ . The nucleus of a deuterium atom is called a deuteron. T represents tritium, the isotope of hydrogen that contains one proton and two neutrons,  $^3\text{H}$ ; its nucleus is called a triton. The advantage of fusing singly charged nuclei is that their electrostatic repulsion is minimized, so the kinetic energy required to overcome this repulsion is minimized as well. As can be seen in figure 1.1, the helium nucleus, or  $\alpha$  particle, has a particularly low potential energy, making it attractive as a product. Starting from the isotopes of hydrogen, the only choice that allows an  $\alpha$  particle as a product is  $D + T$ .

Of the 17.6 MeV from the reaction,  $20\% = 3.5 \text{ MeV}$  goes to the  $\alpha$  particle and  $80\% = 14.1 \text{ MeV}$  goes to the neutron. This follows from momentum conservation. Ignoring the momentum of the incoming thermal D and T, the outgoing energetic particles must be oppositely directed, with equal  $mv$ , giving the neutron four times the speed of the  $\alpha$  particle. The energy of the neutron then,  $(1/2)mv^2/2 = (1/2)m\vec{v} \cdot \vec{v}$ , is four times higher than the energy of the  $\alpha$  particle, since  $mv$  is equal between the two.

To overcome the electrostatic repulsion between even singly-charged nuclei requires a great deal of kinetic energy. For a useful rate of reaction, this must be some 10's of keV. Such energies are easily achieved with simple electrostatic particle accelerators, but the scattering rate is much higher than the fusion rate, so we cannot simply fire beams of deuterons and tritons at each other. They would just scatter all over. What we need is a confined gas of these ions at a temperature in the range of 10 keV (116M K), so they are constantly colliding with each other at energies in the range of 10's of keV.

**Question:** Suppose two deuterons, each with energy equal to the mean particle energy in a 10 keV plasma, collide head on. What is the energy of one of the deuterons in the frame of reference of the other?

Any cloud containing a useful density of ions would immediately blow itself apart from electrostatic repulsion, so we also need to include electrons at very, very nearly the same density. The electrons must also not be too much cooler than the ions, or the ions will lose too much energy as they thermalize collisionally with the electrons. The result is that we need a  $\sim 10$

keV ion-electron gas, a high temperature plasma. The ionization potential of the hydrogen atom is 13.6 eV, so collisions between the free electrons in this plasma and the bound electrons in any hydrogenic atoms present will rapidly drive the system to full ionization.

Evidently, we need to heat this plasma to high temperature in the first place and then keep it hot to produce energy. We can start with externally supplied heating, but we would like the reaction largely to maintain itself, like logs in a fire, where all that is required is to throw new logs in as the old ones burn, and occasionally remove the ash. Neutrons produced by fusion immediately escape a magnetically-confined plasma without interacting, so are useless for plasma heating. Fortunately, however, the  $\alpha$  particles from the DT reaction are born at 3.5 MeV and are themselves positively charged. So if our scheme for holding onto a DT plasma with charged particles at 10's of keV also holds onto MeV-energy charged  $\alpha$  particles, then we can use those  $\alpha$  particles to provide most or all of the power to maintain the temperature of the plasma, rather like the flame from one burning log lighting the next. If the heat is well enough contained, and the plasma is fueled steadily, and the He ash is removed, the plasma will maintain its high temperature and steady burn rate. To achieve all of this, we need to understand the physics of plasmas. The goal is to determine how to contain a hot, dense plasma that will make commercial amounts of fusion power, and at the same time leak heat at a slow enough rate, while remove helium at a fast enough rate, that it can sustain its own temperature largely by fusion, without too much power input from the outside. The requirements for this are addressed quantitatively in chapter 9.

The most successful configuration to date at confining hot fusion plasma is called a “tokamak,” a Russian neologism for “toroidal chamber with magnetic coils.” In a uniform magnetic field, charged particles spiral along the field, as shown in figure 1.13. The circular motion across  $\vec{B}$  arises from the  $q\vec{v} \times \vec{B}$  Lorentz force. Since there is no force along  $\vec{B}$ , the velocity in that direction is constant, and the resulting total motion traces out a spiral along the magnetic field.

If the magnetic field lines are then closed into a toroidal (doughnut-shaped) configuration, the particles largely spiral along the field lines, which face in the toroidal direction, the long way around the doughnut. However, as we will see in chapter 10, a small vertical drift motion is induced by the curvature and gradient of a toroidal magnetic field. A twist, literally, needs to be added to the field as shown in figure 1.14, in order to confine the particle trajectories. With this twist, as a particle moves along a field line the vertical upward drift when it is at the top of the tokamak, taking

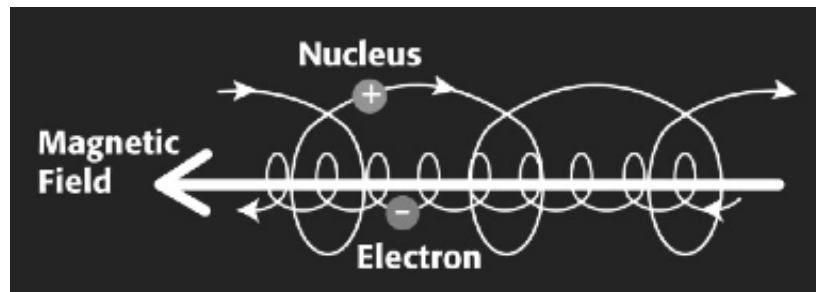


Figure 1.13 Charged particles spiraling along a uniform magnetic field.

the particle outward from the center of the plasma, is compensated by the vertical upward and inward drift when it is at the bottom. In a tokamak, the magnetic field that induces this twist is generated by an electrical current flowing in the plasma itself. This current makes a magnetic field that faces in the poloidal direction, the short way around the doughnut, and the sum of this field with the toroidal field from external magnets provides the overall twist. The poloidal field is much weaker than the toroidal magnetic field, so in tokamaks a field line makes more than one toroidal transit, or circumnavigation, per poloidal transit. Nonetheless, the result is remarkably well confined particle motion, and a plasma configuration that has already produced megawatts of fusion power, for pulses in the range of 0.5 to 5 seconds in laboratory experiments, but not yet self-sustained.

Tritium decays with a half-life of 12.3 years, meaning that one-half of any given quantity of tritium decays away after this time period, or about 5% decays away per year. Tritium does not exist in significant quantities in nature, and must be produced for fusion energy based on the DT reaction. The most efficient reaction for producing tritium is:



Tritium is also produced when neutrons interact with the deuterium in heavy-water reactors, by radiative capture with the emission of a gamma ray, an energetic photon.



The  $n + {}^6Li$  and  $n + D$  reactions can be used to produce tritium in fission reactors in order to start up a limited number of DT fusion systems, but the amount of tritium that will be burned in a fusion power system,  $\sim 400\text{g/day}$ , means that fission reactors are not a practical source for steady supply. The fusion neutrons themselves must be captured by  ${}^6Li$  to provide

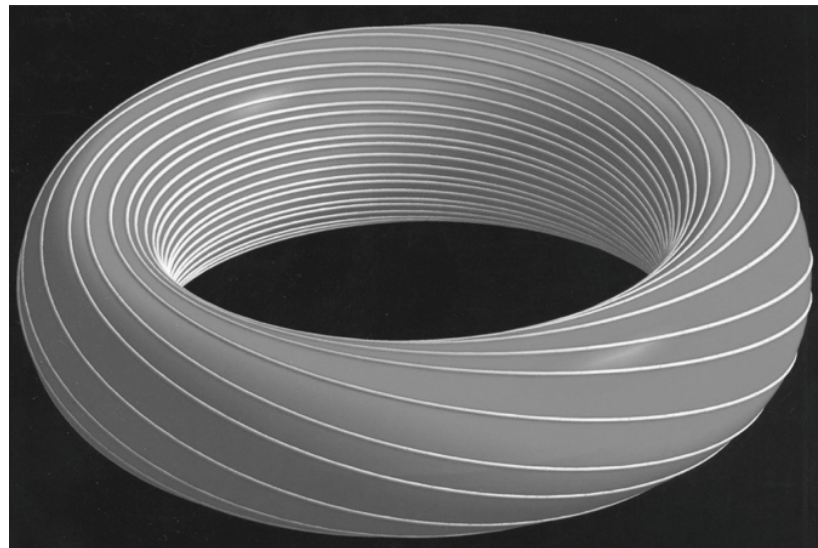


Figure 1.14 Twisted toroidal magnetic field to confine charged particles.  
Source: Jeff Freidberg's book

a steady supply of fuel. Since some neutrons will be absorbed by structural materials and coolant, it is necessary to include elements such as Pb or Be that function as neutron multipliers. When these nuclei are struck by an energetic neutron, two neutrons frequently emerge. Thus the first wall and blanket that surround a fusion plasma must not only capture the heat from the  $\alpha$  particles and neutrons, but also multiply the neutrons and breed the tritium needed to keep the reaction going, as discussed in chapter 16. In sum, the  $\alpha$  particles maintain the temperature of the plasma and the neutrons maintain the fuel supply.

Figure 1.15 illustrates a concept for a pilot fusion power plant based on the tokamak configuration. A vertically-elongated, toroidal plasma is held in the center of chamber. (We will see in chapter 12 that vertical elongation improves a tokamak's ability to contain high pressure.) The plasma is largely surrounded by a first wall and blanket. Some of the heat from the plasma that originated from the fusion  $\alpha$ 's is captured at the first wall, but the majority is channeled into the divertor region, a topic of much modern research, as discussed in chapter 15. It is from this region that the He ash is pumped away as well. The neutrons are captured in the blanket for their heat and to breed tritium. The vacuum vessel separates the fusion fuel from contamination by the atmosphere, and vice-versa. The horizontal ports in the vessel provide access for heating and current drive systems,

and for plasma measurement tools, called “diagnostics.” The vertical ports provide access for maintenance. The TF (toroidal field) coils provide the main toroidally-directed magnetic field. The whole structure is contained in a cryostat, an excellent thermal insulator, to maintain the very low temperature ( $\sim 4K$ ) of the superconducting coils. Superconductors are attractive for fusion magnets, because no energy is consumed in resistive dissipation of the coil current. They do, however, require impressive refrigerators. In the future, fusion systems may move to more advanced high-temperature superconductors.

The central solenoid, essentially a cylindrical magnet, is a key feature of a tokamak. It functions as the primary winding of a large transformer, driving up and sustaining the current in the plasma, which functions as a one-turn secondary winding. When, for example, the central solenoid’s electrical current is reversed from clockwise to counter-clockwise, a substantial vertical  $\partial B / \partial t$  is generated inside the cylinder, which causes a toroidally directed electric field. Hot plasmas are very good electrical conductors, so the electric field drives up millions of amperes of clockwise toroidally directed current. It is this plasma current that provides the necessary twist in the field lines. The magnetic fields created by the PF (poloidal field) coils interact with the plasma current to provide the desired plasma shape. The currents in the top and bottom PF coils attract the toroidal current flowing in the plasma towards the top and bottom, and so elongate the plasma. The resulting field pattern also directs plasma diffusing out from the core to flow into the divertor chambers.

**Question:** Where in Maxwell’s equations does the toroidal electric field come from? What would happen if the sign in this equation were reversed? (This sign is Lenz’s law.)

There are other toroidal configurations that are promising for fusion. The stellarator (or “star-maker,” invented by Princeton astrophysicist Lyman Spitzer) takes a different approach to providing the necessary twist in the magnetic field. Rather than drive an electrical current through the plasma, it uses non-axisymmetric, distorted coils as can be seen in figure 1.16 to coax the magnetic field around in the poloidal direction. This trick, which appears to defy Ampere’s law, but of course does not, provides a firmer cage around the plasma. After all, the poloidal field in a tokamak is primarily generated by the plasma’s own current, so if the plasma moves it carries its magnetic cage with it! This is not the case for a stellarator. Such systems though difficult to build due to their lack of symmetry are less prone to macroscopic disturbances than tokamaks, and their fusion performance is

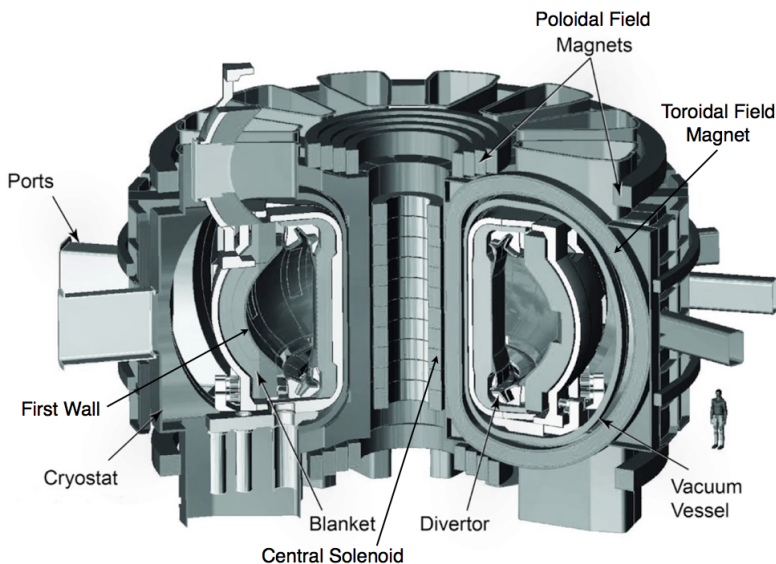


Figure 1.15 Concept for a fusion pilot plant, based on the tokamak magnetic configuration.

in the same range for the same size of device, with the same magnetic field strength.

At the other extreme there are toroidal configurations with weaker toroidal magnetic fields, and even an example that in theory has only a poloidal magnetic field, created by a toroidal current. The plasmas in these configurations are much more unruly, but without the massive toroidal field coils, they are less expensive to build. In some cases there are no magnet coils threading the center of the torus, and the heat flux from the plasma largely escapes along magnetic field lines that lead outside the magnet system, providing considerable engineering simplification. These latter configurations, however, do not even approach the tokamaks of the late 1960's in fusion performance. Nonetheless their advocates are hopeful that they will ultimately make more cost-effective fusion power systems. Some work in this area has attracted private financing, as opposed to the public funding that supports almost all fusion research.

Inertial confinement fusion, discussed in chapter 17, is something completely different. Here the concept is to compress a  $\sim 5$  mm diameter hollow sphere of frozen DT fuel very rapidly, using many powerful laser or particle beams. The center of the sphere is filled with DT gas, in equilibrium with

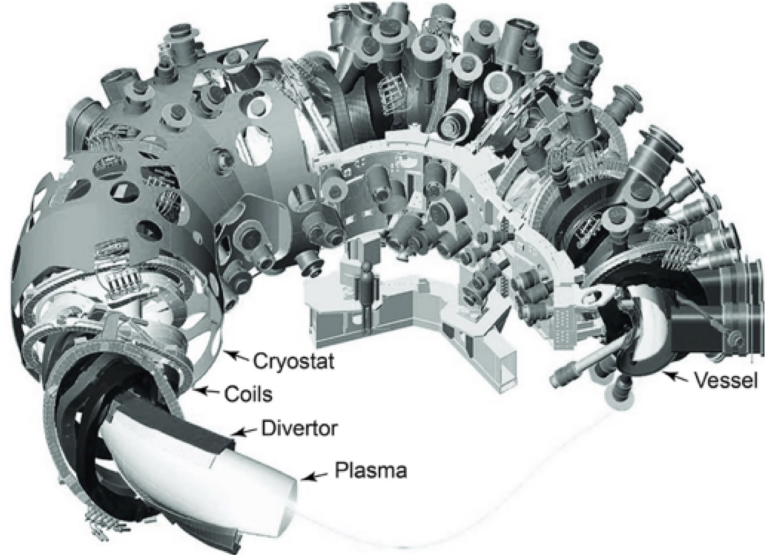


Figure 1.16 Cutaway drawing of the superconducting W7-X stellarator, which began operation in Germany in 2015.

the frozen fuel. When the inward motion, or implosion, stops at the center, kinetic energy is exchanged for heat and pressure, and a tiny, symmetrical, pure DT hot spot is formed at the center of the original sphere, largely from the gas that filled it. This hot spot, comprising only a few % of the fuel, is projected itself to burn vigorously and then ignite an outward propagating burn wave throughout the remainder of the fuel. The fuel is held in place as it burns only by its own inertia, hence the name “Inertial Confinement Fusion,” or ICF. The most advanced approach to ICF at present is to use the intense heat from lasers to fill a small cavity with x-rays, and have the x-rays compress the sphere of fuel, in what is called “indirect drive.” If this sounds like something you have heard of (the hydrogen bomb) you are right. Inertial confinement fusion research is currently funded to help scientists understand the processes going on in nuclear weapons, on a very, very much smaller size and energy scale than an underground test of a nuclear weapon. This research has made progress in recent years, but it is still bedeviled by the challenge of getting the little shells to implode symmetrically. As we will discuss in chapter 17, the implosion process is very unstable and hard to control. We will also discuss the energy application of ICF, which involves producing, targeting, imploding and cleaning up from 5 – 10 of these events per second, making 250 MJ to 600 MJ of fusion energy at each explosion.

**Question:** What might be the advantages and disadvantages of pursuing a form of fusion energy with close links to the physics of nuclear weapons?

### 1.2.2 Why fusion?

Harnessing fusion is clearly scientifically and technologically challenging. What makes fusion attractive as an energy source?

The basic fuels, deuterium and lithium, are abundant. Deuterium forms about 0.03% by mass of the hydrogen in seawater, and can be inexpensively extracted in effectively unlimited quantities.  $^6\text{Li}$  forms about 6.5% of lithium by mass. Identified lithium reserves of 12 million tonnes would allow the full-power operation of 2000 1 GWe power plants for 1500 years, just burning the  $^6\text{Li}$  and leaving the rest for applications such as automotive batteries. It should be economically practical to extract an additional 200 billion tonnes of lithium from seawater for fusion. There have been efforts to extract uranium from seawater; the energy density of lithium in seawater is 2800 times greater for fusion than is the energy density of uranium burned in LWRs.

The CO<sub>2</sub> emissions associated with fusion energy, like with fission, come dominantly from the construction process. This is similar to the levels needed for wind and solar construction, depending on the assumptions made.

Like fission, fusion is a baseload energy source that does not depend on space- and time-varying natural energy flows. Thus it does not incur the additional capital cost of extension of major components of the electrical grid to areas of low population density, where wind or solar power may be most efficiently harvested, nor does it suffer from power loss due to transmission back from those areas. It does not require large-scale energy storage nor backup energy sources operated at low duty factor. It does not require large land use, as needed especially for biomass energy production. It also does not require carbon capture and storage as needed for the most effective use of biomass, and for coal, oil or gas.

There is no equivalent to prompt criticality for fusion. If the pressure in the plasma were to rise, causing increased power output, the system would naturally quench due to physical limits to the plasma pressure.

There is radioactive decay heat in a fusion system, due to radioactivity induced in the material surrounding the plasma. A loss of coolant could result in damage to such components, but could not result in a core meltdown nor the process of self-disassembly seen at Chernobyl and Fukushima.

The radioactive waste from fusion is much less dangerous than that from fission, and much less long-lived, as shown in figure 1.17. The y-axis of this

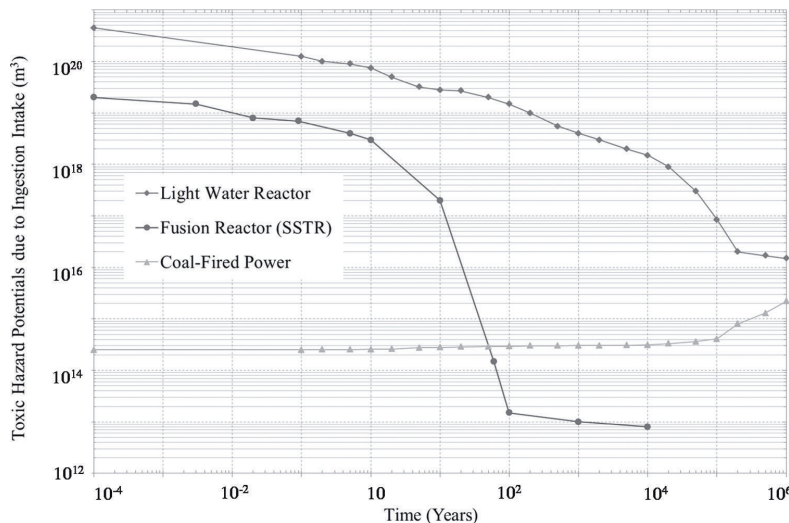


Figure 1.17 Toxic Hazard Potential from lifetime operation of 1 GWe fission LWR, a Japanese fusion power plant concept, SSTR, and coal power plant. Y-axis represents cubic meters of water in which system and waste must be dispersed to reach safe drinking level for all radioactive components. Source: Kikuchi and Inoue, 2002

figure, Toxic Hazard Potential, indicates the volume of water in which a ground-up power source and all of its waste would need to be dispersed so that the water would be considered drinkable. Fission reactors at Chernobyl and Fukushima have indeed exhibited the ability to distribute a significant fraction of their radioactive constituents into the environment, in a manner that is impossible for fusion. After 50 years, fusion wastes drop below that associated with the waste from coal-fired plants, which is not considered a radiological hazard.

The proliferation risks associated with a safeguarded fusion power plant are qualitatively less than those associated with a safeguarded fission reactor. 14.1 MeV neutrons can be used to transmute  $^{238}\text{U}$  to  $^{239}\text{Pu}$  or  $^{232}\text{Th}$  to  $^{233}\text{U}$ , both of which are highly weapons-useable, but since these materials should not be present in any quantity in a fusion system, they should be straightforward to detect. It would be impossible to hide a “clandestine” fusion system capable of producing significant quantities of fissile material from 14.1 MeV neutrons. Finally, in a breakout scenario, it would be straightforward to disable a fusion power plant by military attack on any number of auxiliary systems, without risk of releasing radiation.

One can ask if fusion will be too late to contribute to constraining the maximum temperature rise to  $< 2^{\circ}\text{C}$  above pre-industrial in the year 2100, as targeted by the IPCC. While near-term progress in controlling carbon emissions can be accomplished confidently with existing technologies, costs, risks of failure, and damaging side-effects may grow later in the century without the development of new technologies. Based on IPCC/EMF-27 projections (see figure 1.12), bio-energy plays a crucial role in the second half of the century since it serves as a net carbon sink. CO<sub>2</sub> absorbed by plants from the atmosphere is re-emitted when biomass is burned, but then most of it is captured and stored underground. However bio-energy is projected to require  $\sim 40\%$  as much land area as is presently used for agriculture – in a world with growing population and per capita food demand. Carbon capture and storage (CCS), needed for both bio-energy and low-carbon energy production from other fossil fuels, is projected only to be adequate in volume and distribution if deep saline aquifers are employed later in the century. However R&D on CCS at the needed scale is only now beginning, and whether it will prove to be safe and effective is uncertain. Intermittent electricity sources, solar and wind, are projected to play a dramatically increasing role later in the century, but their effective cost increases as it becomes necessary to provide major enhancements to the electric grid, as well as large scale energy storage and/or large amounts of infrequently used highly dispatchable power. Substantial demand control is also required. Nuclear fission energy is projected to increase by a factor of about seven, but by mid-century will deplete known and projected reserves of uranium, especially in countries with high populations and low uranium reserves. This could lead to large-scale plutonium reprocessing, with its associated high nuclear proliferation risks. From this perspective, it is reasonable to conclude that while existing technologies are well suited to taking the near-term steps along the path to achieving the goals set out by the IPCC, R&D also needs to be aggressively pursued over a broad range of technologies, including fusion, for the longer term.

**Question:** The development of fusion, which may be needed in the second half of this century, is a long-term project that must be pursued today if the research investment is to “pay off” when it may be needed. How should we balance competition for government resources between projects like fusion R&D vs. loan guarantees and subsidies to support the near-term deployment of fission nuclear energy and renewables?

### **1.2.3 Scientific progress**

Soon after WWII scientists and engineers began to consider non-explosive applications of nuclear power in earnest, including both fission and fusion. It is said that they considered magnetic confinement fusion in early meetings at Los Alamos, and Fermi proved that without the twist shown in figure 1.14 particles would not be confined by toroidal fields.

A period of innovation in magnetic confinement configurations followed, which was classified, because it was believed that fusion might be a means to provide the neutrons to produce large quantities of tritium for thermonuclear weapons, using  $D + D \rightarrow T + n$ . Soon, however, it became clear that large quantities of tritium were not needed, because, remarkably, equation 1.5 can be implemented inside of a thermonuclear weapon. The same heavy-water and graphite moderated fission reactors that were used to produce Pu could also produce the small amounts of T that were still required. Therefore the emphasis switched exclusively to power production and the  $D + T$  reaction. In 1953 President Eisenhower announced the “Atoms for Peace” initiative, through which the US would share peaceful nuclear technology with the world. At the second Atoms for Peace conference, in Geneva in 1958, fusion energy research was declassified world-wide and an international collaborative (and sometimes competitive) effort to develop fusion energy began. Fusion provided one of the few channels of communication between Western and Soviet scientists during the Cold War.

A range of magnetic configurations was investigated, including not only toroidal configurations with much greater toroidal magnetic field than poloidal such as the tokamak, pursued in the USSR, and stellarator, pursued in the US, but also ones with higher poloidal field than toroidal, pursued mainly in the US and in the UK. These are called “pinches” because the high plasma current is self-attracting (like currents attract) pinching the plasma together. A series of experiments at Los Alamos was whimsically named “Perhap-satrons,” one of which is shown in figure 1.18. An alternative configuration, known as a “magnetic mirror” was also studied. Here the magnetic field was nearly linear, but higher in value at its two ends, to reflect particles back and forth, as will study in chapter 10.

The Soviets claimed that their tokamak plasmas were achieving much higher temperatures than the other configurations. In 1968 a British team visited the Kurchatov Institute in Moscow, bringing along a new plasma diagnostic that took advantage of the recently invented laser as an intense monochromatic and highly collimated light source. This technique, based on scattering laser light off of plasma electrons to measure their velocity

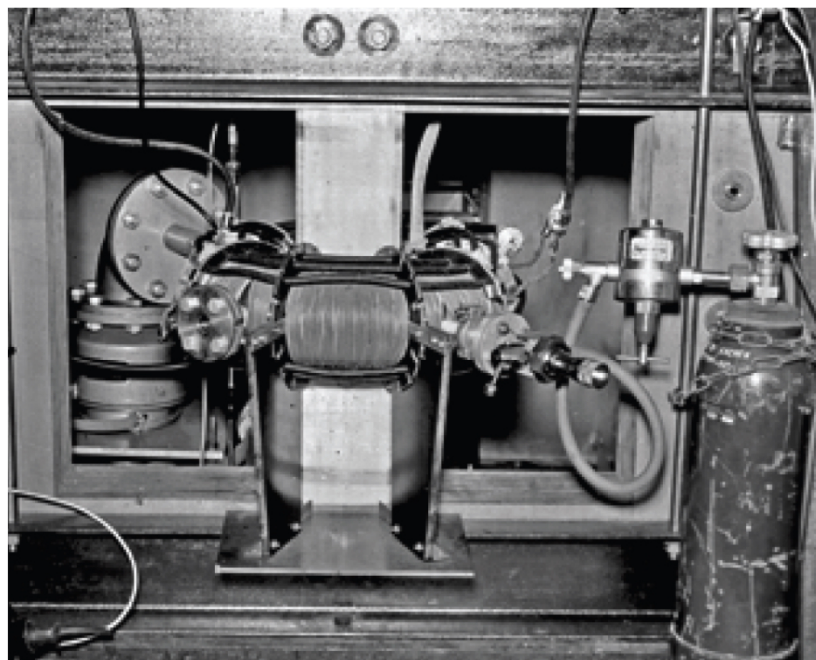


Figure 1.18 One of the early toroidal pinch experiments at Los Alamos, from the “Perhapsatron” series.

distribution, was, and remains, the gold standard for measuring electron temperature. The British found that the Soviet T-3 tokamak achieved electron temperatures above 1 keV, with the very modest plasma heating power that resulted from resistive dissipation of the plasma current =  $I_p^2 R$ , where  $I_p$  is the plasma current and  $R$  the small electrical resistance of the plasma. This was a better result than had been claimed by the Soviet team, and much better than had been achieved in stellarators, pinches and mirror machines.

After these results were reported, most fusion research programs around the world turned to the tokamak configuration. However significant stellarator programs were maintained in Germany and Japan, because the stellarator is a more natural configuration for steady-state operation, as it does not require a plasma current to be sustained with external power. Programs in mirrors and various types of pinches persisted as well, although ultimately at a lower level.

In the intervening decades tremendous progress has been made in the performance of fusion plasmas and in understanding the physics of magnetic confinement, particularly in the tokamak configuration. Experiments in the US and Europe have produced over 10 MW of thermal fusion power, and over

15 MJ of thermal fusion energy. This has led to the current construction of the international ITER (latin for “The Way”) tokamak in southern France. The goal of this project is to produce 100’s of MW of thermal fusion power for hundreds of seconds, at a gain (fusion power divided by external heating power) greater than 10. The entities participating in this project include China, Europe, India, Japan, South Korea, the Russian Federation, and the United States, representing more than one-half of the world’s population. If this project succeeds, it will demonstrate that fusion can be harnessed at the commercial scale. If enough physics and engineering research is performed in parallel with ITER, the nations that do this work will be positioned to construct pilot fusion energy projects capable of putting net electricity on the grid.

It is useful to briefly review the progress in fusion science and technology, and consider the remaining challenges. As an organizing principle, we will follow the power flow through a magnetically confined plasma, and then touch briefly on inertial confinement fusion.

#### *Plasma heating and current drive*

To achieve useful levels of fusion power density, plasmas must be heated to very high temperature, as shown in figure 1.19. This figure shows fusion power per cubic meter,  $p_{fus}$ , as a function of temperature. The pressure of pure fusion fuel plus charge-neutralizing electrons is set equal to 1 MPa. (This is very close to 10 atmospheres.) In computing the plasma pressure it is assumed that  $T_e = T_i = T$ . In addition to its variation with  $T$  shown in the figure,  $p_{fus}$  rises as the square of the particle density, at fixed temperature. This is because, again at fixed temperature, the rate of close encounters between reactants rises linearly with the density of each, which are assumed to be proportional to the total density. Thus, at fixed and equal ion and electron temperatures, the fusion power density rises as the square of the pressure, and can be simply scaled by (Pressure/1 MPa)<sup>2</sup> from figure 1.19.

The center of the ITER plasma will be at a thermal pressure,  $n_e T_e + n_i T_i$ , of about 1 MPa, as used in the figure, but much of ITER’s volume will be at lower pressure and temperature (see for example the temperature profiles shown in figure 1.20). The major radius,  $R_0$ , the distance from the axis of symmetry to the center of the plasma, will be 6.2m. The horizontal minor radius,  $a$ , the distance from the plasma center to its inner and outer edges, will be 2m, and its vertical minor radius,  $b$ , the distance from the plasma center to its top and bottom will be about 3.4m, for a total plasma volume of 840 m<sup>3</sup>. Thus its volume average power density with 500 MW(th) fusion power production will be about 0.6 MW/m<sup>3</sup>.

Incidentally, figure 1.19 also illustrates why the DT reaction is the most likely candidate for producing practical fusion energy. For example, for the same plasma pressure, the  $p - {}^{11}\text{B}$  reaction produces about 2400 times lower power density. Not surprisingly, as we will discuss below, this has severe consequences for the possibility of self-sustainment as well.

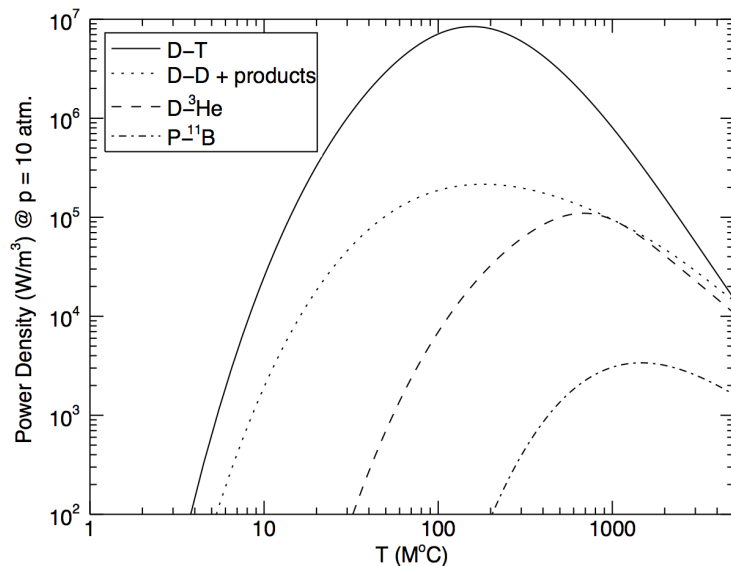


Figure 1.19 Fusion power density as a function of plasma temperature. In all cases the plasma particle kinetic pressure,  $n_e T_e + n_i T_i$ , is fixed at 1 MPa, about 10 atmospheres, and  $T_i = T_e$  is assumed. For the DD reaction, it is assumed that the T and  ${}^3\text{He}$  fusion products are burned as well.

As a very first question, it is eminently reasonable to ask if the required temperatures, as indicated in figure 1.19, can be produced in the laboratory. Remarkably, the answer is yes. Figure 1.20 shows electron and ion temperatures achieved in the Joint European Torus experiment in England with a heating mechanism, neutral beam injection, that predominantly heats the ions. The electrons are subsequently heated by collisions with the hotter ions. This is a dramatic improvement beyond the  $\sim 1\text{-}2$  keV temperatures achieved with Ohmic ( $I_p^2 R$ ) heating alone.

Neutral beam heating involves the injection of high currents of neutral, typically  $\text{D}^0$ , atoms. A single modern neutral beam might inject 20 amperes of 100 keV deuterium atoms into a tokamak plasma, providing 2 MW of

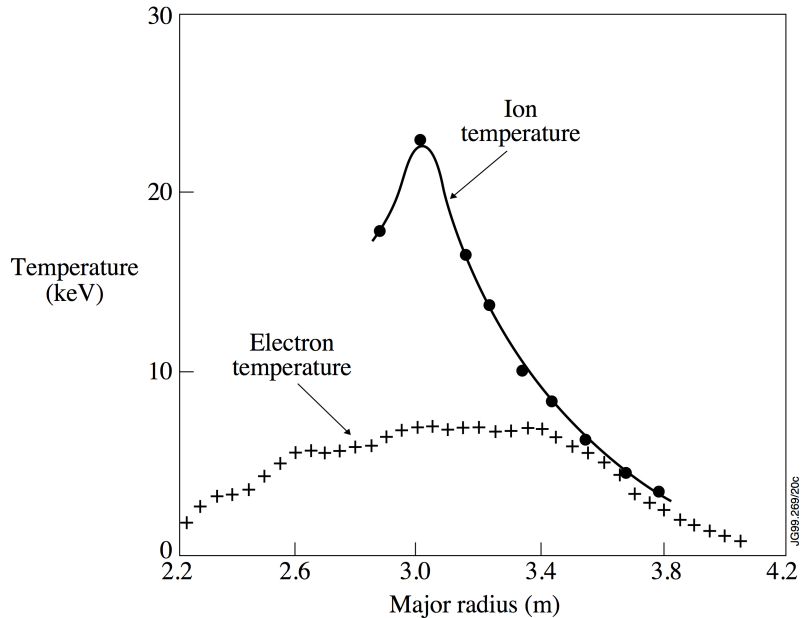


Figure 1.20 Measured ion and electron plasma temperature profiles in the Joint European Torus, across the horizontal midplane. Center of the plasma is at 3m major radius, horizontal minor radius is about 1.2m. (1 keV = 11.6M K).

heating. (The case shown in figure 1.20 had a total of 20 MW of heating power.) Neutral deuterium atoms travel easily across a magnetic field, and then are ionized by collisions with ions and electrons in the plasma. Now they are confined as charged deuterons, and transfer their energy to the bulk plasma. In general this occurs by simple binary collisions, but under some circumstances the fast ions can drive up instabilities. These conditions are now well understood, and even the nonlinear consequences of the fast ions interacting with the instabilities they drive have been characterized and compared successfully with theory. These experiments and the associated theory provide a basis for projecting that in most conditions ITER's injected fast ions and  $\alpha$  particles from fusion will thermalize by binary collisions. We will, however, be able to study conditions where instabilities are predicted to arise.

Other methods of plasma heating have also been developed, generally involving injecting radio waves that interact resonantly with the motion of the ions or the electrons, or even with a "hybrid" of the two motions. The interaction of these waves with the plasma, including how they heat the

plasma electrons or ions preferentially and even drive current in the plasma, is well understood theoretically and confirmed experimentally. There are some challenges, however, in optimizing the efficiency of launching waves into the plasma, especially ones with large wavelength, so large launching structures. But the bottom line is that we are now quite confident that we will be able to drive ITER plasmas to the temperatures required for fusion.

Experiments on the Tokamak Fusion Test Reactor, TFTR and the Joint European Torus, JET, the two tokamaks which have operated in deuterium-tritium, have even shown the beginnings of heating by fusion alpha particles.

The current in the ITER plasma can be sustained by the electric field from the central solenoid for about 400 seconds, but then the solenoid will reach its maximum current and magnetic field. No more  $dB/dt$  of the desired sign, so no more useful toroidal electric field, will be available. For the pulses of up to 3000 seconds planned for ITER, and even longer for a tokamak fusion power plant, it will be necessary to drive the current by external means. Getting the necessary efficiency of external current drive from radio waves and/or neutral beams, and taking advantage of the natural self-driven “bootstrap” current (see chapter 10) in the tokamak, so that not too much fusion power needs to be siphoned off to sustain the plasma current, are challenges that will be studied using ITER and as well as smaller non-DT tokamak experiments. The stellarator, on the other hand, does not have this challenge and is being studied in parallel. Alternatively, one could operate a tokamak with long pulses, recharging the solenoid between pulses. This has the disadvantage of more frequent time-varying thermal and mechanical stresses.

#### *Macroscopic Stability*

Early in the study of fusion plasmas, the biggest challenge was holding the plasma from going macroscopically (large scale) unstable, in effect flinging itself to the walls of the vacuum chamber. Figure 1.21 shows an early British toroidal pinch plasma going unstable and doing exactly that, because of the very high energy in the poloidal field relative to that in the toroidal field. This results in a virulent “kink” instability, as we will study in chapter 12. Tokamaks are much, much more kink-stable than pinches, because the strong toroidal field provides the plasma with the stiffness needed to resist bending or kinking. If the plasma current profile develops too strong a spatial gradient, however, this gradient can nonetheless drive significant macroscopic instabilities in tokamaks, even resulting in the rapid termination of the plasma, called a “disruption.” Disruptions can generally be avoided, but when they do occur they may damage internal components, particularly at

the high plasma current, 15 MA, planned for ITER. This will be a very important area of study and – again – the backup is the stellarator, which can be designed to have no plasma current and, based on current understanding, no violent disruptions.

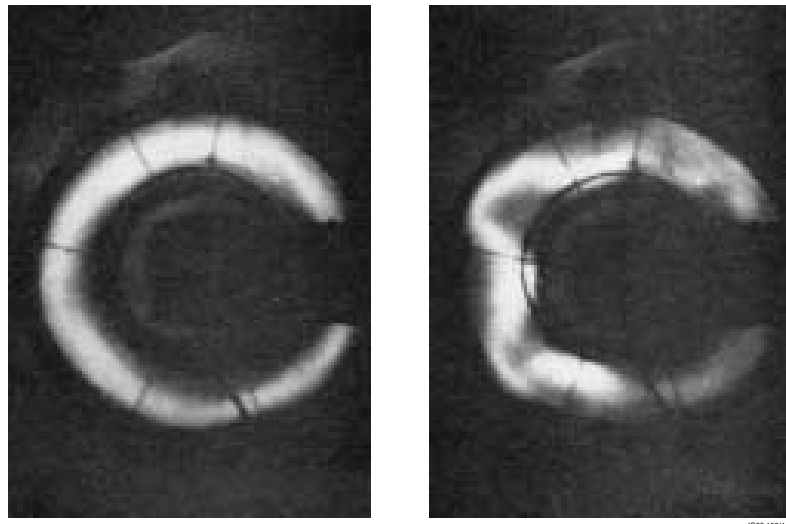


Figure 1.21 Image of a small pinch experiment early in its development, and then after a kink instability has grown up.

Macroscopic instability can be driven not only by poloidal magnetic energy density due to the plasma current, but also by plasma stored energy density, or pressure. A key parameter that characterizes plasma stability as a function of pressure is  $\beta$ , the ratio of plasma pressure to magnetic pressure, discussed in chapter 11.

$$\beta \equiv \frac{p}{B^2/2\mu_0} \quad (1.7)$$

(It can be confusing that the same variable,  $p$ , is used both for pressure and power density. We will mitigate this unavoidable problem by *always* providing a descriptive subscript for power density.)

Generally magnetic configurations are characterized by a  $\beta$  limit, above which the plasma pressure will distort the configuration and allow the confined plasma to escape rapidly. Most aspects of these limits are now well understood for tokamaks, both experimentally and theoretically. Conventional tokamaks, with  $R_0/a \sim 3$  have achieved  $\beta_t \sim 10\%$ , while low aspect ratio tokamaks, or spherical tori, have achieved  $\beta_t \sim 40\%$ , where the  $t$  sub-

script indicates that only the toroidal field is included in the denominator of  $\beta$ . ITER is designed to achieve 500 MW(th) of fusion power at conservative values of  $\beta \sim 2.5\%$ . A cost-effective fusion power source with the size of ITER will need to make more fusion power than this however, and one option will be to operate at higher values of  $\beta$ , closer to the known limits. This will be studied in ITER and in other experimental devices around the world.

Interestingly, since fusion power density,  $p_{fus}$ , rises as the square of pressure,  $p^2$ , at fixed  $T$ , and  $p$  rises as  $B^2$  at fixed  $\beta$ , fusion power density rises as  $B^4$  at fixed  $T$  and  $\beta$ . Thus another approach to achieving higher fusion power at fixed system size is to operate at higher magnetic field. The new high temperature superconductors, such as YBCO, when operated well below their maximum operating temperature, allow higher current densities than present low-temperature superconductors, such as NbSn. These may permit operation at higher magnetic fields and so higher power density without approaching  $\beta$  limits too closely, but more R&D is needed to determine how to take advantage of the properties of this material, and how much advantage can be gained. For example, the critical current density for losing superconductivity is highly sensitive to the orientation of the magnetic field at the conductor. Ultimately, of course, the maximum attainable field will be limited by the strength of the material used to construct the coil.

**Question:** ITER is planned to operate with a toroidal magnetic field of 5.3 T. If that field could be increased to 7 T, roughly how much fusion power could it make at the same value of  $\beta$ ?

#### *Energy confinement*

Referring back to figure 1.19, we can see that the maximum DT fusion power density as a function of temperature in a pure DT plasma with  $T_i = T_e = T$ , and a particle kinetic pressure of 1 MPa, is about 8 MW/m<sup>3</sup>. The ideal gas ratio of 3/2 between energy density and particle kinetic pressure is appropriate for magnetic fusion plasmas, because they have little energy stored in the electrostatic fields around the individual charged particles and in the electromagnetic radiation field within the plasma. Thus a magnetic fusion plasma with a kinetic particle pressure of 1 MPa has an energy density of 1.5 MJ/m<sup>3</sup>. In a practical situation with a finite-size plasma, energy density is continually leaking away, both by thermal transport carried by charged particles leaving the plasma and so draining heat from both the electrons and the ions, and also by radiative loss carried by photons leaving the plasma draining heat from the electrons, as we will discuss in more detail in chapters

9, 13 and 14. Together these two losses constitute a loss power density,  $p_{loss}$ . Let us define a characteristic “energy confinement time,”  $\tau_E$ , as the ratio of the stored energy density to the loss power density, a quantity which has units of time. Specifically, this is the time it would take for the loss power density to drain away all of the energy density, if the loss power density did not change as the plasma cooled and/or rarified.

$$\tau_E \equiv \frac{(3/2)(n_e + n_i)T}{p_{loss}} \quad (1.8)$$

Now we consider that in a useful, steady-state DT fusion plasma  $p_{loss}$  must be largely compensated by the alpha particle power density,  $p_\alpha$ , produced by fusion, since we probably cannot afford to resupply all of the heat needed for steady-state power balance externally. Let us therefore equate the alpha heating power density with a fraction,  $f_\alpha$ , of the power loss density from the plasma:

$$p_\alpha = f_\alpha p_{loss} \quad (1.9)$$

Substituting  $p_{loss}$  derived from equation 1.9 into equation 1.8 and recognizing that  $n_e = n_i = n$  for a pure DT plasma, we have:

$$\tau_E = \frac{3nT}{p_\alpha/f_\alpha} = f_\alpha \frac{p_{fus}}{p_\alpha} \frac{3nT}{p_{fus}} = f_\alpha \frac{15nT}{p_{fus}} \quad (1.10)$$

where we have recognized that  $p_{fus}/p_\alpha = 5$  holds for the DT reaction. Remembering that, with our definitions,  $p = 2nT$ , we can read from figure 1.19 that the minimum needed  $\tau_E$  for full self-sustainment,  $f_\alpha = 1$ , of a pure DT plasma at a pressure of 1 MPa is a little under one second, at  $T$  somewhat above 100M K:

$$\tau_E = f_\alpha \frac{15 \cdot p}{2 \cdot p_{fus}} \approx \frac{7.5 \cdot 10^6}{8 \cdot 10^6} \quad (1.11)$$

Next it is helpful to remember that  $p_{fus}$  and  $p_\alpha$  scale as the square of the plasma pressure,  $p^2$ , at fixed  $T$ . This gives us

$$\tau_E = f_\alpha \frac{15nT}{p_{fus}(1 \text{ MPa}, T)} \left( \frac{1 \text{ MPa}}{2nT} \right)^2 \quad (1.12)$$

as the condition for the minimum energy confinement time required for  $f_\alpha$  fractional self-sustainment. This translates to a requirement on the “fusion triple product”,  $nT\tau_E$ :

$$nT\tau_E = f_\alpha \frac{(15/4)(1 \text{ MPa})^2}{p_{fus}(1 \text{ MPa}, T)} \quad (1.13)$$

For a given desired  $f_\alpha$  there is a minimum requirement on  $nT\tau_E$  as a function of temperature. This optimum occurs at the temperature where  $p_{fus}$  is maximum at fixed pressure. Thus this triple product is a measure of the approach to self-heating, assuming the optimum temperature can be achieved. Figure 1.22 shows progress over time on this parameter in tokamaks.

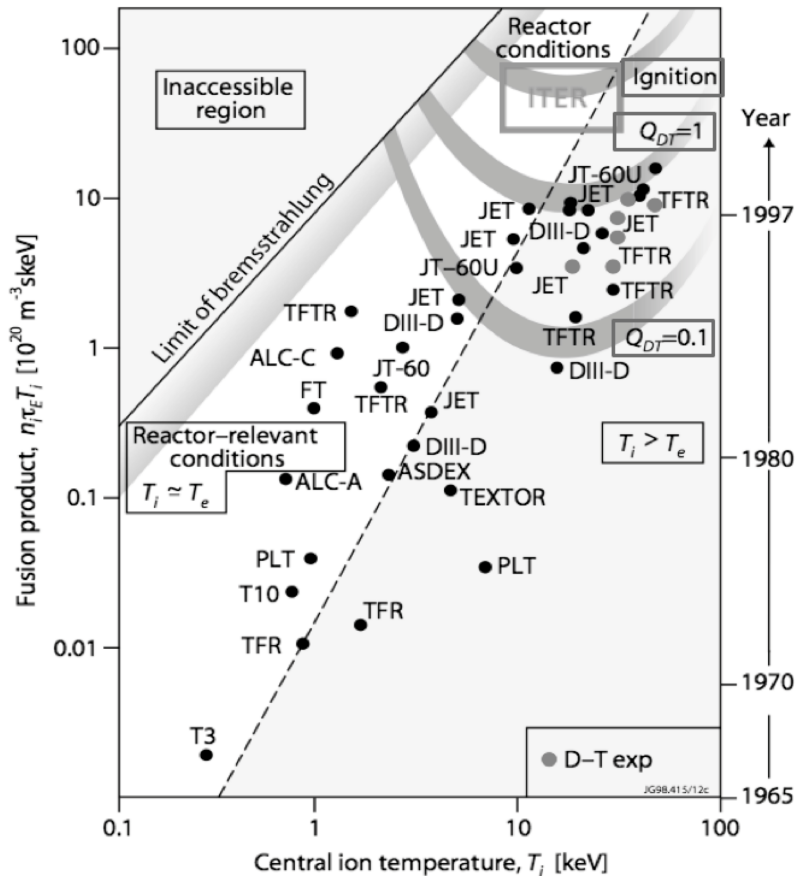


Figure 1.22  $nT\tau_E$  in tokamaks, where  $n_i$  here is the central hydrogenic ion density,  $n_H + n_D + n_T$ ,  $T_i$  is the central ion temperature and  $\tau_E$  is the energy confinement time defined over the full volume of the plasma. Data points are labeled by the experimental tokamak devices on which they were measured, and DT cases are indicated by gray dots. All other cases are DD.

Figure 1.22 has some features that bear explanation. First, since it is not addressing local power balance, but attempting to characterize global fusion performance, it needs some simple way to characterize the  $nT\tau_E$  of the particular plasmas measured. The parameters listed in the figure caption

do a reasonable job of defining a global  $nT\tau_E$  that is proportional to the global  $f_\alpha$ . You will note, however, that the curves on the plot are labeled by the global fusion gain,  $Q$ , which is defined as  $Q \equiv P_{fus}/P_{ext}$ , where  $P_{ext}$  is the total externally applied heating power. The relationship between global  $f_\alpha$  and global  $Q$  in a steady state DT plasma is simple:

$$f_\alpha = \frac{P_\alpha}{P_{loss}} = \frac{P_{fus}}{5P_{loss}} = \frac{P_{fus}}{5(P_{ext} + P_\alpha)} = \frac{P_{fus}}{5P_{ext} + P_{fus}} = \frac{Q}{Q + 5} \quad (1.14)$$

Thus  $Q = 1$  corresponds to  $f_\alpha = 1/6$ ,  $Q = 10$  to  $f_\alpha = 2/3$  and  $Q = \infty$ , or full ignition, to  $f_\alpha = 1$ .

The upper left region is “inaccessible” because of unavoidable radiation of photons from the electrons. When electrons encounter nuclei they are deflected, which amounts to a form of acceleration, and accelerating electrons radiate energy. This process is analogous to how an energetic electron beam stopping in a high-Z material makes X-rays, so it is called “bremsstrahlung”, German for “stopping radiation.” Magnetic fusion plasmas are transparent to this radiation, so it is an unavoidable loss mechanism that limits  $nT\tau_E$  as a function of  $T$ .

The lower right region is the region where the energy confinement time is less than the time it takes ions and electrons to equilibrate in temperature through collisions, so this is a region where, with dominant ion heating,  $T_i > T_e$ . It is not completely accurate to say that this region is not reactor-relevant, since you can see that the ignition region,  $f_\alpha = 1$ , straddles the boundary of this region. However, unless extraordinary measures are taken, the alpha particles from fusion mostly transfer their energy to the electrons in the plasma, so in this region in a fusion power system we are likely to see, if anything,  $T_e > T_i$ . However many of the experimental data points to right on the plot have powerful ion heating, so  $T_i > T_e$ .

It is worth noting that only tokamaks are shown on this plot. Stellarators have achieved parameters towards the middle of the plot, as have very low aspect ratio ( $R_0/a \leq 2$ ) tokamaks, sometimes called Spherical Tokamaks or Spherical Torii. Other devices, various kinds of mirrors and toroidal pinches with different amounts of toroidal field relative to poloidal field, have not yet achieved the  $nT\tau_E$  measured in T-3 fifty years ago. On the other hand, they generally have less externally supplied magnetic energy than T-3, and they each offer potential advantages in their power-plant implementation relative to tokamaks.

**Question:** Some fusion researchers are interested in pursuing the reaction  $p + {}^{11}\text{B} \rightarrow 3\alpha + 8.7\text{ MeV}$  because it does not produce neutrons nor does it require tritium breeding. We noted before that for fixed plasma pressure the

power density from  $p + ^{11}\text{B}$  is  $\sim 2400$  times lower than from D + T. How much higher is its required  $nT\tau_E$ ? On the positive side, note that unlike the DT reaction, all of its fusion products are charged, and so can be counted as heating the plasma.

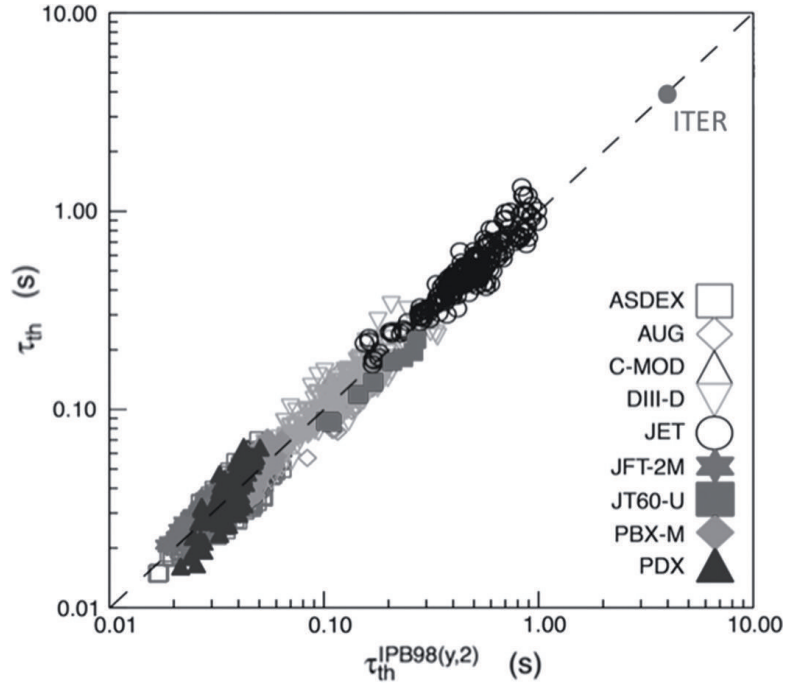


Figure 1.23 Measured energy confinement time, defined as thermal stored energy divided by heating power, on tokamaks world-wide, vs. regression fit.

While figure 1.22 shows dramatic progress over time, it is important that this progress be consistent and predictable, something that you cannot tell from the figure. Empirical trends in the data already observable in the early 1980's accurately predicted the performance of the next generation of much larger devices that began to produce significant experimental results in the late 1980's and beyond. Now, taking all of the data together, a highly consistent database has been accumulated that predicts that ITER will have the desired performance, as shown in figure 1.23. Remarkably, and to the credit of the both the researchers operating these experiments and those making the measurements, the RMS error of this fit is only about 12%.

The experimental progress discussed so far required the construction of

a series of experimental facilities of increasing size. Figure 1.24 shows the largest current tokamak, about twice the size of the devices studied in the 1970's, and half the size of ITER. In parallel with this, however, possibly even more impressive progress has been made in understanding the physics of the small-scale nonlinear turbulence that drives thermal transport in tokamaks. Now massively parallel computer simulations predict the thermal transport in the hot core of tokamak plasmas with good accuracy. In the 1980's the best calculations typically predicted an order of magnitude too much transport in the hot core of the plasma, and an order of magnitude too little transport at the cooler edge. A combination of theoretical insight and massively parallel computing power has completely turned this situation around, as discussed in chapter 14. The results from ITER will provide a very strong test of the

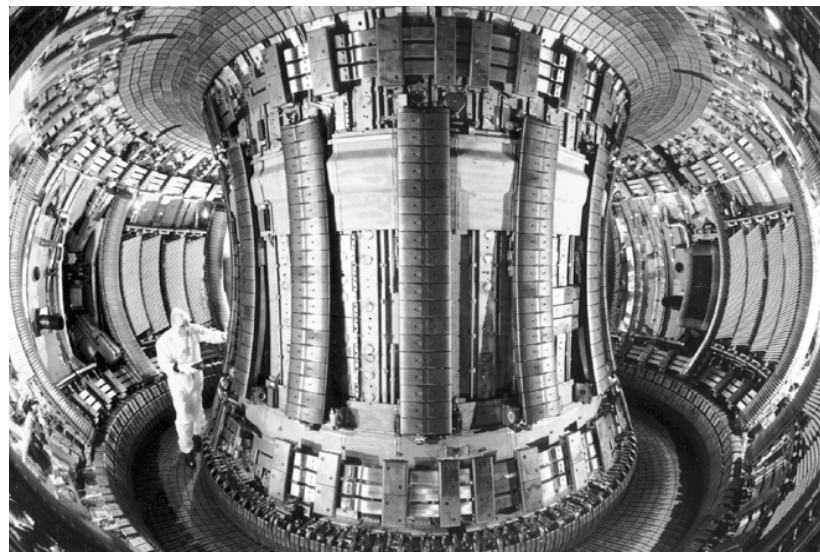


Figure 1.24 Joint European Torus.  $R_0 = 3\text{m}$ ,  $a = 1\text{m}$ .

empirical regression fits and especially of the theoretical projections. ITER should “nail down” experimentally the confinement in large-scale tokamaks in a manner that could not be done by any other means.

#### *Power efflux*

If a DT plasma is successfully heated to fusion temperature, and then it holds onto the power from the alpha particles produced by fusion well enough that a steady high-temperature burn is established, there will be a strong flow of power out of the plasma, equal to the total stored energy in the plasma

divided by the global confinement time. This power flow needs to be handled on material surfaces without damage to plasma-facing components, or impurity influx to the fusion plasma that would deteriorate its performance. If a fusion power plant plasma produces 2500 MW of fusion power at  $Q = 25$ , it necessarily produces 600 MW of loss power. (We leave the neutrons to the next section.) A favorable aspect of magnetic confinement is that magnetic fields are very effective at holding heat in the main plasma. Unfortunately this quality of magnetic confinement extends to the plasma on the field lines in the “scrape-off layer”, or SOL, just beyond the edge of the magnetically confined plasma.

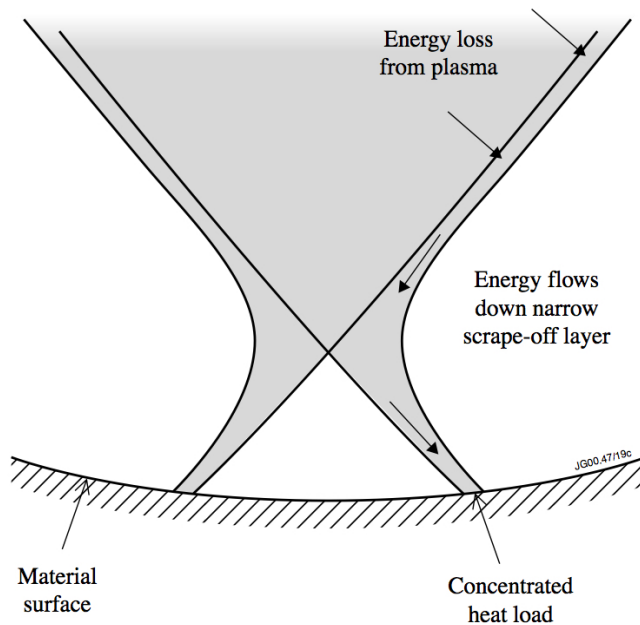


Figure 1.25 Plasma crosses edge of confined plasma into scrape off layer, and is directed to material surfaces.

As shown in figure 1.25, and discussed in chapter 15, the magnetic field lines just outside the edge of the main plasma divert the SOL plasma away from the main plasma towards material surfaces in the “divertor” chamber, which is generally at some distance. A divertor chamber is visible at the bottom of figure 1.24. The plasma flows into the divertor chamber at a fraction of the ion thermal speed, and during the time it takes to get to the divertor target, where it first contacts a material surface, it spreads very little. Recent detailed experimental measurements and a relatively simple “heuristic”

theory that matches the data well, indicate that the spreading may be as little as 1 – 2 mm in ITER. The thermal loss power in ITER with 500 MW of fusion power at  $Q = 10$  is only 150 MW, and the duty factor (fraction of operational time) will be less than  $\sim 5\%$ . While challenging, it appears that at these parameters the heat flux can be handled by intercepting the field lines at a glancing angle, as planned. ITER’s plasma-facing components will also need to handle the transient power efflux from the plasma during disruptions and during bursts of loss from near the edge of the plasma, called Edge Localized Modes. Research is ongoing on means to suppress these transient heat fluxes and to spread the steady heat flux in a fusion power plant with four times higher thermal loss power and near-continuous service. These are problems that will need to be solved by research on ITER and in parallel with ITER operation.

#### *Materials and blanket*

As discussed in chapter 16, the 14.1 MeV neutrons produced by DT fusion are much more energetic than the neutrons even in fast-spectrum reactors. For the most part, however, the damage to materials is similar, because the individual clusters of atomic displacements are very similar. A significant difference, however, is that 14.1 MeV neutrons cause many more  $(n,\alpha)$  reactions, reactions in which a neutron is absorbed and a helium nucleus (or  $\alpha$  particle) is emitted. The helium gas that accumulates as a result in steels and other materials to be used in a fusion power plant can cluster in bubbles along the boundaries between different crystal grains in the material, and cause the material to become very brittle. New steels, however, are being developed with nano-inclusions dispersed within the crystal grains themselves. These inclusions, for example of yttrium oxide, make the steel tougher. Interestingly, they also scavenge helium atoms, and prevent them from accumulating at grain boundaries.

Europe and Japan are working together on the design and R&D for an International Fusion Materials Irradiation Facility, IFMIF, which should provide the neutron fluence needed to irradiate test samples to qualify materials for fusion applications.

In addition to materials that can stand up to the neutron flux, fusion systems will require “blanket” systems constructed of these materials that can absorb the heat from neutrons and transfer it to coolant systems, preferably at high temperature for high efficiency electricity production. These blankets must also multiply neutrons and breed tritium using lithium. ITER will have six test-blanket modules for testing different engineering approaches. ITER will not, however, provide a fluence (flux  $\times$  time) of neutrons that

approaches what a power plant will produce, so the next step facility in the development of fusion, perhaps an energy-producing pilot plant, will need to address this issue, using blankets constructed from materials qualified in an irradiation test facility such as IFMIF.

### *Magnets*

The superconducting magnets for ITER are at the full scale that might be anticipated for a fusion power plant, and produce the magnetic field strength that is called for in some designs. One could say that the practical knowledge that the world is developing from construction of the ITER magnets will complete the magnet technology development needed for fusion. This may be so, but modern high-temperature superconducting magnets may be able to support higher current densities than the magnets now being wound for ITER. As noted before, if this can lead to higher fields, one may be able to make more compact and less expensive fusion systems, so R&D in this area for fusion could be very valuable.

### *Inertial confinement fusion*

Very soon after the laser was invented in 1960, the idea was conceived that a small sphere of frozen DT could be compressed and heated to fusion temperature using this new technology, and so produce net energy. The research to test this new idea was pursued in the U.S. using a series of more and more powerful laser systems, with the primary policy motivation to study the closely related physics of nuclear weapons. The U.S. scientists, however, were also motivated by energy applications, as was a team in Japan.

Two barriers were found to producing significant amounts of fusion energy using high-power lasers. First, when the laser light traverses the plasma that is inevitably produced outside the frozen DT sphere, it can drive up waves in that plasma that deflect the incoming laser beams or even produce energetic electrons that prematurely heat the frozen DT gas. The former is obviously problematic, and the latter makes it more difficult to compress the fuel adequately, since it has too high a pressure to begin with, and pushes back. Second, the best kind of target for inertial confinement fusion is a thin, hollow sphere of fuel, and it is very hard to compress rapidly a very thin, hollow shell without breaking it up. If the originally spherical shell breaks into pieces, it does not fly inwards symmetrically and the kinetic energy per unit mass invested in the motion of the material won't show up as heat and pressure at the exact geometric center of the original sphere. This is what is needed to cause fusion in a small, central "hot spot" containing only a few

% of the fuel, which is then to drive a propagating burn wave through the remaining fuel.

When more energetic lasers are used, it is possible to implode heavier shells, with less acceleration, and so suffer less from instability. Experiments with the current generation of lasers in the National Ignition Facility (NIF), capable of providing about 2 MJ of laser light in 20 nsec, continue to suffer from these two problems. The first round of experiments on NIF clearly pushed the shell far too hard, and achieved only about 2.5 kJ,  $\sim 0.125\%$  of the stated goal of 2 MJ. This goal had been dubbed “ignition,” in a very different sense from ignition in magnetic fusion. If the hot spot in the core of an inertial confinement pellet starts to burn, this is analogous to a match being lit under a pile of logs. If the match sets the fuel on fire, that could be called igniting the fire. When the analogous process occurs, the compressed but initially cold fuel begins to burn due to heating from the hot spot, that is what is called “ignition” in inertial confinement fusion, and the production of 2 MJ of fusion energy would be a good sign of this. Experimenters on NIF in late 2013 tried pre-heating the shell with an early laser pulse so it compressed more weakly, and achieved much more symmetric implosions and about 10x higher fusion output, but still only about 1.3% of the goal. It was a nice accomplishment, however, that the fusion energy produced was greater than the small fraction, less than 1%, of the laser energy that was originally deposited in the DT fuel. One could say that these experiments demonstrated that an inertial confinement fusion match has been lit in the laboratory, but this has not yet resulted in a burn wave in the accumulated fuel.

Measured fusion energy production per pulse from magnetic and inertial confinement fusion experiments are shown in figure 1.26.

#### **1.2.4 Prospects**

The ubiquitous joke about fusion energy is that it is always 20 years away. At the same time the facts show that rapid progress has been made in fusion R&D. Certainly the early pioneers underestimated the difficulty of mastering the science of plasma physics (vis., the “Perhapsatron”), and at later times fusion researchers made projections that depended on funding levels that did not materialize. Four of the ITER partners, China, Europe, Japan and South Korea have articulated specific plans for major next steps, in some cases even before DT results from ITER will be available. As we discuss in chapter 18, R&D is needed in ITER and in parallel with ITER on the issues discussed above, in particular steady-state operation either by current drive

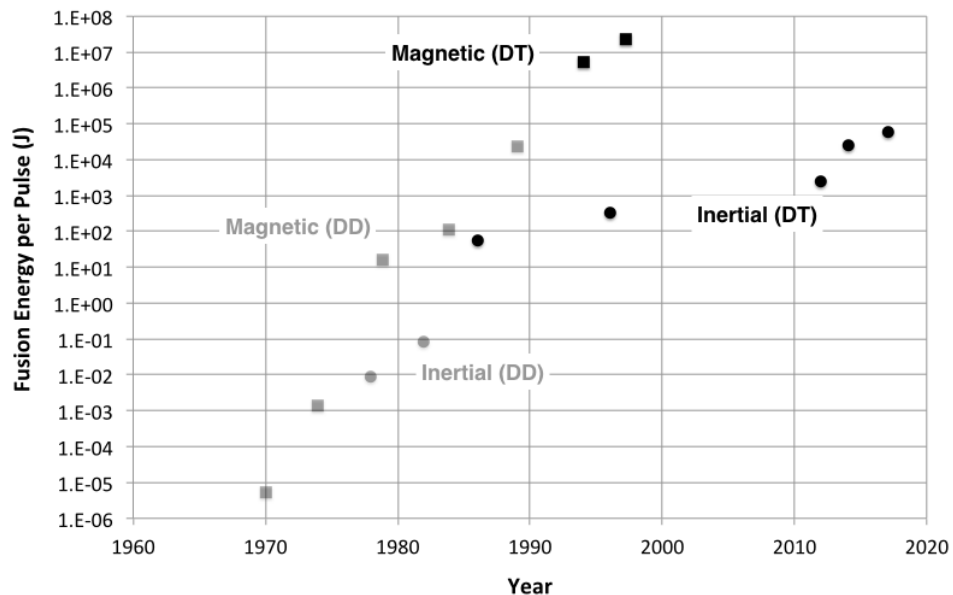


Figure 1.26 Fusion energy produced per pulse in magnetic and inertial fusion, both in deuterium-only (DD) plasmas and in DT plasmas.

in tokamaks or via stellarators, means to handle the very high heat fluxes that emerge from fusion plasmas, and validation of new materials for use in the high flux of energetic neutrons. But with success in these endeavors it should be possible for the next generation of major fusion devices to put net fusion electricity onto the grid.

## Resources

- World Nuclear Association  
Descriptive material on fission energy technologies.  
<http://www.world-nuclear.org>
- International Institute for Applied Systems Analysis, Global Energy Assessment, chapter 14: Nuclear Energy.  
Critical evaluations of fission and fusion energy technologies.  
<http://www.iiasa.ac.at/web/home/research/Flagship-Projects/Global-Energy-Assessment/Chapte14.en.html>
- IAEA Nuclear Technology Review 2017  
Annual review of IAEA-related developments in nuclear technology.

[https://www.iaea.org/About/Policy/GC/GC61/GC61InfDocuments/English/gc61inf-4\\_en.pdf](https://www.iaea.org/About/Policy/GC/GC61/GC61InfDocuments/English/gc61inf-4_en.pdf)

- OECD-NEA/IAEA Uranium 2016: Production, Resources and Demand  
Generally semi-annual assessment of uranium production, resources and demand.  
<https://www.oecd-nea.org/ndd/pubs/2016/7301-uranium-2016.pdf>
- Joint Comprehensive Plan of Action  
Example of extreme constraints and safeguards applied to Iran.  
<http://www.state.gov/e/eb/tfs/spi/iran/jcpoa/>
- Climate Change, Nuclear Power, and Nuclear Proliferation: Magnitude Matters  
Assessment of proliferation risks associated with a large expansion of fission energy, possible role of fusion energy.  
R.J. Goldston, Science and Global Security 19:130–165, 2011  
DOI: 10.1080/08929882.2011.589223
- The World Scientific Handbook of Energy, G.M. Crawley, Editor, World Scientific, 2013, ISBN: 978-981-4343-51-0  
Assessemnt of many energy sources, including fission and fusion
- FUSION: Science, Politics, and the Invention of a New Energy Source, J.L. Bromberg, MIT Press, 1982  
History of the intertwined science and politics of fusion R&D through 1978
- A Piece of the Sun: The Quest for Fusion Energy, D. Clery, Overlook Duckworth, Peter Mayer Publishers, 2013, ISBN-13: 978-1468304930  
More up-to-date history of fusion R&D, with less emphasis on the pioneers.

### **Exercises**

- 1.1 The explosion of 1 kg of TNT is said to release 4.184 MJ of energy. This number is suspicious. Where do you suppose it came from? (Hint: If someone gave you a wooden cube whose edges were all exactly 2.54 cm long... would you suspect something about its time or place of manufacture?) Since the chemical formula for TNT is C<sub>7</sub>H<sub>5</sub>N<sub>3</sub>O<sub>6</sub>, what is its energy release, in eV, per nucleon?
- 1.2 When water goes from the top to the bottom of a water wheel and so loses 10 m in height, how much potential energy, in eV, is freed up per nucleon?
- 1.3 Methane is burned in the reaction CH<sub>4</sub> + 2O<sub>2</sub> → 2H<sub>2</sub>O + CO<sub>2</sub>. The

energy release is 55.2 MJ per kg of methane. How many eV are freed up per nucleon of methane? Per nucleon of methane + oxygen?

- 1.4 Derive the rule of (very nearly) 70, in the limit of small gain per generation. For what gain is the law precisely correct? How far is it off for gain that is twice that value? How far is it off for a gain of 10%?
- 1.5 In setting the priorities for a geological nuclear waste facility, how important do you think it is that spent fuel be recoverable, in order that the uranium and other actinides could be burned in the future? For how long should it be recoverable?
- 1.6 It has been reported that a Turkish consortium will invest 49% in the first nuclear power plant to be constructed in Turkey, by Russia. This is a modification of the basic BOO model. It is interesting that the IAEA does not list Turkey among the “newcomer” nations it is helping. There are reports that the Trump administration is offering to waive any requirement on Saudi Arabia to follow the UAE “gold standard” on enrichment and reprocessing, if Saudi Arabia pays U.S. corporations to construct the reactors it is planning. What do you make of these maneuvers?
- 1.7 Fusion question
- 1.8 Fusion question
- 1.9 Fusion question
- 1.10 Fusion question



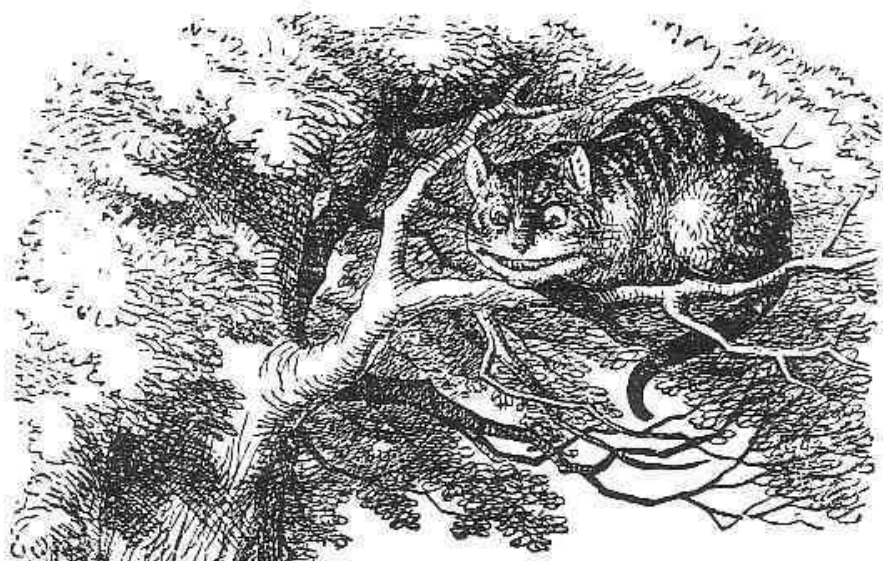
## **PART ONE**

### **FISSION**



## Chapter 2

### Neutron Interactions with Matter



“All right,” said the cat; and this time it vanished quite slowly, beginning with the end of the tail, and ending with the grin, which remained some time after the rest of it had gone.

---

Lewis Carroll, Alice’s Adventures in Wonderland

In this chapter we learn how neutrons interact with matter, such as hydrogen and uranium nuclei. For the most part we are interested in fission, absorption and scattering. But first we review the concepts of beam attenuation, mean free path, and reaction rate in a hard-sphere classical context. Then we explore some aspects of how the Alice-in-Wonderland effects of quantum mechanics play a role in nuclear physics, and finally we look at the specific nuclear processes of interest for producing nuclear energy from fission.

## 2.1 Cross sections

Consider a collection of small, hard spheres, say BBs, flying through a randomly distributed field of larger stationary billiard balls, as illustrated in figure 2.1. Let's say the radius of the BBs is 2 mm, and that of the billiard balls 30 mm. The projection of the billiard balls, along any angle, is of course a circle of radius 30 mm. However if the center of one the BB's is headed to within 32 mm of the center of a billiard ball, and nothing else happens first, they will collide. Thus we define the effective cross-sectional area for this collision, or effective collision cross section, as  $\pi \cdot 0.032^2 \text{ m}^2$ . The more general expression for hard-sphere collisions is  $\sigma = \pi(r_b + r_t)^2$ , where the BB's are denoted by subscript  $b$ , for a moving beam of particles, and the billiard balls are denoted by the subscript  $t$ , indicating a "target" of stationary particles. In nuclear reactor theory, this  $\sigma$  is called the "microscopic" collision cross section.

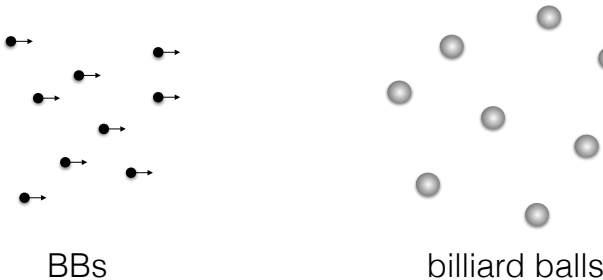


Figure 2.1 Small BBs flying into a field of larger billiard balls.

Now suppose that the density of billiard balls is  $N_t$ , with units  $\text{m}^{-3}$ . Consider that the billiard balls are very much further apart than their diameters, and they are randomly distributed in space. Randomly distribute the BB's as well. Furthermore, for mathematical simplicity, let us assume that the BBs are all flying precisely in the  $x$  direction. Now consider some differentially small incremental distance along their flight path amongst the billiard balls,  $dx$ . The meaning of "differentially small" is that differential values are as small as necessary to make any effects that vary as  $(dx)^2$  negligible as compared with those that vary as  $dx$ . The expected number of billiard balls in the volume formed by a differential area  $dA$ , in the  $y - z$  plane, and depth  $dx$  in the  $x$  direction, is just  $N_t dA dx$ . The sum of all of the cross-sectional areas of each billiard ball is  $N_t \sigma dA dx$ . If we can ignore the possibility that the projection on the  $y - z$  plane of the cross sections overlap, the fraction of the beam that will collide in length  $dx$ , and so be taken out of the unidirec-

tional beam of BBs, is given by the sum of the target cross-sectional areas, divided by the total differential area. Thus the probability of loss from the unidirectional beam in traversing distance  $dx$  given by,

$$P_{loss} = N_t \sigma dA dx / dA = N_t \sigma dx \quad (2.1)$$

So long as the fractional loss is sufficiently small, which can be achieved by making  $dx$  sufficiently small, as we have done by taking it to be differential, we can ignore overlaps. This is because an overlap amounts to two predicted collisions along a straight-line trajectory in the  $x$  direction, and so has probability  $(N_t \sigma dx)^2$ .

In nuclear reactor theory,  $N_t \sigma$  is called the “macroscopic” cross section of the target,  $\Sigma_t \equiv N_t \sigma_t$ , with units  $\text{m}^{-1}$ . You might wonder what to think about a target sphere that straddles the edge of a zone of  $dx$ . It doesn’t really matter; count it on one side or the other, just be consistent in how you do your counting and you will get the same macroscopic  $N_t(x)$  and so the same macroscopic result.

**Question:** What can happen if the billiard balls are arranged in an orderly pattern, rather than randomly?

## 2.2 Beam attenuation and mean free path

Now we are interested to know what happens to the density, which we denote  $n_b$ , of our beam of BBs as it travels through the field of billiard ball target particles. To construct a time-independent problem, consider that there is a constant source of beam particles entering the problem from  $x < 0$ . Using the argument we made in section 2.1, we can say that the fractional change of  $n_b$  in passing through a distance  $dx$  is given by  $dn_b/n_b = -\Sigma_t dx$  or

$$\frac{dn_b}{dx} = -\Sigma_t n_b \quad (2.2)$$

The solution to this equation is well known:

$$n_b(x) = n_0 e^{-\Sigma_t x} \quad (2.3)$$

where  $n_0$  is evidently the value of  $n_b$  at  $x = 0$ . If you are unfamiliar with this solution, you can check it simply by substituting it into equation 2.2.

We are going to find it useful to know the mean, or average, distance beam particles travel before they collide with a target particle. To find this we consider the average, over all the beam particles, of the distance they travel before they collide, which we will call the mean free path,  $\lambda_{mfp}$ . Consider that some differential chunk of beam density  $dn_b = \Sigma_t n_b dx$  collides in each

differential distance  $dx$  around location  $x$ . Multiply the differential chunk of beam density deposited near  $x$  by the local value of  $x$ . Integrating over all of these  $x$ -weighted differential chunks  $dn_b$ , and dividing by the integral of all of the chunks  $dn_b$  of beam density (without the factor of  $x$ ) gives us the average distance to collision for all of the beam particles.

$$\frac{\int_{n_0}^0 x dn_b}{\int_{n_0}^0 dn_b} = \frac{\int_0^\infty \Sigma_t x n_b dx}{\int_0^\infty \Sigma_t n_b dx} = \frac{n_0 \int_0^\infty \Sigma_t x e^{-\Sigma_t x} dx}{n_0 \int_0^\infty \Sigma_t e^{-x \Sigma_t} dx} \quad (2.4)$$

To make progress we need to integrate the numerator of the last term by parts, using

$$\int u dv = uv - \int v du; \quad u = \Sigma_t x; \quad dv = e^{-x \Sigma_t} dx; \quad du = \Sigma_t dx; \quad v = -e^{-x \Sigma_t} / \Sigma_t \quad (2.5)$$

giving us

$$\lambda_{mfp} = \frac{\int_0^{n_0} x dn_b}{\int_0^{n_0} dn_b} = \frac{n_0 \left( -xe^{-\Sigma_t x} \Big|_0^\infty + \int_0^\infty e^{-\Sigma_t x} dx \right)}{-n_0 e^{-\Sigma_t x} \Big|_0^\infty} = \frac{n_0 / \Sigma_t}{n_0} = \frac{1}{\Sigma_t} \quad (2.6)$$

### 2.3 Reaction rates

Sometimes we are interested in the rate at which collisions occur, rather than the distance over which they occur. A reaction with a given reaction rate coefficient is represented, not too surprisingly, by a “rate” equation:

$$\frac{dn_b}{dt} = -\nu n_b \quad (2.7)$$

where  $\nu$  is the reaction rate coefficient, in units of  $s^{-1}$ . We found  $dn_b/dx$  in equation 2.2, and we know that if we move along with the beam particles  $dx/dt = v_b$ , where  $v_b$  is the beam speed. Thus we can, if we like, consider beam attenuation in the framework of equation 2.7 by evaluating the time derivative of the density, traveling with the beam. This will give us the rate at which the beam particles with whom we are traveling are disappearing.

$$\nu = -\frac{1}{n_b} \frac{dn_b}{dt} = -\frac{1}{n_b} \frac{dn_b}{dx} \frac{dx}{dt} = \Sigma_t v_b \quad (2.8)$$

Since all of the particles are suffering the same loss rate as our traveling companions, this gives us an effective reaction rate coefficient  $\nu = \Sigma_t v_b$ .

On the other hand, if the underlying physics is fundamentally characterized by a rate coefficient  $\nu$ , which is independent of the beam velocity, we

can find an *effective* macroscopic cross section for the interaction,  $\Sigma_t$ .

$$\Sigma_t = -\frac{1}{n_b} \frac{dn_b}{dx} = -\frac{1}{n_b} \frac{dn_b}{dt} \frac{dt}{dx} = \frac{\nu}{v_b} \quad (2.9)$$

This result is identical to equation 2.8. Interestingly, we can now write

$$\sigma_t = \frac{\nu/N_t}{v_b} \quad (2.10)$$

So if  $\nu \propto N_t$ , then  $\sigma \propto 1/v_b$ .

As we will see this  $1/v$  dependence of microscopic nuclear cross sections is common at low energies, for reactions that proceed through neutron absorption. This is because the neutron absorption rate coefficient is generally independent of neutron energy at low enough energies, but still linearly dependent on the density of nuclei.

Another quantity of interest is the “volumetric reaction rate,” the number of collisions per unit time, per unit volume. Appropriately, this has units, in SI, of #/(s m<sup>3</sup>). By the physical argument that loss in beam density is exactly reaction density, we have simply for the volumetric reaction rate:

$$-\frac{dn_b}{dt} = \nu n_b = \Sigma_t n_b v_b = \Sigma_t \phi_b \quad (2.11)$$

where  $\phi_b \equiv n_b v_b$  will turn out to be very useful in fission reactor analysis. Note that we didn’t use the fact that the beam was traveling in the  $x$  direction in this analysis, so it could have been going in any direction. Indeed  $\phi_b$  could be composed of many beams traveling in all directions, each attenuating as it goes along. In particular  $\vec{v}_b$  could have been isotropically distributed. For all of these cases, the local volumetric reaction rate is just  $\Sigma_t \phi_b$ . When we have a range of neutron energies we will need to take into account the energy dependences of  $\Sigma_t$  and of  $\phi_b$ . Basically, this is the theme of Chapter 3. But first let’s learn something about the Alice-in-Wonderland world of atomic nuclei.

## 2.4 Elements of non-relativistic quantum mechanics

So far we have been working with BBs and billiard balls, at the familiar spatial scale of millimeters and centimeters. However, if we travel down to the quantum-mechanical world of nuclear physics, where cross sections are measured in barns ( $10^{-28}$  m<sup>2</sup>), things are more Cheshire-Cat like. First of all, according to the rules of quantum mechanics, particles are best understood as wave packets, composed of quantum wave functions,  $\psi$ , with mean wave

number  $k \equiv 2\pi/\lambda$  and mean angular frequency  $\omega \equiv 2\pi f$  given by

$$\begin{aligned}\vec{k} &= \vec{p}/\hbar \\ \omega &= E/\hbar\end{aligned}\tag{2.12}$$

where  $p_x$  is the particle momentum ( $\vec{p} = m\vec{v}$  in the non-relativistic range of  $v^2 \ll c^2$ ) and  $E$  is the total (kinetic + potential) energy of the particle. Both  $\omega$  and  $E$  are conserved as a particle / wave packet enters a potential well, but  $\vec{k}$  and  $\vec{p}$  are not.  $\hbar$  is Planck's constant divided by  $2\pi$ ,  $1.05 \cdot 10^{-34}$  J·s. The quantum wavelength is called the “de Broglie” wavelength, after Louis de Broglie who first proposed, in his 1924 Ph.D. thesis (!), that matter could have wave-like properties, just as light had been shown earlier by Einstein to have particle-like properties, through his study of the photo-electric effect.

**Question:** Albert Einstein was an antagonist of quantum mechanics, and yet he had been the first to show that light has particle-like characteristics. What did his analysis have to do with equation 2.12?

The simplest form for the quantum wave function,  $\psi$ , in free space is the planar solution with the spatio-temporal dependence:

$$\psi(x, t) = \psi_0 e^{i(k_x x - \omega t)}\tag{2.13}$$

where  $\psi_0$  is a complex constant. You might well ask, in the company of a great number of very smart people including Einstein, “*What is  $\psi$ ?*” The name “wave function” conveys little, and it doesn't help that  $\psi$  has an imaginary component. In quantum mechanics, we compute probabilities for what may happen, rather than make deterministic predictions. For example, if we want to know the probability that a particle will be found at a particular location  $x$  at time  $t$ , we use the quantum rule that the real function  $\psi^*(x, t)\psi(x, t)$  is the local probability density for finding the particle. (The “ $*$ ” superscript indicates a complex conjugate.) Integrating  $\psi^*\psi$  over a small range in  $x$ , we arrive at the probability that we will find the particle in that range. Similarly, the quantum formula for the probability density of  $x$ -directed momentum is  $-i\hbar\psi^*(x, t)\partial\psi(x, t)/\partial x$ .

A one-dimensional free-space wave packet localized in  $x$  can be constructed by superposing free-space planar wave functions, like equation 2.13, distributed continuously over a range in  $k_x$ . For example it is a well-known result from Fourier transforms that if we superpose a Gaussian-shaped distribution of waves with mean wavenumber  $k_{x,0}$  and root-mean-square deviation in  $k_x$ ,  $\sigma_{k,x} \equiv \langle (k_x - k_{x,0})^2 \rangle_{wp}^{1/2}$  (where  $\langle \dots \rangle_{wp}$  indicates the average over the wave packet) we get a spatially localized wave packet with  $\sigma_x \equiv \langle (x - x_0)^2 \rangle_{wp}^{1/2} = 1/\langle (k_x - k_{x,0})^2 \rangle_{wp}^{1/2}$ . Such a wave packet is shown in

figure 2.2. Evidently, just from the theory of Fourier transforms we have that  $\sigma_x \sigma_{k,x} = 1$ .

Now we know that probability density and momentum density are each proportional to the square of the amplitude of  $\psi$ , so they are each  $\sqrt{2}$  narrower than  $\psi$ , in  $x$  and  $\hbar k$  respectively (see exercise 2.3). This means that

$$\begin{aligned}\delta x &= \sigma_x / \sqrt{2} \\ \delta p &= \hbar \sigma_{k,x} / \sqrt{2}\end{aligned}\tag{2.14}$$

giving us Heisenberg's uncertainty principle, which expresses the relationship between the uncertainty in a particle's position and its momentum:

$$\delta x \delta p_x \leq \frac{\hbar}{2}\tag{2.15}$$

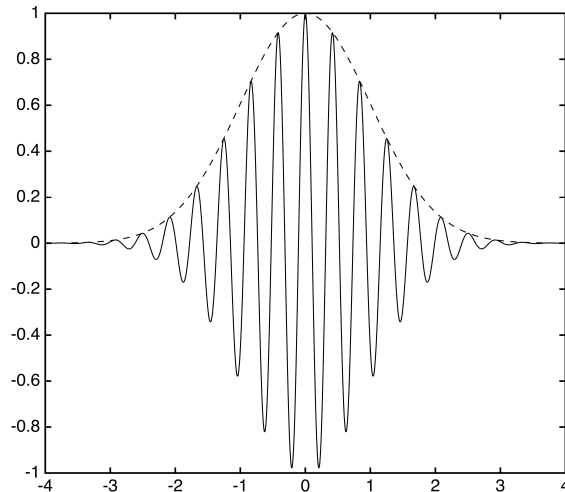


Figure 2.2 Wave packet. Solid line is  $\text{Re}(\psi)$ . Dotted line is  $|\psi| = \sqrt{\psi^*\psi}$ .

Now if we sum wave functions over an isotropic distribution of  $\vec{k}$ , distributed in a Gaussian way around  $\vec{k}_0$ , the spatial part of the wave-function dependence will form a nice spherical quantum fuzz-ball, as illustrated qualitatively in figure 2.3. This is the probability density of a particle produced or selected to be in a particular range of momentum: a mean value with equal uncertainty range in all directions.

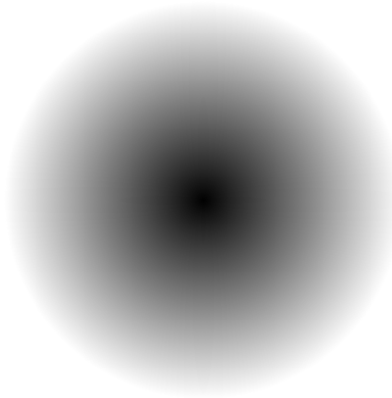


Figure 2.3 Representation of the quantum probability density of a particle.

## 2.5 Elements of nuclear physics

The first formulations of non-relativistic quantum mechanics were developed by Heisenberg and Schrödinger in 1925, and were immediately applied to understanding electron orbitals and energy levels in the electric potential well around nuclei. Then, as new experimental results emerged in the 1930's, these ideas began to be applied to the nucleus itself. To orient ourselves in this world, let us evaluate the neutron energies whose quantum mechanical wavelengths in free space equal some relevant physical sizes. We will use

$$\begin{aligned}\lambda_n &= 2\pi/k_n = h/p_n = h/\sqrt{2m_n E_n} \\ E_n &= h^2/(2m_n \lambda_n^2)\end{aligned}\tag{2.16}$$

where  $h$  is Planck's constant,  $6.63 \cdot 10^{-34}$  J·s, and the “ $n$ ” subscript stands for neutron. This equation is in SI units, so energy is in Joules.

The first observation we can make using table 2.1 is that inter-atomic spacings are typically sub-nanometer ( $1 \text{ nm} = 10^{-9} \text{ m}$ ) in scale, corresponding to number densities in the range of a few times  $10^{28}/\text{m}^3$ . This is comparable to the De Broglie wavelength of thermal neutrons. On the other hand, a thermal neutron's wavelength is vastly larger than nuclear diameters, which are measured in femtometers ( $1 \text{ fm} = 10^{-15} \text{ m}$ ), which are also called “Fermis,” in honor of Enrico Fermi. The wavelength of neutrons emitted by fission are in the range of nuclear diameters, since nuclear energies naturally correspond to neutron wavelengths that “fit” within a nuclear diameter, just as electron wavelengths “fit” within atoms.

Nuclei, however, are fundamentally different from atoms. They do not contain a concentrated central attractant, and the basic force holding nucle-

Table 2.1 *de Broglie wavelengths and Neutron energies*

Comparison	Distance = $\lambda_n$ (m)	Neutron Energy (eV)
Atomic lattice spacing, $\text{UO}_2$	$3.44 \cdot 10^{-10}$	$6.90 \cdot 10^{-3}$
Molecular spacing, $\text{H}_2\text{O}$	$3.10 \cdot 10^{-10}$	$8.50 \cdot 10^{-3}$
Atomic lattice spacing, U metal	$2.75 \cdot 10^{-10}$	$1.09 \cdot 10^{-2}$
Thermal neutron (1/40 eV)	$1.81 \cdot 10^{-10}$	$2.5 \cdot 10^{-2}$
Fission neutron (2 MeV)	$2.02 \cdot 10^{-14}$	$2 \cdot 10^6$
Nuclear diameter, U	$1.67 \cdot 10^{-14}$	$2.92 \cdot 10^6$
Nuclear diameter, O	$6.80 \cdot 10^{-15}$	$1.77 \cdot 10^7$
Nuclear diameter, H	$1.75 \cdot 10^{-15}$	$2.67 \cdot 10^8$

ons (neutrons and protons) together, the strong force, is very short-range. Since the 1970's we have known that the strong force is a manifestation of the color force that acts between the three quarks in a nucleon and "leaks out" to interact with the quarks in other nucleons, but we don't need to go to that level of analysis here. We just need to know that all nucleons attract each other, very similarly, through the strong force. On the other hand, protons repel each other through their positive charges. Furthermore, protons and neutrons – separately – obey Pauli's exclusion principle. You cannot have two neutrons in the same state, so you can have only two, with opposite spin, in each orbital. The same holds true, separately, for protons. One more thing: nuclear spin has a much stronger effect in nuclear physics than in atomic physics. The energetic coupling between spin and orbital angular momentum is relatively weak in atomic physics, giving rise to what is called "fine structure," but this effect is much bigger in nuclear physics. Similarly, the interaction between two nucleons depends very strongly on their spin, with stronger attraction for the same spin direction.

The two most basic, but insight-providing, approaches to understanding the nucleus are to consider it either as a set of orbital shells, like the atom, or to consider it as a drop of a very special nuclear liquid. These are called the "shell" and "liquid drop" models. The shell model can allow us to understand some puzzling features of nuclei quite simply. For example, why are there more neutrons than protons as the atomic number,  $Z$ , increases? Because of Pauli's exclusion principle, larger and larger radius orbitals become occupied with increasing  $Z$ . Meanwhile, however, the protons repel each other through

the long-range electrostatic force, so the attractive short-range strong force between nearby nuclei begins to be balanced by repulsion, with increasing size. It is obviously energetically favorable to fill up the same volume with neutrons as the proton orbitals, to strengthen the strong attraction without adding electrostatic repulsion. However, since the neutrons are not affected by the protons' electric field, they experience a deeper potential energy well at a given radius. As a consequence their wavelengths are shorter and their orbital shells are smaller. Thus more neutrons than protons can be packed into the same space. This effect grows as the long-range electrostatic repulsion competes more and more effectively with the short-range strong force, as the number of protons grows.

Another curious feature of nuclear physics that can be explained using the shell model is that nuclei with even numbers of protons or even numbers of neutrons are energetically favored compared to those with odd numbers. The most stable nuclei have even numbers of both. This is because of the strong spin-spin and spin-orbit couplings that favor even numbers. For example, when spin-spin coupling dominates, two spin up neutrons with equal but opposite orbital angular momenta constitutes a lower energy state than two neutrons with opposite spin with the same orbital angular momentum. When you have an even number of nucleons of a given type, the next one must occupy a significantly higher energy state, with unfavorable spin-orbit or spin-spin coupling.

A powerful result of the alternative *liquid-drop* model is its explanation of the curve of binding energy, seen in figure 1.1. The total negative potential energy in a nucleus can be seen as being dominantly composed of the strong attractive nuclear potential acting between neighbors, minus the long-range electrostatic repulsion between the protons. The strong-force attractive potential well is linear in the total number of nucleons, so long as all nucleons are fully surrounded by neighbors. This approximation breaks down of course for very small numbers of nucleons (as does the liquid drop model in general), but it also needs to be corrected for all of the nucleons near the surface of a large nucleus that have fewer neighbors, and so are less deeply bound. This corresponds to a form of nuclear surface tension, just like for a macroscopic drop of fluid; it takes more energy to have more surface, so the nucleus is forced to a near-spherical shape. By contrast the electrostatic repulsive anti-well goes as the atomic number,  $Z$ , squared, divided by the nuclear radius, since the electrostatic potential goes as  $1/r$ .

Together these do a good job of explaining why the potential energy well per nucleon grows at first, due to the falling fraction of nucleons near the surface, and then falls, due to the growing effect of electrostatic repulsion.

The most famous result of the liquid-drop model is that it shows why if you add enough vibrational energy to a nucleus, you can cause it to break apart, or fission, in analogy to the way that a drop of liquid can break up when its vibrational energy overcomes its surface tension. It is remarkable that this picture, which presupposes in its most primitive form a kind of localization of nucleons, like water molecules, works so well. There is a somewhat similar successful model for the electronic properties of high-Z atoms, in which bound electrons are also considered as forming a fluid. This was developed independently by Llewellyn Thomas and Enrico Fermi in 1927.

The empirical result that the radius of the charge density of a nucleus,  $r_{cd}$ , scales as the cube root of its nucleon number,  $A$ , is consistent with the liquid-like picture of the nucleon as well. It amounts to assuming a constant mass density, such as would be expected in an incompressible fluid like water. The strong nuclear force becomes repulsive at short enough distances, and together with the Pauli exclusion principle, sets this up.

$$r_{cd} \approx 1.35 \text{ fm} \cdot A^{1/3} \quad (2.17)$$

The energy states of neutrons in nuclei shown in figure 2.4 bear some resemblance to electronic states in atoms, but because the potential well,  $V(r)$  is closer to a square well than a  $1/r$  shape, and because of the strong effect of spin, there are some important differences. For example, unlike atomic states, the bound states of neutrons do not become arbitrarily densely packed near the transition to free states.

Furthermore, the wave function of a free neutron is partially reflected by the presence of the steep wall of the nuclear potential. If the neutron wavelength is just right, this can form a positive interference and so a “resonance” that can very strongly enhance the neutron probability density,  $\psi^*\psi$ , in the vicinity of the nucleus, even though the neutron is not energetically confined by the potential well of the nucleus.

Another interesting difference between atomic and nuclear physics is that the stable atomic numbers are different. The most stable atoms are the noble gases, helium, neon, argon, krypton, xenon and radon having  $Z = 2, 10, 18, 36, 54$  and  $86$ . However the most stable numbers of protons ( $Z$ ) and, separately, of neutrons ( $N = A - Z$ , where  $N$  is the number of neutrons) are the so-called “magic numbers”,  $2, 8, 20, 28, 50, 82$  and  $126$ . This difference between atomic and nuclear physics arises from the strong spin-orbit and spin-spin energy coupling of the strong force, that changes the locations of the bigger energy steps between different nuclei. At magic numbers of neutrons, taking away a neutron costs a lot of energy (it is very well bound

in the potential well), and adding a neutron gains less, since it is more lightly bound. The same holds for magic numbers of protons. As  $Z$  and  $A$  increase, both the bound and resonant states become more closely spaced, and narrower in energy. They take on the form of collective oscillations with rather long lifetimes, and so more well defined frequencies and therefore more well defined energies. (This arises from an uncertainty relationship between energy and time, similar to that between momentum and position.)

Here is an interesting question that follows from our discussion: why does the deuteron ( $Z = 1, A = 2$ ) exist, but not the di-neutron ( $Z = 0, A = 2$ ), despite the lack of electrostatic repulsion in either case? The answer is that the proton and neutron in a deuteron can each be in the ground state, and also have the same spin, and so strong mutual attraction. On the other hand, the two neutrons in a putative di-neutron cannot each be in the ground state and also have the same spin, due to the Pauli exclusion principle. The attractive potential energy well is not strong enough for even one bound state to be possible.

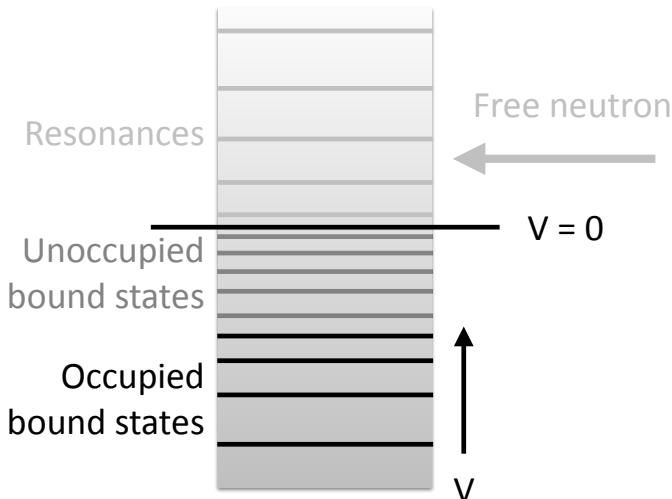


Figure 2.4 Energy states in the vicinity of a nuclear potential field,  $V$ .

There are two fundamental categories of ways in which free neutrons can interact with nuclei. In the first category, they interact internally with the nucleus. In this case they are *absorbed* and form an excited “compound nucleus,” which can then decay to its ground state by  $\gamma$  emission, and/or emit  $\alpha$  or  $\beta$  particles, or emit one or more neutrons. ( $\gamma$ 's are simply photons with MeV-range energy,  $\alpha$ 's are helium nuclei, two protons and two neutrons,

and  $\beta$ 's are electrons. Positrons or anti-electrons,  $\beta^+$ , can also be emitted.) Of greatest interest to us in the absorption category are fission and radiative capture of a neutron. In the latter case, the excess energy associated with a neutron falling into the potential well of a nucleus is radiated away in one or more  $\gamma$  rays.

In the second category of interactions, the neutron's wave function can be *scattered* from the external potential of a nucleus, not interacting directly with its core. This sends it off in a different direction without changing the internal state of the nucleus. Since no energy is transferred between kinetic and potential, this constitutes elastic scattering. Nonetheless, some kinetic energy is transferred to the originally stationary nucleus, so the neutron does lose kinetic energy. *Inelastic scattering* is strictly speaking absorption of the incoming neutron and emission of a neutron ( $n'$ ) at a lower energy, along with a  $\gamma$ , but it is nonetheless categorized in nuclear reactor physics as scattering, as shown in figure 2.5. The standard nuclear physics notation for the main interactions of interest to us are displayed in figure 2.5. The form is “(incoming particle, outgoing particle or particles)”. Fission is an exception, denoted with the letter “f”. The  $\gamma$  emitted in an inelastic collision is usually omitted, as here.

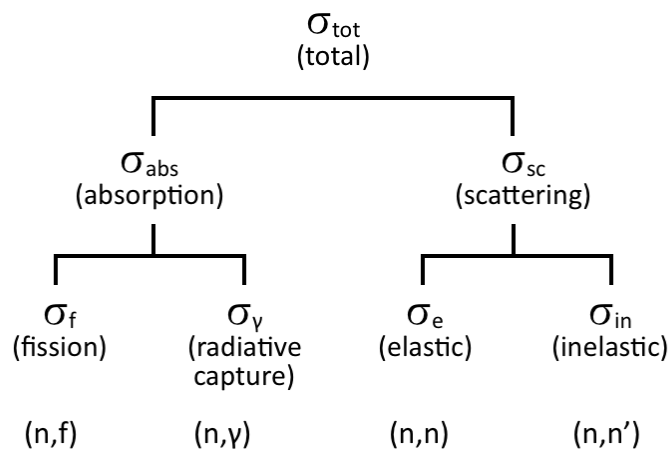


Figure 2.5 Primary neutron-nucleus interactions of interest in reactor physics.

Neutron absorption and scattering can be modeled using what is called the “cloudy crystal ball” model of the nucleus. The idea is that a neutron's wave function is diffracted as it enters the potential field around a nucleus just as light is diffracted as it passes from free space into a crystal with a non-unity

index of refraction. Just as with light, matching conditions are required at the surface, including the neutron wave-function entering the ball and exiting the ball. The “cloudy” feature, which corresponds to absorption, is modeled by including an absorption rate that acts to draw down the probability density within the nucleus. In this picture resonances naturally enhance both absorption and scattering, by greatly enhancing the probability density of the incoming neutron within, and in the vicinity of, the nucleus.

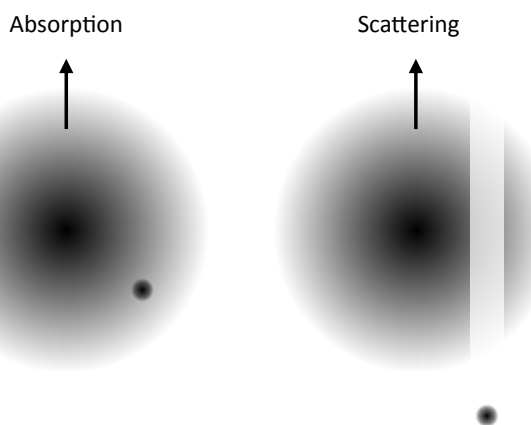


Figure 2.6 Mechanisms of absorption and scattering

The physics of neutron absorption is not well described by the classical cross section picture discussed in section 2.1; it is much more closely related to the discussion of reaction rate coefficients and resulting effective cross sections in section 2.3. The wave packet of a free neutron with thermal energy, or even keV energies, is much, much wider than the diameter of a nucleus, as shown schematically on the left-hand side of figure 2.6. During some or all of the time this wave packet passes through an absorbing medium, its probability density bathes one or more nuclei. So long as the neutron’s energy is far from any resonance, or so long as it is on a very broad resonance, the absorption rate is largely independent of the incident neutron velocity. A low-velocity incoming neutron’s wavelength within the nuclear potential well is determined dominantly by its new-found momentum within the well, corresponding to the MeV-range nuclear potential, not by its much lower free-space momentum. The reaction rate coefficient (equation 2.11) depends on the basic physics of the nucleus, the number density of nuclei (so the time-average number of nuclei within the neutron wavepacket), and the neutron probability density within those nuclei, but not on the free neutron veloc-

ity. As we saw in section 2.10 a reaction rate coefficient that is independent of velocity, but depends linearly on the target density, implies an effective cross section that varies as  $1/v$ . For higher energy neutrons, or in the case of narrow low-energy resonances, this  $1/v$  dependence is lost, but it is a remarkably common feature. At resonances, whether at low energies or higher ones, we see the strong effect of the high neutron probability density inside the nucleus.

Enrico Fermi won the 1938 Nobel Prize in physics for his discovery of new radioactive elements produced by neutron irradiation, and for his discovery that low-energy neutrons are absorbed by many nuclei much more efficiently than high-energy neutrons – to everyone’s surprise at the time. One day he took his neutron activation apparatus off of its customary marble table (it was Rome after all) and placed it on a wooden mantle piece. Suddenly the device made much more activation. This was due to collisions between neutrons and hydrogen nuclei in the wood, which slow the neutrons effectively through elastic collisions as we will discuss in the next chapter. When Fermi went to accept the Nobel Prize in Sweden in 1938, he took his family with him, including his Jewish wife, Laura. He traveled on to the U.S. with the prize money, thus escaping Fascist Italy and Mussolini’s new racial laws. He was a key player in the Manhattan Project to build the atomic bomb during WWII, but he fought against the decision to build the much more powerful hydrogen bomb (see Chapter 7). Lise Meitner’s nephew Otto Frisch made important contributions as well.

**Question:** After Meitner escaped from Germany in 1938, she found a job in neutral Sweden, working for 1924 Nobel Laureate Manne Siegbahn. However Siegbahn was uninterested in her work and provided her little support. In 1943 she was offered a senior position at Los Alamos, with her own research group and unlimited funds. And of course real security from the war. Despite the fact that many of her relatives had disappeared, and she had been forced to live as a refugee, she responded to the offer by saying, “I will have nothing to do with a bomb!” She said that nuclear physics was too beautiful to be used for making weapons. Meitner had seen the consequences of war very personally, having worked for her country, Austria, as a volunteer nurse and X-ray technician during WWI, on the Eastern front. And it was Austrian willing acceptance of German racial laws that forced her to flee to Sweden. Would you have made the same decision to shun work on a nuclear weapon? Even if you would not have, can you understand her decision?

Neutron *scattering* is more like classical scattering than neutron *absorption*, but it still has much of the Cheshire Cat about it. Now, again, the

neutron wave packet is much larger than the nucleus, at least at sub-MeV neutron energies. The nucleus only scatters away the fraction of the probability density contained in the wave packet that passes closest to it, typically at a distance from the center of the nucleus somewhat greater than  $r_{cd}$ . The efficiency of this scattering interaction is proportional to the volume of the cylinder it scatters from the wave packet, as shown on the right side of figure 2.6. This volume is given by the effective area of the neutron wave function scattered by the nucleus perpendicular to its direction of motion,  $\pi a_{sc}^2$ , times its average height. This is the ratio of the volume of the neutron wave packet to its own cross-sectional area:  $(4/3)a_{wp}$  for a sphere. The fraction of the wave packet probability density that is scattered away, which functions as a reduction factor against the geometrical cross section of the wave packet suffering scattering, is then given by:

$$f = \frac{(4/3)a_{wp}\pi a_{sc}^2}{(4/3)\pi a_{wp}^3} = \frac{a_{sc}^2}{a_{wp}^2} \quad (2.18)$$

so the *effective* cross section is just  $f\pi a_{wp}^2 = \pi a_{sc}^2$ , exactly what we would get in the classical case of infinitesimal BBs and finite billiard balls. In the sub-MeV energy range, far from resonances or on a broad resonance, scattering cross sections tend to be independent of energy. Just as with absorption, however, resonances can greatly increase the scattering cross section. For example the proton + neutron (= deuteron) system has a resonance very near  $E = 0$ , so hydrogen has a very large scattering cross section at sub-MeV energies. As we will see the large proton scattering cross section helps to make water a very important component of most modern fission reactors. Perhaps this is why the Cheshire Cat is grinning as it vanishes.

## 2.6 Fission

Let's return to the snowy woods in Sweden, in early 1939, with Lise Meitner and her nephew Otto Frisch. Fermi, in Rome, had been using neutrons to bombard his way up the periodic table, making both new stable and new radioactive nuclei, and had indeed struck uranium. But his chemistry was not good enough, and he had not recognized the fission fragments that emerged. As she was preparing to escape Germany, Meitner had encouraged Otto Hahn to repeat the uranium experiments, and to look more closely. He found unmistakable traces of barium. The nucleus had not been chipped, but split! And yet this was completely contrary to all previous experience. (The female German chemist, Ida Noddack, however, had suggested the possibility of fragmentation to explain Fermi's experiments. She was largely

ignored.) Sitting on a tree trunk in the snow, Meitner realized that while nuclear surface tension and electrostatic repulsion both reduce the strength of binding, the first resists deformation of the shape of the nucleus, since the surface area must grow with deformation, but the other favors such deformation, since like charges are given the opportunity to separate. It is as if the surface tension were decreased by the electric charge. She estimated that at  $Z \approx 100$  these effects would balance, causing large nuclei to be deformable and subject to shape oscillation!

But if a uranium nucleus could be excited into oscillation with a modest amount of energy, could it be split into two parts? She reasoned that if a uranium nucleus could break into two approximately equal parts, there would have to be, at some point along the way, two approximately half-mass and half-charge fragments separated approximately by twice their nuclear radius, as shown in figure 2.7. The electrostatic potential energy associated with this configuration would be

$$U = \frac{e^2 Z^2}{4\pi\epsilon_0(2r_{cd})} \quad (2.19)$$

You can understand this by imagining holding one fission fragment at  $x = -r_{cd}$  and moving the other in from  $x = \infty$  to  $x = +r_{cd}$ . There would be no work done on the stationary fragment, since for it  $Ze\vec{E} \cdot \vec{v} = 0$ , while equation 2.19 corresponds to the work required to bring the second one into place. When they fly apart, work is done by the electrostatic field on both.

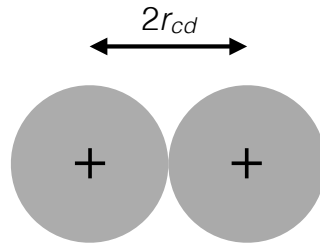


Figure 2.7 Cartoon of two fission-product nuclei “touching”.

**Question:** Calculate the electrostatic energy contained in the system shown in figure 2.7. Assume  $Z = 46$  and  $A = 117$  for each nucleus. Use equation 2.17 for the radii of the nuclei and the SI value  $\epsilon_0 = 8.85 \cdot 10^{-12}$ . Convert from the SI unit of Joules to electron Volts (eV) by dividing by the electron charge,  $e = 1.60 \cdot 10^{-19}$ . Your answer should be about 230 MeV.

So, asked Meitner and Frisch (brushing snow off their clothing), where

could this energy come from? Meitner knew that the binding energy per nucleon falls at the rate of about 1 MeV per nucleon in this range of atomic numbers (see figure 1.1). So just about the right amount of internal energy, 200 MeV or so, would be released by the formation of two half- $Z$  nuclei from a uranium nucleus. This internal energy could be transformed into external electrostatic energy as the nucleus oscillated. Talk about an “aha” moment!

Frisch rushed back to the lab and within a few weeks found the  $\sim$ 100 MeV fission fragments, clearly confirming Meitner’s understanding, about the same time as others around the world did this experiment. Soon it was also found that 2 to 3 neutrons “evaporate” out of the process during fission events, and it became clear to many physicists that a “chain reaction” might be possible, explosively releasing immense amounts of energy. As WWII began, nuclear physicists in America and Britain suddenly stopped publishing about fission. As Fermi put it, “Contrary to their traditions, they set up a voluntary censorship and treated the matter as confidential long before its importance was recognized by the government, and secrecy became mandatory.” Fermi, himself, was a leader of this effort. The unofficial silence about nuclear fission was noted by the Soviets, along with direct reports from British spies about efforts to look into atomic weapons.

Figure 1.2 shows the probability distribution of the neutrons that are produced by fission of uranium. Their average energy is 2 MeV, while their most probable energy is 0.72 MeV. Table 2.2 shows their average number per fission,  $\bar{\nu}$ , when fission is induced by thermal neutrons and also directly by fission neutrons themselves, for uranium and plutonium. An important feature of the overall fission process is that a very small fraction, less than 1%, of the nuclei that result from fission (“fission products”) produce energetic neutrons that are delayed by of order 10 seconds after the fission event itself. This delay, due to the chain of radioactive decays of the fission products, is very important for the controllability of fission reactors.

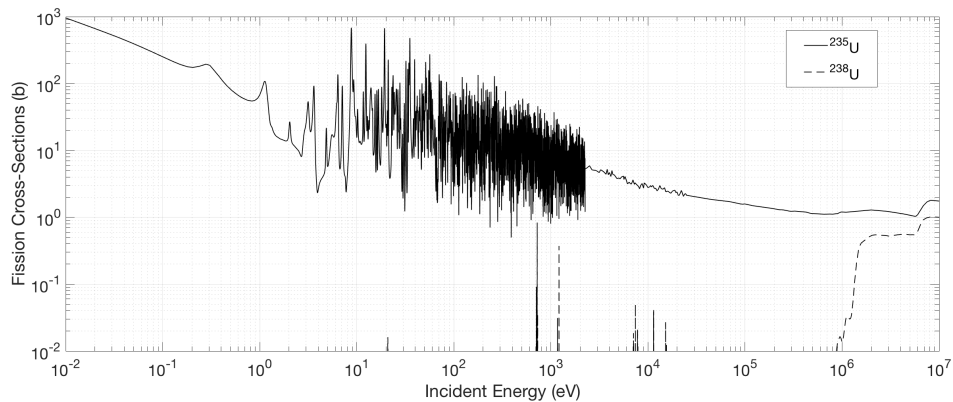
Years later, when Fermi was shown a sketch for the bas-relief to be placed over the entrance to the future Institute for Nuclear Studies at the University of Chicago, he suggested that it depicted a scientist “not discovering fission.” Hahn won the 1944 Nobel Prize in Chemistry for the discovery of fission. Many think that, as Bohr had recommended, Meitner should have won the Nobel Prize in Physics.

Now we are ready to look at fission cross sections for the nuclei of greatest interest to us,  $^{235}\text{U}$  and  $^{238}\text{U}$ , shown in figure 2.8. The  $x$ -axis represents neutron energy in eV. The  $y$ -axis represents cross-sectional area, in barns. 1 barn is  $10^{-28} \text{ m}^2$ . This is convenient, since number densities tend to be in the range of a few times  $10^{28}/\text{m}^3$ , so these large factors cancel in forming a

Table 2.2 Mean number of neutrons produced per fission event

Neutron Speed	Nucleus	$\bar{\nu}$
Thermal	$^{235}\text{U}$	2.44
Thermal	$^{239}\text{Pu}$	2.88
Fast	$^{235}\text{U}$	2.6
Fast	$^{238}\text{U}$	2.6
Fast	$^{239}\text{Pu}$	3.09

macroscopic cross section,  $\Sigma \equiv N_t \sigma$ . A cross section of a few barns, roughly characteristic of nuclear interactions in the MeV energy range, and a number density of a few times  $10^{28}/\text{m}^3$ , gives  $\Sigma \approx 10/m$ , so the mean free path is about 0.1 m, or 10 cm.

Figure 2.8 Fission cross sections vs. energy for  $^{235}\text{U}$  and  $^{238}\text{U}$ .

There are a lot of interesting features in these graphs that we can now understand. First of all, at low energies we see approximately a  $1/v$  dependence, as is expected because fission starts with absorption of a neutron. On log-log graphs of  $\sigma$  vs.  $E_n$ , such as this, a  $1/v$  variation shows up as a fall in  $\sigma$  by one order of magnitude for two orders of magnitude increase in  $E_n$ , since a factor of 10 increase in  $v$ , and so decrease in  $1/v$ , corresponds to a factor of 100 increase in  $E_n$ . Further up in energy we can see many narrow spikes, which are due to the resonances we have discussed, which concentrate neutron probability density at the location of the nucleus, through positive interference. (As you can see, there is also negative interference, where the

neutron probability density is depleted.) Perhaps most interesting, the fission cross sections for  $^{235}\text{U}$  and  $^{238}\text{U}$  are similar (but not entirely equal) above about 1 MeV, but the cross section for  $^{238}\text{U}$  is dramatically lower at low energies. This is because  $^{235}\text{U}$  has an *odd* number of neutrons, 143, while  $^{238}\text{U}$  has an *even* number, 146. When a low-energy neutron is absorbed into a  $^{235}\text{U}$  nucleus, the resulting  $^{236}\text{U}$  nucleus has an even number of neutrons. Conversely, when a  $^{238}\text{U}$  nucleus absorbs a low-energy neutron it has an odd number. A “new” neutron that can pair with an existing neutron drops into a lower energy state, and releases about 1 MeV more energy that can be invested into the deformation and ultimately fission of the nucleus. The  $^{238}\text{U}$  nucleus needs an extra MeV to arrive in the form of neutron kinetic energy in order to have a high probability of fission.

$^{235}\text{U}$  is called “fissile,” because it has a significant probability of fission by thermal neutrons.  $^{238}\text{U}$  is called “fissionable,” because, while it does not have a significant probability of fission by thermal neutrons, it can be fissioned by MeV-energy neutrons.  $^{239}\text{Pu}$  is also fissile, and  $^{240}\text{Pu}$  is fissionable, due to the same underlying physics as the uranium isotopes. Nuclei that produce fissile isotopes when they capture neutrons are called “fertile”. The most important for nuclear energy (and nuclear weapons) applications are  $^{238}\text{U}$ , which produces  $^{239}\text{Pu}$ , and  $^{232}\text{Th}$ , which produces  $^{233}\text{U}$ .

**Question:** Neptunium has  $Z = 93$ , and its most stable isotopes are  $^{236}\text{Np}$  and  $^{237}\text{Np}$ . Which do you think is fissile, and which fissionable?

When uranium fission occurs, about 211 MeV of energy, in all forms, is released. 9 MeV is in the form of anti-neutrinos, which are not stopped in the reactor. The remaining energy is almost all captured within the reactor core. 169 MeV is in the form of fission products (the nuclei that emerge from the fission process), which are stopped within the fuel pin where they are created. The neutrons that emerge from fission carry about 5 MeV of energy, and are mostly stopped within the reactor, while  $\gamma$ 's emitted during fission, almost all stopped within the reactor, carry about 7 MeV. Neutrons that are absorbed in the fuel and structure, without producing further fission, result in about 9 MeV of energy release, mostly in “capture  $\gamma$ 's” (see next section). Many of the fission products are unstable, and emit about 13 MeV of  $\beta$ s and  $\gamma$ s during their decay after the fission process. This is the “decay heat,” or “after-heat” that presents safety challenges.

To put this in macroscopic terms, fission of 1t of uranium or plutonium produces about 960 GWth-days of heat. Since a light-water fission reactor might be 35% efficient, and might run on average, counting refueling and maintenance periods, at 90% of its “nameplate” power (= 90% “capacity

factor”), such a reactor fissions about 1t of “heavy metal” (uranium or plutonium) per year. On the other hand, fission of 1 kg of heavy metal produces the same amount of energy as 17.8 kt of TNT, roughly equal to the yields of the weapons that destroyed Hiroshima and Nagasaki in WWII. The US-Russia “Megatons to Megawatts” program, that lasted from 1993 to 2013, involved down-blending 500t of Russian weapons-grade uranium,  $\approx 90\%$   $^{235}\text{U}$ , to reactor-grade,  $\approx 4\%$   $^{235}\text{U}$ , thus using the explosive material for about 18,000 nuclear weapons to produce fuel for about 450 reactor-years of power, roughly a quarter of US nuclear power production during that period.

There is one last interesting piece of the nuclear physics of fission that we should cover here. When  $^{235}\text{U}$  or  $^{239}\text{Pu}$  fissions due to capture of a thermal neutron, it does not produce many fission products with mass number in the range of 1/2 of the initial mass number, say 118. As shown in figure 2.9 the production is split between higher and lower masses. This is because of the particularly stable nuclei near the magic numbers 50 for protons and 82 for neutrons and, to a lesser degree, 50 for protons and 50 for neutrons. At higher incoming neutron energies the valley in figure 2.9 begins to fill in, since the energetic value of magic numbers becomes less important.

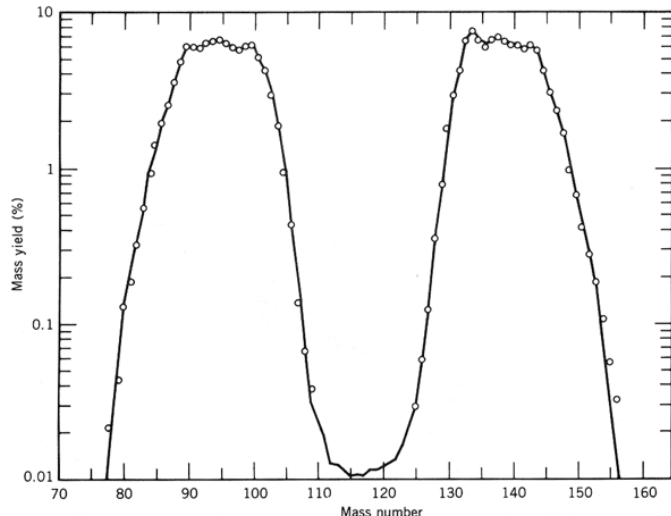


Figure 2.9 Probability of production of masses of fission products from thermal fission of  $^{235}\text{U}$ . The sum of probabilities is 200%, since two fission products are produced per event.

## 2.7 Radiative Absorption

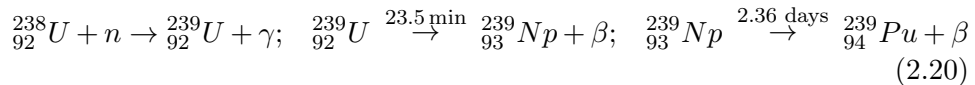
The type of radiative absorption of most interest to us is rather simple. A nucleus absorbs a neutron and becomes a new nucleus in an excited state, with atomic mass increased by unity, but retains its original atomic number. This nucleus then relaxes to its ground state by emitting one or more  $\gamma$  photons in the MeV energy range.

Radiative absorption is important for us in two neutron energy ranges. First, as neutrons slow down from their MeV birth energy range, they encounter sharp resonances in  $^{238}\text{U}$ , that lead to large spikes in the cross section for absorption, as shown in figure 2.10. The databases that are used to make these plots only track individual resonances up to a certain energy, above which the cross section is averaged over resonances. As you can see, the absorption resonances between about 5 and 500 eV dominate over the  $^{235}\text{U}$  fission cross section in the same range, as shown in figure 2.8. This dominance is amplified by the fact that the  $^{235}\text{U}$  enrichment in a fission power reactor is typically only in the range of 4%, meaning that there is 24 times more  $^{238}\text{U}$  than  $^{235}\text{U}$  nuclei. Secondly, radiative absorption by  $^{238}\text{U}$  and, to a lesser degree  $^{235}\text{U}$ , competes at low energy with fission. The  $1/v$  region  $^{238}\text{U}$  absorption cross sections is much smaller than that for fission of  $^{235}\text{U}$ , but again we must remember that there is much more  $^{238}\text{U}$  than  $^{235}\text{U}$  around.

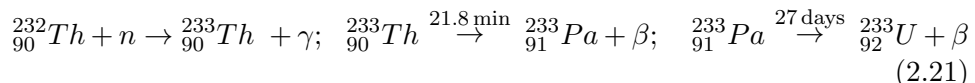
Radiative absorption by  $^{238}\text{U}$  plays a key role in the neutron economy of uranium-based fission reactors, as it removes neutrons from the steady chain reaction necessary to sustain power production. We will discuss this in some detail in Chapter 3. On the other hand, radiative absorption also results in build-up of  $^{239}\text{Pu}$  in a uranium-fueled reactor, which is fissile, and functions as additional fuel. Thus while it hurts the short-term neutron economy of the chain reaction, it helps the long-term fuel economy of the reactor. Depending on parameters, about 1/3 of the energy produced in a LWR may come from the built-up  $^{239}\text{Pu}$ , about making up for the fact that about 1/3 of the initially supplied  $^{235}\text{U}$  does not undergo fission.

In uranium/plutonium “fast breeder” reactors, in which the neutrons are not slowed down to thermal energies, but remain “fast”, the goal is to make more fissile material than is burned, by transmuting  $^{238}\text{U}$  to  $^{239}\text{Pu}$  using neutrons predominantly in the range of  $\sim 100$  keV. It is also possible to breed  $^{233}\text{U}$  from  $^{232}\text{Th}$ , potentially creating a thorium-based fuel cycle. This is in principle achievable even with thermal neutrons. The reaction chains

for these two processes (neglecting anti-neutrino production) are



and



Resonant radiative absorption is also important for the stability of fission reactors. As we will discuss in Chapter 3, there is a Doppler broadening effect that increases radiative absorption as fission fuel heats up. This contributes self-regulation to a fission reactor.

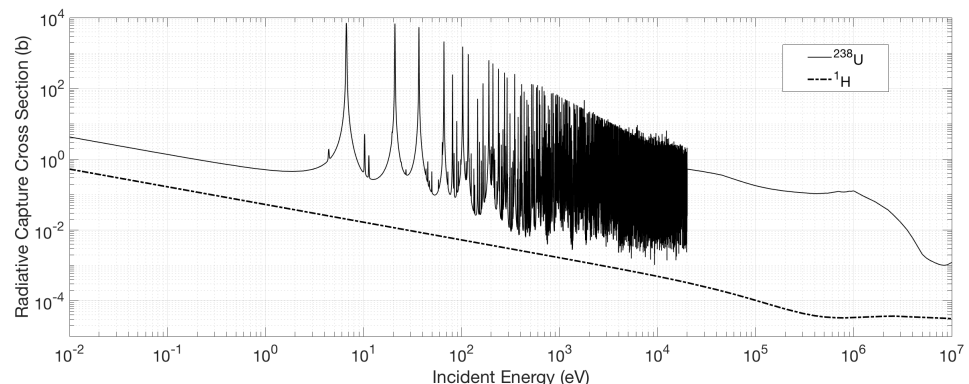


Figure 2.10 Cross sections for radiative absorption of neutrons by  $^{238}\text{U}$  and by protons,  $^1\text{H}$ .

When neutrons slow down to thermal energies,  $1/v$  radiative absorption becomes important in  $^{238}\text{U}$  as discussed above, and to a lesser degree in  $^{235}\text{U}$ . It also becomes important in the elements composing the moderator (the material that slowed the neutrons down in the first place) and in the structural materials that make up the reactor. For a light-water reactor, the dominant absorption is by the hydrogen in the moderating water, whose cross section is also shown in figure 2.10. This absorption is greatly enhanced by the broad resonance of the D-H system (the deuteron) near zero binding energy. Deuterium, oxygen and carbon have  $1/v$  neutron absorption cross sections that are 100 to 1000 times smaller than hydrogen's. This is why heavy water ( $\text{D}_2\text{O}$ ) and graphite can be used as moderators for natural uranium, but light water requires enriched uranium. You do, however, have to be careful about impurities, especially boron in graphite moderators, due to its large  $(n, \alpha)$  cross section.

Finally, neutrons also interact with Pu and fission products as they build up in the reactor core during operation. Pu can undergo fission, and both Pu and fission products are targets for radiative absorption. Pu has the interesting property that as it absorbs neutrons and climbs up from  $^{239}\text{Pu}$  to  $^{240}\text{Pu}$  to  $^{241}\text{Pu}$  to  $^{242}\text{Pu}$ , it goes back and forth from fissile to fissionable. The  $^{135}\text{Xe}$  fission product has an immense radiative absorption cross section of two million barns at thermal energy, so it has a significant effect on reactor operation. As we will see, it has to be managed carefully. Mismanagement of  $^{135}\text{Xe}$  contributed to the Chernobyl accident.

## 2.8 Elastic and Inelastic Scattering

Neutrons can also scatter in angle when they encounter target nuclei. While the internal state of the target nucleus and of the neutron do not change in elastic scattering, in the lab frame the target nucleus does gain kinetic energy as it recoils in an elastic collision, so the neutron loses kinetic energy.

Elastic scattering involves reflection of some of the neutron wave-function off of the nuclear potential, as shown schematically on the right-hand side of figure 2.6, and discussed there. In general, elastic scattering cross sections on light nuclei are independent of the incoming neutron energy over a wide range. This is because the kinetic energy of the neutron within the nuclear potential is far dominated by the depth of the potential well of the nucleus, and the resonances of light nuclei are both broad and spaced well apart. Due to a broad resonance of the deuteron, just above zero energy, hydrogen has a very large scattering cross section, indeed much greater than that of oxygen, as shown in figure 2.11. Since  $r_{cd}$  of the oxygen nucleus is much greater than that of the proton, this illustrates again the power of a resonance. This is such a powerful effect that the mean free path of sub-MeV energy neutrons in light water is in the range of 1cm, rather than the 10 cm for neutrons in most materials.

Notice that over much of the slowing-down range of neutrons, from birth at  $\sim 2$  Mev to thermal energy, the scattering cross sections for hydrogen and oxygen are roughly independent of energy. Again this is because the process is not one of *absorption*, which is characterized by a rate coefficient associated with simply being in the presence of absorbing nuclei; it does not care if a neutron is passing by or standing still. Instead this is *scattering* (albeit quantum-mechanical), which depends on passing target nuclei, and scattering away probability density at each such encounter. In this case the number of encounters per unit distance is what matters, just as in classical scattering, so the effective cross section tends to be independent of energy.

Both reactions, of course, depend linearly on the target density. At the highest energies shown the nuclear structures come into play. The broad resonance of the deuteron system tails off, and the resonance structure of the  $^{17}\text{O}$  nucleus becomes visible. The cross sections increase at the lowest energies also. There are effects associated with the fact that the nuclei are bound in molecules, and with scattering off of more than one nucleus at a time. However the cross section variation shown in these data libraries arises from the fact that at low enough neutron energies the rate of encounter between neutrons and nuclei depends only on the motion of the target nuclei, and is independent of the neutron motion – giving the same  $1/v$  variation as typically characterizes absorption. Indeed if you were to expand these plots to even lower energies you would see a clear  $1/v$  variation at very low energies. In these plots the thermal target motion is assumed to correspond to 293° K.

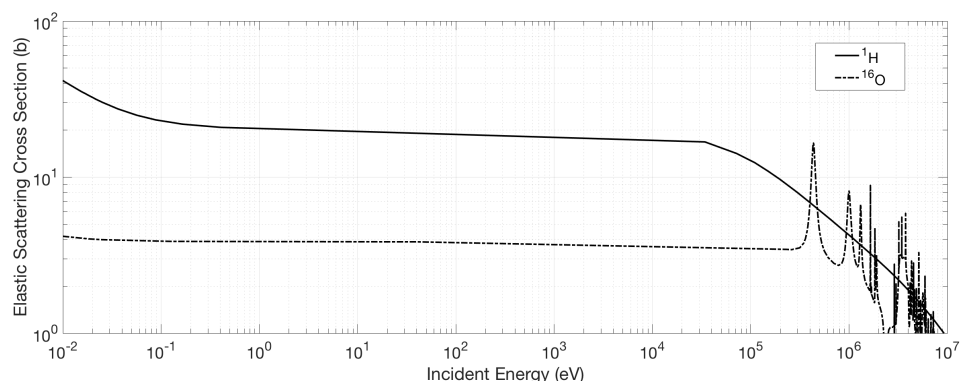


Figure 2.11 Cross sections for elastic scattering of neutrons by protons,  $^1\text{H}$ , and oxygen nuclei,  $^{16}\text{O}$ .

For heavy nuclei, resonances are closely spaced and narrow, and play a role in elastic scattering, as can be seen in figure 2.12, because the neutron wave function is amplified in the region of the nuclear potential. Generally scattering is maximum close to an absorption resonance peak, and – interestingly – is reduced below the peak. This is because the wave function within the nucleus at these energies has a low value near its edge, and so little of the neutron probability density is radiated way. If you smooth the elastic scattering cross section shown in figure 2.12 over the resonances it is  $\sim 15\text{b}$  from 1 keV to where it begins to fall off in the high-energy range.

Inelastic scattering is really a form of absorption of an energetic neutron, formation of an excited state of the target nucleus, followed by emission of

a  $\gamma$  and a neutron of lower energy. In the energy range of interest to us, inelastic scattering is only available for mid-range to heavy nuclei. Inelastic scattering on U reduces the neutron energy to a mean value of (very roughly)  $\sim (E_{Mev}/12)^{0.5}$  MeV, for the majority of fission-energy neutrons. It has a threshold around 45 keV, as shown in figure 2.12. In the energy range below 500 keV, the main excited state that is produced is the lowest, at about 45 keV, so the energy loss is about 45 keV per inelastic collision.

Inelastic scattering is not available in the case of the proton and deuteron, since neither has any bound, excited states.

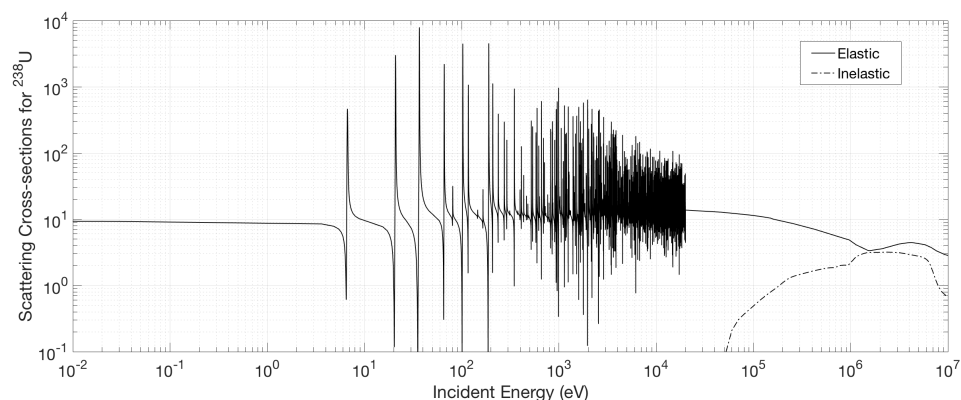


Figure 2.12 Cross sections for elastic and inelastic scattering of neutrons by  $^{238}\text{U}$ .

## 2.9 Try This at Home

There are many places to access nuclear data on line. Each has different advantages and disadvantages. But in all cases it is interesting to use these tools to get a feel for the physics. Here is a bit of a curated list. All of these let you download the data from which plots are made, if you want to plot or manipulate the data yourself.

- <https://www-nds.iaea.org/exfor/endf.htm>  
A bit of a bare-bones interface, but it does let you download figures. You have some control over the formatting; not all of the controls work.
- <http://www.nndc.bnl.gov/sigma/index.jsp?as=10&lib=endfb7.1&nsub=10>  
A simpler interface, but it doesn't let you (on a Mac) download plots except as screen shots. It lets you overlay different cross sections and it lets you do numerical manipulations on the "Plot Cart" data. This is my

“go-to” website. I downloaded the data for the plots in this chapter from here.

- <http://www.oecd-nea.org/janis/>  
A nice interface, and very nice plots. The JAVA version lets you download nice plots. The “books” that are available here are for comparison with experimental data.
- <http://atom.kaeri.re.kr/nuchart/>  
A nicer-yet interface, but doesn’t let you download plots except as screen shots. A unique feature of this interface is that it assumes zero thermal motion of the target nuclei.

You might as well use the latest US library, ENDF/B-VII.1 as of this writing. The ENDF library, and the different interfaces to it have a special language. For the IAEA interface, you need to know that the target nucleus is specified, for example, as U-235. You also need to know that for the cross sections listed below you use SIG for “Quantity.” For average neutron production per fission event you leave “Quantity” blank.

In the ENDF formatting the neutron-nucleus reactions are classed as Incident-Neutron Data, with specific reactions:

- Fission: N,F (#18)
- Radiative absorption: N,G (#102)
- Elastic scattering: N,EL (#3)
- Inelastic scattering: N,INL (#4)
- Average total, prompt plus delayed, number of neutrons released per fission event: N,nu\_tot (#452)
- Average number of delayed neutrons released per fission event: N,nu\_d (#452)

Note that N,NON (#3), “Nonelastic neutron cross section” is just the total cross section, including all interactions, minus the elastic scattering cross section. You can show this by summing N,NON + N,EL to get N,TOT.

## Resources

- “Lise Meitner, a Life in Physics,” Ruth Lewin Sime, University of California Press, Berkeley and Los Angeles, London, 1996
- “Enrico Fermi, Physicist,” Emilio Segre, University of Chicago Press, Chicago and London, 1970
- “Introductory Nuclear Physics,” Kenneth S. Crane, John Wiley and Sons, Hoboken NJ, 1988

- “The Elements of Neutron Interaction Theory,” Anthony Foderaro, MIT Press, Cambridge MA and London, 1971

### Exercises

- 2.1 Write a little Monte-Carlo code to check our derivation of the mean free path, and to evaluate the root-mean-square free path, which you will also derive analytically. This will become an element of your future Monte-Carlo studies.

Start by setting up an array of perhaps 10 million neutrons. Imagine that these neutrons are located at  $x = 0$  and are about to be launched in the  $+x$  direction. Evidently, in order to represent our physical situation, you will have to select how far each of these neutrons should go before suffering its first collision. We know from equations 2.2 and 2.3

$$dn_b = -n_0 \Sigma \exp(-\Sigma x) dx \quad (2.22)$$

We need to translate this into a differential probability,  $dP$ , that a neutron originating at  $x = 0$  will suffer its first collision in a differential range  $dx$ . Physically, this probability corresponds to the fraction of the initial neutrons born at  $x = 0$  that first collide in the range  $dx$ .

$$dP = -dn_b/n_0 = \Sigma \exp(-\Sigma x) dx \quad (2.23)$$

We can integrate this result  $dx$  to find the probability that a neutron suffers its first collision before a given distance,  $x$ :

$$P(x) = \int_0^x \Sigma \exp(-\Sigma x') dx' = 1 - \exp(-\Sigma x) \quad (2.24)$$

Reasonably, the probability of a first collision before  $x = \infty$  is unity. We will find it useful to invert this equation to solve for  $x$  as a function of  $P$ :

$$x(P) = -\frac{\ln(1 - P)}{\Sigma} \quad (2.25)$$

Now here is where the Monte-Carlo magic comes into play. Select  $P$  for each neutron as a random number with equal probability over the range  $0 < P < 1$ , and use equation 2.25 to solve for  $x(P)$ , for each neutron. This procedure, of course, gives equal likelihood for each range of  $dP$  situated between 0 and 1. The varying range  $dx$  that corresponds to each equal differential element of probability,  $dP$ , is then populated with equal total probability, as it should be. Figure 2.13 illustrates that the width of  $\Sigma dx$  varies with  $x$  for fixed  $dP$ . Since  $\Sigma$  is assumed constant

over space, evidently  $dx$  is varying. In particular the fixed probability  $dP$  is distributed over a wider range of  $dx$  as the beam of neutrons is attenuated, so physically the local collision rate is reduced.

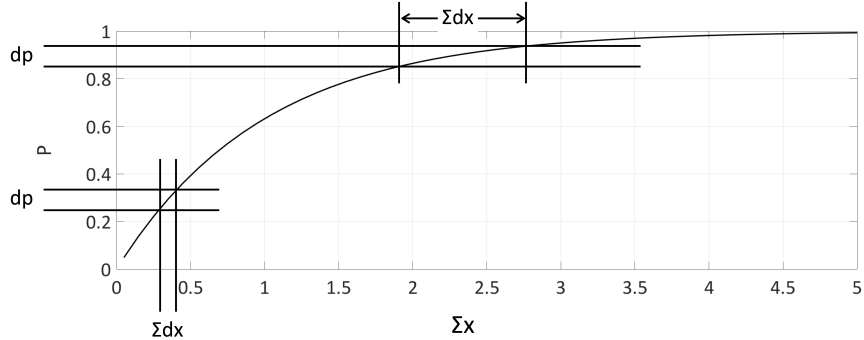


Figure 2.13 Varying ranges of  $\Sigma dx$  corresponding to different but equal-sized ranges of  $dP$  along the curve  $P(\Sigma x)$ .

So, go ahead and produce 10 million random numbers between 0 and 1. Select a single value for  $\Sigma$  for all of neutrons and find the different values for the neutrons' first collision positions,  $x_c$ . Histogram the positions you found from  $x = 0$  to, say,  $10/\Sigma$ , and show that it has the shape you expect. This is easiest using a semi-log plot. The result should reassure you that your method is working. Where do you see the highest noise/signal ratio on your plot? Why?

Now find the mean value of the first-collision positions,  $\langle x_c \rangle$ . Does it agree with our analytic result, equation 2.6? Now find the root-mean-square value of the positions,  $\sqrt{\langle x_c^2 \rangle}$ . How does this compare with the mean value? Calculate the root-mean-square value analytically, using equation 2.4 as the model:

$$\langle x_c^2 \rangle^{1/2} = \left( \frac{\int_{n_0}^0 x^2 dn_b}{\int_{n_0}^0 dn_b} \right)^{1/2} \quad (2.26)$$

You will need to integrate by parts twice! Show that your numerical result agrees with your analytic calculation.

You are taking the mean of 10 million independent, unbiased, but individually lousy estimates of  $\langle x_c \rangle$ . By the rule for the error of the mean, the fractional statistical error in your result should be  $\sqrt{10^{-7}} \approx 0.03\%$ . Is this about the reproducibility that you find when you run your code repeatedly?

## 2.2 Radioactive decay is characterized by a rate equation of the form of

equation 2.7. Consider a large group of nuclei, of a specified isotope, undergoing radioactive decay. Express the mean lifetime of these nuclei in terms of  $\nu$ . What is the mean time at while 1/2 of these nuclei will have decayed? This latter is called the “half-life” of these nuclei. How is it related to the mean lifetime?

- 2.3 Confirm that  $\sigma_x \sigma_{k,x} = 1$  by checking a table of Fourier transforms. Next show that the momentum density in a planar wave function is  $\hbar k \psi^* \psi$ . Now show that if  $\psi(x, t)$  is given by equation 2.13, then  $\psi^* \psi = \psi_0^* \psi_0 = |\psi_0|^2$ . Finally show that if  $g \propto f^2$ , and  $f$  has a Gaussian shape, then  $g$  also has a Gaussian shape with  $\sigma_g = \sigma_f / \sqrt{2}$ .
- 2.4 Los Alamos, New Mexico was selected for the design and construction of nuclear weapons during WWII because General Groves, who managed the whole Manhattan Project, wanted an out-of-the-way location. J. Robert Oppenheimer, who was the Scientific Director of Los Alamos during the war, had attended a private high school there and loved the region. The local residents were ranchers; it is too dry for farming. Presumably this is why the physicists who gathered there chose to measure cross sections in “barns,” as in the expression, “You could not hit the broad side of a ...” Less well known is their unit of time, the “shake”,  $10^{-8}$ s, or 10 ns, presumably honoring the tails of the local lamb population. This is roughly how long it takes a 1 MeV neutron to drive fission in uranium metal. Least well known is the fact that the scientists developed a short-hand code for referring to the fissile and fissionable nuclei of most interest to them, as shown in Table 2.3.

Table 2.3 *Los Alamos Code*

Type	Code Name	Nucleus
Fissile	25	$^{235}\text{U}$
Fissile	49	$^{239}\text{Pu}$
Fissionable	28	$^{238}\text{U}$
Fissionable	40	$^{240}\text{Pu}$

Explain the code and give the code name for  $^{236}\text{Np}$ . What about  $^{237}\text{Np}$ ? Show which one is fissile and which fissionable using the one of the tools for accessing the online ENDF data base. Explain why.

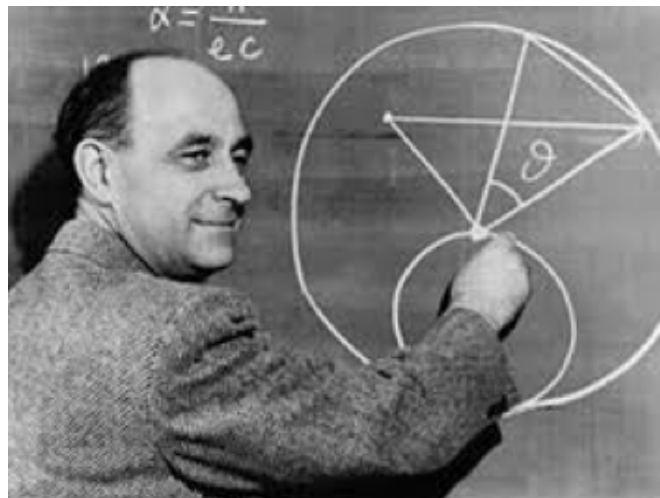
- 2.5 Show how the two fission products that Lise Meitner visualized as touching each other, as in figure 2.7, turn their electrostatic potential energy into kinetic energy. Imagine that the right-hand fission product

starts at location  $x = x_1 > 0$  at time  $t = t_0$ , and the left-hand product starts at  $x = x_2 < 0$  at the same time. Evaluate their acceleration as a function of  $x_1 - x_2$ . Now multiply the acceleration of the right-hand product by  $m_1 v_1$  and the acceleration of the left-hand by  $m_2 v_2$ . Summing these together you have the time derivative of the total kinetic energy. Show that integrating this from  $t_0$  to  $\infty$  gives a kinetic energy equal to the original electrostatic potential energy.

- 2.6 Reproduce the hydrogen scattering cross section shown in figure 2.11 using the IAEA and KAERI interfaces to the ENDF/B-VII.1 library. They are very different at extremely low energies. Why?
- 2.7 Use the IAEA and KAERI interfaces to the ENDF/B-VII.1 data library to examine a resonance of your choosing from the left-hand side of figure 2.10. Show that the two interfaces give quite different results. Estimate the thermal velocity of a  $^{238}\text{U}$  nucleus at 293° K. How much does this change the neutron energy, in the frame of reference of the nucleus? Does this roughly explain the difference?

## Chapter 3

### Neutron Energy Distribution



Indeed the neutrons produced by a primary fission must be used very sparingly in order to keep a positive surplus in spite of the loss due to the large parasitic absorption of U-238. Great care must be exerted in order to make the balance between useful and parasitic absorption of the neutrons as favorable as possible. Since the ratio of the two absorptions depends on the energy of the neutrons and, aside from details, is greater for neutrons of low energy, one of the steps consists in slowing down the neutrons from their initial high energy, which is of the order of 1 MeV, to an energy as low as that of thermal agitation. A simple process to achieve this end has been known for some time. It is based on the fact that when a fast neutron collides against an atom some of its energy is lost as recoil energy of the atom. The effect is greatest for light atoms which recoil more easily and is maximum for hydrogen but quite appreciable for all light elements.

---

Enrico Fermi, Proceedings of the American Philosophical Society,  
Read November, 1945

In this chapter we will learn how the MeV neutrons produced in fission lose energy by colliding with light nuclei in a reactor, and eventually at low energies themselves drive fission through the strong  $1/v$  variation of the

fission cross-section. They transfer from the Fast energy region, above about 1 MeV where it is possible to drive fission of  $^{238}\text{U}$ , through an Intermediate energy region, down to about 1 eV, and finally to the Thermal region where the neutrons have energies characteristic of their thermal environment. This history governs the neutron “lifecycle,” which of course requires each fission neutron to reproduce, on average, exactly one new fission neutron during its lifetime, in order to sustain the reaction at a constant level. We will also look briefly at so-called “fast” reactors, in which the neutrons only slow down to the energy range of some hundreds of KeV, dominantly due to inelastic collisions.

### 3.1 Energy change in elastic scattering

Let us start by examining how neutrons lose energy in elastic collisions, due to the kinetic energy invested in the recoil of target nuclei. As we will see, this process is dominated by collisions with light nuclei. The cross-sections for such collisions (see figure 2.11) can be approximated as independent of energy over a fairly wide range of interest for fission neutrons slowing down to thermal energies.

Consider figure 3.1 showing a neutron-nucleus collision in the lab frame. If we are taking a macroscopic perspective like this, we can consider the neutron and target nucleus as point particles. We assume that before the collision we have a neutron moving with speed  $v_0$  and a stationary target nucleus. After the collision the neutron scatters off at some angle  $\psi$  from its original trajectory, with speed  $v_1$ . The nucleus, of course, recoils, but we will not need to calculate its recoil speed.

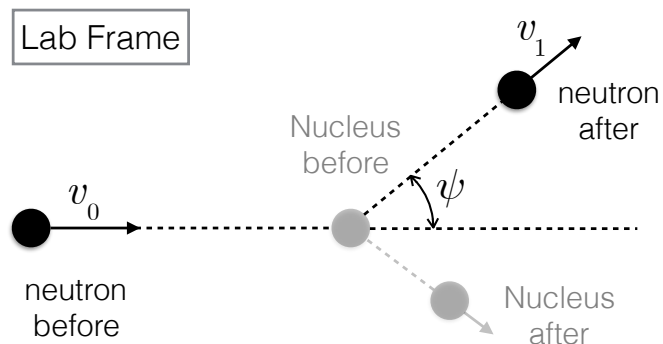


Figure 3.1 Diagram of a neutron-nucleus collision in the lab frame.

In all of our calculations we will assume that the mass of the neutron

can be adequately approximated as a single atomic mass unit, 1u, while the mass of the nucleus can be taken as  $A$ u. Since  $1\text{u} = 1.66 \cdot 10^{-17} \text{ kg} = 931 \text{ MeV}/c^2$ , we can ignore relativistic effects for our neutrons with at most a few MeV of kinetic energy. In general, the accuracy of the approximations we will be making does not justify greater precision than this. The center of mass of the neutron-nucleus system is located at

$$\vec{x}_{CoM} = \frac{A\vec{x}_N + \vec{x}_n}{A + 1} \quad (3.1)$$

where the subscript “N” denotes the target nucleus and “n” denotes the neutron.

The time-derivative of the position of the center of mass (its velocity) follows from the velocity of its components:

$$\vec{v}_{CoM} \equiv \dot{\vec{x}}_{CoM} = \frac{A\dot{\vec{x}}_N + \dot{\vec{x}}_n}{A + 1} = \frac{\vec{v}_0}{A + 1} \quad (3.2)$$

By conservation of momentum, proportional to  $A\dot{\vec{x}}_N + \dot{\vec{x}}_n$ , we can see that the center-of-mass velocity must be conserved, and in particular must be equal before and after a collision.

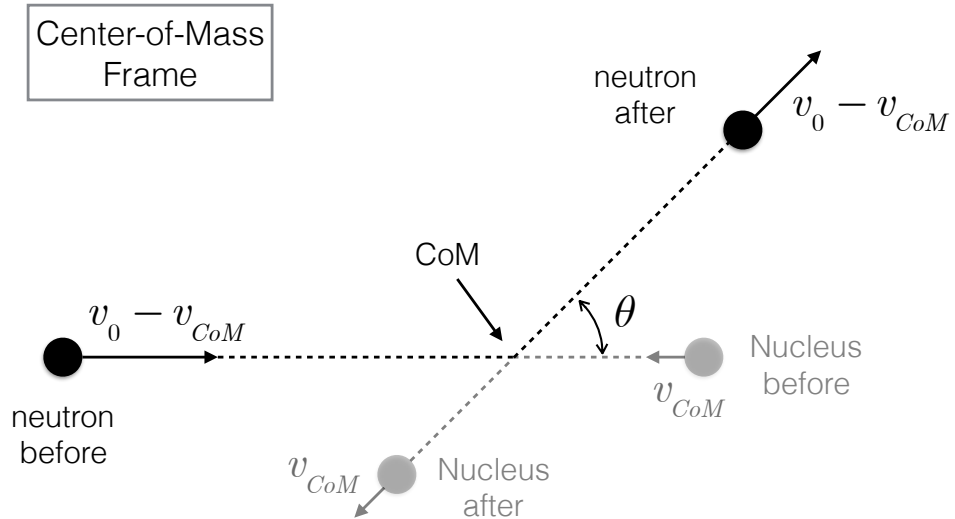


Figure 3.2 Diagram of a neutron-nucleus collision in the center-of-mass frame.

Conservation of  $v_{CoM}$  suggests that it may be convenient to transfer to the center-of-mass frame. In our non-relativistic conditions, to determine velocities in the center-of-mass frame given velocities in the lab frame, we

simply subtract the velocity of the center of mass,  $\vec{v}_{CoM}$ , equation 3.4. Thus the incoming velocity of the neutron in the CoM frame is given by

$$\vec{v}_0 - \vec{v}_{CoM} = \frac{\vec{v}_0(A+1)}{A+1} - \frac{\vec{v}_0}{A+1} = \frac{A\vec{v}_0}{A+1} \quad (3.3)$$

The target nucleus is stationary in the lab frame, so its incoming velocity in the center-of-mass frame is simply given by

$$-\vec{v}_{CoM} = \frac{-\vec{v}_0}{A+1} \quad (3.4)$$

Combining this with the previous equation, we see that the total momentum in the center-of-mass frame is zero.

Since we are considering elastic collisions only, with no changes in potential energy, total kinetic energy must be conserved in this system, while the total momentum is maintained at zero. From this we can deduce that the outgoing speeds of the neutron and the nucleus must equal their incoming speeds, as indicated in figure 3.2. Of course their vector velocities change.

**Question:** Explain, in words if you can, why the outgoing speeds of the neutron and nucleus equal their incoming speeds.

With just these very simple results, we now transfer back to the lab frame. To determine velocities in the lab frame given velocities in the center-of-mass frame, we obviously add the velocity of the center of mass,  $\vec{v}_{CoM}$ , equation 3.4. For the square of the outgoing neutron speed we can write down, using the law of cosines,

$$v_1^2 = (v_0 - v_{CoM})^2 + v_{CoM}^2 + 2(v_0 - v_{CoM})v_{CoM} \cos \theta = \\ \frac{A^2 v_0^2}{(A+1)^2} + \frac{v_0^2}{(A+1)^2} + \frac{2Av_0^2 \cos \theta}{(A+1)^2} = v_0^2 \frac{A^2 + 2A \cos \theta + 1}{(A+1)^2} \quad (3.5)$$

This gives us a simple expression for the outgoing neutron energy in the lab frame, in terms of the incoming lab frame energy. Let us define  $E_0$  as the incoming kinetic energy, and  $E_1$  as the outgoing. Then we have

$$\frac{E_1}{E_0} = \frac{v_1^2}{v_0^2} = \frac{A^2 + 2A \cos \theta + 1}{(A+1)^2} \quad (3.6)$$

The maximum possible lab-frame outgoing energy is for zero-angle scattering – effectively no interaction at all:

$$E_{1, max} = E_0 \frac{A^2 + 2A \cos(\theta = 0) + 1}{(A+1)^2} = E_0 \frac{A^2 + 2A + 1}{(A+1)^2} = E_0 \quad (3.7)$$

while the minimum possible lab-frame outcoming energy is for perfect backscattering:

$$E_{1, \min} = E_0 \frac{A^2 + 2A \cos(\theta = \pi) + 1}{(A + 1)^2} = E_0 \frac{A^2 - 2A + 1}{(A + 1)^2} = E_0 \frac{(A - 1)^2}{(A + 1)^2} \quad (3.8)$$

Let us define a parameter  $\alpha$

$$\alpha \equiv \frac{(A - 1)^2}{(A + 1)^2} \quad (3.9)$$

This allows us to bound the range of outcome energies,  $E_1$ , both from above and from below

$$\alpha E_0 < E_1 < E_0 \quad (3.10)$$

so we can define a range of energy decrements

$$\Delta E = E_0 - E_1 < E_0 - \alpha E_0 \quad (3.11)$$

$$\frac{\Delta E}{E_0} < 1 - \alpha = \frac{4A}{(A + 1)^2} \quad (3.12)$$

We now have the range of possible energy loss, but we need to know the relative probability of any given energy loss to fully understand the slowing-down process. Thus we need to know the relative probability of any given center-of-mass scattering angle,  $\theta$ . Since the de Broglie wavelength of the neutrons of interest is generally much greater than the effective scattering radius of the target nuclei (see table 2.1), a target nucleus “experiences” a nearly isotropic oscillation of the neutron wave function with time, with relatively little difference across the nucleus. This results in an outgoing wave with a probability density that is essentially isotropic. Thus a scattered neutron has equal probability of leaving the target nucleus in any increment of solid angle,  $d\Omega$ , over the full  $4\pi$  available. This isotropy holds in the center-of-mass frame because it is in this frame that the neutron + nucleus system is at rest when the outgoing wave is launched.

We know that a range of solid angle  $d\Omega$  can be expressed as

$$d\Omega = \sin\theta d\theta d\phi = -d\cos\theta d\phi \quad (3.13)$$

Since all ranges of  $d\phi$  are equally probable by the symmetry of the problem, and all ranges of  $d\Omega$  are equally probable as just derived, we can deduce that all ranges of  $-d\cos\theta$  must be equally probable, from  $\cos\theta = 1$  to  $-1$ . (Note that the sign of  $d\cos\theta$  plays no physical role here; it just happens to be

counting downwards in this case.) Starting from equation 3.6 we can deduce

$$dE_1 = E_0 \left[ \frac{2A(d \cos \theta)}{(A + 1)^2} \right] \quad (3.14)$$

so all outcoming lab-frame differential energy increments,  $dE_1$ , in the range from  $\alpha E_0$  to  $E_0$  are equally probable.

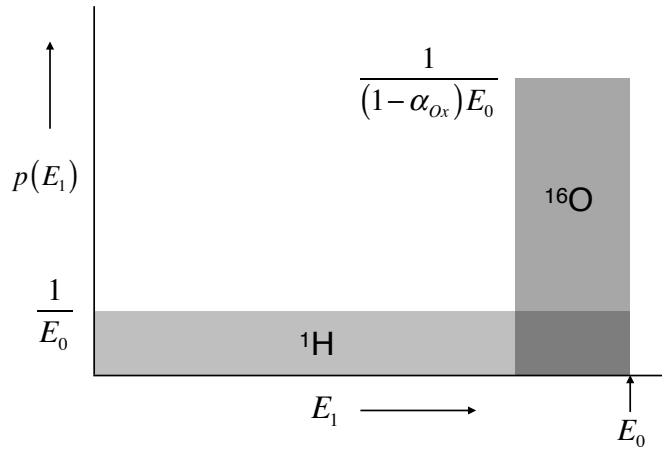


Figure 3.3 Probability of outgoing energy for neutron collision with protons and  $^{16}\text{O}$  nuclei.

**Question:** Explain, perhaps literally by waving your hands around, why it would not be physical to have an even distribution in  $\theta$  as opposed to  $\cos \theta$ .

The probability of  $E_1$  landing in a differential energy increment  $dE$  is given by  $p(E_1)dE$ . Since it must land somewhere, we require

$$\int_0^{\infty} p(E_1) dE_1 = \int_{\alpha E_0}^{E_0} p(E_1) dE_1 = 1 \quad (3.15)$$

from which we derive

$$p(E_1) = \frac{1}{\Delta E_{max}} = \frac{1}{(1 - \alpha)E_0} \quad (3.16)$$

over the range of possible values of  $E_1$  (equation 3.10). Elsewhere  $p(E_1) = 0$ . Figure 3.3 illustrates this for  $^1\text{H}$  and  $^{16}\text{O}$ , with  $\alpha = 0$  and 0.78 respectively.

### 3.2 Logarithmic energy decrement

Fermi noted that the range of possible energy loss at a collision is proportional to the incoming energy, and this loss happens over and over again as a neutron slows down. Thus neutron slowing down can be seen as a process similar to exponential decay of the neutron energy, but with finite-size steps.

Exponential decay is characterized by an equation of the form

$$E_{N_c} = E_0 \exp(-N_c \xi) \quad (3.17)$$

where  $N_c$  is a continuous variable such as distance or time. Following Fermi, however, we will be taking  $N_c$  as an integer, representing the *number of collisions* undergone. We can then write finite-step exponential decay as

$$N_c \xi = \ln(E_0/E_{N_c}) = \ln[(E_0/E_1)^{N_c}] = N_c \ln(E_0/E_1) \quad (3.18)$$

so this finite-step model assumes energy drops in equal “logarithmic energy decrements,”  $\xi$ , with each collision, similar to what we expect. We have previously, in effect, derived a range for the logarithmic energy decrement, which is independent of neutron energy, but we cannot predict the specific value at each collision.

$$\ln(\alpha) < \ln(E_1/E_0) < 0 \quad (3.19)$$

It is particularly daring for the case of hydrogen, but let us press ahead and approximate the energy loss process with a mean logarithmic energy decrement per collision, where the average is taken over all possible energy decrements.

$$\xi \approx \langle \ln(E_0/E_1) \rangle \quad (3.20)$$

This approach gives us the appropriate average for determining the mean number of collisions required to get down to a specified final energy.

$$\langle N_c \rangle = \frac{\ln(E_0/E_{N_c})}{\xi} \quad (3.21)$$

In particular for the energy to drop by one factor of  $e$ , on average  $1/\xi$  collisions are required, or more generally  $1/\xi$  collisions are required per downwards  $e$ -fold in energy.  $\ln(10)/\xi \approx 2.303/\xi$  collisions are required on average for a 10-fold, or order-of-magnitude drop.

Now we can evaluate

$$\xi \equiv \left\langle \ln \left( \frac{E_0}{E_1} \right) \right\rangle \equiv \int_{\alpha E_0}^{E_0} \ln \left( \frac{E_0}{E_1} \right) p(E_1) dE_1 = \frac{1}{(1-\alpha) E_0} \int_{\alpha E_0}^{E_0} \ln \left( \frac{E_0}{E_1} \right) dE_1 \quad (3.22)$$

The derivation simplifies greatly if we define  $\tilde{E} \equiv E_1/E_0$  before we proceed.

$$\xi = \frac{-1}{1-\alpha} \int_{\alpha}^1 \ln(\tilde{E}) d\tilde{E} \quad (3.23)$$

Now we use  $\int \ln x dx = x \ln(x) - x + C$  (which you can check by taking the derivative of both sides) to arrive at

$$\xi = \frac{-1}{1-\alpha} [-1 - \alpha \ln(\alpha) + \alpha] = 1 + \frac{\alpha}{1-\alpha} \ln(\alpha) \quad (3.24)$$

This result is shown in figure 3.4. As noted above,  $\xi$  is the inverse of the

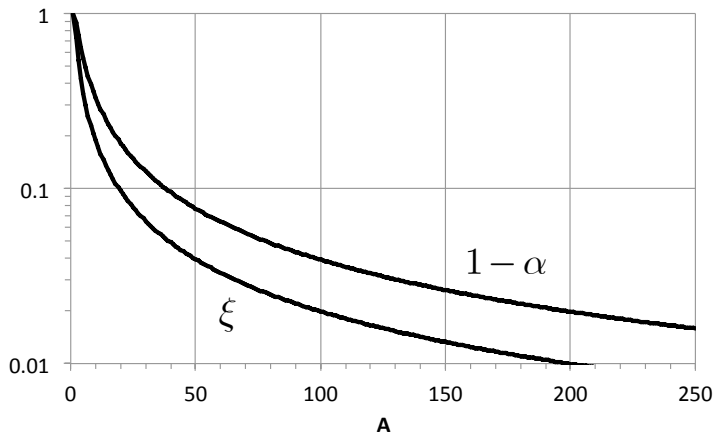


Figure 3.4  $1 - \alpha$  and  $\xi$  vs. atomic mass.

number of collisions required, in Fermi's model, to reduce the energy of a neutron by a factor of  $e$ . For example for  $A = 200$  it takes about  $N_c = 100$  collisions. On the other hand it takes only a single collision with a proton, for which  $\alpha = 0$ . Mathematically this is because  $\ln(\alpha)$  diverges as  $\alpha$  goes to zero more weakly than  $1/\alpha$ . As a result  $\alpha \ln(\alpha)$  goes to zero as  $\alpha$  goes to zero. For  $^{16}\text{O}$  it takes 8.34 collisions to drop the neutron energy by a factor of  $e$ .

$1 - \alpha$  is the maximum fractional energy loss. It is never in fact very far from  $\xi$ , since  $\xi$  is a logarithmically weighted average fractional energy loss.  $1 - \alpha$  is unity for protons, as is  $\xi$ . It is higher than  $\xi$  for greater values of  $A$ , with an asymptotic ratio of two.

To evaluate the power of neutron slowing down we are not only interested in  $\xi$  but also the mean free path between collisions. Since there are two protons for each oxygen nucleus in light water, and the proton elastic scattering

cross-section is about five times higher than that of the oxygen nucleus, it is evident that the oxygen in light water plays an even more modest role in neutron thermalization than indicated by  $\xi$ . To quantify this we first define a total macroscopic elastic scattering cross-section, summed over all species of nuclei (elements and isotopes) present.

$$\overline{\Sigma_e} \equiv \sum_{nuclei} \Sigma_e \quad (3.25)$$

Because  $\Sigma$  is already used for the macroscopic cross-section (section 2.1), we use the overbar to indicate the sum over all elements and isotopes. It is natural to sum macroscopic cross-sections in this way, since they each represent the differential probability of scattering out of a beam,  $-dn/n$ , per differential path length,  $dx$ , along the neutron's path, for a particular type of nucleus (section ??). Now if we are interested in the total differential logarithmic energy decrement per differential path length, we can sum the contributions from each as well, to get the "slowing down power" of a medium.

$$\overline{\xi \Sigma_e} \equiv \sum_{nuclei} \xi \Sigma_e \quad (3.26)$$

Table 3.1 shows the total macroscopic elastic scattering cross-section, slowing down power, radiative absorption cross section, radiative absorption rate coefficient, and slowing-down time (see section 3.3) for the neutron moderators used in nuclear reactors. The elastic scattering cross-sections for hydrogen, deuterium, carbon and oxygen, used as moderators, or components of moderators, in thermal-spectrum reactors, are evaluated at a representative value of 1 keV, midway logarithmically between the MeV and the eV energy range. The radiative absorption rate coefficients,  $\nu_\gamma = \overline{\Sigma_\gamma v}$  are calculated by choosing any point in the  $1/v$  absorption range, and evaluating  $n\sigma_\gamma v$ . In both cases, the sum is then taken over the species of nuclei present. (Oxygen and carbon are nearly mono-nuclidic.) Sodium and lead are used as coolants in fast reactors, in which moderation is undesirable, but of course they still provide some moderation and absorption. Their cross-sections are averaged over the range of 100 to 500 keV, meant to be representative of the neutron spectra found in fast-spectrum reactors. Sodium is mono-nuclidic, but there are four naturally-occurring isotopes of lead, which are averaged appropriately, as indicated.

**Question:**  $(\overline{\Sigma_e})^{-1}$  is the mean free path to an elastic scattering event. What is  $(\overline{\xi \Sigma_e})^{-1}$ ?

As can be seen light water is much more effective than other moderators

Table 3.1 *Total macroscopic elastic scattering cross-section, slowing down power, radiative absorption rate coefficient, and slowing-down time for neutron moderators.*  
*(See text for energies of evaluation.)*

	$N$	$\overline{\Sigma_e}$	$\overline{\xi \Sigma_e}$	$\overline{\Sigma_\gamma}$	$\nu_\gamma = \overline{\Sigma_\gamma v}$	$\tau_s$
Light water	$3.33 \cdot 10^{28}$	132	121	2.22	4890	$1.69 \cdot 10^{-6}$
Heavy water	$3.33 \cdot 10^{28}$	35	18	$4.01 \cdot 10^{-3}$	8.82	$1.13 \cdot 10^{-5}$
Graphite	$1.14 \cdot 10^{29}$	51	8	$4.40 \cdot 10^{-2}$	96.8	$2.55 \cdot 10^{-5}$
Sodium	$2.43 \cdot 10^{28}$	8.91	0.753	$1.69 \cdot 10^{-3}$		
Lead	$3.10 \cdot 10^{28}$	25.1	0.242	$1.17 \cdot 10^{-2}$		

at slowing down neutrons. Its weakness is that the  $(n,\gamma)$  radiative capture reaction on protons — once the neutrons have slowed down — competes strongly with the  $^{238}\text{U}$  fission reaction. As a result, light water can only be used as a moderator with enriched uranium. On the other hand, heavy water and graphite moderators are used with natural or near-natural uranium. This is possible because these moderators do not contain protons that scavenge thermal neutrons, which compensates for the high ratio of  $^{238}\text{U}$  to  $^{235}\text{U}$ . However, as a result of this high ratio radiative capture on  $^{238}\text{U}$  is greatly enhanced relative to fission, so heavy-water and graphite moderated reactors are prodigious producers of Pu, per unit fission power. This makes them attractive for the production of plutonium for weapons.

### 3.3 Slowing Down Time

We are now in a position to use Fermi's continuous slowing-down model to calculate the time required for a neutron to slow down from the MeV energy range to the eV energy range. Working from equations 3.21 and 3.26, we can write

$$\frac{1}{E} \frac{dE}{dt} = \frac{d \ln(E)}{dt} = \frac{dx}{dt} \sum_{nuclei} \left[ \frac{d \ln(E)}{dN_c} \frac{dN_c}{dx} \right] = -v \overline{\xi \Sigma_e} \quad (3.27)$$

which gives us a pretty and simple result:

$$\frac{dE}{dt} \approx -v \overline{\xi \Sigma_e} E \quad (3.28)$$

This equation can be solved straightforwardly for the slowing-down time:

$$\tau_{slow} \approx \int_{E_{min}}^{E_{max}} \left( \frac{dE}{dt} \right)^{-1} dE = \frac{1}{\xi \Sigma_e} \int_{E_{min}}^{E_{max}} \frac{dE}{v(E) E} \quad (3.29)$$

$$= \frac{1}{\xi \Sigma_e} \int_{v_{min}}^{v_{max}} \frac{2vdv}{v^3} = \frac{2}{\xi \Sigma_e} \left( \frac{1}{v_{min}} - \frac{1}{v_{max}} \right) \quad (3.30)$$

For MeV neutrons slowing down to the energy where the spectrum of thermalized neutrons is conventionally taken to dominate,  $\sim 0.5$  eV, we can neglect the  $1/v_{max}$  term. The neutron velocity at 0.5 eV is  $9.8 \cdot 10^3$  m/s, giving a slowing-down time in light water of  $1.69 \mu\text{sec}$ . It is interesting to multiply this slowing-down time by the absorption rate coefficient,  $\nu_\gamma = \overline{\Sigma_\gamma v}$ , shown in table 3.1. We can see that there is less than 1% absorption during the slowing down process in light water, which we will neglect, and truly tiny absorption in heavy water or graphite. As we will see, however, there is significant resonant absorption on  $^{238}\text{U}$  during slowing down, and there is significant absorption by protons after the neutrons thermalize. In a light-water reactor, perhaps 50% of the active volume of the reactor is filled with light water, the rest being structure and fuel. Since neither of these contribute significantly to the slowing-down process, the effective slowing-down time is in practice perhaps twice longer than in pure light water. On the other hand, the effective absorption rate in the moderator is reduced by the same factor, so  $\nu_{abs}\tau_s$  is unchanged.

### 3.4 Neutron flux vs. energy, $\phi(E)$ , and vs. lethargy, $\phi(u)$

In section 2.3 we defined  $\phi \equiv nv$ , in the context of a collection of particles of given density and speed. Now we are interested in working with neutrons that have a wide distribution of speeds and so energies. To define  $\phi(E)$ , neutron flux as a function of energy, let us start by positing that  $\phi$  is the integral over energy of  $\phi(E)$ :

$$\int_0^\infty \phi(E)dE \equiv \phi \quad (3.31)$$

Now we can say that an element of  $d\phi$  is given by

$$d\phi = \phi(E)dE \quad (3.32)$$

allowing us to define

$$\phi(E) \equiv \frac{d\phi}{dE} \quad (3.33)$$

We can use the same analysis to define neutron density as a function of energy.

$$\int_0^\infty n(E)dE \equiv n \quad (3.34)$$

$$n(E) \equiv \frac{dn}{dE} \quad (3.35)$$

It is intuitive to assume  $\phi(E) = n(E)v(E)$ . We can show this formally by considering the case of a narrow energy distribution of neutrons, with width  $\delta E$  around energy  $E$  and corresponding neutron speed  $v(E)$ . This is exactly the case in which we earlier defined  $\phi \equiv nv$ . We can use this case to relate  $\phi(E)$  to  $n(E)$  by noting that

$$\phi = \phi(E)\delta E = nv = n(E)\delta E \cdot v(E) \quad (3.36)$$

$$\phi(E) = n(E)v(E) \quad (3.37)$$

This type of analysis is helpful as a model for the case of a different independent variable. It is not uncommon in nuclear reactor physics to define a quantity called “lethargy” for neutrons, denoted  $u$ , and defined as

$$u \equiv \ln\left(\frac{E_0}{E}\right) \quad (3.38)$$

where  $E_0$  is generally taken to be 10 MeV, to encompass all of the neutrons of interest in a fission system. The idea here is that neutrons become more “lethargic” as they slow down, so lethargy increases with decreasing energy. On the basis of Fermi’s analysis of slowing-down, neutrons make approximately equal steps up in lethargy [down in  $\ln(E)$ ] with each collision. On average, the lethargy of a neutron increases by  $1/\xi$  at a collision, so by 1 at a collision with a hydrogen nucleus and by 1/8.34 at a collision with an oxygen nucleus.

By analogy with the discussion of  $\phi(E)$  we can write down for a given differential increment of  $\phi$

$$d\phi = \phi(E)dE = -\phi(u)du \quad (3.39)$$

where the minus sign arises from the fact that  $u$  varies in the opposite direction from  $E$ . This gives us

$$\phi(E) = -\phi(u)\frac{du}{dE} = \frac{\phi(u)}{E} \quad (3.40)$$

$$\phi(u) = E\phi(E) \quad (3.41)$$

where  $u = \ln(E_0/E)$ . Note that  $E\phi(E)$  has the same units as  $\phi$ ,  $\text{s}^{-1}\text{m}^{-2}$ .

Often  $E\phi(E)$  is plotted, rather than  $\phi(E)$ . The  $x$  axis is almost always chosen to be  $E$  rather than  $-u$ , but if the  $x$  axis has a logarithmic scale, then the layout of the image on the page is equivalent to a plot vs.  $-u$ . For reference, note that an order of magnitude drop in energy,  $E$ , corresponds to a  $\ln(10) = 2.30$  positive increment in lethargy,  $u$ .

An incremental element of  $\phi$  is given by

$$d\phi = \frac{d\phi}{dE} dE = \phi(E) dE = E\phi(E) d(\ln(E)) \quad (3.42)$$

As a result, the visually perceived area under a curve of  $E\phi(E)$ , in some length along the image in the  $x$  direction (when the  $x$  axis has a logarithmic scale), reflects its contribution to  $\phi$ . We will see in section 3.6 that  $\phi(E)$  is nearly proportional to  $1/E$  over a wide range of energy, making a plot of  $E\phi(E)$  more revealing than a plot of  $\phi(E)$  itself. See, for example, figure 3.8 later in this chapter.

### 3.5 Fast energy region $\phi_F(E)$

Now we will look into the neutron flux as a function of energy,  $\phi(E)$ , in three different energy ranges: the Fast energy range, where the direct source of fast neutrons from fission is very important in setting  $\phi_F(E)$  the spectrum of fission neutrons as yet undegraded in energy, the Intermediate energy range, where  $\phi_I(E)$  is set mostly by the slowing down process (although resonant absorption is important towards the lower end), and the Thermal energy range, where neutrons are largely in thermal equilibrium with their environment, although  $\phi_T(E)$  is fed by neutrons slowing down into this range, and neutrons are finally either radiatively absorbed or drive fission. Then, of course, the process starts over again at the top.

This analysis is appropriate for thermal reactors, which take advantage of the favorable  $1/v$  range of the fission cross-section. Later in this chapter we will discuss fast reactors, which are designed to minimize neutron moderation and utilize neutrons with energies of about 100 keV and above. In the next chapter we will discuss the spatial diffusion of neutrons during their lifetime. However in the present chapter we will treat the problem as if the reactor were infinite in spatial extent, with no spatial gradients.

In the Fast energy range, typically taken to include neutrons above about 1 MeV, where it becomes possible to drive fission of  $^{238}\text{U}$ , the main source of neutrons is directly due to neutrons from fission, undegraded in energy, rather than due to slowing-down from higher energies. Experiments have shown that the source of neutrons can be reasonably well approximated by

the Watt probability distribution, for  $^{235}\text{U}$  fission driven by both thermal and MeV-range neutrons. B.E. Watt of Los Alamos first published data supporting a distribution of this form in 1952.

$$\chi(E_{\text{MeV}}) = 0.484 \sinh(\sqrt{2E_{\text{MeV}}}) e^{-E_{\text{MeV}}} \quad (3.43)$$

$\chi(E)$ , as shown in figure 1.2, is normalized such that  $\int_0^\infty \chi(E_{\text{MeV}}) dE_{\text{MeV}} = 1$ .

The more general form is

$$\chi(E_{\text{MeV}}) = \frac{2\exp(-ab/4)}{\sqrt{\pi a^3 b}} \sinh(\sqrt{bE_{\text{MeV}}}) e^{-E_{\text{MeV}}/a} \quad (3.44)$$

It is just a coincidence that a reasonably good fit to the spectrum for uranium fission can be made with  $a = 1$  and  $b = 2$ . More sophisticated fits to the experimental data and models make  $a$  and  $b$  themselves vary somewhat with energy.

Let us define  $S$  as the total volumetric neutron source rate due to fission, with units  $\text{s}^{-1}\text{m}^{-3}$ . Then the neutron source rate per unit energy is given by  $s(E) = S\chi(E)$ . Note that we will work with  $\chi(E)$  in SI units of  $\text{s}^{-1}\text{m}^{-3}\text{J}^{-1}$ . Typical values for  $S$  in commercial light-water reactors are in the range of  $10^{19} \text{ s}^{-1}\text{m}^{-3}$ .

**Question:** Estimate the volume of a reactor with volume average  $S = 10^{19} \text{ s}^{-1}\text{m}^{-3}$ . Assume 3 GW(th) of power production. Take the energy production to be 202 MeV per fission event, and  $\bar{\nu} = 2.44$  neutrons, on average, per fission. If you further assume a cylindrical reactor fuel volume of typical height 4m, what is its radius?

Neutron source rates and power densities are higher in fast-spectrum reactors, and lower in graphite or heavy-water moderated reactors. The fuel rods are more closely packed in liquid-metal-cooled fast-spectrum reactors, in order to minimize moderation, while the fuel is much more widely spaced in graphite or heavy-water moderated reactors, because, as shown in table 3.1, these moderators slow down neutrons less rapidly. As we will see in section 3.6.1, in thermal-spectrum reactors we need to slow down neutrons past the radiative absorption resonances with minimum absorption, in order to maximize their chance of thermalizing and driving fission. If the neutrons drift slowly down in energy, then the ratio of moderator volume to fuel volume needs to be large in order to reduce the chance that a neutron will find the fuel as it passes slowly through the resonant energies of  $^{238}\text{U}$ .

Equation 2.11 describes the depletion, or loss, of a mono-energetic beam of particles due to collisions with target particles. We can apply the same formalism to a small energy range,  $dE$ , of fast neutrons with average energy

*E.* We can also include, for the case at hand, the source rate of fission neutrons. This gives us:

$$\frac{dn_F}{dt} dE = s(E)dE - \Sigma_{loss}(E)\phi_F(E)dE \quad (3.45)$$

Solving this with the assumption of steady state operation we have:

$$\phi_F(E) = s(E)/\Sigma_{loss}(E) \quad (3.46)$$

Now we need to ask ourselves what we mean by  $\Sigma_{loss}(E)$  in this case. Elastic collisions of fast neutrons with heavy nuclei such as uranium or plutonium, with  $\xi \sim 0.008$ , barely change neutron energies, so we can neglect the effect of these collisions on the neutron spectrum. Elastic collisions with protons, with  $\xi = 1$ , cause substantial energy loss, so they can be considered to take neutrons out of the Fast energy spectrum altogether. One can make a similar argument for deuterons, with  $\xi = 0.725$ . Elastic collisions with carbon and oxygen are intermediate cases, with  $\xi = 0.158$  and  $0.120$ , respectively. For present purposes, we will neglect these, although we will see later that their resonances leave some detailed signatures on the shape of the spectrum. Their contribution to slowing down is also reduced because, at fission energies, their center-of-mass scattering is becoming forward-directed, rather than isotropic. This is because the neutron de Broglie wavelength begins to approach the nuclear diameter. Interestingly, even at these same energies scattering on protons remains nearly isotropic in the center-of-mass frame, because the large resonance near zero energy still dominates scattering, and this resonance is spherically symmetric in nature.

Inelastic collisions and radiative absorption should both “count” since they take neutrons out of the Fast spectral region. Hydrogen and deuterium cannot support inelastic scattering, since they do not have bound excited states. The thresholds for inelastic scattering on carbon and oxygen are at 5 MeV and 6 MeV, respectively, where the Watt spectrum has fallen to low values, so we can neglect inelastic scattering on them. However inelastic collisions on zirconium in LWR fuel rod cladding can have some effect, since the threshold is quite a bit lower. We will neglect here other such “parasitic” absorption mechanisms. Fission events extract neutrons, but also inject them, so we can include fission events as absorptions, but we must also count them within  $s(E)$  defined to include contributions from fission driven both by thermal neutrons and by fast ones,  $s(E) = s_T(E) + s_F(E)$ . The energy spectrum of neutrons from fission due to neutrons in the Fast energy region is not significantly different from that due to thermal neutrons.

Fast neutrons have mean free paths of about 4 cm or more in most mate-

rials, including both water and uranium dioxide fuel. Fuel pins are about 1 cm in diameter, and they are spaced apart by of order 1 cm. Thus we can assume, rather roughly, that  $\phi_F(E)$  is equal in the fuel, the cladding, and the moderator, in a light-water reactor. Thus the fuel, cladding and moderator contribute to the overall loss in proportion to their own volume and macroscopic cross-section, giving

$$\begin{aligned} V^{tot}\Sigma_{loss}(E)\phi_F(E) &= V^{mod}\overline{\Sigma_e^{mod}}(E)\phi_F(E) + V^{clad}\overline{\Sigma_{in}^{clad}}(E)\phi_F(E) \\ &+ V^{fuel}\left[\overline{\Sigma_f^{fuel}}(E) + \overline{\Sigma_\gamma^{fuel}}(E) + \overline{\Sigma_{in}^{fuel}}(E)\right]\phi_F(E) \end{aligned} \quad (3.47)$$

This is equivalent to “homogenizing” the materials, but it is physically based on the (imperfect) assumption that  $\phi_F(E)$  is homogeneous. Not surprisingly, this is called the “homogeneous approximation.” In practice, fast neutrons are slightly denser in the fuel, where they are produced, than in the moderator. This is taken into account using a “fast advantage factor,” but we will neglect it here.

Dividing by  $V^{tot}\phi_F(E)$  we have

$$\begin{aligned} \Sigma_{loss}(E) &= \frac{V^{mod}}{V^{tot}}\overline{\Sigma_e^{mod}}(E) + \frac{V^{clad}}{V^{tot}}\overline{\Sigma_{in}^{clad}}(E) \\ &+ \frac{V^{fuel}}{V^{tot}}\left[\overline{\Sigma_f^{fuel}}(E) + \overline{\Sigma_\gamma^{fuel}}(E) + \overline{\Sigma_{in}^{fuel}}(E)\right] \end{aligned} \quad (3.48)$$

where the superscripts on the  $\bar{\Sigma}$ 's indicate the volumes over which the constituent  $\Sigma$ 's are summed, and the subscripts indicate elastic scattering (only on hydrogen or deuterium), inelastic scattering on cladding and fuel nuclei, and absorption on fuel nuclei, including both fission and a small amount of radiative absorption. Radiative absorption on moderator and cladding nuclei is negligible in the fast energy region, and fission is of course impossible.  $V$  with superscripts indicates the volume of moderator, cladding, and fuel, as well as the total volume.

We are now in a position to evaluate the neutron multiplication in the fast energy region, conventionally denoted  $\epsilon$ . First we write down our equation for  $\phi_F$  including fission induced both by thermal and fast neutrons:

$$\phi_F(E) = \frac{s_T(E) + s_F(E)}{\Sigma_{loss}(E)} = (S_T + S_F) \frac{\chi(E)}{\Sigma_{loss}(E)} \quad (3.49)$$

as well as the equation for the production rate of neutrons by this spectrum,

$$S_F = \frac{V^{fuel}}{V^{tot}} \int_0^\infty \phi_F(E) \overline{\nu_F \Sigma_f^{fuel}}(E) dE \quad (3.50)$$

where the integral corresponds to summing the neutron production from each differential range,  $dE$ , of energy.  $\overline{\nu_F}$  represents the mean neutron production per fission event, due to fast neutrons, for each type of nucleus.

Substituting equation 3.49 into equation 3.50 we have:

$$S_F = (S_T + S_F) \frac{V^{fuel}}{V^{tot}} \int_0^{\infty} \frac{\overline{\nu_F \Sigma_f^{fuel}}(E)}{\Sigma_{loss}(E)} \chi(E) dE \quad (3.51)$$

To simplify the algebra over the next few steps, let us define

$$X \equiv \frac{V^{fuel}}{V^{tot}} \int_0^{\infty} \frac{\overline{\nu_F \Sigma_f^{fuel}}(E)}{\Sigma_{loss}(E)} \chi(E) dE \quad (3.52)$$

So can break equation 3.51 into

$$S_F(1 - X) = S_T X \quad (3.53)$$

Thus we have

$$\frac{S_T + S_F}{S_T} = \frac{(S_T + S_F)X}{S_T X} = \frac{S_F}{S_F(1 - X)} = (1 - X)^{-1} \quad (3.54)$$

Substituting back in for  $X$  we have

$$\frac{S_T + S_F}{S_T} = \left[ 1 - \frac{V^{fuel}}{V^{tot}} \int_0^{\infty} \frac{\overline{\nu_F \Sigma_f^{fuel}}(E)}{\Sigma_{loss}(E)} \chi(E) dE \right]^{-1} \quad (3.55)$$

Since we have already made a number of approximations to this point, it is conventional to eliminate the integral by using fission-spectrum weighted values for  $\Sigma_{loss}(E)$  and  $\Sigma_f(E)$  of the form

$$\begin{aligned} \Sigma_{F,loss} &\equiv \int_0^{\infty} \chi(E) \Sigma_{loss}(E) dE \\ \Sigma_{F,f} &\equiv \int_0^{\infty} \chi(E) \Sigma_f(E) dE \end{aligned} \quad (3.56)$$

where we have taken advantage of the normalization of  $\chi(E)$  arranged to make its integral  $dE$  from 0 to  $\infty$  equal to unity. This gives us a simplified result:

$$\frac{S_T + S_F}{S_T} = \frac{S}{S_T} \approx \left[ 1 - \frac{V^{fuel}}{V^{tot}} \frac{\overline{\nu_F \Sigma_f^{fuel}}}{\Sigma_{F,loss}} \right]^{-1} \quad (3.57)$$

Next we would like to know what fraction of  $S = S_T + S_F$  is delivered to the Intermediate energy range. This fraction should equal the fraction of slowing down terms in  $\Sigma_{F,loss}$ . This is just

$$\frac{V^{tot}\Sigma_{F,loss} - V^{fuel}\overline{\Sigma}_{F,f}^{fuel} - V^{fuel}\overline{\Sigma}_{F,\gamma}^{fuel}}{V^{tot}\Sigma_{F,loss}} = 1 - \frac{V^{fuel}(\overline{\Sigma}_{F,f}^{fuel} + \overline{\Sigma}_{F,\gamma}^{fuel})}{V^{tot}\Sigma_{F,loss}} \quad (3.58)$$

Lastly, we would like to know the ratio of the neutrons delivered to the Intermediate energy range divided by those delivered to the Fast energy range, due to thermal fission, which will just be the enhancement in the fission rate, equation 3.57, multiplied by the probability of escaping the Fast spectrum by slowing down, equation 3.58. This “fast fission factor” is conventionally denoted  $\epsilon$ . As we will see,  $\epsilon$  is close to unity in thermal reactors, not close to zero as might be expected from the choice of nomenclature.

$$\epsilon = \frac{1 - \frac{V^{fuel}}{V^{tot}} \frac{(\overline{\Sigma}_{F,f}^{fuel} + \overline{\Sigma}_{F,\gamma}^{fuel})}{\overline{\Sigma}_{F,loss}}}{1 - \frac{V^{fuel}}{V^{tot}} \frac{\overline{\nu}_F \overline{\Sigma}_{F,f}^{fuel}}{\overline{\Sigma}_{F,loss}}} \quad (3.59)$$

**Question:** Simplify equation 3.59 in the limit of small  $\epsilon - 1$ . Explain why the result makes intuitive sense.

Table 3.2 provides relevant fission-spectrum weighted “Fast” microscopic cross-sections, and Table 3.3 relevant number densities, for evaluating equation 3.59. Sodium and lead are included, anticipating that we will want to calculate  $\epsilon$  for liquid-metal-cooled fast-spectrum reactors.

Since the fuel volume is generally quite a bit less than the total volume, and the fission cross-section is quite a bit less than the sum of all the cross-sections that extract neutrons from the fast spectrum, this “fast fission factor” is generally only about  $5 \pm 2\%$  above unity in light-water reactors. The higher values occur when the fuel corresponds to a larger fraction of the total volume, and the lower values when this fraction is smaller. Let’s compute an example. A typical fuel pin diameter in an LWR is 1 cm, within which the zircaloy cladding might be 0.5 mm thick. The spacing between fuel rod centers (the so-called “lattice pitch”) might be 1.3 cm. This gives  $V^{fuel}/V^{tot} = 0.376$ ,  $V^{clad}/V^{tot} = 0.088$ , and  $V^{mod}/V^{tot} = 0.535$ . Let us assume fresh 4% enriched uranium fuel.

We can derive the macroscopic cross-sections from tables 3.2 and 3.3. For  $\Sigma_{F,loss}$  we start from the Watt-spectrum averaged version of equation 3.48. It is convenient that 1 barn =  $10^{-28} m^2$ , and typical densities are in the  $10^{28} m^{-3}$  range. Thus one doesn’t need to carry along these two large

Table 3.2 *Watt-spectrum weighted (Fast) microscopic cross-sections (barns =  $10^{-28} m^2$ ) and  $\bar{\nu}$*

Atom	At. Mass	$\sigma_{F,f}$	$\sigma_{F,\gamma}$	$\sigma_{F,e}$	$\sigma_{F,in}$	$\bar{\nu}$
Hydrogen	1	—	$5.02 \cdot 10^{-5}$	4.01	—	—
Deuterium	2	—	$7.12 \cdot 10^{-6}$	2.54	—	—
Carbon	12	—	$2.51 \cdot 10^{-5}$	2.33	$1.01 \cdot 10^{-2}$	—
Oxygen	16	—	$1.20 \cdot 10^{-4}$	2.74	$2.46 \cdot 10^{-3}$	—
Sodium	23	—	$2.66 \cdot 10^{-4}$	2.72	0.513	—
Magnesium	Natural	—	$3.74 \cdot 10^{-4}$	3.14	0.327	—
Iron	Natural	—	$3.06 \cdot 10^{-3}$	2.60	0.644	—
Zirconium	Natural	—	$9.70 \cdot 10^{-3}$	5.07	0.687	—
Lead	Natural	—	$2.88 \cdot 10^{-3}$	5.72	0.704	—
Uranium	235	1.23	$9.52 \cdot 10^{-2}$	4.35	1.98	2.48
Uranium	238	0.303	$7.11 \cdot 10^{-2}$	4.87	2.59	2.71
Uranium	Natural	0.309	$7.13 \cdot 10^{-2}$	4.87	2.59	2.7
Uranium	2% $^{235}\text{U}$	0.340	$7.21 \cdot 10^{-2}$	4.85	2.57	2.69
Uranium	4% $^{235}\text{U}$	0.340	$7.21 \cdot 10^{-2}$	4.85	2.57	2.67
Uranium	20% $^{235}\text{U}$	0.488	$7.59 \cdot 10^{-2}$	4.77	2.47	2.59
Plutonium	239	1.85	$4.10 \cdot 10^{-2}$	4.38	1.59	3.18
Plutonium	240	1.39	$8.31 \cdot 10^{-2}$	4.57	1.78	3.11
Plutonium	241	1.62	$9.39 \cdot 10^{-2}$	4.27	1.79	2.93
Plutonium	242	1.15	$8.09 \cdot 10^{-2}$	4.79	2.01	3.05

factors in evaluating macroscopic cross-sections, since they cancel.

$$\begin{aligned} \Sigma_{F,loss} &= 0.535 \cdot 6.69 \cdot 4.01 + 0.088 \cdot 4.31 \cdot 0.687 \\ &\quad + 0.376 \cdot 2.34 \cdot [0.34 + 0.0721 + 2.57] = 17.2 \text{ m}^{-1} \end{aligned} \quad (3.60)$$

which is dominated by elastic scattering on hydrogen, but with a significant

Table 3.3 Molecular weights, mass densities and number densities

Material	Atoms	Molecular Weight g/mole	Mass Density $\text{kgm}^{-3}$	Number Density $\text{m}^{-3}$
Graphite	C	12.011	2267	$1.14 \cdot 10^{29}$
Water	O	18.016	1000	$3.35 \cdot 10^{28}$
	H			$6.69 \cdot 10^{28}$
	D			$6.69 \cdot 10^{28}$
Sodium	Na	22.99	997	$2.43 \cdot 10^{28}$
Iron	Fe	55.84	7874	$8.49 \cdot 10^{28}$
Zirconium	Zr	91.22	8520	$4.31 \cdot 10^{28}$
Lead	Pb	207.2	10660	$3.10 \cdot 10^{28}$
Uranium metal	U	238.03	19100	$4.83 \cdot 10^{28}$
$\text{UO}_2$	U	270.3	10500	$2.34 \cdot 10^{28}$
	O			$4.68 \cdot 10^{28}$

Table 3.4 Example LWR Square Lattice Cell

Parameter	Value
Fuel pin diameter	0.01 m
Zirconium cladding	0.0005 m
Lattice pitch	0.013 m
$V^{fuel}/V^{tot}$	0.376
$V^{clad}/V^{tot}$	0.088
$V^{mod}/V^{tot}$	0.535

contribution from inelastic scattering on  $^{238}\text{U}$ . We can also calculate

$$\begin{aligned}\overline{\Sigma_{F,f}^{fuel}} &= 2.34 \cdot 0.34 = 0.796 \text{ m}^{-1} \\ \overline{\Sigma_{F,\gamma}^{fuel}} &= 2.34 \cdot 0.0732 = 0.171 \text{ m}^{-1} \\ \overline{\nu_F \Sigma_{F,f}^{fuel}} &= 2.67 \cdot 0.796 = 2.13 \text{ m}^{-1}\end{aligned}\tag{3.61}$$

The fast fission cross-section for  $^{238}\text{U}$  is about 1/4 of that for  $^{235}\text{U}$ , but we

are only considering 4% enrichment, so the fission terms are dominated by collisions with  $^{238}\text{U}$ . From these three results, and  $V^{fuel}/V^{tot} = 0.376$  found in table 3.4 we arrive at

$$\begin{aligned}\epsilon &= (1 - 0.376 \cdot (0.796 + 0.171)/17.2)/(1 - 0.376 \cdot 2.13/17.2) \\ &= 1.03\end{aligned}\quad (3.62)$$

**Question:** Qualitatively, do you expect  $\epsilon$  to decline rapidly with fuel burn-up? You can ignore fast neutron absorption or scattering on built-up fission products.

### 3.6 Intermediate energy region $\phi_I(E)$

Now we are interested in the Intermediate energy region, between about 1 Mev keV and about 1 eV. Evidently this region covers a broad range, some six orders of magnitude in energy. We will use our results on slowing down by elastic collisions to calculate the neutron flux spectrum in this region. The key findings we will use are

- An elastic collision causes a neutron of energy  $E_0$  to fall to an energy between  $\alpha E_0$  and  $E_0$
- For isotropic center-of-mass scattering, the neutron falls with equal probability to any energy within this range.

Once we have derived the resulting “slowing down” spectrum, we will discuss the effects of the key neutron loss mechanism near the lower end of this energy range, resonant radiative absorption. Because of this process, the Intermediate energy range is also called the “resonance region.” We can neglect fission due to neutrons in the Intermediate energy range, since it is much weaker than absorption – in part because thermal-spectrum reactors generally have uranium enriched to at most 5%  $^{235}\text{U}$ , and this energy range is below the threshold for fission of  $^{238}\text{U}$ . Finally we will calculate the “resonance escape probability,”  $p$ , the probability that a neutron entering the Intermediate energy range will escape being captured by the resonances, and will be delivered to the next energy range down, the Thermal energy range.

To make progress we need to define a new quantity,  $q(E)$ , which represents the flux of neutrons downwards in energy across energy  $E$ . The units of  $q(E)$  are the same as those of the source rate of neutrons into the Intermediate energy range,  $\epsilon S_T$ ,  $\text{m}^{-3}\text{s}^{-1}$ . Indeed everywhere above the range of significant

resonant radiative absorption  $q(E)$  must equal  $\epsilon S_T$ , if neutrons are not going to pile up above  $E$  with time.

In some differentially short interval of time,  $dt$ , the only neutrons that can cross energy  $E$  are those with initial energy  $E'$  in the range  $E/\alpha > E' > E$ . This is because their final energies must be at least  $\alpha$  times their initial energies and must be below their initial energies. We can ignore the case of more than a single collision in this calculation, because we are considering a differentially short period of time and the probability of two collisions is differentially small compared with the probability of one. The energy range available to the neutron after the collision is from  $E'$  down to  $\alpha E'$ . These initial and final ranges are shown in figure 3.5.

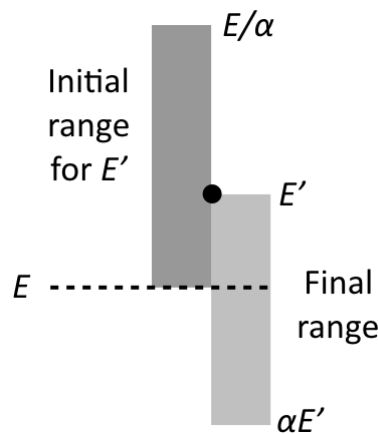


Figure 3.5 Initial and final energy ranges for a neutron crossing energy  $E$ .

Assuming isotropic center-of-mass scattering, the probability that a collision will cause a neutron of energy  $E'$  to cross energy  $E$  is proportional to the fraction of its final energy range below  $E$ ,  $(E - \alpha E')/(E' - \alpha E')$ . The rate of neutrons crossing energy  $E$  in the absence of losses is given by

$$q(E) = \epsilon S_T = \int_E^{E/\alpha} \Sigma_e(E') \phi_I(E') \left( \frac{E - \alpha E'}{E' - \alpha E'} \right) dE' \quad (3.63)$$

where the integral corresponds to a sum over  $dE'$  of the rate of neutrons crossing  $E$ , including the probability that such a crossing happens at a collision.

If we define  $\tilde{E}' \equiv E'/E$  and change the integration variable from  $E'$  to  $\tilde{E}'$

( $E$  is fixed since we are evaluating  $q(E)$  at a given  $E$ ) this becomes

$$q(E) = \epsilon S_T = E \int_1^{1/\alpha} \Sigma_e(E\tilde{E}') \phi_I(E\tilde{E}') \left( \frac{1/\tilde{E}' - \alpha}{1 - \alpha} \right) d\tilde{E}' \quad (3.64)$$

The term in parentheses, which weights the integral over  $\Sigma_e(E\tilde{E}')\phi_I(E\tilde{E}')$ , has no explicit energy dependence. This implies that the only way for  $q(E)$  to be independent of energy, as required in the absence of losses, is for  $\Sigma_e(E)\phi_I(E)$  to be proportional to  $1/E$ . Thus to simplify the algebra from here we express  $\Sigma_e(E\tilde{E}')\phi_I(E\tilde{E}')$  as  $\psi/(E\tilde{E}')$  where  $\psi$  is a constant. Uniquely in this case can the  $E$  dependence of  $q$  drop out.

We now proceed to evaluate the integral in equation 3.64, using our result that  $\Sigma(E)\phi(E) = \psi/E$ , where  $\psi$  is a constant.

$$\begin{aligned} q(E) &= \epsilon S_T = \frac{\psi}{1 - \alpha} \int_1^{1/\alpha} \left( \frac{1/\tilde{E}' - \alpha}{\tilde{E}'} \right) d\tilde{E}' = \frac{\psi}{1 - \alpha} \left[ -\frac{1}{\tilde{E}'} - \alpha \ln(\tilde{E}') \right]_1^{1/\alpha} \\ &= \frac{\psi}{1 - \alpha} \left[ -\alpha + 1 + \alpha \ln(\alpha) \right] = \psi \left( 1 + \frac{\alpha \ln \alpha}{1 - \alpha} \right) = \psi \xi \end{aligned} \quad (3.65)$$

giving the simple result

$$\phi_I(E) = \frac{\psi}{E\Sigma_e(E)} = \frac{\epsilon S_T}{E\xi\Sigma_e(E)} \quad (3.66)$$

This shows why  $E\phi_I(E) = \phi_I(u)$  is a convenient plotting variable in the wide Intermediate energy range, where  $\Sigma_e(E)$  varies modestly.

**Question:** Outline how to take into account multiple types of scatterers, arriving at equation 3.67.

$$\phi_I(E) = \frac{\epsilon S_T}{E\xi\Sigma_e(E)} \quad (3.67)$$

To do this, assume that the elastic scattering cross-sections vary slowly over the range  $\Delta E = Ee^\xi$  the characteristic range above  $E$  from which neutrons scatter down through  $E$ . In this case you may make the approximation of removing  $\Sigma_e$  from under the integral in equation 3.64.

If we want to extend the slowing-down neutron flux spectrum to higher energies, we can approximate that the source of slowing-down neutrons is that fraction of  $\chi(E)$  that lies above the energy under consideration. This

allows a generalization:

$$\phi_I(E) = \frac{eS_T}{E\xi\Sigma_e(E)} \int_E^\infty \chi(E)dE \quad (3.68)$$

where we have taken advantage of the fact that  $\xi$  is normalized such that its integration from 0 to  $\infty$  equals unity.

You might think this is a wild approximation. Indeed you would be justified in being doubtful, especially for slowing down on hydrogen where the individual steps can be very large. However you will show in a little Monte-Carlo study, exercise 3.3, that this approximation is extremely good for slowing-down on hydrogen, with its large steps, and on higher-mass nuclei for which the downward steps in energy,  $\Delta E = Ee^{-\xi} \ll 1$  MeV, so that neutrons undergo multiple scatters within the bulk of the Watt spectrum as they slow down. Even the intermediate case is not bad.

### 3.6.1 Resonant absorption

While the neutrons are slowing down due to elastic scattering, they can undergo other collisions. Inelastic scattering is largely cut off except at the very highest energy end of the intermediate energy region. Fission and resonant absorption on  $^{235}\text{U}$  are generally neglected and fission on  $^{238}\text{U}$  is almost non-existent. However resonant absorption on  $^{238}\text{U}$  does play a significant role in the energy range below about 10 keV. As is characteristic of quantum-mechanical calculations, the energy dependence of the absorption cross-section for stationary nuclei, the so-called “natural” line shape, is given by a Lorentzian profile, in this case multiplying the background  $1/v$  variation of absorption.

$$\sigma_\gamma(E) = \left(\frac{E_r}{E}\right)^{1/2} \frac{\sigma_0}{1 + 4(E - E_r)^2/\Gamma^2} \quad (3.69)$$

The peak value of this function is  $\sigma_0$  and its width at half-maximum is  $\pm\Gamma/2$ . By the uncertainty principle relating uncertainty in energy to uncertainty in time,  $\Gamma = \hbar/\tau$  where  $\tau$  is the lifetime of the excited state of the nucleus after it absorbs the neutron.

These absorption lines in uranium are generally quite narrow. Figure 3.6 shows the “natural” line width of the  $^{238}\text{U}$  resonance near 102.6 eV. It has a width of only about  $\pm 0.075$  eV at half-height. The same figure also shows the effect on the line profile of thermal motion of the uranium nuclei at 300° K, resulting in a line width of about  $\pm 0.2$  eV at half height.

Let us assume that the thermal motion of the nuclei corresponds to that

of the atoms in an ideal gas, which is a decent first-order approximation. Thus the energy of motion in each degree of freedom should be  $\approx T/2$ , with  $T$  expressed in energy units. At 300° K the average total energy of thermal motion corresponds to about  $(3/2) \cdot 0.026\text{eV}$ . Because of the much greater mass of uranium nuclei compared with neutrons, the speed of the nuclei corresponds to that of a neutron with energy reduced from this by a factor of 238. The energy of a neutron with this speed would be just  $1.6 \cdot 10^{-4}$  eV.

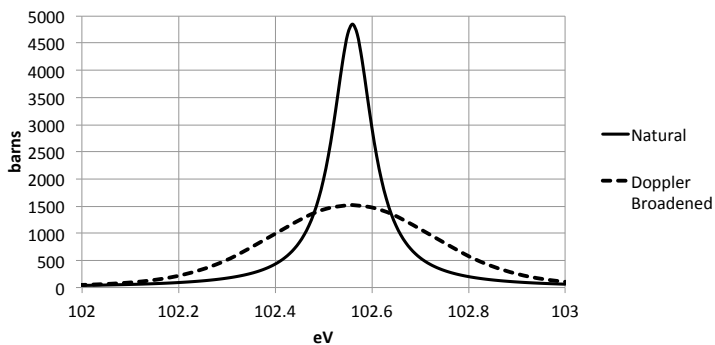


Figure 3.6 Natural and Doppler broadened resonant absorption line in  $^{238}\text{U}$ .  $T = 300^\circ \text{ K}$ .

How can this tiny effective neutron energy cause a significant spreading of the line profile? The answer is that the energy of an incoming neutron in the frame of a moving nucleus is found by first adding the two velocities as a vector sum. The energy of a neutron in the frame of a moving nucleus is then given by

$$E = \frac{1}{2}m_n v^2 = \frac{1}{2}m_n(v_n^2 - 2v_n v_N \cos\theta + v_N^2) \quad (3.70)$$

where  $m_n$  is the neutron mass,  $v_n$  is the incoming neutron speed in the lab frame,  $v_N$  is the speed of the incoming nucleus in the lab frame and  $\theta$  is the angle between their lab-frame velocities. The third term is negligible,  $1.6 \cdot 10^{-4}$  eV as calculated above. But the spreading due to the second term is of order  $\sqrt{E_n E_N / A} = \sqrt{102.6 \text{ eV} \cdot 1.6 \cdot 10^{-4} \text{ eV}} = 0.128 \text{ eV}$ . Thus a nucleus undergoing thermal motion will have a chance to absorb neutrons over a considerably wider range of incoming energies than indicated by the natural absorption line width – higher neutron energies if the nucleus is moving away from the incoming neutron, and lower energies if the nucleus is moving towards it. Concomitantly, neutrons right on the resonance peak in the lab frame will have a lower chance of being absorbed, since many

nuclei are moving fast enough that the neutron, in the frame of the nucleus, is well off the resonance peak.

Neutrons that slow down into an absorption resonance, and enter a fuel rod before slowing down further, have a substantial probability of being absorbed. Fuel rods are typically about 1 cm in diameter, and the number density of uranium in uranium dioxide fuel is  $2.4 \cdot 10^{28} \text{ m}^{-3}$ . Thus an absorption cross-section of 1000 b gives a mean free path of less than 1/2 mm, and neutrons striking the fuel will be absorbed even fairly far from the resonance. Thus as the resonance broadens due to heating of the fuel, absorption will be increased. The absorption cross-section on peak is very much overkill, so the broadening of the wings increases the ability of the fuel to scavenge neutrons, without sacrificing any significant probability of absorption at the peak.

The depletion of the neutron slowing down flux,  $q(E)$ , across the absorption band of resonance  $i$  is given by

$$\begin{aligned}\Delta q(E) &= \phi(E) \Delta E_{eff,i} N_{238U} \sigma_{\gamma,eff,i} V^{fuel} / V^{tot} \\ &= q(E) \frac{\Delta E_{eff,i} N_{238U} \sigma_{\gamma,eff,i} V^{fuel}}{E_i \xi^{mod} \Sigma_e^{mod} V^{mod}}\end{aligned}\quad (3.71)$$

Note that both sides of this equation characterize neutrons in units of  $\text{m}^{-3} \text{s}^{-1}$ . Thus the absorption process depletes the downward flow in energy of the neutrons.  $\Delta E_{eff}$  is an “effective” energy width of the resonance and  $\sigma_{\gamma,eff}$  takes into account the fact that much of the uranium near the center in energy of the resonance and near the geometrical center of the fuel rod sees very little neutron flux, so the “effective” cross-section is reduced. In fact, of course, the nuclear cross-section is unchanged, but the neutron flux is depleted, especially in the core of the fuel, at energies near resonance. We have used  $q(E)$ , rather than  $S$ , in the definition of  $\phi(E)$ , to take into account the depletion of the flux of neutrons downward in energy, at energy  $E$ , by resonances at energies greater than  $E$ . For small drops in  $q(E)$ , we can express the probability of a neutron traversing from above to below the resonance as

$$p_i = \exp \left( -\frac{\Delta E_{eff,i} N_{238U} \sigma_{\gamma,eff,i} V^{fuel}}{E_i \xi^{mod} \Sigma_e^{mod} V^{mod}} \right) \quad (3.72)$$

If we want to know the probability of slowing down through all of the resonances without absorption, we can multiply these probabilities for each

resonance to find the overall “resonance escape probability”,  $p$ .

$$p = \exp \left( -\frac{N_{238}U IV^{fuel}}{\xi^{mod} \Sigma_e^{mod} V^{mod}} \right) \quad (3.73)$$

where

$$I = \sum_i \frac{\Delta E_{eff,i} \sigma_{\gamma,eff,i}}{E_i} \quad (3.74)$$

Now we have hidden the complex calculation of the effective line widths and absorption cross-sections in  $I$ , which has units of barns. Fortunately there are reasonable approximations for this sum in cases of interest. For the case where we can ignore the fact that a fuel rod partially shields its neighbors at near-resonance energies, we can approximate, for uranium dioxide fuel rods of diameter  $2 \text{ mm} < D < 3.5 \text{ cm}$ ,

$$I \approx [4.45 + 16.7D_{cm}^{-1/2}] [1 + 6 \cdot 10^{-3}(T_K^{1/2} - 300^{1/2})] \quad (3.75)$$

where  $D$  is measured in centimeters, and  $T$  in Kelvins. For fuel rods that partially shield one another,  $I$  is somewhat reduced.

An interesting feature of equation 3.73 is that it is very sensitive to the slowing down power of the moderator,  $\xi^{mod} \Sigma_e^{mod}$ . This suggests a significant problem for heavy-water or graphite moderators, whose slowing down power is much less than that of light water, as shown in table 3.1. As we discussed when we looked at power densities in different types of reactors, this problem is compensated by increasing  $V^{mod}/V^{fuel}$ . This has the result that reactor cores based on heavy-water or graphite moderators are much larger, for a given power output, than those based on light-water moderators. This is, of course, a major economic attraction for LWRs, and largely why they have dominated the market. As we will see later, however, heavy-water and graphite-moderated reactors are very attractive for would-be proliferators.

A typical temperature operating point for the fuel in an LWR might be about  $1000^\circ \text{ K} = 727^\circ \text{ K}$ , considerably above the temperature of the coolant/moderator. The fission heat is largely deposited in the fuel in the form of fission fragments, and must diffuse down a strong temperature gradient to the coolant. This provides a very favorable negative feedback characteristic of nuclear reactors that depend on thermal neutron fission; it means that the reaction rate will be slowed as the fuel heats and the slowing-down neutrons are increasingly absorbed. If the reaction rate and so power production begin to increase, say because a neutron absorbing control rod is partially withdrawn from the reactor, the fuel temperature will of necessity

also begin to rise. Now, however, so long as the control rod was not withdrawn too far, the reaction rate will be held from increasing indefinitely, because the radiative neutron absorption will increase at higher temperature and the reactor power will come to a new equilibrium.

The resonances for  $^{235}\text{U}$  and  $^{239}\text{Pu}$  are similar in magnitude to those for  $^{238}\text{U}$ , and they are divided in the outcome of neutron capture between fission and radiative absorption. Since the density of fissile material in a thermal reactor is always much less than the density of  $^{238}\text{U}$ , the net effect of all of the resonances is absorption, but there is an order 1% effect on neutron generation during slowing down in the resonance region, which we have neglected for our purposes here.

Let us evaluate  $p$  for the light-water reactor we considered at the end of section 3.5, described in table 3.4. The fuel diameter is  $D = 0.9$  cm, and let us take  $T = 1000^\circ \text{ K}$ . This gives  $I = 23.9$  b. Using table 3.3 multiplied by 0.96 for the number density of  $^{238}\text{U}$  in the enriched uranium dioxide fuel and table 3.1 for the stopping power of light water, we arrive at  $p = 0.73$ . Note that we have divided the numerator and denominator of the fraction within the argument of the exponential by  $V^{tot}$ .

$$p = \exp\left(-\frac{0.96 \cdot 2.34 \cdot 23.9 \cdot 0.376}{121 \cdot 0.535}\right) = 0.732 \quad (3.76)$$

In sum, we note that  $p$  is an important and sensitive factor in the neutron lifecycle. It typically takes on values in the range of 0.6 – 0.85. The number of neutrons per second per  $\text{m}^2$  slowing down into the Thermal energy region equals  $\epsilon S_{TP}$ .

We can include this effect, very approximately, in the slowing down neutron flux spectrum by depleting the flux spectrum from 10 keV down to the lowest  $^{238}\text{U}$  resonance, at 7 eV. For energies above 10 keV we retain equation 3.68, while for energies below 10 keV we can write

$$\phi_I(E) = \frac{\epsilon S_T}{E \xi \Sigma_e(E)} \left[ 1 - (1-p) \frac{4 - \log_{10}[\text{Max}(E_{eV}, 7)]}{4 - \log_{10}(7)} \right] \quad (3.77)$$

where the integral of  $\chi$  from  $E$  to  $\infty$  has been set to unity at these low energies. Of course this is very approximate, not tracking the energy dependence of the depletion particularly accurately, and not capturing the strong depletion at individual resonances.

### 3.7 Thermal energy region $\phi_T(E)$

After neutrons slow down from the Fast energy region through the Intermediate energy region, it is clear that eventually they must stop, on average, losing energy. What happens is that they begin to gain energy from collisions predominantly with the nuclei of the moderator, due to the thermal motion of these nuclei, and come towards thermal equilibrium with them. This is called the Thermal energy region. The neutrons in this region are close to Maxwellian in their energy distribution, but never fully in equilibrium with their surroundings, because they are “fed” energetic neutrons from the intermediate energy region, and lose neutrons by radiative absorption and driving fission, whose rate coefficients are independent of energy in the low-energy “ $1/v$ ” region. As a result the spectrum is hotter than the moderator, and “harder” than a Maxwellian, with a greater high-energy tail than a corresponding bell-shaped Maxwellian distribution. The expression for a Maxwellian distribution, as a function of energy, is given by

$$n_M(E) = \frac{dn_M}{dE} = n_M \sqrt{\frac{4E}{\pi T^3}} e^{-E/T} \quad (3.78)$$

where  $T$  is expressed in the same energy units as  $E$ , for our purposes Joules.  $T = k_B T_K$ , where  $k_B$  is Boltzmann’s constant and  $T_K$  is temperature in Kelvins.

**Question:** Why do neutrons share energy more easily with nuclei in the moderator than with fuel nuclei?

We can calculate the density of neutrons in the thermal energy region, under steady conditions, by equating the source rate of neutrons with their loss rate

$$q(1eV) = \epsilon S_T p = n_T \nu_{T,abs} = n_T \overline{\Sigma_{T,abs}} v \quad (3.79)$$

where  $q(1eV)$  is the flux of neutrons downwards in energy into the Thermal energy range. The subscript “ $T$ ” indicates that we are considering the thermal energy range. In this energy range we assume that  $\Sigma_{T,abs}$  varies dominantly as  $1/v$ , so we can take  $\nu_{T,abs}$  to be independent of energy. Conventionally we evaluate all thermal cross-sections,  $\Sigma_T$ , at  $E = 0.0253$  eV, where the neutron velocity,  $v$ , is 2200 m/s. This also allows to calculate the mean lifetime of a thermalized neutron:

$$l_T = (\nu_{T,abs})^{-1} = (\overline{\Sigma_{T,abs}} v)^{-1} \quad (3.80)$$

consistent with the expected

$$n_T = \epsilon S_T p l_T \quad (3.81)$$

This allows us to evaluate the Thermal flux spectrum:

$$\phi(E) = \frac{dn_M}{dE} v(E) = \epsilon S_T p l_T \sqrt{\frac{4E}{\pi T^3}} e^{-E/T} \cdot 1.383 \cdot 10^4 \sqrt{E_{eV}} \quad (3.82)$$

$\Sigma_{abs} \propto 1/v$ , which is key for this analysis, is a good assumption for uranium fuel, but not for plutonium fuel.  $^{239}\text{Pu}$  has a strong resonance in the vicinity 0.3 eV. This resonance produces about 60% fission, 40% radiative absorption. Furthermore, this reaction has  $\bar{\nu}$  of about 2.9, so it is clearly a net contributor of neutrons.  $^{241}\text{Pu}$  has a resonance in the vicinity 0.26 eV that produces about 70% fission, 30% radiative absorption, so is also a net contributor. On the other hand  $^{240}\text{Pu}$  has a very strong radiative absorption resonance just above 1 eV. A mitigating factor is that all of these resonances are strong enough that they are strongly self-shielding, in part due to the fact that their width is reduced as a result of the low incoming neutron energy. In this work we will retain  $\Sigma_{abs} \propto 1/v$  even for Pu, but we should keep this caveat in mind. In particular, the large low-energy resonances of fissile Pu can compete with (but not reverse) the stabilizing influence of the radiative absorption resonances of the much larger fraction of  $^{238}\text{U}$ . They also can take quite a bite out of the thermal neutron spectrum, reacting as they do with the neutrons before they fully thermalize.

Remembering that fission is a form of absorption (in this case, obviously, in the evaluation of the distribution of thermal neutrons), we can write

$$\overline{\Sigma}_{T,abs} = \frac{V^{fuel}}{V^{tot}} \left( \overline{\Sigma}_{T,f}^{fuel} + \overline{\Sigma}_{T,\gamma}^{fuel} \right) + \frac{V^{mod}}{V^{tot}} \overline{\Sigma}_{T,\gamma}^{mod} + \frac{V^{clad}}{V^{tot}} \overline{\Sigma}_{T,\gamma}^{clad} \quad (3.83)$$

At thermal energies the strong absorption cross-sections can result in a fairly short mean free path for neutrons within the fuel rods, resulting in some depletion of  $\phi_T$  in the fuel rod compared to its value in the moderator, thus reducing the absorption by the fuel. This is taken into account sometimes by a “thermal disadvantage factor,” which we neglect here, as we neglected the “fast advantage factor” in the Fast energy region.

With the above caveats we can evaluate equation 3.80 for the thermal neutron lifetime,  $l$ , in our example light-water reactor. Using table 3.4 for the volume ratios, table 3.3 for the number densities of the different elements, and table 3.5 for the microscopic thermal cross-sections, neglecting the tiny absorption on oxygen, and recognizing that the velocity at which these are

all evaluated is 2200 m/s, we get

$$l_T = \{[0.376 \cdot (23.4 + 6.52) \cdot 2.34 + 0.088 \cdot 0.191 \cdot 4.31 + 0.535 \cdot 0.322 \cdot 6.69] \cdot 2200\}^{-1} = 16.5 \mu\text{s} \quad (3.84)$$

This result is significantly longer than the slowing down time of  $3.2 \mu\text{s}$  estimated from table 3.1, by dividing the neutron slowing down time in light water by the fraction of the moderator volume over the total volume. For a graphite or heavy-water moderated reactor the slowing down time is much longer, but the fraction of the moderator volume is greater and the absorption is slower (in part because these reactors operate with natural or low-enriched uranium), so again the slowing down time is less than the lifetime against absorption.

Returning to our example light-water reactor, we can calculate

$$n_T = \epsilon S_T p l_T = 1.03 \cdot 0.732 \cdot 1.0 \cdot 10^{19} \cdot 1.65 \cdot 10^{-5} = 1.24 \cdot 10^{14}/\text{m}^3 \quad (3.85)$$

Real reactors are significantly more complex than our “example” light-water reactor loaded with fresh 4% enriched fuel. There are sources of parasitic absorption, occurring neither in the uranium fuel, nor in the cladding or pure moderator. These include

- Fuel assembly and reactor structures
- “Burnable poison,” e.g., gadolinium included in fresh fuel
- “Chemical shim,” e.g., boron added to moderator in form of boric acid
- Control rods and associated structure

Furthermore, the composition of the fuel itself evolves over time, affecting the the absorption of thermal neutrons:

- Build-up of fission products, especially  $^{135}\text{Xe}$  and  $^{149}\text{Sm}$
- Depletion of  $^{235}\text{U}$  due to fission and  $(n, \gamma)$  reactions
- Build-up and evolution of Pu isotopes, fissile and fertile
- Build-up of  $^{236}\text{U}$  from  $(n, \gamma)$  reactions with  $^{235}\text{U}$

Fuel is designed to produce excess neutron multiplication when it is fresh, because it inevitably produces lower multiplication as it burns. So absorbing elements are used to increase radiative absorption when there is more fresh fuel present, and reduce this absorption when there is less. Burnable poisons deplete as the fuel itself becomes less reactive, and the level of boric acid in the moderator can be reduced as well to compensate. Control rods are movable absorbers used to adjust the power output.

In this context it is worth taking a bit of a tour through table 3.5, which displays relevant cross-sections in the Thermal energy region. These have

Table 3.5 *Thermal microscopic cross-sections evaluated at  $v = 2200 \text{ m/s}$  (barns =  $10^{-28} \text{ m}^2$ ) and  $\bar{\nu}$*

Atom	At. Mass	$\overline{\sigma_{T,f}}$	$\overline{\sigma_{T,\gamma}}$	$\overline{\sigma_{T,e}}$	$\overline{\sigma_{T,\alpha}}$	$\bar{\nu}$
Hydrogen	1	—	0.322	30.1	—	—
Deuterium	2	—	$5.05 \cdot 10^{-4}$	4.25	—	—
Boron	Natural	—	0.104	4.51	764	—
Carbon	12	—	$3.86 \cdot 10^{-3}$	2.74	—	—
Oxygen	16	—	$9.56 \cdot 10^{-3}$	2.74	—	—
Magnesium	Natural	—	$6.27 \cdot 10^{-2}$	3.60	—	—
Iron	Natural	—	2.56	11.29	—	—
Zirconium	Natural	—	0.191	6.83	—	—
Cadmium	Natural	—	$2.45 \cdot 10^3$	7.58	—	—
Xenon	135	—	$2.66 \cdot 10^6$	$2.99 \cdot 10^5$	—	—
Samarium	149	—	$4.05 \cdot 10^4$	185	—	—
Gadolinium	Natural	—	$4.86 \cdot 10^4$	171	—	—
Uranium	235	585	98.5	15.1	—	2.44
Uranium	236	0.0473	5.16	8.84	—	2.37
Uranium	238	$1.68 \cdot 10^{-5}$	2.69	9.25	—	—
Uranium	Natural	4.21	3.38	9.29	—	2.44
Uranium	2% $^{235}\text{U}$	11.7	4.61	9.37	—	2.44
Uranium	4% $^{235}\text{U}$	23.4	6.52	9.48	—	2.44
Uranium	20% $^{235}\text{U}$	117	21.9	10.4	—	2.44
Plutonium	239	751	274	7.99	—	2.88
Plutonium	240	$6.43 \cdot 10^{-2}$	291	0.958	—	—
Plutonium	241	1013	363.3	4.27	—	2.94
Plutonium	242	$1.04 \cdot 10^{-3}$	19.27	7.75	—	—

each been evaluated at the  $v = 2200 \text{ m/s}$ , or  $E = 0.0253 \text{ eV}$ . Surveying this table we can find some interesting physics. The large, broad resonance of the proton + neutron (= deuteron) system near zero energy shows up as a large elastic scattering cross-section for hydrogen. This is enhanced by

the thermal motion of the hydrogen itself. Next we can see the very small radiative absorption cross-section for deuterium, which is why heavy water is an effective moderator even for natural uranium fuel. Boron is unremarkable, except for the very strong reaction  $^{10}\text{B} + \text{n} \rightarrow ^7\text{Li} + ^4\text{He} + 2.31 \text{ MeV}$ . This is called an  $(\text{n},\alpha)$  reaction, specifically  $^{10}\text{B}(\text{n},\alpha)^7\text{Li}$ . It is not included in the schema shown in figure 2.5; this is the main place that reactions like this are seen in nuclear reactor physics. In reactors, boric acid is dissolved in the water coolant, and – evidently – a rather small fraction can strongly increase its neutron absorption. Boric acid can also, however, lead to corrosion of low-alloy and carbon steels, as was discovered most dramatically in 2002 at the Davis-Besse nuclear power plant, in Ohio on Lake Erie. A football-sized cavity had been eaten out of the reactor pressure vessel.

We see that carbon and oxygen have very low radiative absorption cross-sections. Magnesium has an attractively low radiative absorption cross-section, so was used in the British Magnox graphite-moderated reactors, that both produced power and plutonium for weapons. It is also used in the North Korean plutonium production reactors for fueling nuclear weapons. It is not compatible with water over long periods of time, however, which makes it difficult to work with. Iron has rather a high radiative absorption cross-section at thermal energies, and a high number density (see table 3.3), which makes it unattractive for thermal-spectrum reactors. Zirconium is much better for fuel cladding.

$^{113}\text{Cd}$ ,  $^{135}\text{Xe}$ ,  $^{149}\text{Sm}$ ,  $^{155}\text{Gd}$  and  $^{157}\text{Gd}$  are all powerful neutron absorbers. They each have substantial low-energy resonances, so their cross-sections do not vary as  $1/v$  over the full Thermal energy region. Cadmium is often present in control rods that are used to adjust a reactor's neutron multiplication. Xenon and Samarium are the main fission products that reduce neutron multiplication. Xenon also contributes multi-hour dynamics to reactor behavior, that notoriously contributed to the Chernobyl disaster. We will discuss the effects of these fission products in sections 5.4 and 5.5. Gadolinium is sometimes mixed into reactor fuel. It is so reactive that it is consumed during operation, so as it burns up its loss partially compensates for the reduction in neutron production due to the depletion of  $^{235}\text{U}$ . Of course the production of  $^{239}\text{Pu}$  also partially compensates for this loss.

The uranium and plutonium sections of the table illustrate the very high effective fission cross-sections that are found at thermal energies. However, you should note that the radiative absorption cross-sections also rise in the Thermal energy region, so the competition between fission and radiative absorption remains important. The table shows that the ratio of the two is strongly modified by enrichment level. In both the U and Pu sections you

can see that nuclei with odd numbers of neutrons have much greater thermal fission cross-sections than those with even numbers. One interesting feature is the very low thermal scattering cross-section of  $^{240}\text{Pu}$ . This is because of a resonance at 1.06 eV, which suppresses scattering on its low-energy wing.

Since we are interested in following neutrons right to the point where they drive fission, we next calculate the “fuel utilization factor,”  $f$ , the fraction of the thermal neutrons that are absorbed in the fuel, divided by the total absorbed. Here we again neglect the “thermal disadvantage factor” that takes into account reduction of  $\phi_T$  within the fuel, and assume fresh 4% enriched fuel, with no poisons.

$$f = \frac{V_{\text{fuel}} (\overline{\Sigma}_{T,f}^{\text{fuel}} + \overline{\Sigma}_{T,\gamma}^{\text{fuel}})}{V_{\text{fuel}} (\overline{\Sigma}_{T,f}^{\text{fuel}} + \overline{\Sigma}_{T,\gamma}^{\text{fuel}}) + V_{\text{mod}} \overline{\Sigma}_{T,\gamma}^{\text{mod}} + V_{\text{clad}} \overline{\Sigma}_{T,\gamma}^{\text{clad}}} \quad (3.86)$$

To evaluate this expression for our “example” LWR, we again use table 3.4 for the volume ratios (dividing top and bottom by  $V^{\text{tot}}$ ), table 3.3 for the number densities of the different elements, and table 3.5 for the microscopic thermal cross-sections, neglecting the tiny absorption on oxygen. We get

$$\begin{aligned} f &= \frac{0.376 \cdot (23.4 + 6.52) \cdot 2.34}{0.376 \cdot (23.4 + 6.52) \cdot 2.34 + 0.088 \cdot 0.191 \cdot 4.31 + 0.535 \cdot 0.322 \cdot 6.69} \\ &= 0.955 \end{aligned} \quad (3.87)$$

This is a very high value, because we are starting with fresh fuel and no poisons. As we will see, this leads to a high multiplication value. In a realistic situation, either with poisons at startup or with much less fissile material after considerable burnup, this value is more typically in the range of 0.65 to 0.85.

The final step is to determine the efficiency of thermal neutrons captured in the fuel to produce fast neutrons through fission. This is called the “thermal efficiency” factor,  $\eta_T$ , but can be seen simply as the neutron multiplication in the fuel. As such, it is given by:

$$\eta_T = \frac{\overline{\nu \Sigma}_{T,f}^{\text{fuel}}}{\overline{\Sigma}_{T,f}^{\text{fuel}} + \overline{\Sigma}_{T,\gamma}^{\text{fuel}}} = \frac{\overline{\nu \sigma}_{T,f}^{\text{fuel}}}{\overline{\sigma}_{T,f}^{\text{fuel}} + \overline{\sigma}_{T,\gamma}^{\text{fuel}}} \quad (3.88)$$

where the second equality comes from the fact the fuel density cancels out. This is evaluated, as a function of neutron energy, in figure 1.3.

Again assuming 4% enrichment in our “example” reactor we can use table

3.5 to arrive at

$$\eta_T = \frac{2.44 \cdot 23.4}{23.4 + 6.52} = 1.91 \quad (3.89)$$

As shown on the left-hand side of figure 1.3,  $\eta_T$  depends strongly on the level of enrichment of the fuel. Thus this factor also drops with the burnup of  $^{235}\text{U}$ .

The number of neutrons per second per  $\text{m}^2$  that are produced from fission driven by thermal neutrons,  $S_T$ , equals  $f\eta_T$  times the influx of neutrons per second per  $\text{m}^2$  from the Intermediate energy region. At the end of section 3.6.1 we saw that this influx was  $\epsilon p S_T$ . If we multiply these together we have

$$S_T = \epsilon p f \eta_T S_T \quad (3.90)$$

For this equation to be satisfied we require

$$\epsilon p f \eta_T = 1 \quad (3.91)$$

This is known as Fermi's Four Factor Formula. If it is not satisfied, the neutron production, and so power production (in our infinite system) is either falling ( $\epsilon p f \eta_T < 1$ ) or rising ( $\epsilon p f \eta_T > 1$ ) in time. We will examine the so-called "kinetics" of the time-dependent process in Chapter 5.

In our case we found relatively high values for  $f$  and  $\eta_T$ , since we did not include the full panoply of poisons and parasitic absorbers and we did not consider any burn-up of the fuel. As a result our "example" LWR has  $\epsilon p f \eta_T = 1.03 \cdot 0.732 \cdot 0.955 \cdot 1.91 = 1.38 > 1$ . Note that just as this calculation is not completely realistic for the neutron multiplication, the absorption time would be less with more poisons present at the start of operations, and greater at later times as fuel is burned up, so the large macroscopic fission cross-section falls, and poisons are removed.

### 3.8 Visualizing the four-factor formula

Fermi's four-factor formula for the neutron economy of an infinite thermal fission reactor, is generally presented in terms of the life cycle of a single neutron. In essence, steady operation of such a reactor requires that the life cycle of a neutron close precisely, with one parent neutron ultimately producing exactly one child.

$$k_\infty \equiv \epsilon p f \eta_T = 1 \quad (3.92)$$

where the  $\infty$  subscript again reminds us that we are considering an infinite system, with no spatial losses. Every fast neutron produced from thermal fission results in  $\epsilon$  neutrons delivered to the intermediate energy range.  $\epsilon p$

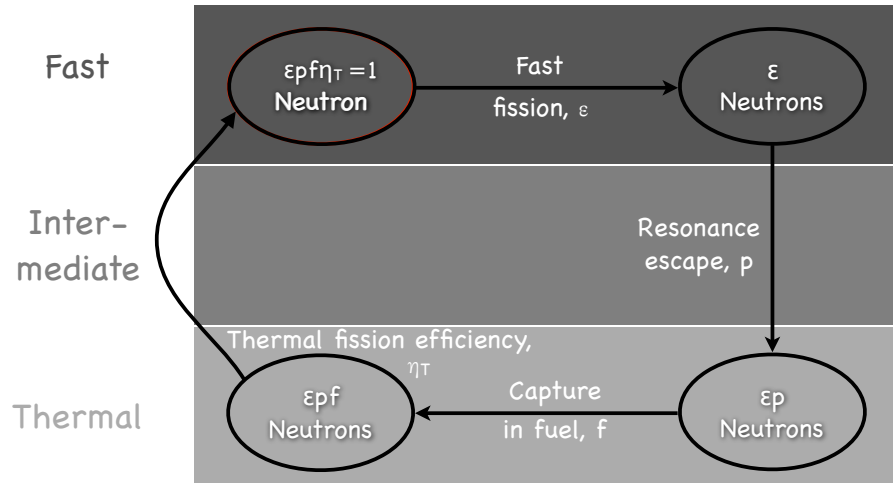


Figure 3.7 Fermi's neutron life cycle

neutrons escape the resonances as they slow down and are then delivered to the thermal energy range.  $\epsilon p f$  thermal neutrons are captured in the fuel, and this then produces  $\epsilon p f \eta_T$  neutrons from thermal fission. For the reactor to operate at a steady rate of fission, every neutron produced by thermal fission must ultimately replace itself with exactly one neutron from thermal fission, as expressed in Fermi's formula. This is shown diagrammatically in figure 3.7.

**Question:** If Fermi's four-factor formula is satisfied, does it guarantee that a neutron leaving the intermediate energy region will precisely reproduce itself with a neutron entering the intermediate energy region? (This is a little tricky. Don't jump to the "obvious" conclusion.)

### 3.9 Neutron flux spectrum in the example Light Water Reactor

We have made a number of approximations in our analytic derivations of the Fast, Intermediate, and Thermal flux spectra in our "example" LWR. It is

interesting, therefore, to compare our analytic results with a full numerical calculation. The Monte Carlo N-Particle code, MCNP, was used to calculate the average neutron flux spectrum in our “example” LWR. This code tracks millions of neutrons from their “birth” at fission to their absorption, as they undergo all of the processes we have discussed, simulating collisions using a random sampling process (hence the name Monte Carlo). The spatial profile of neutron birth is obtained by iteration over initial batches of neutrons, and noting where they undergo fission.

The results from a Monte-Carlo code such as MCNP are usually tallied as cumulative neutron “track lengths” within predetermined spatial zones and energy intervals. To interpret these cumulative track lengths we assume that the volume of the system under consideration is  $V_{tot}$ , and that the neutrons we are simulating are born over some time period  $\tau_{tot}$ , much longer than the lifetime of the individual neutrons in the system. Now we have that the average volumetric source rate of neutrons being simulated is  $S_{sim} = N_{sim}/(V_{tot}\tau_{tot})$ , where  $N_{sim}$  is the total number of neutrons in the simulation. We define the summed track lengths in a spatial zone and energy interval of interest as  $\Sigma(\Delta L)$ . Each individual track length,  $\Delta L$ , that contributes to the cumulative  $\Sigma(\Delta L)$  represents a time,  $\Delta t$ , spent by one neutron in the spatial zone and energy interval of interest, multiplied by its speed,  $v$ . Each  $\Delta t/(\tau_{tot} V_{zone})$  represents an incremental contribution to the number density within the spatial zone and energy interval, since this is the fraction of the total time one neutron spent in the spatial range and energy internal of interest. By the same token  $v\Delta t/(\tau_{tot} V_{zone}) = \Delta L/(\tau_{tot} V_{zone})$  from this neutron must be its incremental contribution to the neutron flux,  $\phi \equiv nv$ , in the spatial zone and energy interval. From this we have that  $\Sigma(\Delta L)/(\tau_{tot} V_{zone})$  is the calculated  $\Delta\phi$ , in the expected units of  $\text{m}^{-2}\text{s}^{-1}$ . Since  $\phi(E) \equiv d\phi/dE$  we have  $\phi(E) \approx \Delta\phi/\Delta E = \Sigma(\Delta L)/(\tau_{tot} V_{zone} \Delta E)$ . Finally, to determine the prediction for a real case, we multiply by  $S/S_{sim}$ , resulting in an equation for  $\phi(E)$  in a spatial zone and energy interval of interest:

$$\phi(E) \approx \frac{\Sigma(\Delta L)}{\tau_{tot} V_{zone} \Delta E} \frac{S}{N_{sim}/(V_{tot}\tau_{tot})} = \frac{SV_{tot}}{N_{sim}} \frac{\Sigma(\Delta L)}{V_{zone} \Delta E} \quad (3.93)$$

The standard output of MCNP, for each predetermined spatial zone and energy interval, is the summed track length per unit volume,  $\Sigma(\Delta L)/V_{zone}$ . Thus to arrive at a  $\phi(E)$  of interest, you must multiply by  $SV_{tot}/(N_{sim}\Delta E)$ .

**Question:**  $\tau_{tot}$  dropped out of the result. Does this make sense? Also, confirm that the units on the R.H.S. of this equation are correct.

The calculation shown in figure 3.8 was done for a single lattice cell with specularly reflecting boundary conditions, as if it were bounded by identical (but mirror-image!) lattice cells undergoing the identical Monte-Carlo calculation. This corresponds to the assumption in this chapter, where we have ignored neutron spatial transport, but it does capture spatial variation of the structures within a cell, and in particular self-shielding of the capture resonances. The spatial zone for the tally, however, is the full cell, so the plot represents the volume-average neutron flux within the cell. The energy resolution is  $\Delta E/E = 11\%$ . The results from equations 3.46, 3.68, 3.77, and 3.82 are overlaid on the Monte-Carlo calculation. We have assumed a total (thermal + fast) neutron production rate of  $10^{19} \text{ s}^{-1}\text{m}^{-3}$ . Note that  $\epsilon S_T$  appears in equations 3.68, 3.77, and 3.82. Using equation 3.57 we can write

$$S_T = S \left[ 1 - \frac{V^{fuel}}{V^{tot}} \frac{\overline{\nu_F} \Sigma_f^{fuel}}{\Sigma_{F,loss}} \right] \quad (3.94)$$

and then using equation 3.59 we have the convenient result:

$$\epsilon S_T = S \left[ 1 - \frac{V^{fuel} (\overline{\Sigma}_{F,f}^{fuel} + \overline{\Sigma}_{F,\gamma}^{fuel})}{V^{tot} \Sigma_{F,loss}} \right] \quad (3.95)$$

An interesting implementation detail is that MCNP tracks a generation composed of many independent neutrons from the neutrons' births at fission events until their first absorptions, and fission events are considered as such absorptions. The resulting fission neutrons, whether from Fast or Thermal region fission events, are all counted as part of the following generation. This is unlike Fermi's definition of a generation, which includes Fast region neutron multiplication within a single generation. Nonetheless, if the approximations in the Fermi approach are good, an MCNP spectrum should be close to a Fermi-based spectrum. A Fermi spectrum starts with only the source of neutrons arising from Thermal region fissions, and increases that Thermal spectrum source by the multiplication that gives the total source, Thermal + Fast – exactly what is used in calculating the MCNP spectrum. The two approaches then deplete the number of neutrons entering the Intermediate region from the Fast region, and the Thermal region from the Intermediate region, by the same processes.

The different definitions of a generation of neutrons between MCNP and the Fermi approach do, however, have an effect on the evaluation of  $k_\infty$ , when  $k_\infty \neq 1$ , as derived in exercise 3.11. Conceptually, the shorter life of a generation in MCNP implies  $k_\infty$  closer to unity than in Fermi's approach, to get the same physical growth or decay of the neutron population per unit

time. Adjusting the MCNP value to the same basis as Fermi's approach, using the result in exercise 3.11, we get  $k_\infty = 1.42$ , reasonably close to the Fermi value of 1.38 derived in this chapter.

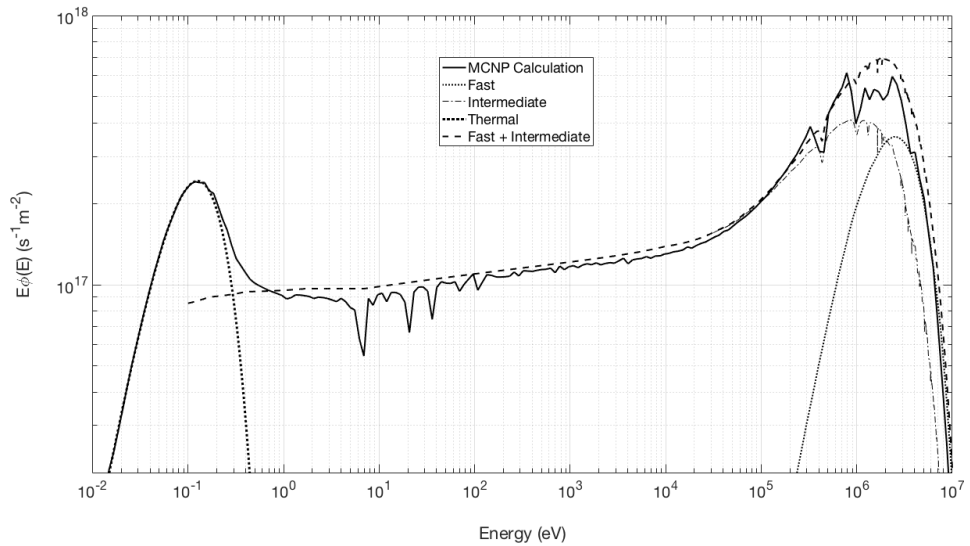


Figure 3.8 Neutron flux spectrum in the “example” LWR, MCNP vs. analytic results. MCNP simulation by Julien de Troullioud de Lanversin

The agreement between the analytic spectrum and the numerical calculation is surprisingly close. In the energy range around 1 MeV we can see some structure in the numerical result that is not well reflected in the analytic calculations. This structure is due to the  $^{16}\text{O}$  elastic scattering resonances that can be seen clearly in figure 2.11. These highly localized resonances are not considered in the Fast spectrum calculation, and are not handled appropriately in the slowing-down calculations. For example the resonance just above 400 keV depletes neutrons at this energy and moves them down on average to 350 keV and the resonance at about 1 MeV moves them on average to 880 keV.

**Question:** Why does elastic scattering on oxygen move neutrons down, on average, by 12% in energy?

When we add the undegraded Fast and extended Intermediate slowing-down spectra together, they somewhat exceed the MCNP result. This is probably because inelastic scattering is not included in the slowing-down calculation. The significant contribution of the high-energy end of the nominally Intermediate spectrum, suggests that  $\epsilon$  may be somewhat underesti-

mated by considering only undegraded neutrons. Paradoxically, such an underestimate, potentially explaining the difference in  $k$ , could also explain the slightly higher analytic vs. MCNP spectrum in the bulk of the Intermediate range of energy.

In the energy range around 100 keV, the shape of the slowing down spectrum is affected by the variation of the hydrogen scattering cross-section with energy. This is remarkably similar to the numerical result. In the bulk of the Intermediate range of energy, the analytic calculation runs less than 10% below the fully numerical result, while both traverse some five orders of magnitude in energy and  $\phi(E)$ . This is a remarkable tribute to Fermi's analysis of neutron slowing down. Note that, as expected, our simple inclusion of the resonance escape probability does not exhibit the strong depletion at resonances observed in the numerical simulation. Note that the energy bin-width in the MCNP calculation, at each energy, is 11% of the that energy, so the downward depletion spikes are not fully resolved in the plot.

The Thermal flux spectrum is fit here with a temperature of 0.063 eV = 693° K, which is modestly above the moderator temperature, taken here to be 600° K, so this reflects heating and hardening by the slowing-down neutrons.

### 3.10 Fast reactors

Fast-neutron-spectrum reactors, sometimes called simply (but confusingly) “fast reactors,” operate quite differently from the thermal-neutron-spectrum reactors we have discussed so far in this chapter. Sustainment of the chain reaction in the case of fast reactors involves closing the neutron life cycle at energies between above about 25 keV, thus avoiding the greatest effects of resonant absorption. This requires enrichment in the range of 20% to achieve  $\eta$  acceptably above unity, as can be seen in figure 1.3. If neutrons could be held (magically) at 2 MeV one could operate at lower enrichment, since  $^{238}\text{U}$  fissions at such high energies, but inelastic scattering just on the fuel itself rapidly degrades such neutrons to the range of one hundred keV, making this impossible.

A signature feature of fast reactors is that the coolant, which extracts power from the fuel rods, does not contain low-Z materials, such as hydrogen, deuterium or carbon – used for slowing down neutrons in thermal-spectrum reactors. The most common coolant is liquid sodium, but lead and lead-bismuth have been used, and high-temperature helium gas is proposed. A problem with gaseous He as a coolant is that it has very low volumetric heat capacity. This has the two consequences: it must flow through the reactor

very quickly and it provides very little thermal “ballast” against temperature excursions.

Let us start to analyze fast reactors using the same approach for the Fast energy spectrum in a fast reactor, composed of neutrons undegraded in energy, as we did for the ‘Fast energy region of thermal spectrum reactors. One important difference is that there is no significant low-Z moderator present to extract neutrons from this energy region. You might think that sodium with  $\xi = 0.0845$  is not so different from carbon with  $\xi = 0.158$ , but a graphite-moderated reactor has a very large ratio of moderator to fuel volume, while the coolant volume is generally less than the fuel volume in a fast reactor. Sodium also has a much lower number density than graphite.

Let us define the region into which the undegraded neutrons move after inelastic scattering as the Fast Reactor Intermediate, or FR-I region, in analogy to the Intermediate region in LWRs. There is no equivalent, of course, of the Thermal region. It is unusual to use this approach for fast reactors, but it will provide us with some useful insights.

We start by essentially copying equation 3.46:

$$\phi_F(E) = \frac{S\chi(E)}{\Sigma_{loss}(E)} = \frac{s(E)}{\Sigma_{loss}(E)} \quad (3.96)$$

As can be seen from Table 3.2 the dominant neutron interaction with both the moderator, which we will take to be sodium, and with the cladding and other structure, which we will take for simplicity to be iron, is inelastic scattering. Radiative capture on sodium and iron can be neglected. Special stainless steels, which are iron alloys, are best suited to the neutron environment of a fast reactor.

Next we need to modify equation 3.48 to recognize that the coolant affects the spectrum by inelastic, rather than elastic, scattering

$$\begin{aligned} \Sigma_{F,loss}(E) &= \frac{V^{cool}}{V^{tot}} \overline{\Sigma_{F,in}^{cool}}(E) + \frac{V^{clad}}{V^{tot}} \overline{\Sigma_{F,in}^{clad}}(E) \\ &\quad + \frac{V^{fuel}}{V^{tot}} \left[ \overline{\Sigma_{F,f}^{fuel}}(E) + \overline{\Sigma_{F,\gamma}^{fuel}}(E) + \overline{\Sigma_{F,in}^{fuel}}(E) \right] \end{aligned} \quad (3.97)$$

Then we take the Watt-spectrum average of our modified equation:

$$\begin{aligned} \Sigma_{F,loss} &= \frac{V^{cool}}{V^{tot}} \overline{\Sigma_{F,in}^{cool}} + \frac{V^{clad}}{V^{tot}} \overline{\Sigma_{F,in}^{clad}} \\ &\quad + \frac{V^{fuel}}{V^{tot}} \left[ \overline{\Sigma_{F,f}^{fuel}} + \overline{\Sigma_{F,\gamma}^{fuel}} + \overline{\Sigma_{F,in}^{fuel}} \right] \end{aligned} \quad (3.98)$$

We can now take over directly equation 3.59 for the fast reactor situation:

$$\epsilon \equiv \frac{S_{FR-I} + S_F}{S_{FR-I}} = \frac{1 - \frac{V_{fuel}}{V^{tot}} \frac{(\overline{\Sigma}_{F,f}^{fuel} + \overline{\Sigma}_{F,\gamma}^{fuel})}{\overline{\Sigma}_{F,loss}}}{1 - \frac{V_{fuel}}{V^{tot}} \frac{\overline{\nu}_F \overline{\Sigma}_{F,f}^{fuel}}{\overline{\Sigma}_{F,loss}}} \quad (3.99)$$

where  $S_{FR-I}$  represents the source of neutrons from fission due to neutrons that have first suffered an energy-losing inelastic collision.

Most thermal reactors use a square grid of fuel rods, but fast reactors generally use a hexagonal grid, to allow a larger fraction of fuel volume. For our nominal fast reactor, let us assume the parameters shown in table 3.6, where the lattice pitch in this case is the distance between the centers of adjacent fuel pins in the hexagonal grid.

Table 3.6 *Example Sodium-Cooled Fast Reactor Hexagonal Lattice Cell*

Parameter	Value
Fuel pin diameter	0.009 m
Iron cladding	0.0006 m
Lattice pitch	0.011 m
$V_{fuel}/V^{tot}$	0.455
$V_{clad}/V^{tot}$	0.219
$V^{mod}/V^{tot}$	0.325

We can carry along the result for the fast-region spectrum equation 3.49, taking into account both the neutrons due to the FR-I spectrum, and the multiplication in the Fast spectrum itself.

$\epsilon$  is generally a much more significant factor in fast reactors than in thermal reactors, since the large loss of fast neutrons by collisions with hydrogen is not present. Let us again work an example, using tables 3.2 and 3.3 to compute the desired macroscopic cross-sections. For our nominal case, assuming uranium oxide fuel enriched to 20%  $^{235}\text{U}$ , we have

$$\begin{aligned} \Sigma_{F,loss} &= 0.325 \cdot 2.43 \cdot 0.513 + 0.219 \cdot 8.49 \cdot 0.644 \\ &\quad + 0.455 \cdot 2.34 \cdot [0.488 + 0.0759 + 2.47] = 4.83 \text{ m}^{-1} \end{aligned} \quad (3.100)$$

which is dominated by inelastic scattering on uranium, but with a significant contribution from inelastic scattering on the coolant and cladding plus

structure. We can also calculate

$$\begin{aligned}\overline{\Sigma_{F,f}^{fuel}} &= 2.34 \cdot 0.488 = 1.14 \text{ m}^{-1} \\ \overline{\Sigma_{F,\gamma}^{fuel}} &= 2.34 \cdot 0.0759 = 0.178 \text{ m}^{-1} \\ \overline{\nu_F \Sigma_{F,f}^{fuel}} &= 2.67 \cdot 1.14 = 3.04 \text{ m}^{-1}\end{aligned}\quad (3.101)$$

Fast fission in this case is again mainly due to collisions with  $^{238}\text{U}$ , but there is significant enhancement by  $^{238}\text{U}$  fission, due to the 20% enrichment level. From these results we can find

$$\epsilon = \frac{1 - 0.455 \cdot (1.14 + 0.178)/4.83}{1 - 0.455 \cdot 3.04/4.83} = 1.23 \quad (3.102)$$

This term is much enhanced compared with a thermal-spectrum reactor, mostly due to the absence of low-A moderation, but partly also due to greater enrichment.

It is difficult to calculate analytically the lower-energy neutron spectrum in a fast reactor. This spectrum is “fed” from above by inelastic scattering of the primary fission neutrons. It is shaped by further inelastic scattering and some drag on the coolant, and is ultimately depleted by fission and radiative absorption. Spectra vary from one design to another, but  $E\phi(E)$  for the lower-energy region tends to peak at around 100 keV.

To roughly match our Monte-Carlo simulation results, shown in figure 3.9, we will approximate the FR-I spectrum as giving  $E\phi(E)$  proportional to a so-called “log-normal” function. This is just a function that looks like a normal, or Gaussian, distribution, shifted from the origin, when it is displayed against a logarithmic  $x$ -axis. It looks most familiar when the  $y$ -axis is linear. To reasonably fit the simulation, without being overly fussy, we center the distribution of  $E\phi_{FR-I}(E)$  on 100 keV, with  $1-\sigma$  width of a factor of 4 in either direction, i.e., with r.m.s. width spanning from 25 keV to 400 keV. This log-normal distribution is

$$\phi_{FR-I}(E_{eV}) \propto \frac{1}{E_{eV}} \exp \left\{ -\frac{[\log_{10}(E_{eV}) - 5]^2}{2 [\log_{10}(4)]^2} \right\} \quad (3.103)$$

We average cross-sections over  $\phi_{FR-I}$  and denote them as, for example for fission,  $\sigma_{FR-I,f}$ ,  $\Sigma_{FR-I,f}$  and  $\overline{\Sigma_{FR-I,f}}$ . As a particular case,

$$\sigma_{FR-I,f} \equiv \frac{\int_0^\infty \phi_{FR-I}(E) \sigma_f(E) dE}{\int_0^\infty \phi_{FR-I}(E) dE} \quad (3.104)$$

Comparing the  $^{238}\text{U}$  and  $^{235}\text{U}$  fission cross-sections averaged over this

$\phi_{FR-I}$  (table 3.7) to the Watt-spectrum averaged cross-sections (table 3.2), we see that the  $^{238}\text{U}$  fission largely drops out of the picture in the FR-I region.

**Question:** Remind yourself of the definitions of each of the kinds of cross-sections in table 3.7.

Table 3.7 *Fast-Reactor microscopic cross-sections (b) and  $\bar{\nu}$ , averaged over  $\phi_{FR-I}$  defined in equation 3.103.*

Atom	At. Mass	$\sigma_{FR-I,f}$	$\sigma_{FR-I,\gamma}$	$\sigma_{FR-I,e}$	$\sigma_{FR-I,in}$	$\bar{\nu}$
Oxygen	16	—	$6.41 \cdot 10^{-5}$	3.88	$2.03 \cdot 10^{-4}$	—
Sodium	23	—	$1.57 \cdot 10^{-3}$	4.98	$4.48 \cdot 10^{-2}$	—
Iron	Natural	—	$8.94 \cdot 10^{-3}$	3.69	$6.00 \cdot 10^{-2}$	—
Lead	Natural	—	$5.05 \cdot 10^{-3}$	9.22	$3.60 \cdot 10^{-2}$	—
Uranium	235	1.73	0.479	9.00	0.575	2.45
Uranium	238	$1.51 \cdot 10^{-2}$	0.269	10.7	0.754	2.74
Uranium	4% $^{235}\text{U}$	$8.37 \cdot 10^{-2}$	0.277	10.6	0.747	2.50
Uranium	20% $^{235}\text{U}$	0.358	0.311	10.3	0.718	2.46
Plutonium	239	1.62	0.376	9.24	0.756	2.92
Plutonium	240	0.230	0.453	10.3	0.689	2.99
Plutonium	241	2.30	0.385	8.22	0.744	2.96
Plutonium	242	0.147	0.364	11.5	0.683	3.07

There is no analog to the resonance escape probability,  $p$ , in the case of a fast reactor, since neutrons are not slowed down past resonances. But we can estimate  $f$  and  $\eta_{FR-I}$ , with the goal of ending up with a three-factor formula,  $\epsilon f \eta_{FR-I}$ .

Now we are in a position to evaluate  $f$ , the fuel utilization factor, in analogy to how we evaluated it in the thermal case. Again  $f$  is defined as the absorption in the fuel divided by all forms of absorption.

$$f = \frac{V_{fuel} \left( \overline{\Sigma_{FR-I,f}^{fuel}} + \overline{\Sigma_{FR-I,\gamma}^{fuel}} \right)}{V_{fuel} \left( \overline{\Sigma_{FR-I,f}^{fuel}} + \overline{\Sigma_{FR-I,\gamma}^{fuel}} \right) + V_{cool} \overline{\Sigma_{FR-I,\gamma}^{cool}} + V_{clad} \overline{\Sigma_{FR-I,\gamma}^{clad}}} \quad (3.105)$$

where again, all of the cross-sections are averaged over the log-normal FR-I distribution. Note that we are not including elastic or inelastic scattering in determining loss from the FR-I spectrum, since such scattering moves neutrons downwards in energy but does not remove them. We have, in practice, included these effects in the assumed log-normal shape of the FR-I spectrum we selected.

For our nominal fast reactor case, we can now evaluate  $f$ . Its numerator and denominator (each divided by  $V_{tot}$ ) and its resulting value are given by:

$$\begin{aligned} f_{num} &= 0.455 \cdot 2.34 \cdot (0.358 + 0.311) = 0.712 \\ f_{den} &= 0.455 \cdot 2.34 \cdot (0.358 + 0.311) + 0.325 \cdot 2.43 \cdot 1.57 \cdot 10^{-3} \\ &\quad + 0.219 \cdot 8.49 \cdot 8.94 \cdot 10^{-3} = 0.730 \\ f &= 0.976 \end{aligned} \tag{3.106}$$

where we have neglected the very small radiative absorption by the oxygen in the fuel.

The final step is to evaluate  $\eta_{FR-I}$  the ratio of neutrons produced in the fuel to those captured, in the FR-I region of the energy spectrum. By analogy with the thermal calculation we have:

$$\eta_{FR-I} = \frac{\overline{\nu\sigma}_{FR-I,f}^{fuel}}{\sigma_{FR-I,f}^{fuel} + \sigma_{FR-I,\gamma}^{fuel}} \tag{3.107}$$

For our nominal fast reactor this evaluates to

$$\eta_{FR-I} = \frac{2.46 \cdot 0.358}{0.358 + 0.311} = 1.32 \tag{3.108}$$

Summarizing the neutron life-cycle for our nominal fast reactor, we have

$$\epsilon f \eta_{FR-I} = 1.23 \cdot 0.976 \cdot 1.32 = 1.58 \tag{3.109}$$

Thus we see that fast reactors, running with 20% enriched uranium fuel, can have significantly more multiplication than light-water reactors. This is rather understated in the present calculation, because it is easier to avoid parasitic absorption of fast spectrum neutrons than thermal neutrons. Fast-reactor cores tend to have higher power density and be smaller than LWRs, and fast neutrons have longer mean-free paths than thermal neutrons. As a result the spatial loss of neutrons (discussed in the next chapter) tends to be greater for fast reactors. A significant fraction of the extra 0.55 neutrons produced in the neutron life-cycle, in our example case, may be lost from the reactor core that contains the fissile material. However if the core is surrounded by a “blanket” composed of  $^{238}\text{U}$  fuel assemblies, then there

is a high probability that the lost neutrons will suffer radiative absorption and  $^{239}\text{Pu}$  nuclei will be produced. This is in addition to the  $^{239}\text{Pu}$  that is produced by the Fast and FR-I spectra in the core itself. As a result, a fast reactor can, in principle, produce more fissile material than it consumes. A fast reactor with a natural uranium blanket surrounding the core, called a “breeder reactor,” can theoretically produce as much as  $1.5x$  more fissile material than it consumes. Alternatively, the energetic neutron spectrum in a fast reactor containing a minimum of  $^{238}\text{U}$  can theoretically burn significantly less reactive fuel than uranium, such as the plutonium and other transuranics (sometimes called “minor actinides”) that are left in the spent, or used, fuel of thermal-spectrum reactors. Theoretically such a fast reactor, called a “burner reactor” can reduce its transuranic material inventory by about  $1/2$  as much as it burns, i.e., making only about one transuranic nucleus per two transuranics burned. Such systems in principle produce energy from what would otherwise be considered waste, and arguably reduce the burden of waste for future generations. These in-principle capabilities have proven difficult to achieve practically, and their associated fuel cycles can carry with them considerable risk of the diversion of materials usable in nuclear weapons, but they attract reactor designers to fast-spectrum systems.

### 3.11 Neutron flux spectrum in the example Fast Reactor

Finally, we would like to calculate the neutron flux spectrum in our “example” fast reactor. The average power density in the core of a fast reactor tends to be higher than in a thermal reactor, if only because the relative fuel density is higher. For a typical value in some of the existing and planned designs, let us take  $350 \text{ MW/m}^3$ , which gives a fission rate of  $1.08 \cdot 10^{19}/\text{m}^3\text{s}$ , or a neutron source rate of about  $2.7 \cdot 10^{19}/\text{m}^3\text{s}$ .

Equations 3.96 and 3.97 provide the Fast spectrum in the fast reactor.

We plan to compare with the MCNP calculation, with its definition of a neutron generation, so the “feed” to the FR-I region of the spectrum is not enhanced by multiplication in the Fast region, but rather is depleted by the numerator in the equation for  $\epsilon$ , equation 3.99.

Since the source of neutrons to the FR-I region must balance their loss,

we can write

$$\begin{aligned}
& S \left[ 1 - \frac{V^{fuel}}{V^{tot}} \frac{\left( \overline{\Sigma}_{F,f}^{fuel} + \overline{\Sigma}_{F,\gamma}^{fuel} \right)}{\Sigma_{F,loss}} \right] \\
&= \int_0^\infty \phi_{FR-I}(E) \left[ \frac{V^{fuel}}{V^{tot}} \left( \overline{\Sigma}_f^{fuel}(E) + \overline{\Sigma}_\gamma^{fuel}(E) \right) \right. \\
&\quad \left. + \frac{V^{cool}}{V^{tot}} \overline{\Sigma}_\gamma^{cool}(E) + \frac{V^{clad}}{V^{tot}} \overline{\Sigma}_\gamma^{clad}(E) \right] dE \\
&= \int_0^\infty \phi_{FR-I}(E) dE \\
&\quad \times \left[ \frac{V^{fuel}}{V^{tot}} \left( \overline{\Sigma}_{FR-I,f}^{fuel} + \overline{\Sigma}_{FR-I,\gamma}^{fuel} \right) + \frac{V^{cool}}{V^{tot}} \overline{\Sigma}_{FR-I,\gamma}^{cool} + \frac{V^{clad}}{V^{tot}} \overline{\Sigma}_{FR-I,\gamma}^{clad} \right]
\end{aligned} \tag{3.110}$$

by the definition of the FR-I-averaged cross-sections. Evidently this gives us the normalization for our log-normal FR-I spectrum:

$$\begin{aligned}
& \int_0^\infty \phi_{FR-I}(E) dE \\
&\quad S \left[ 1 - \frac{V^{fuel}}{V^{tot}} \frac{\left( \overline{\Sigma}_{F,f}^{fuel} + \overline{\Sigma}_{F,\gamma}^{fuel} \right)}{\Sigma_{F,loss}} \right] \\
&= \frac{V^{fuel}}{V^{tot}} \left( \overline{\Sigma}_{FR-I,f}^{fuel} + \overline{\Sigma}_{FR-I,\gamma}^{fuel} \right) + \frac{V^{cool}}{V^{tot}} \overline{\Sigma}_{FR-I,\gamma}^{cool} + \frac{V^{clad}}{V^{tot}} \overline{\Sigma}_{FR-I,\gamma}^{clad}
\end{aligned} \tag{3.111}$$

which we have used in figure 3.9.

The agreement is reasonable, given the somewhat arbitrary fit function. One can see that the flux of energetic neutrons is about one order of magnitude higher than for our example LWR, due on the one hand to the higher power density, and on the other to the absence of a hydrogen-bearing moderator. As in the example LWR spectrum, there are spiky features that are not captured in the analytic approach. You are asked to identify the causes of some these in exercise 3.10.

Remarkably, when the MCNP  $k_\infty$  is adjusted to the same basis as Fermi's approach, we arrive at very close to the same answer as we derived analytically; in the MNCP case  $k_\infty = 1.55$ .

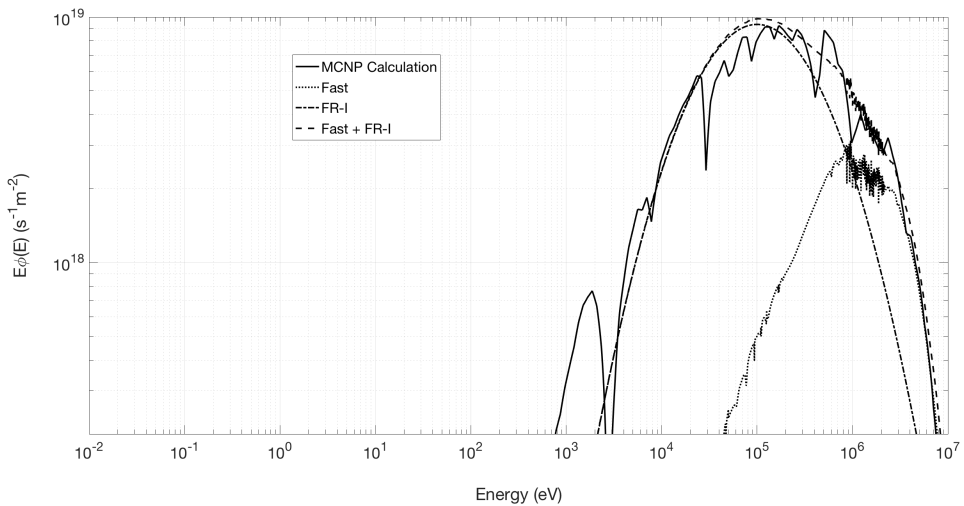


Figure 3.9 Neutron flux spectrum in the example FR, MCNP vs. analytic results. MCNP simulation by Julien de Troullioud de Lanversin

## Review

### Resources

### Exercises

- 3.1 Derive the asymptotic ratio of  $1 - \alpha$  to  $\xi$  for high values of  $A$ . To do this, define  $\epsilon \equiv 1 - \alpha$  and include terms as small as quadratic in  $\epsilon$ . Explain this result based on the physics. Use it to estimate the number of collisions required for an  $e$ -fold downwards of neutron energy for target nuclei of  $A = 200$  and  $A = 238$ .
- 3.2 Derive  $\phi_I(E)$  in Fermi's continuous slowing down approximation. First draw a diagram, analogous to figure 3.5, that depicts the differential energy range of neutrons that will cross energy  $E$  in differential time  $dt$ , given  $dE/dt$ . Using equation 3.35, determine the density of neutrons contained in this energy range and so the downward flux of neutrons crossing  $E$ , in units of  $\text{m}^{-3}\text{s}^{-1}$ . You should have:

$$q(E) = S = -\frac{dn}{dE} \frac{dE}{dt} = -n(E) \frac{dE}{dt} \quad (3.112)$$

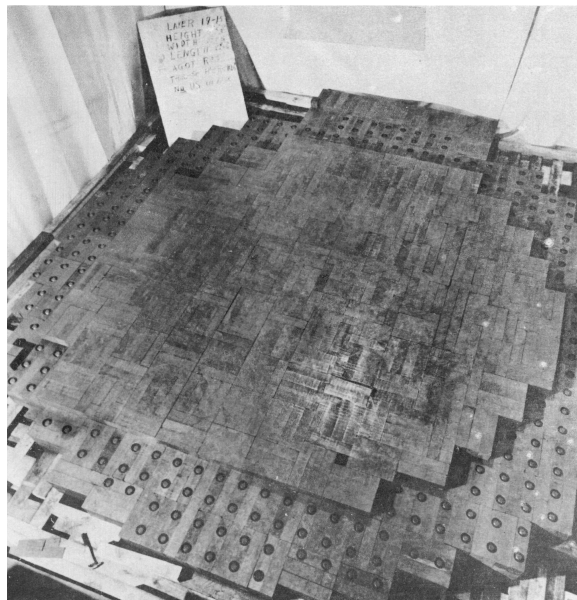
Using Fermi's slowing-down formula, equation 3.28, show that this analysis gives the same result as equation 3.66, but generalized for multiple species of nuclei.

- 3.3 Build a Monte Carlo code to simulate slowing down, and show how good the high energy approximation is.

- 3.4 Develop an equation for a putative  $\epsilon'$  that takes into account only  $(n, \gamma)$  depletion of the flux downwards in energy from the “fast” energy region. How large is the effect of radiative absorption?
- 3.5 Estimate the volume-average value of  $\phi_F(E)$  at 1 MeV for an LWR. Estimate the volume-average value of  $E\phi_I(E)$  ignoring resonant absorption. Estimate the volume-average value of  $\phi_T(E)$  near its peak. Assume a 4 m tall reactor, 1m in radius, producing 3 GW(th), with 25% of its power being produced by Pu fission. Ignore fission with fast neutrons.
- 3.6 Verify 2 rows, chosen at random, in each of tables 3.2, 3.3 and ???. You can download the tabular data and do your own averaging, or you can use the calculation feature at the bnl.gov website. In the latter case be careful that the limits of integration are set by the limits you place on the Plot Cart graphs. To weight a dataset by the Watt spectrum you can set the lower limit to some very low value, the upper limit to 10 MeV, and calculate using
- $$y0*0.4865*\sinh(\sqrt{2*x/1.0e6})*exp(-x/1.0e6)*10$$
- where  $y0$  is the data set that you want to weight. Then look at the average value displayed. Your result should be close to (but not equal to) the  $^{252}\text{Ca}$  spectrum weighted average value that is provided automatically.
- 3.7 Consider, magically, that the thermal and fast reactors we considered in this chapter contained  $^{233}\text{U}$  as their fissile component, rather than  $^{235}\text{U}$ . Explain, qualitatively, how this would affect each factor,  $\epsilon$ ,  $p$ ,  $f$ , and  $\eta_T$  for the thermal reactor, and then  $\epsilon$ ,  $f$ , and  $\eta_{FR_I}$  for the fast reactor: higher, lower, or about the same? Illustrate your answer with cross-section figures where appropriate.
- 3.8 Four factors for graphite and/or heavy water reactors.
- 3.9 Fissile material production in LWRs. How about pure U-238 rods?
- 3.10 There are some pretty impressive drops in the fast reactor neutron spectrum around 3 keV, 30 keV, and 400 keV, as shown in figure 3.46. What is the cause of these?
- 3.11 Relate Fermi and MCNP  $k$ 's.

## Chapter 4

### Neutron Spatial Distribution



Chicago Pile 1, layers 1 - 18 plus partially completed layer 19. Note uranium slugs interspersed in graphite blocks.

Since only a small amount of metal (about six tons) was available and since our graphite was of various brands of different purity it had been planned originally to construct the pile in an approximately spherical shape, putting the best materials as near as possible to the center. ... During the construction as a matter of precaution, appreciably before reaching [the] critical layer, some cadmium strips were inserted in suitable slots. They were removed once every day with the proper precautions in order to check the approach to the critical conditions. The actual construction was carried in this way to the 57th layer, about one layer beyond the critical dimensions. When all the cadmium is removed the effective reproduction factor of the structure is about 1.0006.

---

Enrico Fermi, "Experimental Production of a Divergent Chain Reaction," AECD-3269, declassified Nov. 7, 1951

In Chapter 3 we discussed the slowing down of neutrons and their resulting distribution in energy. We ignored any large-scale spatial variation of the neutron density, although we did take into account the localized fuel self-shielding at radiative absorption resonances. We drove this calculation through to the evaluation of the neutron multiplication factor, appropriately called “ $k_\infty$ ”. Here we will address the spatial motion of neutrons on the scale of the full system. We will use a simple, but powerful, approximation equivalent to treating the neutrons as a sort of gas composed of particles with only one speed, which collide only with the background nuclei and not with each other. This will allow us to take into account the leakage of neutrons from the edges of a reactor and so evaluate the true multiplication factor in finite geometry,  $k$ , also sometimes called  $k_{eff}$ .

#### 4.1 Neutrons as a one-speed gas

The neutron gas that we are about to consider is a bit of a peculiar one. We will assume that all of the neutrons have the same speed,  $v_n$ , and that their velocity is everywhere close to isotropically distributed in direction. This means that the magnitude of the *average* flow of our neutron gas is much less than the neutron speed itself, or

$$|\langle \vec{v} \rangle| \ll v_n \quad (4.1)$$

The signature of a continuum theory of gases is that it develops equations for local quantities such as the number density,  $n$ , and the momentum density,  $nm_n\langle \vec{v} \rangle$ , based in large part on the flows of particles and of momentum, combined with any local sources or sinks of particles and momentum. For our case we ignore the flow of energy, since we are assuming a fixed one-speed system with little energy in the flow itself.

Consider now figure 4.2, where we depict a differential cube of volume  $dxdydz$ . Since we are interested in the net flow of neutrons into or out of this cube, we need to evaluate the flows of neutrons through its surfaces. Let us look first at the back, shaded surface, whose four corners, progressing in the counter-clockwise direction, are located at  $(x, y, z)$ ,  $(x+dx, y, z)$ ,  $(x+dx, y+dy, z)$  and  $(x, y+dy, z)$ . Now consider the time interval  $\partial t$ . We use partial derivatives in this analysis, since we are not evaluating time derivatives moving with the average neutron motion, but time derivatives in the lab frame. During this time interval we can consider that, in effect, a differential volume of particles,  $\partial V$ , moves through the surface we are considering. This volume is given by  $\partial V = dxdy\langle v_z \rangle_{(x,y,z)}\partial t$ , where the subscripted  $(x, y, z)$  here means “evaluated at.” We can ignore the random isotropic motion of

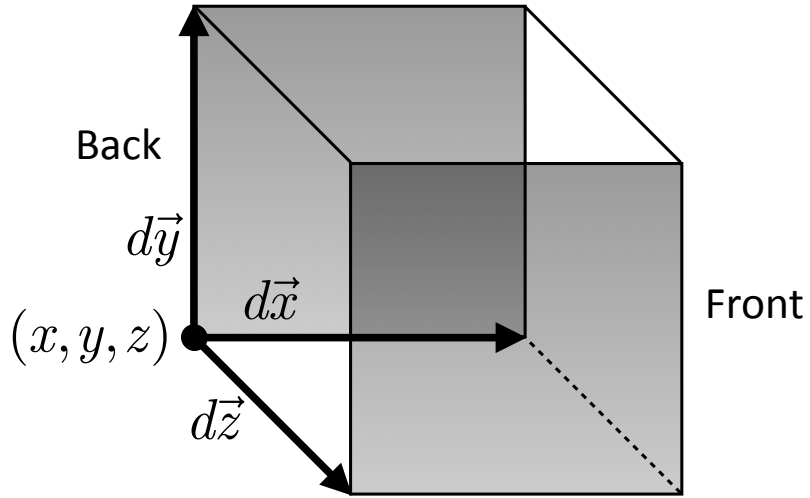


Figure 4.2 A differential cube with its left, lower, back corner located at  $(x, y, z)$ .

neutrons and only consider the small average flow, since the random isotropic motion does not result in net neutron flow through the surface. The number of particles moving into our differential cube through the surface we are now considering is then

$$\partial N_{(x,y,z)} = (n\partial V)_{(x,y,z)} = dx dy (n\langle v_z \rangle)_{(x,y,z)} \partial t \quad (4.2)$$

where  $N$  here denotes a dimensionless number of neutrons, since it is a number density multiplied by a volume. Note that if  $\langle v_z \rangle$  is negative, this corresponds to a negative number of particles moving into the cube, another way to say particles moving out.

Next look at the front shaded surface, whose four corners are located at  $(x, y, z + dz)$ ,  $(x + dx, y, z + dz)$ ,  $(x + dx, y + dy, z + dz)$  and  $(x, y + dy, z + dz)$ . By the same logic as above, the number of particles moving through the surface into the differential volume is given by

$$\partial N_{(x,y,z+dz)} = -dx dy (n\langle v_z \rangle)_{(x,y,z+dz)} \partial t \quad (4.3)$$

where the minus sign arises from the fact that positive  $z$  velocity is *out* of the volume.

If we sum  $\partial N$  due to  $z$ -directed flows through these two surfaces we arrive at the total effect due to flow in the  $z$  direction, since flow in the  $z$  direction only affects the arrival of particles (or their exit) in the differential volume through the two surfaces we have considered so far. Both  $x$  and  $y$  flows are

parallel to these surfaces, and so do not deliver (or extract) particles through our two surfaces.

$$\frac{\partial N_{z\text{-}flow}}{\partial x dy \partial t} = (n\langle v_z \rangle)_{(x,y,z)} - (n\langle v_z \rangle)_{(x,y,z+dz)} \quad (4.4)$$

Recognizing that we are dealing with differential quantities we can simplify the right-hand side to give

$$\frac{\partial N_{z\text{-}flow}}{\partial x dy \partial t} = -dz \frac{\partial}{\partial z} n\langle v_z \rangle \quad (4.5)$$

Dividing both sides by  $dz$  and noting that  $dV = dx dy dz$  we have

$$\frac{\partial n_{z\text{-}flow}}{\partial t} = -\frac{\partial}{\partial z} n\langle v_z \rangle \quad (4.6)$$

If we include the other two pairs of surfaces by analogy, we arrive at the final result that takes into account flows in all three directions, given by

$$\frac{\partial n}{\partial t} = -\frac{\partial}{\partial x} n\langle v_x \rangle - \frac{\partial}{\partial y} n\langle v_y \rangle - \frac{\partial}{\partial z} n\langle v_z \rangle = -\vec{\nabla} \cdot \langle \vec{v} \rangle n \quad (4.7)$$

In our situation where there can be sources and sinks of neutrons, not just effects from flows, we include any local volumetric source or sink, in units of number per second per unit volume, on the right-hand side.

$$\frac{\partial n}{\partial t} = -\vec{\nabla} \cdot n\langle \vec{v} \rangle + s \quad (4.8)$$

This is the particle conservation equation, commonly called the “continuity” equation. Perhaps not surprisingly, if the neutron flow “diverges” in the absence of a source of neutrons, the density of neutrons drops over time.

Now we come to something a bit more complex, the momentum conservation or force balance equation. Consider first the flow of  $z$ -directed momentum through the back surface of our differential cube. This momentum, of course, is carried by individual neutrons, each of which carries  $m_n v_z$  of momentum. By analogy with equation 4.2, we can evaluate the neutron momentum crossing through this surface in a differential time  $\partial t$  as

$$\partial(N m_n v_z)_{(x,y,z)} = nm_n \langle v_z \partial V_{(x,y,z)} \rangle = dx dy (nm_n \langle v_z^2 \rangle)_{(x,y,z)} \partial t \quad (4.9)$$

The reason that we find  $\langle v_z^2 \rangle$  coming into this equation is that in this case the depth of  $\partial V$  in the  $z$  direction is a function of the  $v_z$  of the individual neutrons not  $\langle v_z \rangle$ , the averaged flow speed. Here the random motion does deliver the quantity of interest, momentum, across the surface.

**Question:** Show that the flow of  $z$ -directed momentum in the  $z$  direction

due to the average flow varies as  $\langle v_z \rangle^2$ , not  $\langle v_z^2 \rangle$ , and so is quadratically smaller in  $\langle v_z \rangle / v_n$  than the momentum flow due to random motion.

Taking into account the front surface we arrive at, in analogy to equation 4.6,

$$\frac{\partial(nm_nv_z)_{z\text{-flow}}}{\partial t} = -\frac{\partial}{\partial z}n\langle m_nv_z^2 \rangle \quad (4.10)$$

Recognizing that for our nearly isotropic velocity distribution

$$n\langle m_nv_x^2 \rangle = n\langle m_nv_y^2 \rangle = n\langle m_nv_z^2 \rangle = nm_nv_n^2/3 \quad (4.11)$$

We can sum over all of the surfaces to get

$$\frac{\partial nm_n \vec{v}}{\partial t} = -\frac{mv_n^2}{3}\vec{\nabla}n + \vec{s}_{mom} \quad (4.12)$$

where we have taken advantage of our assumption that  $v_n$  is constant over time and space. We have allowed for a local source or sink of momentum, indicated by  $\vec{s}_{mom}$ , which has units of kg (m/s) m<sup>-3</sup>s<sup>-1</sup> = kg m<sup>-2</sup>s<sup>-2</sup>.

**Question:** Using the fact that in a conventional gas  $p = (2/3)U$ , where  $U$  is the kinetic energy density, show that  $p = nm_n\langle v^2 \rangle/3$ . Thus the first term on the right-hand side is analogous to  $\nabla p$ , as we find in standard fluid mechanics.

Note that we have neglected any flow of momentum other than the momentum in the same direction as its flow. For example when we examined momentum flow in the  $z$  direction, we neglected the  $z$ -directed flow of any  $x$ -directed momentum. This follows from our assumption that the neutron velocity distribution is very nearly isotropic, since under this assumption  $\langle v_i v_j \rangle$ , which comes into the flow in the  $i$  direction of  $j$ -directed momentum, is much larger for  $i = j$  than for  $i \neq j$ . Perhaps it helps to see this if we consider that neutrons moving, for example, in the  $+z$  direction carry  $+z$  momentum in the  $z$  direction, and neutrons moving in the  $-z$  direction carry  $-z$  momentum in the  $-z$  direction. These two flows of momentum have the same sign, so they add together; they do not cancel. In an isotropic distribution, however, if we consider neutrons moving at a given speed  $v_z$  there are just as many neutrons moving at  $-v_x$  as at  $+v_x$  and these, of course, cancel.

You might reasonably ask, “What does the positive  $z$ -directed flow of  $z$  momentum mean? Its sign depends on the coordinate system we choose!” The answer is that the flow of momentum does not impart any net force if it is spatially constant; it is only the divergence of the flow of momentum that imparts a force.

We will see later in this chapter that the assumption of velocity isotropy breaks down when the neutron density varies significantly over a distance approaching the neutron mean free path, and how we can account for this at the edge of a fission system. (In Chapter 11 we will study the conditions at the edge of fusion plasmas where flow speeds can be of the same order as the ion thermal speed, making the ion velocity distribution highly anisotropic.)

## 4.2 The one-speed neutron diffusion equation

To make progress towards a closed form for neutron transport, let us consider the  $s_{mom}$  term in the force balance equation. If the neutron gas has some local average flow velocity,  $\langle \vec{v} \rangle$ , the flow will be dissipated by collisions with the nuclei that are present, which randomize the direction of motion of the neutrons. Furthermore, neutron momentum is of course lost to the background nuclei by any form of neutron absorption, including fission. Since we are solving for the *transport* of neutrons in space, the neutron mean free path for momentum loss is denoted  $\lambda_{tr}$ , where the subscript “*tr*” stands for “*transport*.” The rate coefficient for momentum loss, with dimension  $s^{-1}$ , is then  $v_n/\lambda_{tr}$ .  $v_n$  comes into this rate coefficient rather than  $|\langle \vec{v} \rangle|$  because it is  $v_n$  that determines the frequency with which neutrons encounter nuclei and undergo scattering or absorption. Of course we evaluate the cross-sections at the assumed neutron energy, so we get the correct rate coefficients for absorption processes that have  $1/v$  effective cross-section. Thus we can write

$$s_{mom} = -nm_n \langle \vec{v} \rangle v_n / \lambda_{tr} \quad (4.13)$$

Now let us consider situations where the characteristic time over which the neutron momentum density changes,  $nm\langle v \rangle / (\partial nm\langle v \rangle / \partial t)$  is long compared with the time scale for collisional dissipation,  $\lambda_{tr}/v_n$ . This allows us to neglect the left-hand side of equation 4.12, which represents neutron inertia, giving a balance between force and dissipation:

$$0 = \frac{v_n^2}{3} \vec{\nabla} n + \frac{n \langle \vec{v} \rangle v_n}{\lambda_{tr}} \quad (4.14)$$

which can be solved for the vector neutron flux,  $n\langle \vec{v} \rangle$ . In neutronics calculations, this is referred to as the “neutron current,” to distinguish it from the scalar neutron flux,  $\phi \equiv nv_n$  in our one-speed approximation, and given the label  $\vec{J}$ .

$$\vec{J} \equiv n\langle \vec{v} \rangle = -\frac{v_n \lambda_{tr}}{3} \vec{\nabla} n \quad (4.15)$$

Equations of this form, where the flow of particles is down the density gradient and proportional to the strength of the gradient, are examples of “Fick’s Law.” Here we see how Fick’s Law arises in the context of neutron transport. It is worth noting that if the scale length of the density gradient,  $n/|\vec{\nabla}n|$ , approaches  $\lambda_{tr}$  the flow speed approaches  $v_n$ , which violates our original assumption of near isotropy.

Now we can take the step of combining equation 4.15 with the continuity equation, 4.8. This gives us

$$\frac{\partial n}{\partial t} = \vec{\nabla} \cdot \frac{v_n \lambda_{tr}}{3} \vec{\nabla} n + s \quad (4.16)$$

In conventional physics analysis, partial differential equations of this form are referred to as “diffusion” or “heat” equations, which have the generic form

$$\frac{\partial f}{\partial t} = \vec{\nabla} \cdot D_{phys} \vec{\nabla} f + s \quad (4.17)$$

For our case we can identify  $f = n$  and  $D_{phys} = v_n \lambda_{tr}/3$ . Note that the units of  $D_{phys}$  are  $\text{m}^2\text{s}^{-1}$ .

In neutronics analysis, it is conventional to solve for  $\phi \equiv nv_n$  and the neutron diffusion equation is cast as

$$\frac{1}{v_n} \frac{\partial \phi}{\partial t} = \vec{\nabla} \cdot D \vec{\nabla} \phi + s \quad (4.18)$$

with  $D = \lambda_{tr}/3$ . We will use this equation to define  $D$ , with  $D_{phys} \equiv v_n D$ .

To complete the development of the neutron diffusion equation, we need to look a little more deeply at  $\lambda_{tr}$ , the mean free path for momentum loss. Radiative absorption and  $(n,\alpha)$  events obviously extract all of the momentum from an incoming neutron, since it just disappears from the system. Absorption followed by fission gives back little of the incoming neutron momentum to the fission neutrons. Elastic and inelastic scattering on heavy nuclei also extract essentially all of the momentum from an incoming neutron. In each case, momentum contained in the isotropically distributed  $m_n \vec{v}_n$  is lost, but this is of no consequence for momentum balance. What is of interest to us, is that any general momentum loss also carries away  $\langle m_n \vec{v} \rangle$ .

**Question:** Where does the neutron momentum go in the case of radiative absorption? In the case of fission? In the latter case, roughly how much is given back to the neutron “fluid”?

By contrast with the above, a neutron does not, on average, lose all of its incoming momentum, composed of both  $m_n \vec{v}_n$  and  $\langle m_n \vec{v} \rangle$ , when it undergoes

an elastic collision on a light nucleus. For example, a lab-frame 180° or “head-on” collision of a neutron with an assumed equal-mass stationary proton transfers all of the neutron’s momentum to the proton. The proton proceeds with the original neutron velocity, and the neutron stops dead. However any other possible lab-frame collision angle leaves the neutron with some forward velocity. While you can show this analytically (see exercise 4.1), you can also test it out on a pool table. Thus, in the case of the lightest nucleus, on average the neutron must not lose all of its momentum.

Let us examine, then, the average loss of momentum for a neutron that suffers a collision with a nucleus of finite mass. Let us consider, for this calculation, elastic scattering that is isotropic in the center-of-mass frame. The absolute value of equation 3.3 gives us the speed of the neutron, both incoming and outgoing, in the center-of-mass frame.

$$|\vec{v}_0 - \vec{v}_{CoM}| = \frac{Av_0}{A + 1} \quad (4.19)$$

where we remember that  $\vec{v}_0$  is the incoming lab-frame velocity. Meanwhile, equation 3.2 gave us

$$\vec{v}_{CoM} = \frac{\vec{v}_0}{A + 1} \quad (4.20)$$

The outgoing lab-frame velocity,  $\vec{v}_1$ , is the vector sum of the velocity of the center of mass plus the velocity of the scattered neutron in the center of mass. If we say that the neutron has scattered through an angle  $\theta$  in the center-of-mass frame, the component of the lab-frame outgoing velocity in the direction of the lab-frame incoming velocity is given by:

$$\vec{v}_1 \cdot \frac{\vec{v}_0}{v_0} = \frac{v_0}{A + 1} + \frac{Av_0}{A + 1} \cos\theta \quad (4.21)$$

Thus the remaining fraction of the velocity of the neutron in its original direction, after an elastic scattering event, is given by

$$\frac{\vec{v}_1}{v_0} \cdot \frac{\vec{v}_0}{v_0} = \frac{A \cos(\theta) + 1}{A + 1} \quad (4.22)$$

For the case of no scattering,  $\theta = 0$ , we get the expected result of no change in the forward momentum of the neutron. For perfect backscattering,  $\theta = \pi$ , at  $A = 1$  we have full momentum transfer, and in the limit of high  $A$  we have reversal of the original momentum. Evidently if we were to average this over all scattering angles, assuming isotropy in the center-of-mass frame, we would get that the surviving fraction of the original neutron momentum would be  $1/(A + 1)$ . This is not, however, consistent with our assumption

of a one-speed neutron distribution, since part of why the neutrons lose momentum in these collisions is that they lose speed.

To model a scattering event where speed and energy are not lost, we note that equation 3.6 gives the speed and energy reduction at an elastic collision, as a function of  $\theta$ . We can “boost” the speed of the lab-frame scattered neutron back up to its original value by multiplying the surviving momentum, associated with the lab-frame final speed,  $v_1$ , by  $v_0/v_1$ . For thermal neutrons, this could be due to gaining energy, on average, from the thermal motion of the target nuclei with which the neutrons are nearly in equilibrium. Using this approach we get

$$\frac{\vec{v}_1 \cdot \vec{v}_0}{v_0^2} = \frac{A\cos(\theta) + 1}{\sqrt{A^2 + 2A\cos(\theta) + 1}} \quad (4.23)$$

Now we would like to average the fractional surviving momentum over scattering angle, assuming isotropy in the center-of-mass frame. This is given by

$$\begin{aligned} \langle \frac{\vec{v}_1 \cdot \vec{v}_0}{v_0^2} \rangle &= \frac{1}{4\pi} \int_0^{2\pi} d\phi \int_0^\pi \sin(\theta) d\theta \frac{A\cos(\theta) + 1}{\sqrt{A^2 + 2A\cos(\theta) + 1}} \\ &= \frac{1}{2} \int_{-1}^1 dx \frac{Ax + 1}{\sqrt{A^2 + 2Ax + 1}} = \frac{2}{3A} \end{aligned} \quad (4.24)$$

where a table of integrals or a computer algebra system can help us with the last step. This is the conventional result. It is usually obtained, without discussion of the topic of energy loss, by averaging  $\cos(\psi)$  over isotropic center-of-mass scattering, where  $\psi$  is the lab-frame scattering angle. See exercise 4.2.

We are now in a position to evaluate  $\lambda_{tr} = 1/\overline{\Sigma_{tr}}$ , where we remember that  $\Sigma$  represents a macroscopic cross-section,  $N\sigma$ , and the overbar indicates a sum over all of the species of nuclei present. As for any set of collisional effects acting at the same time, we need to sum up all of the various  $\Sigma$ s to include all of the processes that extract momentum from the neutrons, and then invert that sum to get the overall mean free path for momentum loss.

$$\lambda_{tr}^{-1} = \overline{\Sigma_{tr}} = \overline{\Sigma_\gamma} + \overline{\Sigma_f} + \overline{\Sigma_{(n,\alpha)}} + \overline{(\Sigma_e + \Sigma_{in})[1 - 2/(3A)]} \quad (4.25)$$

where we have “boosted” all scattering events, both elastic and inelastic. However at the energies of interest, inelastic scattering is essentially only a high-A phenomenon.

Finally, we may have a source or sink of neutrons in our system. In a system where neutron multiplication is taking place we can represent this

as

$$s = (k_\infty - 1)(\overline{\Sigma_\gamma} + \overline{\Sigma_f} + \overline{\Sigma_{(n,\alpha)}})\phi = (k_\infty - 1)\overline{\Sigma_{abs}}\phi \quad (4.26)$$

since for each neutron absorbed  $k_\infty$  are produced. We are here ignoring any time delay between the production of these neutrons at high energy and their arrival at the energy under consideration. We will look at the interesting question of time dependence in chapter 5. We are similarly ignoring spatial motion of the neutrons between their birth and their arrival at our assumed energy, although we will include that effect later in this chapter. Also, you should remember that the basic derivation of the diffusion equation assumed that the neutron flow speed is much less than the random one-speed neutron motion. We showed as well that the requirement of flow speed much less than  $v_n$  implied that the scale length of the neutron density gradient,  $n/|\vec{\nabla}n|$ , had to be much greater than  $\lambda_{tr}$ . With these caveats, the reactor-analysis version of the neutron diffusion equation including sources and sinks is, finally, rather beautiful and compact:

$$\frac{1}{v_n} \frac{\partial \phi}{\partial t} = \vec{\nabla} \cdot \frac{\lambda_{tr}}{3} \vec{\nabla} \phi + (k_\infty - 1)\overline{\Sigma_{abs}}\phi \quad (4.27)$$

### 4.3 1-D $\delta$ -function initial condition without boundaries

In order to develop some physical intuition about neutron diffusion, it is helpful to start by considering the one-dimensional physics version of the one-speed diffusion equation, without sources or sinks, given by

$$\frac{\partial n}{\partial t} = \frac{\partial}{\partial x} D_{phys} \frac{\partial n}{\partial x} \quad (4.28)$$

with  $D_{phys} = v_n \lambda_{tr}/3$ . We use the physics version, in part, to maintain contact with a large volume of literature about this equation.

Consider an initial condition of a  $\delta$ -function of neutron density located at  $x = 0$  and uniform vs.  $y$  and  $z$  at time  $t = 0$ ,  $n(t = 0) = \delta(x = 0)$ . The solution to the time evolution of  $n$  vs. time and space is well known:

$$n(x, t) = \frac{1}{\sqrt{4\pi D_{phys}t}} \exp\left(\frac{-x^2}{4D_{phys}t}\right) = \frac{1}{\sqrt{2\pi\sigma_x^2(t)}} \exp\left(\frac{-x^2}{2\sigma_x^2(t)}\right) \quad (4.29)$$

where the last step comes from properties of the “normal” (or Gaussian) distribution.  $\sigma_x(t)$  is the root mean square deviation of such a distribution from its mean value at time  $t$ . You can show that this form solves equation 4.28 for  $t > 0$  by substitution. You can also show that its integral over all  $x$  is unity, independent of time. See exercise 4.3. Figure 4.3 shows the solutions for various values of  $Dt$ .

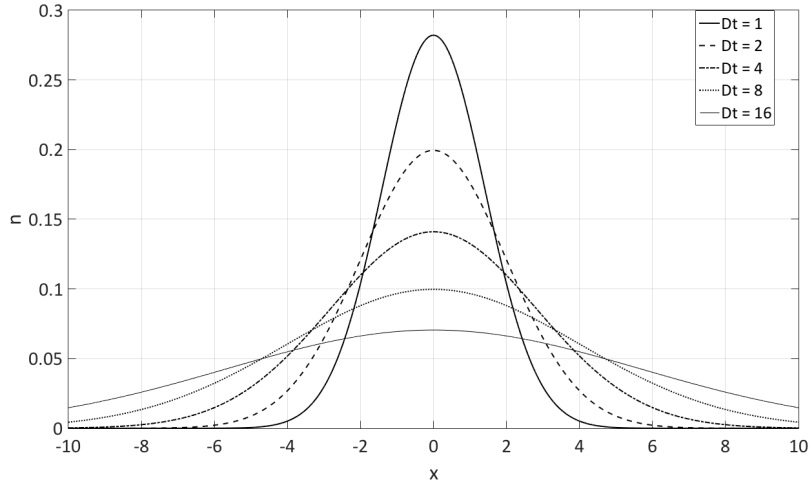


Figure 4.3 Evaluation of equation 4.29 for  $Dt = 1, 2, 4, 8$ , and  $16$ .

The major physics observation from this result is that the mean square deviation of the spatial distribution of neutrons grows linearly with time,  $\sigma_x^2(t) = 2D_{phys}t$ . This reflects a fundamental property of the diffusion equation. In this equation time is fundamentally related to spatial scale length squared divided by  $D_{phys}$ . If you have a steel rod that is twice longer than my steel rod, it takes heat four times longer to diffuse from one end to the other of your rod than mine. If, however, your longer rod is made of aluminum or copper (which have roughly four times the thermal diffusivity of steel), your diffusion time is reduced back down to close to mine.

#### 4.4 Statistical interpretation of the neutron diffusion equation

It is interesting to compare the above continuum result for a  $\delta$ -function initial condition with a statistical analysis of the same problem. In one form, the Central Limit Theorem (CLT) of statistics considers many lists of  $n$  uncorrelated random numbers,  $\Delta x_i$  for  $i = 1 \dots n$ , with mean value  $m$  and variance  $\sigma^2$  defined by

$$\sigma^2 \equiv (1/n) \sum_1^n (\Delta x_i - m)^2 \quad (4.30)$$

The theorem states that the average sum of these lists approaches  $nm$  as the number of lists goes to infinity,

$$\langle x \rangle = \left\langle \sum_{i=1}^n \Delta x_i \right\rangle \rightarrow nm \quad (4.31)$$

This should come as no surprise. The CLT further states, more interestingly, that the average variance of the sums of the many lists approaches  $n\sigma^2$  for large numbers of lists.

$$\langle (x - nm)^2 \rangle \rightarrow n\sigma^2 \quad (4.32)$$

Thus the average variance of the sums grows linearly with the number of steps. It further states that for large  $n$  the probability distribution function of the sums will approach a “normal” (or Gaussian) distribution. Evidently the CLT is closely related to the solution of the generic diffusion equation given in equation 4.29.

Consider that after a decorrelation time of the neutron flight direction,  $\tau_{decor}$ , a neutron lands a distance in  $x$ ,  $\Delta x$ , away from its starting point. For a homogeneous medium and a random initial direction of motion, obviously the mean value of  $\Delta x$ ,  $\langle \Delta x \rangle$ , equals 0. For our case  $m = 0$  in the CLT. But what is the decorrelation time, and what is the mean square value of the step  $\langle \Delta x^2 \rangle$  that corresponds to the CLT’s  $\sigma^2$ ?

The mean decorrelation time of the neutron flight direction is  $\tau_{decor} = \lambda_{tr}/v_n$ , since  $v_n/\lambda_{tr}$  is the rate coefficient for momentum loss. (Without a little more analysis, the CLT is not directly relevant to the case where neutrons are absorbed. We will come back to this in section 4.5.) Thus for our case the number of steps,  $n$ , in the CLT is given by

$$n = t/\tau_{decor} = tv_n/\lambda_{tr} \quad (4.33)$$

Now we would like the mean square distance to decorrelation. If we say that the mean distance to decorrelation is  $\lambda_{tr}$ , we can evaluate the mean square distance to decorrelation by analogy with equation 2.4. Here we use  $s$  as the variable along the randomly-oriented original flight direction, and we average  $s^2$  over the exponential distribution of neutron decorrelation events.

$$\langle \Delta s^2 \rangle = \frac{\int_0^\infty s^2 e^{-\Sigma_{tr}s} ds}{\int_0^\infty e^{-\Sigma_{tr}s} ds} = \overline{\Sigma_{tr}} \int_0^\infty s^2 e^{-\Sigma_{tr}s} ds = \frac{1}{\overline{\Sigma_{tr}^2}} \int_0^\infty \tilde{s}^2 e^{-\tilde{s}} d\tilde{s} = 2\lambda_{tr}^2 \quad (4.34)$$

where the last step can be accomplished through two integrations by parts. (You did this integral before if you completed exercise 2.1.) Since this is the mean square distance to decorrelation in a randomly-oriented initial

direction, we have  $\langle \Delta x^2 \rangle = \langle \Delta s^2 \rangle / 3 = 2\lambda_{tr}^2 / 3$ . This is then the  $\sigma^2$  for a single step that should appear in the CLT for our case. Let us now compare our diffusion equation result for the growth of the variance with time, equation 4.29, to the CLT result.

$$\begin{aligned} \text{Diffusion equation: } & \sigma_x^2(t) = 2D_{phys}t \\ \text{CLT: } & \sigma_x^2(t) = 2n\lambda_{tr}^2/3 = 2tv_n\lambda_{tr}/3 \\ & \Rightarrow D_{phys} = v_n\lambda_{tr}/3 \end{aligned} \quad (4.35)$$

Thus the value of  $D_{phys}$  we derive from comparing the diffusion equation with the statistical CLT analysis is the same as that we derived from our fluid neutron diffusion model. The CLT is equivalent to a very simple “kinetic” model that works directly from single particle motion. It provides an alternative and perhaps more intuitive sense for why diffusive neutron spreading grows as the square root of time. This is simply the way that random steps add, by summing their variance. Suppose a sequence of random steps have summed to net progress in one direction. A subsequent step may add or subtract from that progress. This may seem like no progress, but if you want to get many step lengths further, you are more likely to get there with more random steps. This is also how statistical errors add. While errors may cancel, the overall breadth of uncertainty increases with more sources of error.

Note that the CLT is only valid for large values of  $n$ , the length of the list of random numbers. The width of the CLT Gaussian is much greater than the root mean square step size only for large  $n$ , so the criteria for validity of the CLT analysis and our diffusion analysis are the same – many step sizes over a gradient scale length. A weakness in the simple statistical analysis presented here is that we have not included absorption in our statistical picture. However in the fluid picture it is evident that absorption corresponds to momentum loss, so must be included in  $\lambda_{tr}$ .

#### 4.5 1-D $\delta$ -function steady source without boundaries

We can gain additional useful physical understanding by looking at another simple version of the unbounded diffusion equation. This time let us consider an infinite, homogeneous, net absorbing medium ( $k_\infty < 1$ ), with a steady extrinsic source of neutrons at  $x = 0$ . The one-dimensional time-independent neutronics-analysis diffusion equation for this case is

$$0 = \frac{\partial}{\partial x} \frac{\lambda_{tr}}{3} \frac{\partial}{\partial x} \phi + (k_\infty - 1) \overline{\Sigma_{abs}} \phi + S_2 \delta(x) \quad (4.36)$$

where  $S_2$  indicates a two-dimensional (infinite in  $y$  and  $z$ ) steady extrinsic source of neutrons, in units of neutrons per second per meter<sup>2</sup>. Second order differential equations in general have two solutions and the solutions of this equation are simple exponential growth and simple exponential decay as a function of  $x$ . We should assume, in this net absorbing medium, that the solutions must go to zero at  $x = \pm\infty$ . Therefore we choose decay for  $x > 0$  and growth for  $x < 0$  (i.e., decay vs.  $-x$ ). Matching the solutions at  $x = 0$  we obtain

$$\phi = \phi_0 \exp\left(\mp x \frac{\sqrt{1 - k_\infty}}{L}\right) \quad (4.37)$$

$$L \equiv \sqrt{\frac{\lambda_{tr} \lambda_{abs}}{3}} = \sqrt{\frac{D}{\Sigma_{abs}}}$$

where the  $\mp$  is negative for  $x > 0$  and positive for  $x < 0$ .  $L$  is the decay length due to the competition between diffusion and absorption, in the absence of fission. It is called the “diffusion length.” Note that the actual decay length of the neutron density in our case goes to infinity as  $k_\infty$  approaches unity, meaning that near-critical systems are strongly coupled over space. Figure 4.4 shows the solution for various values of  $L$  for the case of  $k_\infty = 0$ .

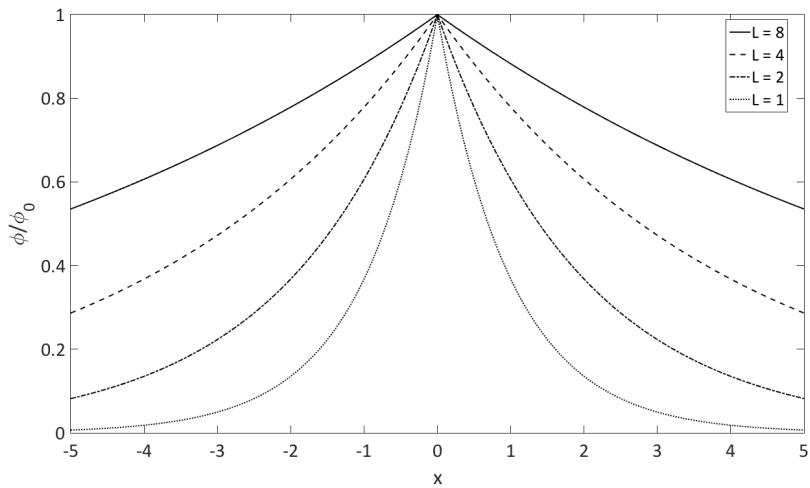


Figure 4.4 Evaluation of equation 4.37 for  $k_\infty = 0$  and  $L = 1, 2, 4$ , and 8.

Let us evaluate  $\phi_0$ . To do this we look close to  $x = 0$ , choosing a point close enough that there cannot have been much multiplication of the source neutrons, so  $x \ll \lambda_{abs}$ , but where the diffusion equation should be applicable,  $x \gg \lambda_{tr}$ . Let us also choose to look where  $x \ll L/\sqrt{1 - k_\infty}$ . This

means that one-half of  $S_2$  must be flowing in each of the directions  $\pm x$ . Using equation 4.15, the one-speed neutron diffusion version of Fick's Law, we have

$$S_2 = 2 \frac{\lambda_{tr}}{3} \frac{\partial}{\partial x} \phi = 2 \frac{\lambda_{tr}}{3} \phi_0 \frac{\sqrt{1 - k_\infty}}{L} = 2 \phi_0 \sqrt{1 - k_\infty} \sqrt{\frac{\lambda_{tr}}{3\lambda_{abs}}} \quad (4.38)$$

so

$$\phi_0 = \frac{S_2}{2} \sqrt{\frac{3\lambda_{abs}}{\lambda_{tr}(1 - k_\infty)}} \quad (4.39)$$

**Questions:** Show that it is possible to chose an  $x$ , near  $x = 0$ , that meets all of the conditions we are imposing. You may assume  $\lambda_{abs} \gg L \gg \lambda_{tr}$ , so that diffusion is applicable in this case in the first place.

Now it is interesting to evaluate the total number of neutrons absorbed, per second per  $\text{m}^2$ , from  $x = -\infty$  to  $+\infty$ . Since, in this case, all of the neutrons produced are absorbed somewhere, the total number of neutrons absorbed must correspond to the sum of the source neutrons plus those produced from fission.

$$\begin{aligned} \int_{-\infty}^{\infty} \Sigma_{abs} \phi dx &= \frac{S_2}{\lambda_{abs}} \sqrt{\frac{3\lambda_{abs}}{\lambda_{tr}(1 - k_\infty)}} \int_0^{\infty} \exp\left(\mp x \frac{\sqrt{1 - k_\infty}}{L}\right) dx \\ &= \frac{S_2}{L\sqrt{1 - k_\infty}} \frac{L}{\sqrt{1 - k_\infty}} = \frac{S_2}{1 - k_\infty} \end{aligned} \quad (4.40)$$

This result indicates that the total multiplication of the system is  $1/(1 - k_\infty)$ . This is exactly what we expect, since for  $S_2$  source neutrons per second per meter<sup>2</sup> produced (and absorbed) there are  $k_\infty S_2$  second generation neutrons produced (and absorbed) per second per meter<sup>2</sup>, the third generation comprises  $k_\infty^2 S_2$  per second per meter<sup>2</sup>, and so on. And we know

$$S_2(1 + k_\infty + k_\infty^2 + k_\infty^3 + \dots) = S_2/(1 - k_\infty) \quad (4.41)$$

rather a satisfying result, with the correct limits as  $k_\infty$  goes to 0 and 1.

It is also interesting to know the mean distance at which a fission event at the origin induces a fission event elsewhere. Since we have a simple exponential fall-off of  $\phi$  to the left and right of the source at  $x = 0$ , and a uniform medium so the fission density is proportional to  $\phi$ , we can use the same form of calculation as that of the mean free path, equation ??, to get this mean distance. The result, in this one dimensional case, is  $L/(1 - k_\infty)^{1/2}$ .

If we would like to know the mean square distance in any one direction, say  $x$ , over which a fission event induces a fission event elsewhere, we can

use the same form of calculation as that of the mean square distance to decorrelation in equation 4.34. Considering that our fission event occurred at  $x = 0$  we find that the mean square location of a further fission event is

$$\langle x^2 \rangle = 2L^2/(1 - k_\infty) \quad (4.42)$$

If we are interested instead in the mean square distance over which a neutron is absorbed, we can use the same equation with  $k_\infty \rightarrow 0$ . This result, of course, is calculated here from the diffusion equation, implying that we can only be certain that it holds when  $\lambda_{tr} \ll \lambda_{abs}$ , a limit that we will sometimes challenge.

Interestingly, we can show easily that this result holds for arbitrary  $\lambda_{tr}/\lambda_{abs}$ , by extending our kinetic analysis based on the Central Limit Theorem. Taking the step size for transport to be  $\lambda_{tr}$  and otherwise ignoring absorption for the moment, we can calculate the mean square displacement in the  $x$  direction, after  $n$  collisions, to be

$$\langle x^2 \rangle_n = \frac{2n\lambda_{tr}^2}{3} \quad (4.43)$$

Now at each collision event, there is a probability of the particle being absorbed, rather than scattered, given by

$$p_{abs} = \frac{\overline{\Sigma_{abs}}}{\overline{\Sigma_{tr}}} = \frac{\lambda_{tr}}{\lambda_{abs}} \quad (4.44)$$

Thus the probability of a particle surviving to event  $n$ , and then being absorbed at that event, is given by

$$p_n = (1 - p_{abs})^{n-1} p_{abs} \quad (4.45)$$

**Question:** Physically, what value must  $\sum_1^\infty p_n$  take? Prove mathematically that it does so.

Now we can write down the mean square  $x$  location of absorption as,

$$\begin{aligned} \langle x^2 \rangle &= \sum_{n=1}^{\infty} (1 - p_{abs})^{n-1} p_{abs} \frac{2n\lambda_{tr}^2}{3} = \frac{2p_{abs}\lambda_{tr}^2}{3} \sum_{n=1}^{\infty} n(1 - p_{abs})^{n-1} \\ &= \frac{2p_{abs}\lambda_{tr}^2}{3} \sum_{n=0}^{\infty} n(1 - p_{abs})^{n-1} = -\frac{2p_{abs}\lambda_{tr}^2}{3} \frac{d}{dp_{abs}} \sum_{n=0}^{\infty} (1 - p_{abs})^n \\ &= -\frac{2p_{abs}\lambda_{tr}^2}{3} \frac{d}{dp_{abs}} p_{abs}^{-1} = \frac{2\lambda_{tr}^2}{3p_{abs}} = 2L^2 \end{aligned} \quad (4.46)$$

This has two important consequences. First, it shows that  $2L^2$  is the

correct value for  $\langle x^2 \rangle$  even in the case where absorption is a large fraction - or even all - of the momentum loss. And second, since in the diffusive limit it gives the same result as the diffusive model, it validates the inclusion of absorption in the definition of  $\lambda_{tr}$  used in our one-speed diffusion equation. For a numerical investigation of this result, see exercise ??.

**Question:** Show simply that in the extreme limit, where there is only absorption, you get the same result for  $\langle x^2 \rangle$ .

## 4.6 Boundary conditions

Now we are interested in moving on to finite systems. To do this we need to set boundary conditions for the diffusion equation. Often fission reactors are surrounded by “reflectors” that bounce neutrons back into the reactor, in order to minimize neutron losses. In thermal reactors this is generally just a region of moderator without fuel assemblies. In fast “breeder” reactors that are designed to produce net fissile material, a “blanket” of fuel assemblies with natural or depleted uranium reflects neutrons, but also absorbs them to produce  $^{239}\text{Pu}$ . Alternatively, or in addition, a fast reactor may include a thick steel reflector to minimize neutrons escaping from the system.

It is evident that  $\phi$  must be continuous across the interface between dissimilar media. The diffusion equation cannot support an infinite gradient in  $\phi$ , even at a discontinuity in  $D$ , since this would correspond to an infinite flux of neutrons. Calling the two sides of the discontinuity the + and – sides, we can express this as

$$\phi_+ = \phi_- \quad (4.47)$$

The diffusion equation also cannot support a discontinuity in the flow of neutrons, since this would correspond to an infinite positive or negative local divergence of the flow. Thus we have another boundary condition at any interface,

$$\hat{n} \cdot D_+ \vec{\nabla} \phi_+ = \hat{n} \cdot D_- \vec{\nabla} \phi_- \quad (4.48)$$

where  $\hat{n}$  indicates a unit vector pointing directly across the interface.

There is a different kind of boundary condition at the edge of a nuclear system, say at an interface with air, where the neutron mean free path is long enough that a neutron is very unlikely ever to return when it crosses the interface. This means that within a distance of  $\lambda_{tr}$  of the edge the angular distribution of neutron velocities inside the nuclear material is highly anisotropic; there are very few inwards-directed neutrons. Such a physical

condition violates the fundamental assumption of near-isotropy inherent in the one-speed diffusion equation.

As an approximation to this condition, let us assume that the angular distribution of neutrons at the edge of a nuclear system is hemispherically isotropic, meaning that for outgoing neutrons all elements of solid angle,  $d\Omega$ , are equally populated with neutrons, but there are no neutrons populating the incoming hemisphere. In this simple case it is easy to calculate the relationship between the outgoing neutron flux and the neutron density, particularly in our one-speed approximation. Take  $\hat{n}$  to be the outgoing direction, and define  $\theta$  with respect to this  $\hat{n}$  direction. To get the outgoing neutron “current” we need only average  $\cos\theta$  over the populated hemisphere, recognizing that  $d\Omega = \sin\theta d\theta d\varphi = -d\cos\theta d\varphi$ , giving

$$\vec{J} \cdot \hat{n} = n \langle v_{\hat{n}} \rangle = nv_n \langle \cos\theta \rangle = \phi \frac{\int_0^1 \cos\theta d\cos\theta}{\int_0^1 d\cos\theta} = \phi \int_0^1 x dx = \frac{\phi}{2} \quad (4.49)$$

This result illustrates the perhaps obvious fact that we cannot have a finite neutron flux across the outgoing interface without a finite neutron density at that interface. Thus the boundary condition at the interface with long mean free path material, such as air, cannot be  $\phi = 0$ .

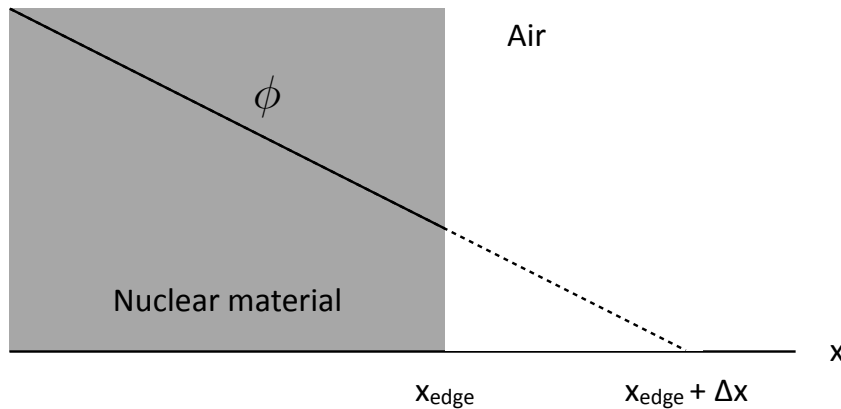


Figure 4.5 Linear extrapolation of  $\phi$  from the edge of nuclear material

If we match the diffusive flux to this very simple “kinetic” edge calculation, we have, at the edge

$$\hat{n} \cdot D \vec{\nabla} \phi = -\phi/2 \quad (4.50)$$

Now consider a boundary of some nuclear material at  $x = x_{edge}$ , as illustrated in figure 4.5. At the boundary of the material, but inside of it, we

have  $d\phi/dx = -\phi/(2D)$ . If we extrapolate this gradient outside, we can find the distance at which the extrapolated line strikes  $\phi = 0$ .

$$\begin{aligned}\phi + \Delta x \frac{d\phi}{dx} &= \phi - \Delta x \frac{\phi}{2D} = 0 \\ \Delta x &= 2D = 2\lambda_{tr}/3 \equiv \lambda_{ext}\end{aligned}\quad (4.51)$$

$\lambda_{ext}$  is given the name “extrapolation length.” It is important to understand that this model for the edge is not accurate within a few  $\lambda_{tr}$ ’s of the edge within the material, and bears no relationship to the actual neutron flux outside of the material. However it does provide a reasonably good model for the global effect of the fact  $\phi \neq 0$  at the boundary. Furthermore, it is important to remember that the edge of the material is at  $x_{edge}$ , not at  $x_{edge} + \lambda_{ext}$ . Finally, this procedure is only valid if  $\phi$  is reasonably linear near the boundary.

As a final, final remark, full kinetic calculations for an infinite planar interface give  $\lambda_{ext} = 0.7104\lambda_{tr}$ .

#### 4.7 Bounded Systems

Now we are in a position to solve the one-speed neutron diffusion equation in some informative geometries. We will simplify the problem by assuming that  $D = \lambda_{tr}/3$ ,  $\overline{\Sigma_{abs}}$ , and  $k_\infty$  are all constant across the reactor core. In practice burnable poisons can be distributed with a spatial profile, and the process by which fuel assemblies are replaced (typically 1/3 of the total every 18 months in commercial LWRs) and moved about, or “shuffled,” during the replacement process, means that this assumption is not really justified for practical cases. As we will see, the profiles we find are peaked, and operators prefer to have more nearly uniform burn-up of the nuclear fuel.

All that said, it is informative to solve the diffusion equation for uniform material properties. We are interested in a time-independent solution. Dividing equation 4.27 through by  $D\phi$  we have

$$\frac{1}{D\phi v_n} \frac{\partial \phi}{\partial t} = 0 = \frac{1}{\phi} \nabla^2 \phi + (k_\infty - 1) \frac{\overline{\Sigma_{abs}}}{D} = \frac{1}{\phi} \nabla^2 \phi + \frac{k_\infty - 1}{L^2} \quad (4.52)$$

Note that we will need  $k_\infty > 1$  to sustain a chain reaction, since neutrons will escape across the boundaries of this system. Reactor designers use some special “lingo” to describe the two terms on the far right of equation 4.52.

$$\begin{aligned}B_g^2 &\equiv -\frac{1}{\phi} \nabla^2 \phi \\ B_m^2 &\equiv \frac{k_\infty - 1}{L^2}\end{aligned}\quad (4.53)$$

$B_g$  is called the “geometric buckling” which can be thought of as the degree to which  $\phi$  is bent, or buckled, by the presence of the boundary conditions. If the boundaries are far away from the center of the system, the buckling is slight, but as they are moved inwards the buckling increases. The sign of the associated curvature means that  $\nabla^2\phi$  is everywhere negative, resulting in net outflow of neutrons from every volume element, and thus the need for neutron production to compensate the outflow and sustain steady state. The neutron production is supplied by the “material buckling,”  $B_m$ . In this version of the neutron diffusion equation we have isolated all of the geometrical effects to the first term and all of the material effects to the second.

For steady operation, or criticality, we need  $B_m = B_g$ . If  $B_m > B_g$ , the system is supercritical and  $\phi$  grows with time, while for  $B_m < B_g$ , the system is subcritical and  $\phi$  decays with time. The dimension of both  $B_g$  and  $B_m$  is  $\text{m}^{-1}$ . It is interesting to note that  $1/B_m^2$  is equal to the square of the scale length of the solution to the one-dimensional unbounded case, equation 4.37. However  $\nabla^2\phi$  in that case is everywhere positive, since an inflow of neutrons is required to balance  $k_\infty - 1 < 0$ .

#### 4.7.1 Cuboids

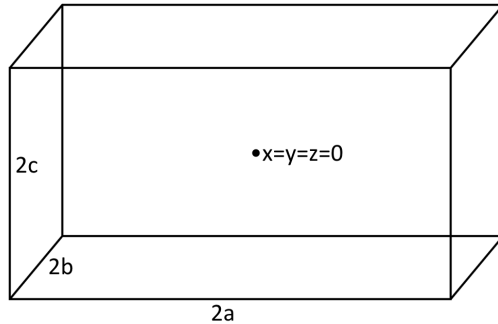


Figure 4.6 Cuboid reactor core.

Let us start by considering the simplest finite case, a cuboid-shaped reactor core. Technically this is a “right cuboid,” because we will assume that all of the intersections between the rectangular surfaces are at right angles. We will take the reactor core to occupy a volume defined by  $|x| < a$ ,  $|y| < b$ , and  $|z| < c$ , as shown in figure 4.6. Using the approximation that  $\phi = 0$  at the extrapolated boundaries, the boundary conditions for a solution are

$\phi = 0$  at

$$\begin{aligned} x &= \pm(a + \lambda_{ext}) = \pm\tilde{a} \\ y &= \pm(b + \lambda_{ext}) = \pm\tilde{b} \\ z &= \pm(c + \lambda_{ext}) = \pm\tilde{c} \end{aligned} \quad (4.54)$$

where the meaning of a constant with a “tilde” is that it represents an extrapolated boundary.

Now we will solve this equation by the method of separation of variables. This amounts to making the *ansatz*, or assumption, that the solution will take the form

$$\phi(x, y, z) = \phi(x)\phi(y)\phi(z) \quad (4.55)$$

In rectilinear coordinates, equation 4.52 becomes

$$\begin{aligned} \frac{\nabla^2 [\phi(x)\phi(y)\phi(z)]}{\phi(x)\phi(y)\phi(z)} + B_m^2 &= \\ \frac{1}{\phi(x)} \frac{\partial^2 \phi(x)}{\partial x^2} + \frac{1}{\phi(y)} \frac{\partial^2 \phi(y)}{\partial y^2} + \frac{1}{\phi(z)} \frac{\partial^2 \phi(z)}{\partial z^2} + B_m^2 &= 0 \end{aligned} \quad (4.56)$$

Since we have assumed that  $B_m^2$  is spatially uniform we need each of the other terms to be spatially uniform as well, since they cannot balance out any spatial variation in one another. The solution also needs to match our boundary conditions. The two potential solutions for this case, with  $k_\infty - 1 > 0$ , are sine and cosine. It is easy to see that if we use either a sine or cosine function for  $\phi$ , the first three terms will be spatially uniform, but only cosine can match the boundary conditions. We conclude

$$\phi(x, y, z) = \phi_0 \cos\left(\frac{\pi x}{2\tilde{a}}\right) \cos\left(\frac{\pi y}{2\tilde{b}}\right) \cos\left(\frac{\pi z}{2\tilde{c}}\right) \quad (4.57)$$

and

$$B_g^2 = \left(\frac{\pi}{2\tilde{a}}\right)^2 + \left(\frac{\pi}{2\tilde{b}}\right)^2 + \left(\frac{\pi}{2\tilde{c}}\right)^2 \quad (4.58)$$

We require, furthermore, that  $B_g^2 = B_m^2$  to achieve self-consistency between the neutron loss due to the finite system size and the excess of  $k_\infty$  above unity. For a given  $B_m$ , the size of the reactor set by  $\tilde{a}$ ,  $\tilde{b}$ , and  $\tilde{c}$  cannot be too small, or the chain reaction is quenched by neutron losses. By the same token the size cannot be too large, or the reaction runs away. For a cuboid reactor with one or more dimensions infinite (an infinite slab or infinite square-cross-section rod) the infinite dimensions play no role in determining  $B_g$  and therefore the necessary  $B_m$ . But if one dimension is too short, for

example  $\tilde{a} < \pi/(2B_m)$ , it doesn't matter how long the others are made, the system can never achieve criticality. As a reminder, the physical reactor only extends to  $x = \pm a$ ,  $y = \pm b$ , and  $z = \pm c$ , not to the extrapolated boundaries,  $\tilde{a}$ ,  $\tilde{b}$ , and  $\tilde{c}$ .

Note that this type of analysis does not determine the absolute value of  $\phi_0$  and so, for example, the level of power production of a reactor. In practice the operating power of a reactor is set by the fact that  $k_\infty$  is a function of the temperature of the reactor. For example, a light water reactor are designed to operate "under-moderated," meaning that if there were more moderator present,  $k_\infty$  would increase, and by the same token less moderation reduces  $k_\infty$ . As a result, as the moderator temperature increases, and the water expands – reducing its density and so neutron moderation –  $k_\infty$  decreases. Thus as the power level of a reactor is slowly brought up, and its temperature increases,  $k_\infty$  decreases. The equilibrium power of the reactor is where  $k_\infty - 1$  just drops to the point where it balances the neutron losses. That point can be adjusted by inserting "control rods" that, in effect, reduce  $k_\infty$  at any temperature, by absorbing neutrons.

**Questions:**  $\phi_0 \cos [3\pi x/(2\tilde{a})]$  is a solution to the neutron diffusion equation that matches the required boundary conditions for a slab infinite in the  $y$  and  $z$  directions. By what factor would  $k_\infty - 1$  need to increase to support this solution? And why is this solution, standing alone, not physical anyway?

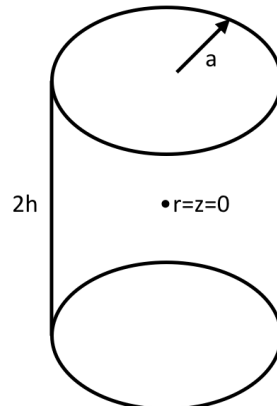


Figure 4.7 Cylindrical reactor core.

### 4.7.2 Cylinders

Now we move on to a more realistic case for a reactor, a right circular cylinder of finite length. Let the radius of the cylinder be  $a$ , and its height  $2h$ , the latter in violation of the conventional definition of  $h$ , but consistent with our practice here, making the named dimension half of the edge-to-edge distance. See figure 4.7. In cylindrical coordinates, and assuming cylindrical symmetry, equation 4.52 becomes

$$\frac{1}{\phi(r)r} \frac{\partial}{\partial r} r \frac{\partial}{\partial r} \phi(r) + \frac{1}{\phi(z)} \frac{\partial^2 \phi(z)}{\partial z^2} + B_m^2 = 0 \quad (4.59)$$

where we have already performed the separation of variables, as in equation 4.56. The first two terms sum to  $-B_g^2$ . Again each term must be spatially uniform.

To address the first term on the left-hand-side, we take advantage of the fact that the 0'th Bessel function of the first kind,  $J_0$ , obeys the equation,

$$\frac{1}{J_0(\gamma r)} \frac{1}{r} \frac{d}{dr} r \frac{d}{dr} J_0(\gamma r) = -\gamma^2 \quad (4.60)$$

making this special function a candidate for our solution. The 0'th Bessel function of the second kind,  $Y_0$ , is the other solution to this equation, but it diverges as  $r$  goes to zero, so we reject it. Let us therefore take

$$\phi(r) \propto J_0(\gamma r) \quad (4.61)$$

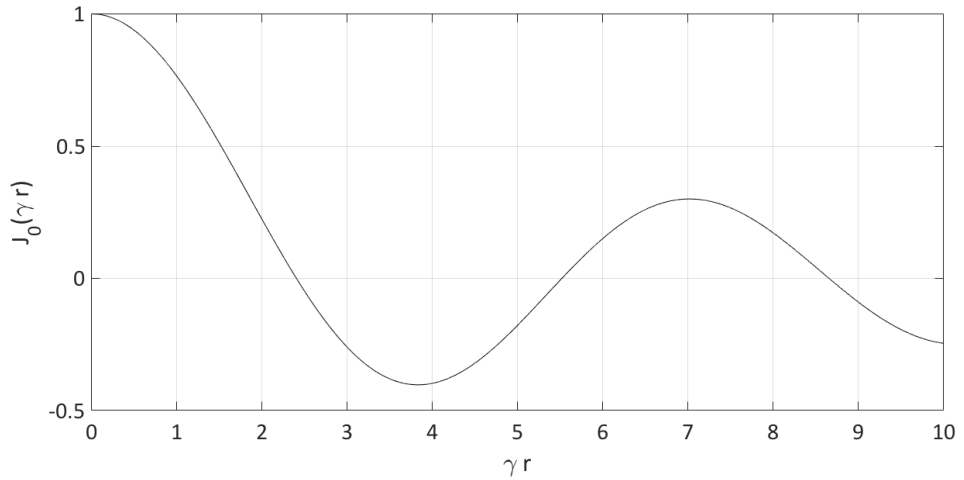


Figure 4.8 0'th Bessel Function of the first kind vs.  $\gamma r$  for  $\gamma = 2.405$

Figure 4.8 shows the 0'th Bessel function of the first kind. It has its first

zero at  $\gamma r = 2.405$ . Thus to match our boundary condition that sets  $\phi = 0$  at  $r = \tilde{a}$  we require

$$\begin{aligned}\gamma\tilde{a} &= 2.405 \\ \gamma &= 2.405/\tilde{a}\end{aligned}\quad (4.62)$$

Thus we have

$$\phi(r) \propto J_0(2.405r/\tilde{a}) \quad (4.63)$$

and  $\gamma^2 = (2.405/\tilde{a})^2$  is the contribution to  $B_g^2$  from this term.

The second term of equation 4.60 is familiar from the cuboid case. Its solution, taking into account the boundary conditions at  $\pm\tilde{h}$ , is

$$\phi(z) \propto \cos\left(\frac{\pi}{2}\frac{z}{\tilde{h}}\right) \quad (4.64)$$

Bringing these together we have

$$\phi(r, z) = \phi_0 J_0\left(\frac{2.405r}{\tilde{a}}\right) \cos\left(\frac{\pi}{2}\frac{z}{\tilde{h}}\right) \quad (4.65)$$

and

$$B_g^2 = \left(\frac{2.405}{\tilde{a}}\right)^2 + \left(\frac{\pi}{2\tilde{h}}\right)^2 \quad (4.66)$$

#### 4.7.3 Spheres

Finally we consider a spherical reactor, with extrapolated radius  $\tilde{a}$ . This is the configuration that reaches criticality, for given  $B_m$ , with the least mass of material. Equation 4.52 in spherical coordinates, assuming spherical symmetry, is

$$\frac{1}{\phi r^2} \frac{\partial}{\partial r} r^2 \frac{\partial}{\partial r} \phi + B_m^2 = 0 \quad (4.67)$$

Now we try an ansatz,  $\phi = \psi/r$ .

$$\begin{aligned}\frac{r}{\psi r^2} \frac{\partial}{\partial r} r^2 \frac{\partial}{\partial r} \left(\frac{\psi}{r}\right) + B_m^2 &= 0 \\ \frac{1}{\psi r} \frac{\partial}{\partial r} \left(r \frac{\partial \psi}{\partial r} - \psi\right) + B_m^2 &= 0 \\ \frac{1}{\psi r} \left(\frac{\partial \psi}{\partial r} + r \frac{\partial^2 \psi}{\partial r^2} - \frac{\partial \psi}{\partial r}\right) + B_m^2 &= 0 \\ \frac{1}{\psi} \frac{\partial^2 \psi}{\partial r^2} + B_m^2 &= 0\end{aligned}\quad (4.68)$$

**Question:** Give a plausibility argument, in terms of volume and surface area, for why the sphere might be the most efficient shape for achieving criticality with a fixed amount of fissile material.

This is the same equation that we solved for the cuboid reactor, but in this case the variable is  $\psi$ , not  $\phi$ . Furthermore the boundary conditions are different. We know that sine and cosine are valid solutions to the equation for  $\psi$ , but now we must reject cosine, because if  $\psi$  takes on a cosine variation  $\phi$  goes to infinity at the origin, which is unphysical. Thus we need a sine solution for  $\psi$ , and we require  $\phi = 0$  and therefore  $\psi = 0$  at  $\tilde{a}$ . This leaves us with

$$\phi = \phi_0 \left( \frac{\tilde{a}}{\pi} \right) \frac{\sin(\pi r/\tilde{a})}{r} \quad (4.69)$$

giving

$$B_g^2 = \frac{1}{\psi} \frac{\partial^2 \psi}{\partial r^2} = \left( \frac{\pi}{\tilde{a}} \right)^2 \quad (4.70)$$

and again we require that  $B_g^2 = B_m^2$ , setting the self-consistency between the neutron loss and the excess of  $k_\infty$  above unity.

**Questions:** Why does the factor  $\tilde{a}/\pi$  appear in the equation for  $\phi$ ? What is  $\partial\phi/\partial r$  at the origin, and why is this necessary?

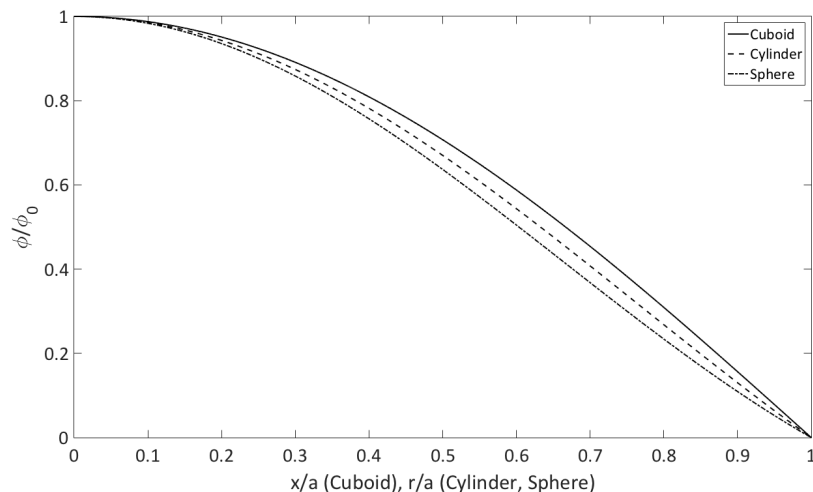


Figure 4.9 Profiles of neutron flux for cuboid, cylindrical, and spherical geometries.

Figure 4.9 shows the spatial profiles of neutrons for the three cases we have considered here. Evidently they are quite similar, but the cuboid is

flattest, the cylinder slightly less flat and the sphere most peaked. This is because surface losses affect the outer part of the profile most strongly in the case where the surface curves around the outer part in two dimensions, the sphere, less in the case where the surface curves around the outer part in only one dimension, the cylinder, and least in the case of a planar surface, with no curvature.

#### **4.7.4 Reflectors**

Nuclear reactor cores are generally surrounded by neutron “reflectors,” as discussed at the beginning of this section, 4.7, on bounded systems. Their purpose is to use inexpensive non-fuel material to reduce neutron loss from the reactor core by reflecting escaping neutrons back into the core. As we will see momentarily, the consequent reduction in neutron loss shows up as a decrease in the size required for criticality, so for fixed material buckling,  $B_m$ , the system can be made smaller. Alternatively, for fixed size  $B_m$  can be reduced, so a lower  $k_\infty$  is required for criticality. Furthermore, the flux profile is flattened, giving more uniform fuel burn.

For simplicity, let us consider a planar reactor, confined in the region  $|x| < a$ , with reflectors in the regions  $|x| > a$ . If the reflectors were to extend to  $\pm\infty$ , the flux profile in the reflectors would be the same as that for a planar source in a net absorbing medium, given in equation 4.37 with  $k_\infty = 0$ . Covering both  $x < 0$  and  $x > 0$  we have, for  $\phi$  in the reflectors,

$$\phi_r(x) = \phi_a \exp\left(-\frac{|x| - a}{L_r}\right) \quad (4.71)$$

where  $\phi_r(x)$  is the neutron flux in the reflector region,  $\phi_a$  is the neutron flux at the interfaces between the reactor core and the reflectors, where  $|x| = a$ , and  $L_r$  represents the neutron diffusion length in the reflectors. In a realistic case, of course, the reflectors do not extend to  $\pm\infty$ , but if they extend for a distance much greater than  $L_r$  they act largely as if they did. To get a feel for the maximum effects of reflectors, with a minimum of mathematics, let us consider this infinite case.

The left-right symmetric one-dimensional solution for  $\phi$  in the core region is

$$\phi_c(x) = \phi_0 \cos(xB_g) \quad (4.72)$$

by the definition of  $B_g$ , equation 4.53. It is important to note that  $B_g$  must still equal  $B_m$  for steady-state conditions. What we will find below is that

$aB_g$ , and so  $aB_m$ , can be lower with a reflector. This gives the result that the core size and/or  $k_\infty$  can be smaller, all else being equal.

The boundary conditions (equations 4.47 and 4.48) that will determine  $B_g$  in this case are given, first, by matching  $\phi$  at the core-reflector interfaces,

$$\phi_c(a, -a) = \phi_0 \cos(aB_g) = \phi_r(a, -a) = \phi_a \quad (4.73)$$

where  $\phi_c$  is the flux profile in the core region.

Next we must match the neutron flow out of the core at  $\pm a$  with that into the reflector at  $\pm a$ , giving

$$\begin{aligned} -D_c \frac{d\phi_c}{dx} \Big|_{a,-a} &= \pm D_c \phi_0 B_g \sin(aB_g) = \\ -D_r \frac{d\phi_r}{dx} \Big|_{a,-a} &= \pm D_r \phi_a / L_r = \pm D_r \phi_0 \cos(aB_g) / L_r \end{aligned} \quad (4.74)$$

where  $D_c$  and  $D_r$  are the neutronics diffusion coefficients,  $\lambda_{tr}/3$ , in the core and reflector, respectively. This gives us

$$B_g \tan(aB_g) = D_r / (L_r D_c) \quad (4.75)$$

If we multiply both sides by  $a$  we arrive at

$$aB_g \tan(aB_g) = aD_r / (L_r D_c) \quad (4.76)$$

Transcendental equations of this type (and *much* more complicated) are endemic to calculations about reflectors. They can be solved for quantities like  $aB_g$  using numerical root finders, or for graphic display the problem can sometimes be made easier by evaluating quantities like  $aD_r/(L_r D_c)$  as a function of  $aB_g$ , but then plotting  $aD_r/(L_r D_c)$  on the  $x$  axis. Figure 4.10 shows the solution to this equation, as well  $\phi_a/\phi_0 = \cos(aB_g)$ , a measure of the degree of the flattening within the core provided by reflection. We display  $B_m$  rather than the equivalent  $B_g$  to emphasize that the size and/or  $k_\infty$  can be reduced by using a reflector.  $aB_m$  is divided by  $\pi/2$ , to allow direct comparison with the no-reflector case.

There is valuable physical insight to be gained from figure 4.10. The number of diffusive transport steps required to traverse a mean square distance  $\langle X^2 \rangle$  is given by  $N = \langle X^2 \rangle / \lambda_{tr}^2$ . Thus, remembering the definition  $D = \lambda_{tr}/3$ , and taking the characteristic length in the core to be  $a$  and that in the reflector to be  $L_r$ , the abscissa of figure 4.10 can be re-expressed in terms of the ratio of collisions a neutron experiences while in the core to

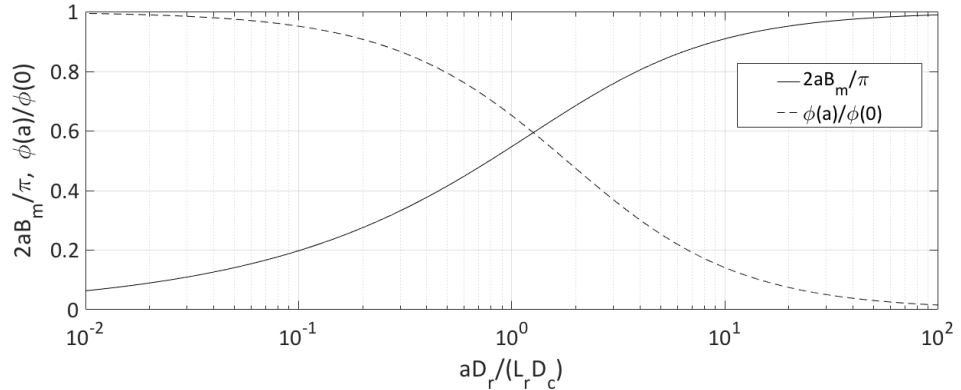


Figure 4.10 Normalized material buckling and profile flattening as functions of normalized diffusion length, in a slab reactor.

those it experiences in the reflector:

$$\frac{aD_r}{L_r D_c} = \frac{a}{\lambda_{tr,c}} \frac{\lambda_{tr,r}}{L_r} = \left( \frac{N_c}{N_r} \right)^{\frac{1}{2}} \quad (4.77)$$

For high values of the abscissa of figure 4.10 many more collisions are required to escape the core than to be absorbed in the reflector. In this limit the solution reasonably converges to the no-reflector case (neglecting the extrapolation length), where we showed  $\tilde{a}B_m = \pi/2$ . For low values of the abscissa, on the other hand, neutrons collide many fewer times in the core than in the reflector, so the reflector has room within  $L_r$  to do its job ... reflect neutrons. Thus the core profile is flattened, as implied by low values of  $2aB_m/\pi = 2aB_g\pi$ . Furthermore,  $a$  and/or  $k_\infty$  can be reduced. Of course  $k_\infty - 1$  cannot be negative for criticality.

Figure 4.11 shows the profiles of  $\phi(x/a)$  for five conditions,  $aD_r/(L_r D_c) = 0.1, 0.3, 1, 3$ , and  $10$ , corresponding to  $2aB_m/\pi = 0.198, 0.332, 0.548, 0.759$ , and  $0.910$ . In the reflector region, the profile shape is given by equation 4.71.

**Question:** When the analysis for a reflected system gives  $a$  greater than  $\tilde{a} - \lambda_{ext}$  from the analysis for an unreflected system, clearly something has gone wrong. Adding a reflector, however inefficient, should not increase the size needed for criticality. What do you suppose has happened? Exercise 4.11 checks your intuition.

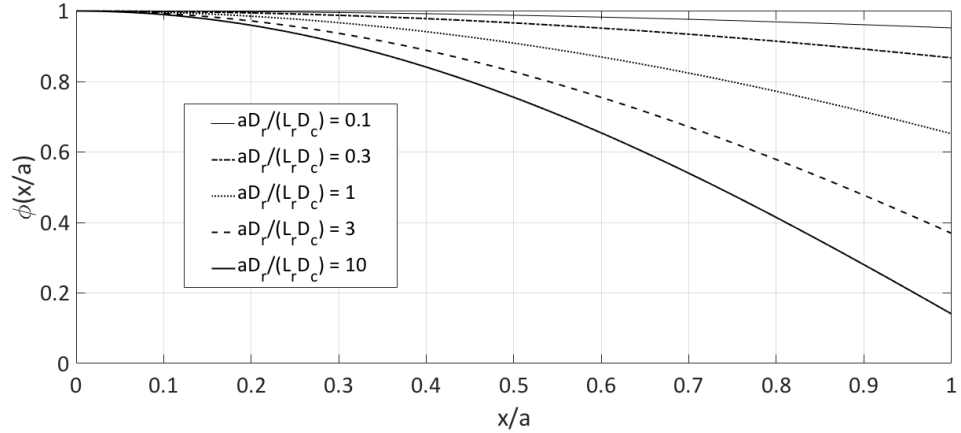


Figure 4.11 Core flux profiles for a range of values of  $aD_r/(L_r D_c)$  in a planar reactor.

#### 4.8 Non-leakage probability

Now we are interested to know, within the framework of the one-speed model, the probability that a neutron born in a bounded volume is absorbed in that volume, rather than escapes across its boundary. As it turns out, Gauss's theorem performs rather nice magic in allowing us to answer this question. Let us use this theorem to evaluate the rate of neutron loss, in neutrons/s, across the boundary of the system (not, in this case, the extrapolated boundary):

$$\begin{aligned} \int_A n\langle \vec{v} \rangle \cdot d\vec{A} &= \int_V \vec{\nabla} \cdot n\langle \vec{v} \rangle dV = \int_V -\vec{\nabla} \cdot D\vec{\nabla}\phi dV \\ &= \int_V DB_g^2 \phi dV = DB_g^2 \int_V \phi dV \end{aligned} \quad (4.78)$$

where  $A$  represents the surface area of the bounded volume, and  $V$  its volume. We have used our established definition,  $B_g^2 \equiv -\nabla^2\phi/\phi$ . Because  $B_g^2$  and  $D$  are assumed to be spatially uniform, each element of volume, on net, loses neutrons in proportion to its local value of  $\phi$ , and the total neutron loss per second across the boundary can be evaluated quite simply.

Conveniently, the local absorption rate is also proportional to the local neutron flux,  $\phi$ , because we have assumed that, along with everything else, the macroscopic cross-section for absorption is spatially uniform at the large scale. So let us evaluate the total absorption rate, in neutrons/sec:

$$\int_V \overline{\Sigma_{abs}} \phi dV = \overline{\Sigma_{abs}} \int_V \phi dV \quad (4.79)$$

Thus the probability that a neutron is *not* lost across the boundary, and so is ultimately absorbed, the non-loss probability, is given by

$$P_{nl} = \frac{\text{neutrons absorbed/s}}{\text{neutrons absorbed/s} + \text{neutrons lost/s}} = \frac{\overline{\Sigma}_{abs}}{\overline{\Sigma}_{abs} + DB_g^2} \quad (4.80)$$

where we have divided both numerator and denominator by  $\int_V \phi dV$ .

Now we use the definition of  $L$ , equation 4.37, to write  $D = L^2 \overline{\Sigma}_{abs}$  and we divide numerator and denominator by  $\overline{\Sigma}_{abs}$ , giving

$$P_{nl} = \frac{1}{1 + L^2 B_g^2} \quad (4.81)$$

for any reactor with homogeneous materials. It seems reasonable then that the criticality criterion for a finite system would be given by:

$$\frac{k_\infty}{1 + L^2 B_g^2} = 1 \quad (4.82)$$

To confirm this, let us return to the steady-state one-speed neutron diffusion equation, equation 4.52.

$$\frac{1}{D\phi v_n} \frac{\partial \phi}{\partial t} = 0 = \frac{1}{\phi} \nabla^2 \phi + \frac{k_\infty - 1}{L^2} = -B_g^2 + \frac{k_\infty - 1}{L^2} \quad (4.83)$$

This reminds us that for an infinite, homogeneous medium, one with no “geometric buckling” so  $B_g^2 \rightarrow 0$ , we require  $k_\infty = 1$  for criticality, which meets the requirement of time independence. For a bounded system, we can immediately write

$$\begin{aligned} B_g^2 &= \frac{k_\infty - 1}{L^2} \\ 1 + L^2 B_g^2 &= k_\infty \\ \frac{k_\infty}{1 + L^2 B_g^2} &= P_{nl} k_\infty = 1 \end{aligned} \quad (4.84)$$

Thus we can define a  $k$  such that

$$k \equiv P_{nl} k_\infty = 1 \quad (4.85)$$

is required for time independence, nicely consistent with our earlier Gauss’s Theorem derivation of  $P_{nl}$ . Often  $P_{nl} k_\infty$  is instead denoted  $k_{eff}$ .

#### 4.9 Spatial diffusion in thermal reactors

We just determined the effect of the boundary on our very simple one-speed diffusion model for a fission reactor. Let us consider now, one by one, the

three energy regions that we discussed in the last chapter: Fast, Intermediate, and Thermal. We will see if we can improve those calculations by taking into account a finite medium.

The goal of our calculation in the Fast energy region was to evaluate  $\epsilon$ , the fast fission multiplication factor, that enhances the number of number of neutrons slowing down into the Intermediate energy region, compared to those produced from thermal fission. We derived this in equation 3.59. reproduced here.

$$\epsilon = \frac{1 - \frac{V_{fuel}}{V^{tot}} \frac{(\overline{\Sigma}_{F,f}^{fuel} + \overline{\Sigma}_{F,\gamma}^{fuel})}{\overline{\Sigma}_{F,loss}}}{1 - \frac{V_{fuel}}{V^{tot}} \frac{\overline{\nu}_F \overline{\Sigma}_{F,f}^{fuel}}{\overline{\Sigma}_{F,loss}}} \quad (4.86)$$

The second term in the denominator corresponds to  $k_\infty$  in the Fast energy region, and its role in the denominator arises from the fact that

$$\frac{1}{1 - k_\infty} = 1 + k_\infty + k_\infty^2 + k_\infty^3 \dots \quad (4.87)$$

and so sums over the generations of neutrons in the Fast energy region. However, each generation has a non-loss probability,  $P_{nl,F}$ , that must be included in a bounded case. Furthermore the numerator represents the fraction of fission neutrons produced that make it down to the Intermediate energy region, so it, too, needs to multiplied by  $P_{nl,F}$ . This can be accomplished with an overall prefactor. The result is a version of  $\epsilon$  appropriate for use in a bounded system,

$$\epsilon_{bnd} = P_{nl,F} \frac{1 - \frac{V_{fuel}}{V^{tot}} \frac{(\overline{\Sigma}_{F,f}^{fuel} + \overline{\Sigma}_{F,\gamma}^{fuel})}{\overline{\Sigma}_{F,loss}}}{1 - P_{nl,F} \frac{V_{fuel}}{V^{tot}} \frac{\overline{\nu}_F \overline{\Sigma}_{F,f}^{fuel}}{\overline{\Sigma}_{F,loss}}} \quad (4.88)$$

It is a little tricky to evaluate  $P_{nl,F}$ , because at energies in the Watt spectral range, elastic scattering is no longer isotropic in the Center-of-Mass frame. This can be included through a correction factor on  $\sigma_e$  of  $1 - \langle \cos\theta \rangle$ , the fraction of forward momentum lost in an elastic collision in the Center-of-Mass frame. Table ?? provides these factors for 2 MeV, the mean energy of the Watt spectrum, and 100 keV the logarithmic center of the  $FR - I$  spectrum.

NEED THE TABLE HERE.

Table 4.1 gives  $\lambda_{tr}$ ,  $L$  and  $v_n$  for the example thermal reactor core we considered in sections 3.5 through 3.8. The elastic scattering term in  $\lambda_{tr,F}$  has been adjusted for forward scattering in the center-of-mass frame.

Table 4.1 *Mean free paths for momentum loss and absorption, diffusion length, and neutron speed for various media in thermal reactors. Thermal speed corresponds to energy of 0.0253 eV; Watt spectrum speed corresponds to 2 MeV.*

Medium	$\lambda_{tr}$	$\lambda_{abs}$	$L$	$v_n$	Spectrum
Nominal LWR Core	0.0119	0.0363	0.0120	$2.2 \cdot 10^3$	Thermal
Nominal LWR Core	0.0119	0.0363	0.0120	$1.96 \cdot 10^7$	Watt
H <sub>2</sub> O	0.0128	0.457	0.0442	$2.2 \cdot 10^3$	Thermal
H <sub>2</sub> O	0.0128	0.457	0.0442	$1.96 \cdot 10^7$	Watt
4% enriched UO <sub>2</sub>	$9.57 \cdot 10^{-3}$	0.0143	$6.75 \cdot 10^{-3}$	$2.2 \cdot 10^3$	Thermal
4% enriched UO <sub>2</sub>	$9.57 \cdot 10^{-3}$	0.0143	$6.75 \cdot 10^{-3}$	$1.96 \cdot 10^7$	Watt
Natural Zirc	0.0340	1.21	0.117	$2.2 \cdot 10^3$	Thermal
Natural Zirc	0.0340	1.21	0.117	$1.96 \cdot 10^7$	Watt
D <sub>2</sub> O	0.0360	28.2	0.582	$2.2 \cdot 10^3$	Thermal
D <sub>2</sub> O	0.0360	28.2	0.582	$1.96 \cdot 10^7$	Watt
Graphite	0.0338	22.7	0.506	$2.2 \cdot 10^3$	Thermal
Graphite	0.0338	22.7	0.506	$1.96 \cdot 10^7$	Watt

The Intermediate energy region is not amenable to treatment by our one-speed model, since the neutrons are anything but mono-energetic. They are spread out over some six orders of magnitude in energy, a factor of nearly fourteen in lethargy. However we can take advantage of the insight we have gained from the diffusion model to consider the loss of neutrons during the slowing down process, following once again an analysis by Fermi.

Consider a differential time period,  $dt$ . During this time, neutrons slow down by an amount of energy

$$dt = dE \left( \frac{dE}{dt} \right)^{-1} \approx \frac{-dE}{v\xi \Sigma_e E} \quad (4.89)$$

where we have used Fermi's continuous slowing-down approximation, equation 3.28. Now during this time  $dt$  we expect the differential increment in the mean-square spreading of the neutrons in any direction, for example  $x$ ,

to be given by

$$\frac{d\langle(\Delta x)^2\rangle}{2} = D_{phys}dt = \frac{-\lambda_{tr}dE}{3\xi\Sigma_e E} \quad (4.90)$$

where the  $v$  has disappeared because we are using the “physics” definition of  $D$ .

Integrating over the Intermediate range of energy traversed by neutrons, from 1 Mev to 1 eV (so  $dE$  itself is negative), we have quite simply

$$\frac{\langle(\Delta x)^2\rangle}{2} = \int_{1\text{eV}}^{1\text{MeV}} \frac{\lambda_{tr}}{3\xi\Sigma_e E} dE \approx \frac{\lambda_{tr}}{3\xi\Sigma_e} \ln(10^6) = 4.60 \frac{\lambda_{tr}}{\xi\Sigma_e} \equiv \tau_{Fermi} \quad (4.91)$$

where we have used the approximation of energy-independent cross-sections across the full energy range. We can use the values at 1 keV, as the mid-point of the Intermediate energy range. This spreading, with dimension of  $m^2$ , is called the “Fermi Age,”  $\tau_{Fermi}$ . It is hard to find a logic for this nomenclature. It is Fermi’s calculation – but why call it an “age”?

It is interesting to show that this spreading of Intermediate energy neutrons is analogous to  $L^2$  for one-speed neutrons. The expected spreading in the one-speed diffusion equation, equation 4.29, is

$$\frac{\langle(\Delta x)^2\rangle}{2} = \frac{\sigma^2}{2} = D_{phys}\tau_{abs} = \frac{D_{phys}}{\Sigma_{abs}v_n} = \frac{D}{\Sigma_{abs}} = L^2 \quad (4.92)$$

where we have used  $\tau_{abs}$  as the mean time to absorption. The analogy is that neutrons are lost from the Intermediate energy region when they slow down to thermal energies, and thermal neutrons are “lost” when they are absorbed, so  $\tau_{Fermi}$  plays an equivalent role for Intermediate energy neutrons to that played by  $L^2$  for thermal neutrons.

We now can take the point of view that if a group of neutrons in the Intermediate energy region spreads spatially in any one dimension by a mean square distance of  $\tau_{Fermi}$  during slowing down, while a one-speed group of neutron spreads spatially in any one dimension by a mean square distance of  $L^2$  in the time it takes be absorbed, then the non-loss probability of neutrons traversing the Intermediate energy range should be given by

$$P_{I,nl} = \frac{1}{1 + \tau_{Fermi}B_{I,g}^2} \quad (4.93)$$

Note that this approximation, which neglects the difference between exponential decay over time and a more or less predictable loss time, focusing only on the mean time, is on top of the approximation of assuming continuous slowing down even when collisions with hydrogen play the dominant role.

Finally we come to the thermal distribution, where our one-speed model is

most reasonably applicable. Here we evaluate  $L$  using thermal cross-sections, to give

$$P_{T,nl} = \frac{1}{1 + L_T^2 B_{T,g}^2} \quad (4.94)$$

This gives a six-factor formula for criticality

$$k = P_{I,nl} P_{T,nl} \epsilon p f \eta_T = 1 \quad (4.95)$$

In the cases where  $\tau_{Fermi} B_{I,g}^2$  and  $L_T^2 B_{T,g}^2$  are both much less than unity, and the difference between the Intermediate and Thermal values for  $B_g$  is negligible, we multiply together  $P_{I,nl} P_{T,nl}$  to get

$$P_{nl} = P_{I,nl} P_{T,nl} = \frac{1}{(1 + \tau_{Fermi} B_{I,g}^2)(1 + L_T^2 B_{T,g}^2)} \approx \frac{1}{1 + M^2 B_g^2} \quad (4.96)$$

where  $M^2 = \tau_{Fermi} + L^2$ .  $M$  in this context is called the “migration length.” This brings us to a still-alliterative Fermi five-factor formula. For our model light water reactor,  $\tau_{Fermi}^{1/2} = 0.0334$  m,  $L = 0.0120$  m and  $M = 0.0355$  m. Taking a 4 m tall reactor of radius 1 m (see exercise 3.5), we have  $B_g^2 = (2.405)^2 + (\pi/4)^2 = 6.40\text{m}^{-2}$ , giving  $P_{nl} = 0.99$ .

It is interesting that while spatial loss is a minor correction to the overall neutron economy in a full-scale light water reactor, spatial diffusion is still very important; it governs the flux profile within the reactor. For spatially uniform material properties, and no reflectors, the neutron sink at the edge results in a much lower total power production than would be obtained with a flat flux profile equal to the peak value. In effect the loss at the edge turns itself down by reducing the neutron production rate close to the edge. Spatial loss is more important in fast reactors, and can be important in heavy water and graphite reactors, especially smaller “research reactors.”

#### 4.10 Spatial diffusion in fast reactors

In Chapter 3 we developed a model for fast-spectrum reactors involving two energy regions. The higher region, characterized by a Watt spectrum, was analogous to the Fast region for thermal reactors, with neutron energy largely above about 1 MeV. However because of the weak moderation by the coolant in fast reactors,  $\epsilon$ , the fast multiplication factor is much higher. The second region we called the Fast Reactor Intermediate, *FR-I*, region, with a log-normal distribution peaked at 100 keV, falling off with  $1 - \sigma$  width of a factor of 4 in either direction.

Table 4.2 gives  $\lambda_{tr}$ ,  $L$  and  $v_n$  for the nominal reactor cores we considered

in sections 3.5 through 3.8 (our example thermal reactor) and section 3.10 (our example fast reactor), and for some representative reflector materials. The example fast reactor blanket is assumed to have the same configuration as the core, but the uranium is pure  $^{238}\text{U}$ . The last four lines anticipate a criticality calculation we will do when we look at nuclear weapons in chapter 7.

## 4.11 Integrated numerical modeling

NEED to fill in the table in this section.

### Review

### Resources

### Exercises

- 4.1 Show that a neutron recoiling off a proton (of assumed equal mass), never has any component of velocity in the reverse direction of its incoming velocity. In other words,  $\vec{v}_0 \cdot \vec{v}_1 > 0$  in the nomenclature of figure 3.1.
- 4.2 Show that the solution for momentum loss for finite-A is also consistent with just considering the average of the cosine of the scattering angle in the lab frame.
- 4.3 Show by substitution that equation 4.29 solves equation 4.28. Also show that the spatial integral of equation 4.29 equals unity, independent of time.
- 4.4 Let's prove an interesting part of the Central Limit Theorem, equation 4.32. Indeed more generally, we will prove that if we add a list of numbers with variance  $\sigma_1^2$  to another list of numbers with variance  $\sigma_2^2$  the variance of the sum is  $\sigma_1^2 + \sigma_2^2$ . Start with a list of  $x_i$  and another list of  $\Delta X_i$ . For simplicity, assume each list has mean value of 0. Thus the variance of the sum is  $\sigma^2 = \sum (x_i + \Delta x_i)^2$ . Show that so long as  $x_i$  is uncorrelated with  $\Delta x_i$ ,  $\sigma^2 = \sigma_1^2 + \sigma_2^2$ .
- 4.5 Consider the infinite, homogeneous, time-independent version of equation 4.27. Add a volumetric extrinsic neutron source term,  $S_{ext}$ . Now calculate  $\phi$ , and the volumetric absorption rate, for the case of  $k_\infty < 1$ . Why is the absorption rate greater than the extrinsic source rate? Explain your result in terms of the meaning of  $k_\infty$ . By the way, what is wrong with your solution if  $k_\infty > 1$  ?

- 4.6 Simulate the 1-D source problem with Monte Carlo.
- 4.7 show that if you use equation 4.50 for the boundary condition in a slab reactor you get the same result for  $\lambda_{tr} \ll x_0$ .
- 4.8 Show that for a cuboid reactor, the highest  $k$
- 4.9 Spherical reflector
- 4.10 Finite size reflector?
- 4.11 Let's understand what has gone wrong when an analysis with a poor reflector gives a size,  $a$ , greater than  $\tilde{a} - \lambda_{ext}$  from the unreflected analysis – for the same  $B_m$ . Start by defining  $\epsilon \equiv \pi/2 - a_r B_m$  where, for clarity, we define  $a_r$  as the solution in the reflected case. We will use  $a_u$  for the unreflected case. Invert both sides of equation 4.76 and solve it for  $\epsilon$ , assuming  $\epsilon \ll 1$ . Set  $B_g = B_m$  as required for criticality. Next substitute back in for  $\epsilon$ , using its definition, while replacing  $\pi/2$  with  $\tilde{a}_u B_m$  from the unreflected solution. Now solve for  $\tilde{a}_u - a_r$  and set this equal to  $\lambda_{ext}$  for the condition of marginal breakdown. What physics assumption has broken down near this point?

Table 4.2 *Mean free paths for momentum loss and absorption, diffusion length, and neutron speed for various media in thermal reactors. Thermal speed corresponds to energy of 0.0253 eV; FR – I speed corresponds to 100 keV; Watt spectrum speed corresponds to 2 MeV.*

Medium	$\lambda_{tr}$	$\lambda_{abs}$	$L$	$v_n$	Spectrum
Nominal LWR Core	0.0119	0.0363	0.0120	$2.2 \cdot 10^3$	Thermal
Nominal LWR Core	0.0119	0.0363	0.0120	$2.2 \cdot 10^3$	Thermal
H <sub>2</sub> O	0.0128	0.457	0.0442	$2.2 \cdot 10^3$	Thermal
H <sub>2</sub> O	0.0128	0.457	0.0442	$2.2 \cdot 10^3$	Thermal
4% enriched UO <sub>2</sub>	$9.57 \cdot 10^{-3}$	0.0143	$6.75 \cdot 10^{-3}$	$2.2 \cdot 10^3$	Thermal
4% enriched UO <sub>2</sub>	$9.57 \cdot 10^{-3}$	0.0143	$6.75 \cdot 10^{-3}$	$2.2 \cdot 10^3$	Thermal
Natural Zirc	0.0340	1.21	0.117	$2.2 \cdot 10^3$	Thermal
Natural Zirc	0.0340	1.21	0.117	$2.2 \cdot 10^3$	Thermal
D <sub>2</sub> O	0.0360	28.2	0.582	$2.2 \cdot 10^3$	Thermal
D <sub>2</sub> O	0.0360	28.2	0.582	$2.2 \cdot 10^3$	Thermal
Graphite	0.0338	22.7	0.506	$2.2 \cdot 10^3$	Thermal
Graphite	0.0338	22.7	0.506	$2.2 \cdot 10^3$	Thermal
Nominal FR Core	–	–	–	$4.37 \cdot 10^6$	FR-I
Nominal FR Core	–	–	–	$1.96 \cdot 10^7$	Watt
Nominal FR Blanket	–	–	–	$4.37 \cdot 10^6$	FR-I
Nominal FR Blanket	–	–	–	$1.96 \cdot 10^7$	Watt
Sodium metal	0.0322	19.5	0.458	$4.37 \cdot 10^6$	FR-I
Sodium metal	0.0366	38.5	0.685	$1.96 \cdot 10^7$	Watt
20% enriched UO <sub>2</sub>	$9.57 \cdot 10^{-3}$	0.0143	$6.75 \cdot 10^{-3}$	$2.2 \cdot 10^3$	FR-I
Natural UO <sub>2</sub>	$9.57 \cdot 10^{-3}$	0.0143	$6.75 \cdot 10^{-3}$	$2.2 \cdot 10^3$	Watt
Natural Iron metal	0.0322	19.5	0.458	$4.37 \cdot 10^6$	FR-I
Natural Iron metal	0.0366	38.5	0.685	$1.96 \cdot 10^7$	Watt
<sup>235</sup> U metal	0.0213	0.136	0.0311	$4.37 \cdot 10^6$	FR-I
<sup>235</sup> U metal	0.0271	0.156	0.0376	$1.96 \cdot 10^7$	Watt
<sup>238</sup> U metal	0.0210	1.71	0.109	$4.37 \cdot 10^6$	FR-I
<sup>238</sup> U metal	0.0265	0.553	0.0699	$1.96 \cdot 10^7$	Watt

# Chapter 5

## Safety

Neutrons can go wild.

### 5.1 The neutron “kinetic” equation

### 5.2 Including delayed neutrons

#### 5.2.1 *Finding $\tau$ 's that solve the equation*

### 5.3 Consequences for reactor stability

### 5.4 Behavior over longer time scales

### 5.5 Chernobyl

### 5.6 Fukushima

### 5.7 Regulatory response

### 5.8 Effects of radiation on human health

### 5.9 Impacts of Chernobyl and Fukushima

#### Review

#### Resources

#### Exercises

##### 5.1 Jumping jacks

##### 5.2 Pushups

##### 5.3 Running in place

# Chapter 6

## The Nuclear Fuel Cycle

Digging it up, burning it, and burying it.

### 6.1 Mining

### 6.2 Enrichment

### 6.3 Burnup

### 6.4 Interim storage

### 6.5 Geological repository

### 6.6 Reprocessing for thermal reactors

### 6.7 Fast reactors and reprocessing

### Review

### Resources

### Exercises

6.1 Jumping jacks

6.2 Pushups

6.3 Running in place

## Chapter 7

### Nuclear Weapons and Nuclear Proliferation



I am become death, the destroyer of worlds.

---

J. Robert Oppenheimer at the Trinity test, 1945

**7.1 How nuclear weapons work**

**7.2 History of nuclear proliferation**

**7.3 Proliferation risks going forward**

**7.4 Means to manage risks**

**Review**

**Resources**

**Exercises**

7.1 Pushups

7.2 Running in place

7.3 General Groves, who managed the Manhattan Project, commissioned Princeton Professor Henry DeWolf Smyth to write a report about the basic principles employed in the construction of nuclear weapons. Stalin had the report translated and distributed to his nuclear scientists. Arguably, while it did not release details, it indicated which paths had been pursued in the Manhattan project, and which had succeeded. Much later, Edward Teller argued that ideas developed in the U.S. inevitably leaked to the Soviet Union within about six months. Remarkably, he used this to argue against hiding the basic ideas behind advances in nuclear weapons, while accelerating nuclear weapons R&D. There are websites that purport to discuss the science and technology of nuclear weapons. What do you think about secrecy in nuclear weapons development?

# **Chapter 8**

## **Advanced Reactors**

Trying to address the issues of safety, waste and nuclear proliferation.

### **8.1 Generation III and III+ reactors**

### **8.2 Generation IV reactors**

### **8.3 Thorium cycle**

### **8.4 Breed and burn in place**

#### **Review**

#### **Resources**

#### **Exercises**

8.1 Jumping jacks

8.2 Pushups

8.3 Running in place

## **PART TWO**

### FUSION



# Chapter 9

## Power and Particle Balance

Need enough power and not too much helium.

### **9.1 Fusion reactions**

### **9.2 Plasma heating**

### **9.3 Heat loss**

### **9.4 Energy gain!**

### **9.5 Particle balance**

#### **Review**

#### **Resources**

#### **Exercises**

9.1 Jumping jacks

9.2 Pushups

9.3 Running in place

# Chapter 10

## Particle Motion

Combining general drifts and torus. Should I do the polarization drift and correct radial acceleration?

**10.1 Uniform electric and magnetic fields**

**10.2 Curved magnetic field**

**10.3 Perpendicular gradient in magnetic field strength**

**10.4 Parallel gradient in magnetic field strength**

**10.5 Drifts in toroidal magnetic field**

**10.6 Passing particle orbits**

**10.7 Trapped particle orbits**

**10.8 Bootstrap current**

**Review**

**Resources**

**Exercises**

10.1 Jumping jacks

10.2 Pushups

10.3 Running in place

# Chapter 11

## Plasmas as Fluids

Reference neutron fluid derivation of diffusion.

### 11.1 Plasmas as fluids?

### 11.2 Equilibrium in a cylinder

### 11.3 Plasma control

### 11.4 Stellarators

### 11.5 2-fluid model and parallel force balance

#### Review

#### Resources

#### Exercises

11.1 Jumping jacks

11.2 Pushups

11.3 Running in place

# Chapter 12

## Macroscopic Stability

Should we dig a little deeper into Troyon scaling?

**12.1 Ideal MHD stability**

**12.2 Interchange and ballooning modes**

**12.3 Kink modes**

**12.4 Plasma shaping**

**12.5 Stellarators**

**Review**

**Resources**

**Exercises**

12.1 Jumping jacks

12.2 Pushups

12.3 Running in place

# Chapter 13

## Collisions and their Effects

Should we include ion-electron thermal equilibration? NRL formulary?

**13.1 Coulomb collisions**

**13.2 Debye shielding**

**13.3 Small-angle scattering**

**13.4 Collisional cross-field transport**

**13.5 Other collisional effects**

**Review**

**Resources**

**Exercises**

13.1 Jumping jacks

13.2 Pushups

13.3 Running in place

# Chapter 14

## Turbulent Transport

Need better intuitive derivation of drift waves.

**14.1 Bohm and GyroBohm**

**14.2 Turbulence and flows – simulation**

**14.3 Turbulence and flows – measurement**

**14.4 Transport barriers**

**14.5 Global scaling**

**Review**

**Resources**

**Exercises**

14.1 Jumping jacks

14.2 Pushups

14.3 Running in place

# Chapter 15

## Divertors, Scrape-off layers, and Plasma-Facing Components

Get into the vapor box?

### 15.1 Divertors

### 15.2 Scrape-off layers

### 15.3 Transient events

### 15.4 Plasma-facing components

Review

Resources

Exercises

15.1 Jumping jacks

15.2 Pushups

15.3 Running in place

# **Chapter 16**

## **Neutron Interactive Materials, Blankets; Safety, Waste and Proliferation**

Text to allow proper formatting.

### **16.1 Neutron interactive materials**

### **16.2 Blanket designs**

### **16.3 Safety**

### **16.4 Waste**

### **16.5 Nuclear proliferation**

**Review**

**Resources**

**Exercises**

16.1 Jumping jacks

16.2 Pushups

16.3 Running in place

# Chapter 17

## Inertial Fusion Energy

17.1 Vision and status

17.2 Batch burn vs. hot-spot ignition

17.3 Drivers

17.4 Targets and chambers

Review

Resources

Exercises

17.1 Jumping jacks

17.2 Pushups

17.3 Running in place

# Chapter 18

## Power Plant Concepts, Development Path and Deployment

$$\begin{aligned} q_{\parallel} &= \kappa_e, \parallel \frac{dT_e}{d\ell}; \quad \frac{dq_{\parallel}}{d\ell} = n_e^2 c_z L_z \\ \frac{1}{2} \frac{dq_{\parallel}^2}{d\ell} &= n_e^2 T_e^2 F_z \kappa_0 T_e^{1/2} L_z \frac{dT_e}{d\ell} \\ q_{\parallel, det} &= n_{e, sep} T_{e, sep} \sqrt{2 \int_{T_{e, det}}^{T_{e, sep}} F_z \kappa_0 T_e^{1/2} L_z dT_e} \end{aligned} \quad eq.1$$

### 18.1 Power plant concepts

### 18.2 Development path

### 18.3 Deployment

#### Review

#### Resources

#### Exercises

18.1 Jumping jacks

18.2 Pushups

18.3 Running in place